WESTERN SYDNEY UNIVERSITY

Early Detection of Alzheimer’s Disease in Experimental and Natural Animal Models Using Novel Biologics

Thesis presented to Western Sydney University in fulfilment of the requirements for the degree of Doctor of Philosophy by

Umma Habiba

Supervisory Panel:

Primary Supervisor: **Associate Professor Mourad Tayebi**

Co-supervisor: **Professor John Morley**

School of Medicine

Western Sydney University

October 2021

Statement of Authentication

I hereby declare that the work presented in this thesis in fulfillment of the requirements of the degree of Doctor of Philosophy (PhD) at the Western Sydney University is to the best of my knowledge, original except for those parts as acknowledged in the text. I also certify that the material has not been submitted either in part or in full for any other degree, whether enrolled at this university or any other institution

[redacted]

Umma Habiba

24.10.2021

Acknowledgements

I express my deepest gratitude to the Almighty Allah for giving me the patience and strength to fulfill my dreams.

I would like to thank my parents for their continuous support and inspiration.

My primary supervisor, Associate Professor Mourad Tayebi has not only been an outstanding supervisor but also a great mentor to guide me throughout my PhD and future career development. I have been extremely blessed to have a supervisor who cared so much about my work, and who responded to my questions and queries so promptly. I am forever grateful for his contributions, motivations, guidance, and assistance.

I also would like to thank my co-supervisor, Professor John Morley for his suggestions and guidance in facilitating my research.

I would like to express my gratitude to Professor Tim Karl and his team for helping me with sample collections. Also, I would like to thank Associate Professor Bang Bui from the University of Melbourne for our collaboration work and for providing constructive feedback throughout my research. I want to express my gratitude to Dr. Sindy Kueh for technical support, and Nikola Mills for training and support. I am also thankful to Dr Hong Yu from Westmead institute of medical research (WMIR) for her continuous support on microscopic analysis and data collection.

I am grateful to the Neuroimmunology laboratory at Western Sydney University and all the members of the team. I would like to express special thanks to Utpal Kumar Adhikari, Sachin Kumar and Rizwan Khan for their advice.

My deep appreciation to Western Sydney University for providing me the opportunity to complete my Doctoral degree, for giving me all the educational support and access to all the advanced laboratory technologies.

Finally, this research took the work of many collaborators to complete, and to all of them I would like to say thank you for all of your help, patience and understanding.

Thank you

Umma Habiba

Thesis contents

List of Figures

List of Tables

List of Abbreviations

Abbreviations	**Full forms**
AD	Alzheimer's disease
MCI	Mild cognitive impairment
CCD	Canine cognitive dysfunction
dAD	Dog'zheimer
Aβo	Amyloid beta oligomer
Aβp	Amyloid beta plaque
CAA	Cerebral amyloid angiopathy
p-Tau	Hyperphosphorylated microtubule-associated tau protein
ONL	Outer nuclear layer
OPL	Outer plexiform layer
INL	Inner nuclear layer
IPL	Inner plexiform layer
GCL	Ganglion cell layer
OCT	Optical coherence tomography
H&E	Hematoxylin and eosin
CR	Congo red
IHC	Immunohistochemistry
IF	Immunofluorescence
TFS	Ten Field Score
mTFS	mean Ten Field Score values

Abstract

According to the World Alzheimer report published in 2020, 50 million people are currently living with dementia and this number is predicted to rise to 150 million in 2050. Alzheimer's disease (AD) is the most common form of dementia (60% - 70% of cases). Early and accurate diagnosis of AD is a major goal in order to reduce the impact of dementia and also represents an urgent unmet medical need globally.

Canine Cognitive Dysfunction (CCD) in aged dogs is a progressive neurodegenerative disorder exhibiting gradual decline of cognitive function and memory loss similar to human AD. In parallel with progressive amyloid beta (Aβ) neuropathology, aged dogs display progressive decline in measures of learning and memory. Of importance, for both AD in human and CCD in dogs, the abnormal accumulation of amyloid beta plaques (Aβp) in the brain is one of the major pathological lesions associated with this devastating disorder.

Aβ is subdivided into three major assemblies, including monomers, oligomers, and fibrils of which Aβ soluble oligomers (Aβo) are the most neurotoxic to neurons. Aβo is believed to trigger the pathophysiology of AD and is normally detected two decades before clinical onset of the disease. Similarly, aged dogs affected with CCD display cognitive decline which occurs prior to accumulation of Aβp in the canine brain, suggesting that earlier assembly states of Aβ (e.g., oligomers) may be the neurotoxic species in dogs, as described for human AD. This thesis particularly focused on the early detection of Aβo with the aim of developing a cost-effective diagnostic test for AD before neuropathological and clinical deficits have ensued. Also, to provide an insight to develop the dog as a natural translational model of AD.

For the initial optimisation and development phase, I collected brains, eyes, and whole blood at different time points during disease progression from 5xFAD and APP/PS1 AD mice models in order to assess the detection limit of intraneuronal Aβo in these tissues and fluids. In study I (Chapter 3), I used 5xFAD AD mouse model and demonstrated the presence of intraneuronal

Aβo in the retina and showed that its accumulation inversely correlated with retinal Aβp deposition, indicating an age-related conversion. Furthermore, in study II (Chapter 4) I used APP/PS1 AD mouse model and showed that Aβo accumulates simultaneously in the retina and peripheral blood which also precedes cognitive decline and deposition in the brain. Taken together these two studies confirmed that Aβo could potentially be used as an early retinal biomarker for AD.

Although the importance of transgenic model is undisputed, they do not fully recapitulate key clinical and pathological aspects observed in huma AD. To investigate whether AD neuropathology in aged dogs affected with CCD resembles lesions associated with human AD (study III -Chapter 5) and further characterise the 'aged dog' as a natural disease model for AD, I used a range of antibodies with the ability to detect Aβo, Aβp and hyperphosphorylated tau (p-Tau). These dogs were previously shown to exhibit Aβp, CAA, and ubiquitin granules (UBQ), however, the presence of hyperphosphorylated microtubule-associated Tau protein (p-Tau) was not conclusive. In study III (Chapter 5), following the development of a new experimental protocol, I demonstrated the presence of p-Tau in dogs' brain with CCD, in addition to Aβo and Aβp. Interestingly, in this study, I showed that p-Tau and Aβo co-localized away from the plaques in dogs' brain.

Similar to humans, the dog's life span has increased substantially over the last two decades. In cognitively healthy humans, Aβo was shown to deposit at a very young age and is believed to trigger p-Tau deposition. Therefore, it is important to understand the significance of these neuropathological lesions in cognitively intact individuals, which may help predict individuals at higher risk to develop AD. Young and cognitively healthy dogs can help characterize and identify early molecular and pathological events that could resemble the preclinical cascade associated with human AD. In study IV (Chapter 6), I investigated the presence of Aβ and p-Tau accumulation in the retina of young (1-5 years old), middle (6-10 years old) and old (≥11 years old) age groups of cognitively healthy dogs. The major goal of this study was to provide insight into the retinal accumulation of Aβo, Aβp and p-Tau in a diverse group of cognitively unimpaired dogs. After immunostaining with Aβo nanobodies, widespread $A\beta_{1-40}$ and $A\beta_{1-42}$ oligomers were observed in the retinal layers of all age groups, whereas Aβp were detected in the middle and old age groups and p-Tau deposits were observed only in four old dogs. I also show that Aβo co-localized with Aβp in the middle and old age groups of dogs' retina. Importantly, I demonstrated that p-Tau co-localized with intracellular Aβo in the retinal layers of old age groups of dogs. This study has provided new information related to retinal AD related changes in cognitively healthy dogs and showed the importance of retinal detection of Aβ and p-Tau before appearance of brain pathology. These finding suggest that early identification of these neuropathological lesions may help predict AD at a very early stage.

In conclusion, accumulating evidence described in my thesis suggested that retinal changes and pathophysiological processes could provide valuable insights into early diagnosis of AD. This thesis provides a strong basis to further validate dogs as a natural AD model where all the AD neuropathological hallmarks have been observed in the brain and retina. Finally, such a model will certainly facilitate the development and clinical applications of an easily accessible, inexpensive, and non-invasive retinal imaging of preclinical AD diagnostic platform to predict and diagnose early stages of AD and monitor disease therapies.

Publications and Conference Presentations

Peer reviewed journal articles

1. **Habiba U**, Merlin S, Lim JKH, *et al;* Age-Specific retinal and cerebral immunodetection of amyloid-β plaques and oligomers in a rodent model of Alzheimer's disease. J Alzheimer's Dis. 2020;76(3):1135-1150.
2. **Habiba U**, Descallar J, Kreilaus F, *et al;* Detection of retinal and blood Aβ oligomers with nanobodies. Alzheimer's Dement (Amst). 2021;13(1):e12193.
3. **Habiba U**, Makiko O, James K. C, *et al;* Neuronal deposition of amyloid beta oligomers and hyperphosphorylated tau is closely connected with cognitive dysfunction in aged dogs. (Journal of Alzheimer's Disease Reports, pp. 1-12, 2021. DOI: 10.3233/ADR-210035

Manuscript

4. **Habiba U**, Leandro T, John M, Mark K, Brian S, Richard D, Mourad T*, Amyloid beta oligomers and phosphorylated Tau deposition in the retina of cognitively unimpaired dogs. (*In preparation*)

Conference Presentations

- **Umma Habiba**; can 'EYE' predict Alzheimer's disease? 3MT oral presentation 2020; Western Sydney University, NSW, Australia.
- **Umma Habiba**; Westmead Research Hub Art in Science 2020; University of Sydney, Australia.
- **Umma Habiba**; Optical detection of Alzheimer's disease in mice with single domain antibody fragments; 3rd innovation and state of the art Alzheimer's and Dementia Research 2019; Oral presentation, London, UK.

- **Umma Habiba**; Optical detection of Alzheimer’s disease in mice with single domain antibody fragments; Macquarie Neurodegeneration Meeting 2019; Poster presentation; Organised by Centre for Motor Neuron Disease Research, Macquarie University, NSW, Australia
- **Umma Habiba**; Optical detection of Alzheimer's disease; Health Beyond Research & Innovation Showcase 2019; Poster presentation; NSW, Australia.
- Utpal K. Adhikari, **Umma Habiba** and Mourad Tayebi; Immunoinformatics Analysis of ‘SAFE’ B-Cell Epitopes for Alzheimer’s Disease Therapy; Health Beyond Research & Innovation Showcase 2019; Poster presentation; NSW, Australia
- **Umma Habiba**; EYE: the diagnostic window for Alzheimer’s disease; 3MT oral presentation 2019; Western Sydney University, NSW, Australia.
- **Umma Habiba**; DOGZHEIMER’S: An Alzheimer-like disorder in dogs with cognitive deficits similar to human Alzheimer; Health Beyond Research & Innovation Showcase 2018; Poster presentation; NSW, Australia.
- Shital K. Barma, **Umma Habiba** and Mourad Tayebi; Alzheimer-like pathology in dog osteosarcoma; Health Beyond Research & Innovation Showcase 2018; Poster presentation; NSW, Australia.

Chapter 1
General Introduction

1.1. Alzheimer's disease

Alzheimer's disease (AD) is an irreversible progressive neurodegenerative disorder associated with gradual decline in cognitive function[1]. It is the most common cause of dementia comprising 60-70% of all dementia cases[2]. AD was first described by a German doctor named 'Alois Alzheimer' in a patient known as Auguste D in 1906. According to the World Health Organisation (WHO), the number of people aged over 60 years has reached 1 billion in 2020 and is expected to increase to 2.1 billion by 2050 (WHO dementia report 2020). AD is the most common cause of death in an aging population[2]. Overall, it is the 6th leading cause of death worldwide, between 2000 and 2018 the number of deaths from AD increased by 146.2 % as compared to other major causes of death including cancer, heart disease, HIV **(Figure 1)**[3]. Recent studies have reported that the worldwide prevalence of AD is 50 million and by 2050 approximately more than 150 million people will be affected by this devastating disease[4-7]. AD has a huge socioeconomic impact and healthcare challenges, specifically the cost of medical and formal and informal social care. The global cost of dementia was estimated to be US $ 1.3 trillion in 2019 and is expected to rise to more than US$ 2.8 trillion by 2030[2,8-10].

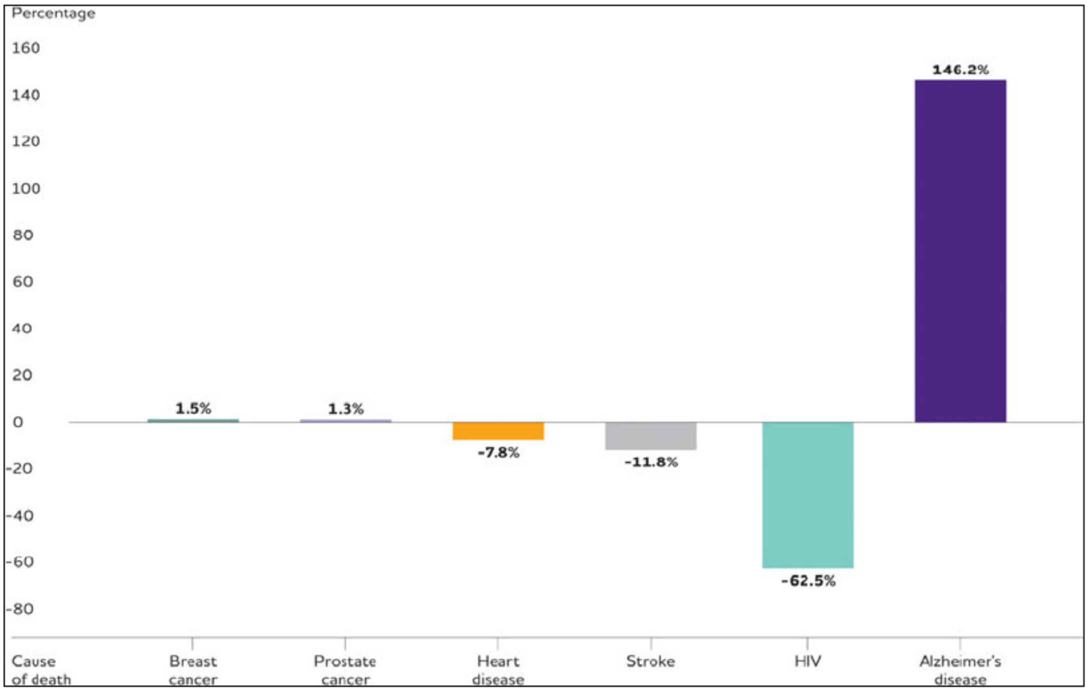

Figure 1. Percentage changes in selected causes of death (all ages) between 2000 and 2018. Between 2000 and 2018, the number of deaths from **Alzheimer's disease** has more than doubled, increasing **146.2 percent**, while the number of deaths from the number one cause of death (heart disease) decreased 7.8 percent[3]. Figure adapted from 2020 Alzheimer's disease facts and figures.

1.2.Types of Alzheimer's diseases

There are two different types of AD, including familial and sporadic AD. Familial Alzheimer's disease (FAD) is rare in people in their 40s or 50s, and is also known as early-onset AD, whereas sporadic Alzheimer's disease (SAD) or late-onset AD is the most common type of AD, usually starting to appear after the age 65[11]. Studies have reported that FAD is usually caused by inherited mutation(s) in amyloid precursor protein (APP), Presenilin 1 (PSEN1) and/or Presenilin 2 (PSEN2) genes, in contrast, SAD appears to be influenced by both environmental and genetic factors[11-13]. Polymorphism of apolipoprotein E (APOE) gene is believed to be a risk factor in the development of SAD[14,15]. In addition other comorbidities including diabetes, cardiovascular disease, inflammation etc. might potentially increase the risk of SAD[16].

1.3. Clinical sign

The clinical signs and symptoms of AD gradually progress over time with various disease stages and is subdivided into preclinical stage, mild or early stage, moderate or middle stage and severe or late stage[17]. The most common clinical symptoms are the gradual decline in memory function, difficulty in learning, recognizing family members, impulsive behavior, problem with communication, difficulty with eating etc. and over time the symptoms become worse and apparent[18]. However, recent studies have reported that AD has a long preclinical phase, and the neuropathology begins decades before clinical onset, providing an opportunity for the development of early diagnostic tests and potential therapeutic approaches[19].

1.4. Pathological features

The neuropathological hallmarks of AD include the presence of extracellular deposition of amyloid beta plaques (AβP), intracellular deposition of hyper phosphorylated Tau (p-Tau) protein as neurofibrillary tangles (NFTs), ubiquitin, neuropil threads, cerebral amyloid angiopathy (CAA), severe synaptic loss and neuronal death[20-22].

1.4.1. Amyloid Beta (Aβ)

Alois Alzheimer was first to describe the accumulation of extracellular Aβp in an AD brain in his original case report[20,23,24]. Aβ peptides are derived from a larger protein, namely APP[25]. Three different subtypes of secretase enzymes, including α, β, and γ secretase sequentially cleave APP into amyloidogenic and non-amyloidogenic peptides[26] **(Figure 2)**. The α-secretase cleaves APP within the Aβ sequence, between amino acids 16 and 17 and generate a soluble APPsα ectodomain and a membrane-bound carboxy-terminal fragment (APP-CTFα) and then the fragments are degraded in lysosomes. The amino terminal fragment generated through α- or β-secretase are called secreted APP (sAPP) α or β, and the carboxyterminal fragments (CTF) are called CTF83 and CTF99, respectively[23]. The Beta-site APP cleaving enzyme 1 (BACE1) is the major β-secretase in the brain. Further the γ-Secretase cleavage of CTF83 and CTF99 results in the generation of p3 and Aβ, respectively, as well as the amino-terminal APP intracellular domain (AICD)[23,24,27]. However, in the non-amyloidogenic pathway, β and γ secretase sequentially cleave APP to produce the 4 kDa Aβ peptide fragments (36–43 amino acids) that aggregate and deposit as plaques[26,28,29] **(Figure 2).**

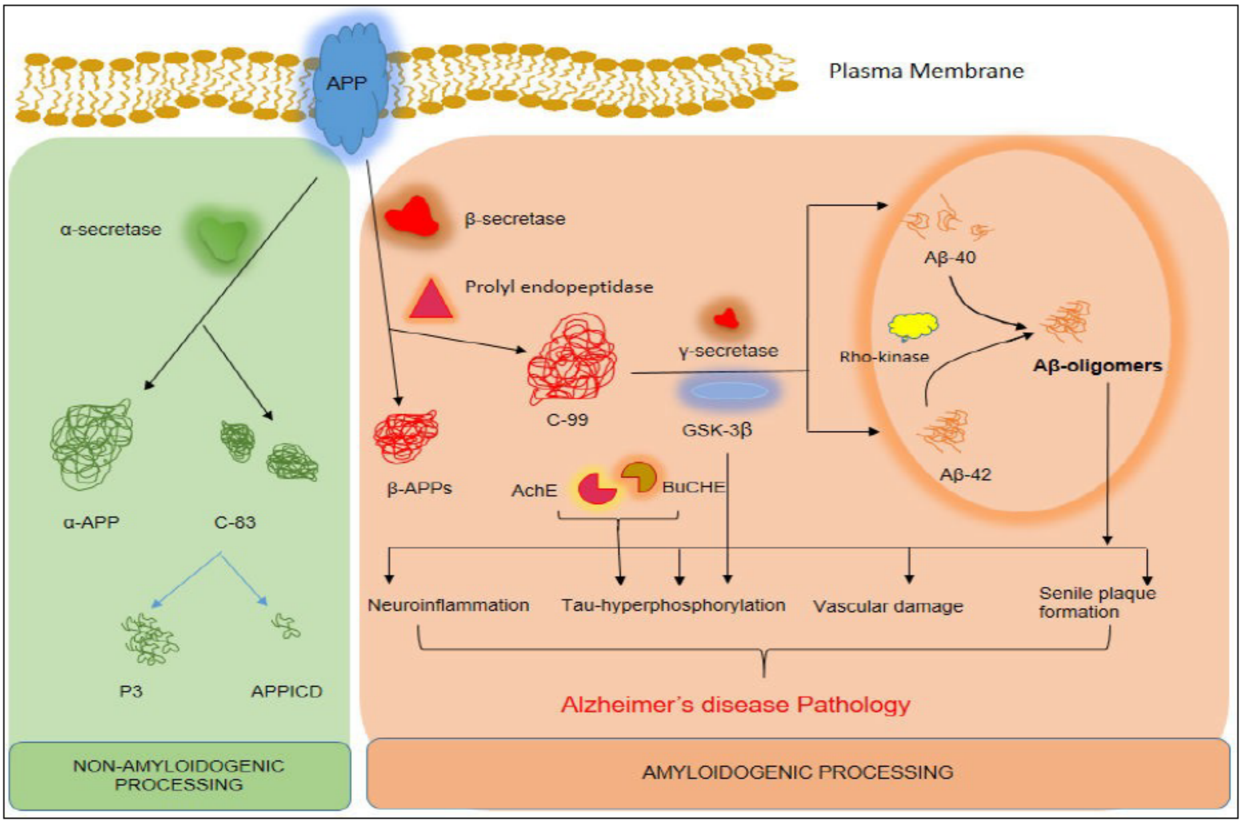

Figure 2. Schematic presentation of enzymes involved in amyloidogenic and non-amyloidogenic processing of APP[30].

Usually, two different types of Aβp are observed in AD brain including diffuse plaques, non-neuritic structures that lack the central cored fibrillary beta pleated sheet structure. In contrast, the dense core or neuritic plaques are made of densely cored beta-pleated sheet often associated with synaptic loss and glial cell activation[20,31-33]. Moreover, there are two major isoforms of Aβ, including $Aβ_{40}$ (80–90%) and $Aβ_{42}$ (5–10%) and the latter is believed to be the most toxic to neurons[34,35]. Also, three major assemblies of Aβ have been reported[36-39]; monomeric Aβ: composed of low molecular weight dimers and trimers; Aβ soluble oligomers (Aβo): containing 12-24 monomers which become elongated to form protofibrils and insoluble fibrils[28,39,40]. In recent years, it has been shown that, among these three stages, Aβo are the most toxic to neurons and inhibit long-term potentiation (LTP), causes synaptic dysfunction[41] and are responsible for triggering the pathophysiology associated with AD[42-47]. A study by Walsh *et al* reported that administration of Aβo to rats caused disruption of LTP and synaptic plasticity[48]. In fact, a study by Lesne *et al* showed that a reduction in oligomer levels corresponded to improved memory function in Tg2576 mice while Aβp were still present, suggesting that Aβp are not the main causative factor for memory decline[49]. Also, another important aspect of Aβo is their accumulation begins in animal models and human AD brain two decades before clinical onset[41,50,51]. It was previously shown that Aβo can be detected in middle aged individuals before the onset of clinical symptoms and the level of Aβo increased gradually with age[52]. Similarly, I demonstrated the presence Aβo in whole blood and in retina of 3-month-old APP/PS1 mice model before accumulation in the brain (see chapter 4)[53]. These studies suggest that the larger aggregates are not responsible for neurodegeneration, but instead the smaller soluble oligomers represent the toxic species of Aβ that initiate the disease pathogenesis and neuropathology that potentially form an early biomarker for AD diagnosis[52,54]. In contrast, the aggregated Aβp are considered less toxic and may act as reservoirs for oligomers synthesis[45].

1.4.2. Cerebral amyloid angiopathy

Aβ was shown to deposit in cerebral blood vessel walls and cause cerebral amyloid angiopathy (CAA) which usually is observed in more than 80% of AD cases. CAA is mostly present in the leptomeningeal arteries and cortical capillaries. Parietal and occipital lobes are most severely affected regions in the brain[55]. A study by Yamada and colleagues reported that CAA is frequently present in AD patients as compared to the non-AD elderly individuals and correlated to AD related pathology[56]. The authors examined 201 cases (aged 62-104 years), including 82

AD patients and found that among 82 AD cases, 87% of patients have CAA as compared to 119 normal aged individuals with 35% frequency of CAA[56].

1.4.3. Neurofibrillary tangles (NFTs)

Another pathological hallmark of AD is the intracellular deposition of hyperphosphorylated Tau protein as neurofibrillary tangles (NFTs). NFTs are composed of paired helical filaments (PHFs) and there are three morphologically different NFTs distinguished in human AD including diffuse pre-NFTs, mature intraneuronal NFTs (i-NFTs) and ghost or extraneuronal NFTs (eNFTs)[57,58]. Physiologically, Tau is a microtubule associated protein which helps stabilize the integrity of neuronal skeleton and responsible for axonal transport, neuronal development, and synaptic function[59]. Tau protein is composed of 352–441 amino acids divided into six isoforms including microtubule binding repeats 3R Taus (0N3R, 1N3R, and 2N3R) and 4R Taus (0N4R, 1N4R, and 2N4R)[60,61]. However, in AD, Tau become misfolded, hyperphosphorylated and aggregated to form NFTs due to abnormal chemical changes, post-translational modifications and/or depolymerisation[20,62]. There are approximately 70 serine or threonine phosphorylation sites on Tau protein among these, Tyr18, Thr212, Ser202/Thr205, Thr231, Ser199, Ser205, Ser214, Ser262, Ser396, Ser422, Ser404, Ser413 and so on are abnormally phosphorylated and form PHFs and NFTs in human AD[61]. However, hyperphosphorylation and tangles build up are still not fully understood, albeit one hypothesis proposes a correlation between Aβo and hyperphosphorylated Tau (p-Tau)[63], where Aβo is considered as the trigger. Recent reports have shown that these two misfolded proteins are interdependent, in other words, Aβo may act as a catalytic factor to develop NFTs and may act together synergistically to enhance neurotoxicity and synaptic dysfunction[45,64]. A histopathological study by Manczak and colleagues[65] which used brain frontal cortex from 20 different post-mortem AD patients and age matched controls, demonstrated this pathological interaction between Aβo and p-Tau which co-localised in the frontal cortex of AD patient brain.

The authors suggested that the synergistic interaction between Aβo and p-Tau leads to neuronal damage and cognitive dysfunction in AD patient[65]. Moreover, a study by Shin and colleagues[63] demonstrated that Aβo can act as a catalytic factor to enhance Tau seeding process and triggers intracellular Tau aggregation in human neuroblastoma cells and transgenic mice primary hippocampal neurons[63]. Another study by De felice and colleagues also reported that Tau hyperphosphorylation in mature hippocampal neurons and neuroblastoma cells is accelerated by Aβo[66]. Together, these studies suggested that Aβo-p-Tau synergistic interaction and Aβo mediated Tau aggregation can be a potential biomarker at prodromal stage of AD. In this thesis, I demonstrated both independent accumulation and interdependent co-accumulation of Aβo and p-Tau in Chapters 5 and 6.

1.4.4. Disturbances in endocytic pathway

Another early pathological impact of Aβ is to interfere with the endocytic pathway and impairment of the maturation of auto phagosomes to lysosomes[67]. Endocytic pathway is usually responsible for recycling, modification and degradation of proteins and it consists of early endosomes, late endosomes, and lysosomes. Normally, Aβ is degraded within lysosomes but in AD patients, intra-neuronal Aβ can accumulate in lysosomal compartment and destabilizes its membrane[68], which leads to the presence of Aβ in the cytosolic compartment. A study by Zheng *et al*, which used human neuroblastoma cell line and rat cortical neurons and after double labelling of $Aβ_{40}$ or $Aβ_{42}$ with different organelle markers, showed that disturbances in Aβ clearance leads to excess deposition of intracellular lysosomal $Aβ_{40}$ and $Aβ_{42}$[69]. Another study by Yu *et al* reported that impairment of clearance or excessive production of Aβo leads to brain Aβ deposition[70]. The authors investigated the effect of $Aβ_{42}$ oligomer on mice neuroblastoma cell line and showed that inhibition of clathrin mediated endocytosis did not inhibit intraneuronal accumulation of $Aβ_{42}$ oligomer and its neurotoxic effect. However, dynamin mediated pathway inhibition had a positive effect on $Aβ_{42}$ oligomer induced neurotoxicity and suggested that RhoA and dynamin regulated endocytosis is involved in intracellular Aβo deposition and neurotoxicity[70].

1.5. Pathological stages of AD

Topographic distribution of extracellular Aβp and intracellular NFTs were first described by Braak and Braak[71]. For progressive distribution of cortical Aβp, there are three stages proposed by Braak and Braak[71], subsequently modified by Thal *et al*[72] proposing five stages of descendant Aβp progression. In Braak and Braak stage A, Aβp deposits in the basal portion of the neocortex, mostly in poorly myelinated perirhinal and ectorhinal areas of temporal lobes. Then in stage B, Aβp depositions progress to the association neocortical areas and hippocampus. In the hippocampus, Aβp distributed from the subiculum to the molecular layers of CA1 and fascia dentata. Finally, in stage C, Aβp deposits spread throughout the entire cortex including primary cortices, subcortical nuclei, and cerebellum. Braak and Braak also reported that cloud-like diffuse plaques transformed into well-developed sharply delineated globular plaques with the advancement of AD affecting mostly the neocortex layer III and Va as compared to layers IV and Vb.

However, Thal *et al* proposed that in phase 1, diffuse Aβ deposits are found in layers II, III, IV, and V of frontal, parietal, temporal, or occipital neocortex. Then in phase 2, Aβ plaques progress towards the entorhinal cortex, hippocampal formation, amygdala, cingulate gyrus, presubicular region and molecular layer of the fascia dentata. In phase 3, in addition to regions described in phase 1 and 2, subcortical regions such as caudate nucleus, basal forebrain nuclei, thalamus, hypothalamus, and white matter exhibit Aβ plaque depositions. In phase 4, Aβ plaques were further deposited in the brain stem including inferior olivary nucleus, medulla oblongata, substantia nigra and midbrain. Finally, in phase 5, Aβ plaques deposited in the pons including pontine nuclei, raphe nuclei, locus coeruleus, parabrachial nuclei, dorsal tegmental nucleus and reticulotegmental nucleus and the molecular layer of cerebellum.

Intracellular NFTs were reported to spread in a more predictable manner than that of Aβp distribution and Braak and Braak[71,73] have demonstrated six stages of NFTs distribution in the cerebral cortex. In Braak and Braak proposed stage I, NFTs first appear in the transentorhinal cortical neurons in the temporal lobe which then spread into the entorhinal region in stage II. Braak and Braak also reported that, stage I and II are the early pathological development without the presence of Aβ plaque pathology. Then in stage III the progressive development of NFTs proceed towards the hippocampus and temporal proneocortex and in stage IV reaches the adjoining neocortex including amygdala, thalamus, and claustrum. Finally, in stage V and stage VI, NFTs deposit superolaterally at the neocortical areas and primary areas of the neocortex including sensory, motor, and visual areas respectively. Braak and Braak reported that the prevalence of neocortical stages V and VI increased with age. All the stages of Aβp and NFTs are summarised in **Table 1**.

Table 1-Topographic distribution of AD neuropathological hallmarks

Braak and Braak proposed Aβp stages	**Thal *et al* proposed Aβp stages**	**Braak and Braak proposed NFTs stages**
Stage Ⅰ: Basal portions of the neocortex including frontal, temporal and occipital lobes	**Stage Ⅰ:** Starting from neocortex	**Stage Ⅰ:** Transentorhinal cortex
Stage II: All associated neocortical areas and hippocampus	**Start II:** Progress to allocortex including entorhinal cortex, hippocampal formation, and amygdala.	**Stage II:** Entorhinal region proper and CA1 region of hippocampus
Stage III: The entire cortex including primary neocortical areas, cerebellum, and subcortical nuclei.	**Stage III:** Subcortical nuclei including striatum, thalamus and hypothalamus, and white matter	**Stage III:** Subiculum of the hippocampus and the temporal pro-neocortex
	Stage IV: Involvement of brainstem structures.	**Stage IV:** Adjoining neocortex including amygdala, thalamus, and claustrum
	Stage V: Finally, Aβ deposited in the pons and cerebellum	**Stage V:** All over the neocortical areas
		Stage VI: All the previously associated areas become severely affected and also involve primary areas of the neocortex including sensory, motor, and visual areas

1.6. Diagnosis

Over the years, various predictive diagnostic techniques of AD have been developed including clinical examination and neuropsychological screening, genetic testing, biomarker identification in blood and cerebrospinal fluid (CSF) and brain imaging including magnetic resonance imaging (MRI), computed tomography (CT scan), positron emission tomography (PET scan) and electroencephalography (EEG)[74,75]. However, there is no definite neuropsychological test for AD, and neurologists and neuropsychologists together with the help of other specialists usually use a variety of approaches such as an individual's previous medical history, physical and neurological examination and cognitive status tests which includes Mini-Mental State Exam (MMSE), Mini-Cog test, Alzheimer's Disease Assessment Scale-Cognitive (ADAS-Cog) etc.[76,77]. Moreover, the biomarker based diagnostic approaches including CSF[78] and PET imaging are very expensive, invasive and have limited acceptability and availability, as it requires exclusive laboratory set up to process and store sample, assay standardization, regulation and validation[76]. However, the blood-based approach is less expensive and less invasive and can be a potential diagnostic method for AD, albeit rigorous validation and predictive accuracy still requires confirmation[79,80]. Thus far, unfortunately, the only confirmatory diagnosis of AD is post-mortem histopathological identification, Therefore, there is an increasing need for a non-invasive and cost-effective tool, allowing identification of individuals in the preclinical or early clinical stages of AD. Development and implementation of such tests may facilitate early and potentially achieve more effective diagnostic, therapeutic and preventative strategies for AD. Researchers have been exploring ways to detect the disease at an early stage before it affects the brain and one of the major possible non-invasive methods for the early detection and monitoring of AD is the eye, believed to play a key role in AD pathogenesis.

1.7. Eye and Alzheimer's disease

Complications in the eye are one of the early complaints in AD patients[81,82]. The most common ocular changes are the loss of colour vision and peripheral vision, impaired contrast sensitivity and visual acuity[83]. Retina is considered a part of the central nervous system, connected to the brain's visual cortex via the optic nerve **(Figure 3)**. The optic nerve is composed of retinal ganglion cell axons which convey signals from photoreceptor cells and transmit to the brain. In human AD patients, retinal vascular and morphological changes have extensively been reported in many studies[84]. The common changes include impaired retinal blood flow[85], ganglion cell loss[82] and thinning of the retinal nerve fibre layer (RNFL)[85-87], optic nerve damage[88], optic nerve fibre loss[89] and pyramidal cell loss in the visual cortex[90]. Recent development in retinal photography techniques such as optical coherence tomography (OCT)[91,92], scanning laser ophthalmoscopy (SLO), ocular fundus photography[93], can enable the noninvasive visualisation of the retinal ganglion cell layer (GCL) and retinal microvasculature. Also, some studies have reported that retinal imaging can predict MCI [94] and AD[85,95] and distinguish between AD and other diseases with high sensitivity and specificity[76,96]. A study by O'Bryhim and colleagues demonstrated that non-invasive optical coherence tomographic angiography (OCTA) imaging exhibited early retinal morphological and microvascular changes in individuals with preclinical AD[97]. Moreover, a meta-analysis study by Coppola and colleagues[98] and a cross-sectional study by Ascaso and colleagues[99] reported that changes in the thickness of retinal nerve fibre layer (RNFL) are associated with MCI and AD when compared to cognitively healthy individuals and suggested that RNFL thickness can be a potential predictor of AD.

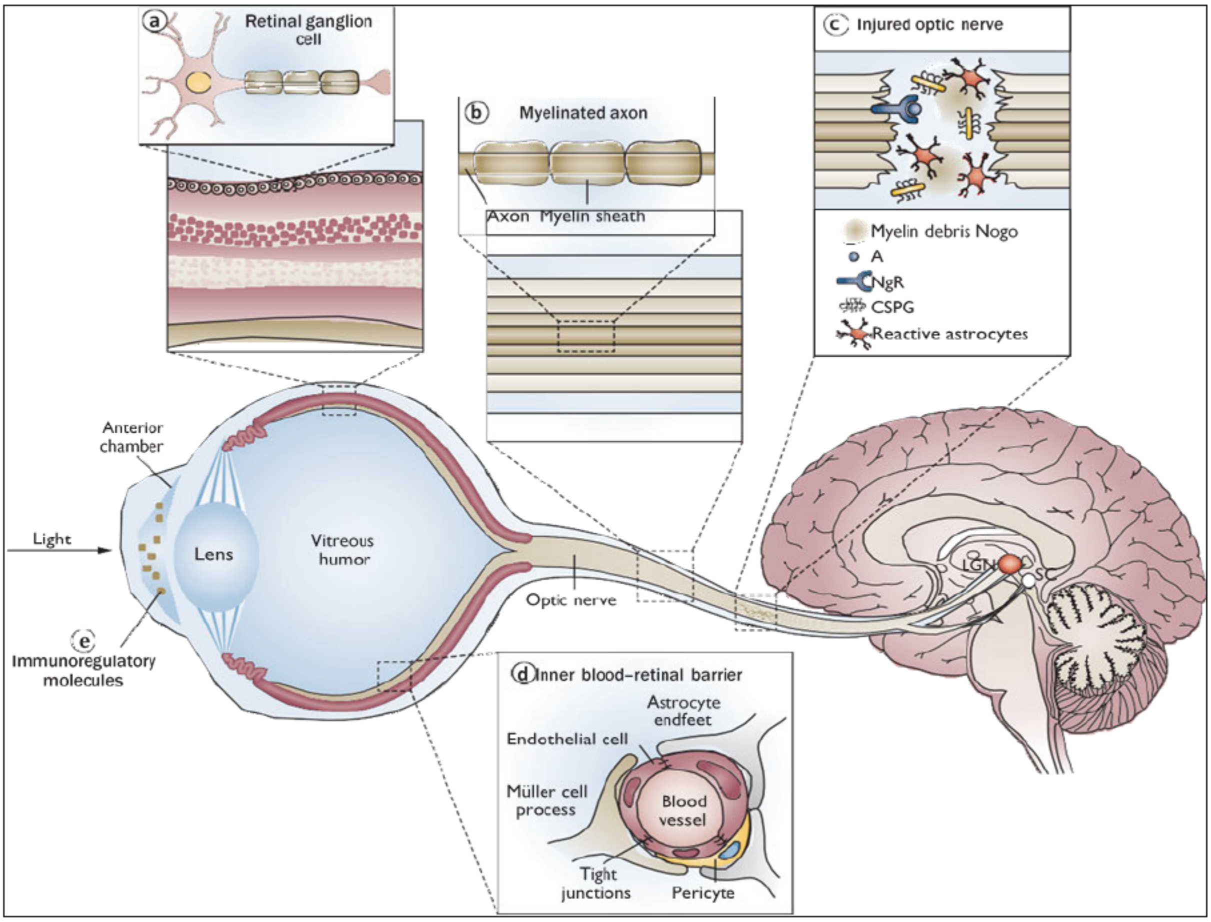

Figure-3. The eye as an extension of the CNS.
CSPG: chondroitin sulphate proteoglycan; LGN: lateral geniculate nucleus; SC: superior colliculus[100].

1.8. Retinal manifestation of AD pathology

Several studies have demonstrated retinal manifestation of AD related pathological hallmarks including Aβ oligomers[53,101], Aβ plaques[102] and p-Tau [103-105]. Koronyo and colleagues after specific immunostaining, have shown the presence of Aβp in post-mortem retinal inner layers of AD patients and after systemic administration of curcumin to APP/PS1 mouse model. The authors demonstrated the presence of solid lipid curcumin fluorochrome tagged retinal Aβp in live mouse via non-invasive scanning laser ophthalmoscopy (SLO) imaging[102].

Moreover, another important retinal manifestation of AD is the impairment of retinal blood flow and changes in the retinal microvasculature. Cerebral and retinal vasculature have common anatomical and physiological properties[106] and dysregulation of cerebral and retinal blood flow is associated with AD pathogenesis. A study by Feke and colleagues was able to distinguish between MCI, AD and control individuals by comparing the retinal blood flow using retinal laser doppler flowmetry[107]. Another study by Williams and colleagues investigated two large cohorts, including 213 AD participants and 294 cognitively normal controls to quantify the different retinal microvascular parameters including calibre, tortuosity, bifurcation and so on. The authors found that retinal microvascular changes may able to predict cerebral vascular alterations, when comparing AD patients and cognitively normal individuals using non-invasive retinal imaging[108]. Further, it was also shown that the presence of Aβ in the vasculature may lead to narrowing of blood vessels and impairment of cerebral and retinal blood flow[85,109]. A study by Lee and colleagues[110] measured the retinal distribution of extracellular and intracellular Aβ in ten neuropathologically confirmed AD post-mortem cases using anti-Aβ 12F4 and 6F/3D antibodies. The authors found that intracellular retinal Aβ were inversely correlated with brain neuritic plaque loads whereas extracellular retinal Aβ loads increased with higher brain CAA scores. This was also highlighted by the recent studies that showed that Aβ accumulation in pericytes can dysregulate the blood flow and may contribute to the retinal microvascular changes[111]. A recent study by Shi and colleagues reported that impairment of vascular platelet-derived growth factor receptor-β (PDGFRβ) signalling is involved in the disruption of both blood-brain barrier (BBB) and blood–retinal barrier (BRB) integrity which leads to the accumulation of abundant $A\beta_{40}$ and $A\beta_{42}$ in the retinal vasculature[112]. Importantly the toxic effects of Aβo on the retina has been reported by Naaman and colleagues. The authors showed that $A\beta_{42}$ oligomers cause extensive retinal neurotoxicity when compared to fibrillary $A\beta_{40}$ and $A\beta_{42}$[113]. The authors administered oligomeric $A\beta_{42}$ and fibrillary $A\beta_{40}$ and $A\beta_{42}$ intravitreally to rats, then assessed with electroretinography (ERG) and showed excessive retinal dysfunction with $A\beta_{42}$ oligomers, mild deficits with $A\beta_{42}$ fibrils and no significant changes with $A\beta_{40}$ fibrils. A large body of research showed that blood Aβo levels can predict brain degeneration in AD[114]. Although the above studies provided a better understanding of AD related pathological changes in the retina and confirms the potential use of Aβo in the retina as an early biomarker, however, no attempts were made to diagnose AD and MCI via early detection of Aβo and which retinal layers are affected most with Aβo deposits.

Furthermore, more recent studies highlighted the deposition of p-Tau in post-mortem AD retina, which also could potentially be used as an early retinal biomarker for non-invasive AD diagnosis[104,105,115]. A study by de Ruyter and colleagues reported the presence of Tau isoforms 3R and 4R and p-Tau Ser202/Thr205 in the retinal inner plexiform layer (IPL) and outer plexiform layer (OPL) of AD post-mortem eyes[115]. Furthermore, Chiasseu and colleagues[116] demonstrated an age-dependant p-Tau accumulation in the retina in AD transgenic mice, which started to appear from 3-months of age, before brain deposition and cognitive impairment. Additionally, the authors reported that p-Tau accumulation in the retina impairs the retinal ganglion cell axonal transport to the visual cortex, effects reversed with siRNA that led to improvement of axonal transport[116].

1.9. Animal models and Alzheimer's disease

Transgenic mice are the most used experimental animal models for the study of AD, and mostly rely on the overexpression of human APP genes related to familial type AD (FAD) that results in the development of Aβ pathology[117,118]. Tg2576, APP/PS1, 5xFAD, 3xTg, J20, and PDAPP transgenic mice models are widely used[117-119] and have provided critical knowledge for understanding the pathogenesis underlying AD. However, translation of therapeutic studies conducted in these mice largely failed to be replicated in human clinical trials[118,120,121]. This has led many researchers to explore the development of new effective animal models; including large models that would spontaneously develop AD. Three transgenic AD rat models have been developed such as McGill-R-Thy1-APP[122], TgF344-AD[123] and PSAPP[124]. The rat model is believed to share more similarities with human AD over transgenic mice. However, like transgenic mice, the rat models were also developed based on APP mutations. Interestingly, the rat model, and unlike the mice, develops Tau pathology, reported to be similar to human Tau pathology; likely due to the six Tau isoforms present in rat[123]. The extent of APP mutations and associated neuropathology and their association with cognitive deficits in the rat models are yet to be investigated more comprehensively [122]. Therefore, despite the development of these rodent models, these have not translated into developing effective detection systems and therapies for AD and arguably only replicate FAD but not SAD pathophysiological processes which represents 80-90% of the total AD proprotion[125,126].

Other animals that have been investigated as good models for human AD include dogs, cats, and monkeys, as these naturally replicate the neuropathological features related to SAD without any genetic manipulation[127-129].

1.10. Canine cognitive dysfunction

Similar to human, advancement of veterinary medical interventions and nutrition helped increase the life expectancy of pet dogs, which also increased the prevalence of age-related disease burden in dogs[130]. Canine cognitive dysfunction (CCD) is one of the most common age-related brain disorders, leading to the development of a neurobehavioral syndrome in senescent dogs similar to human AD.

1.10.1. Common clinical Signs of canine cognitive dysfunction

The characteristic behavioural changes found in dogs affected with CCD comprise deficits in learning, memory and spatial awareness, restlessness, disorientation and deterioration of socio-environmental interaction, house soiling, trying to pass through narrow space, increased barking, changes of sleeping pattern and activity [131-135]. Several questionnaires have been developed as an aid to effectively diagnose CCD in dogs by owners [136-138]. These include the canine cognitive dysfunction rating scale (CCDR), considered as the most accurate (98.9%)

and significant in identifying dogs with CCD[139]. CCDR consists of 13 behavioural questions related to cognitive decline. In addition to the behavioural alterations, dogs with CCD display other abnormalities related to gait, posture, olfaction and perception[139,140]. A study by Ozawa and colleagues reported a strong relationship between cognitive dysfunction of dogs aged 10 years or older with their physical disturbances[141]. The authors found that physical changes, including altered vision, olfaction and head ptosis were associated with CCD which started to appear before cognitive dysfunction[141].

1.10.2. Pathological features of canine cognitive dysfunction

Cognitively impaired aged dogs naturally develop human AD related neuropathological lesions including the presence of extracellular Aβp, ubiquitin, CAA, severe synaptic loss, and neuronal death. However, intracellular NFTs have not been demonstrated conclusively in dogs with CCD[142-144].

Similar to human AD, amyloid pathology is one of the major constituents involved with CCD progression. Canine APP and Aβ share 98% and 100% homology with their human counterparts respectively. In dogs, Aβ peptides are also derived from the enzymatic cleavage of APP, which then become misfolded and aggregated to form Aβp. Dogs with CCD usually develop diffuse plaques, that lack the dense core normally observed in human AD; and start to appear from 6-8 years of age[129,145]. It was previously suggested that absence of neuritic or dense core plaques in dogs could be explained by the shorter life span of this species[129,136] and that brain regional distribution of Aβp is related to age and disease progression in dogs affected with CCD [146]. Studies by Head and colleagues reported that plaques start to develop from 6-8 years of age in beagle and first appear in the prefrontal cortex and entorhinal cortex[145], a structure associated with poor executive function and visual learning ability and also comparable with Braak and Braak stage 'A' of human AD[129,147,148]. However, there is an ongoing debate on the pathological significance of diffuse plaques in dogs' brain where some studies showed that diffuse plaque deposition is age related[138,149] while others reported it to be related to the severity of CCD[150]. Ozawa and colleagues have conducted an histopathological study for the identification/distribution of diffuse Aβp in 16 dogs aged 10-18 years and correlated with the severity of cognitive dysfunction[149]. The authors found that the number of diffuse Aβp increased with age starting from 10 to 14 years, albeit no significant correlation with cognitive deficits was identified[149]. Likewise, Rofina and colleagues performed a semiquantitative analysis of diffuse Aβp deposition in a group of 30 dogs aged between 1 month to 19 years[138]. The authors showed that diffuse plaque deposition was significantly higher in dogs older than 11 years and demonstrated that this increase of diffuse plaque burden significantly related to the age of dogs as opposed to the severity of cognitive impairment[138]. Moreover, recent reports have suggested Aβo are responsible for cognitive decline in Beagles[26,36]. A study by Head and colleagues included 30 Beagles with age ranging between 4.5 – 15.7 years and compared the CSF $A\beta_{42/40}$ ratio with the brain Aβ [26]. The authors found that levels of Aβo in CSF inversely correlated with brain Aβ. Another study by González-Martínez and colleagues assessed plasma of $A\beta_{42/40}$ ratio in a total of 88 dogs aged 1–4 years, 5–8 years, and ≥9 years of age cognitively unimpaired as well as ≥9 years of age cognitively impaired [151]. The authors found that plasma $A\beta_{42/40}$ ratio inversely correlated with age and extent of cognitive impairment. The authors also reported that mild cognitively impaired dogs had higher plasma $A\beta_{42/40}$ level than severely impaired dogs, which mimic the patterns observed in human MCI and AD[129,151-153].

However, when compared to human AD, the presence of NFTs in dogs have been observed in a limited number of studies. Few Tau phosphorylation sites were reported in dog brain, including p-Tau Ser396[143,144,154], Ser189, Ser207[155], Thr181[142], Thr205, Ser422[143] and Ser202/Thr205[143]. A study by Abey and colleagues investigated the presence p-Tau in six different breeds of cognitively impaired dogs aged between 14-17 years using anti-p-Tau

Ser202/Thr205 (clone AT8) and anti p-Tau Ser396 antibodies[144]. AT8 positive labelling was confirmed in only one dog but all dogs were positive for p-Tau Ser396. This study failed to demonstrate the presence of NFTs[144]. Another study by Schmidt and colleagues used anti-pT205, AT8, AT100, PHF-1 and anti-pT422 antibodies to detect hyperphosphorylated Tau in 24 different breeds of dogs aged between 2-19 years[143]. Only 3 dogs aged 13 to 15 years exhibited NFT-like appearence[143]. Therefore, and for the first time, I have shown extensive distribution of human AD like AT8 positive p-Tau deposits in cerebral cortex and hippocampal regions of cognitively impaired aged dogs (Chapter 5).

Aging in human and identifying AD related biomarkers in cognitively normal young and/or middle age individuals is a central focus in the field of AD research[54,156,157]. Several studies have demonstrated the presence of Aβo, Aβp and p-Tau in cognitively unimpaired human[52,54]. AD has a long preclinical period which could be 'used' to help identify individuals at high risk of developing MCI and AD and also moving toward the development and application of disease-modifying therapies at the early asymptomatic stage. As discussed above, transgenic mice may not be able to exactly replicate the crucial neuropathological aspects of AD, because of variable genetic background and enzymatic interference by the transgenic mice's own APP[158,159,160]. Consequently, it has become vital to develop a natural translational model for AD that mimics closely human AD; and the dog appears to provide this opportunity and could potentially allow better understanding of AD and/or ageing in the pre-symptomatic phase before clinical onset. There are a very limited number of studies that investigated AD related biomarkers in young cognitively normal dogs[161] and to date no reports have shown the presence of Aβ and p-Tau in dogs' retina. Therefore, to my knowledge, this is the first time that the presence of retinal Aβo, Aβp and p-Tau was investigated in cognitively normal young, middle, and old dogs (Chapter 6).

1.10.3. Importance of the dog as a natural model for human AD

Dogs share a more common and closer DNA sequence, approximately 84%, with human than rodents[162,163]. A study by Johnstone *et al* showed that $A\beta_{1-42}$ amino acid sequence is identical in dogs and humans but in rats and mice it differs from the human sequence by three amino acids[164]. Dogs are very compliant with behavioural tasks whereas rodent models are not freely motivated toward behavioural and/or cognitive testing so their stress response may interfere with cognitive measures[165]. Also, human age (40-60 years) is similar to middle-aged dogs (5 - 9 years) and over 9 years of dog age is equivalent to humans aged over 66 years[166]. Remarkably, Beagles exhibit cognitive decline, and neurobehavioral changes around 6-7 years (middle age), exacerbated with age; similar to age progression in human[145]. However, a fundamental caveat in AD research is the ability of existing animal models to accurately replicate the subtle clinical and pathological features associated with AD that would enable the establishment and development of effective diagnostic and therapeutic approaches. Approximately, a staggering 98% of therapeutic approaches for AD failed in phase III clinical trial[167,168]. This thesis conclusively demonstrates that the dog is a strong natural disease and translational model for AD and consideration and efforts should focus on elevating this model to become the number one choice for scientists investigating AD.

1.11. Hypothesis

Human Alzheimer's Disease (AD) and Canine Cognitive Dysfunction (CCD) are both progressive neurodegenerative disorders exhibiting gradual decline of cognitive function and memory loss. Many of the molecular and pathological features associated with human AD are mirrored in the naturally occurring age-associated neuropathology in dogs. Also, the age variance between dog and human may help to better comprehend the prodromal cascade of AD. Therefore, dogs can be used as a strong translational model to understand the early pathophysiological stages of CCD and human AD.

Among the three major assemblies of Aβ, Aβo are the most toxic to neurons that lead to the loss of synaptic plasticity and impaired learning and memory. Also, in AD patients, Aβo can be detected more than two decades before clinical onset; and in dogs Aβo were reported to be involved in cognitive decline. Therefore, detection of Aβo may help diagnose AD and CCD at the pre-clinical stage of disease progression.

The eye is considered as a natural 'window' to the brain because retina is part of the central nervous system (CNS) and the only optically accessible nervous tissue. Neurodegenerative changes observed in the brain associated with AD are also accompanied by structural and functional changes in the retinal layers and ocular vasculature. Therefore, optical detection of Aβo through the development of a simple non-invasive, easily accessible, and cost-effective eye imaging platform may open a new possibility towards AD diagnostic and therapy.

In conclusion, incorporating dogs as a natural translational model with the development of an eye imaging platform in the field of AD research may provide a great opportunity to diagnose AD at pre-clinical stage and may lead to identifying individuals at risk of developing AD at a later stage in life.

1.12. Aims

Developmental study: Age specific immunodetection of Aβ oligomer (Aβo) and Aβ plaque (Aβp) in the brain and retina of AD mouse models (5xFAD and APP/PS1)

1. Immunodetection of Aβo and Aβp in the brain and retina.
2. Correlation between brain and retinal amyloid beta pathology
3. Understanding the age dependant progression of Aβo and Aβp in the brain and retina.
4. Immunodetection of Aβo in blood and correlation with retinal and brain pathological progression.

Validation and characterisation of dog model

1. Histopathological characterisation of the dog model as a model of human AD:

1.1. Immunodetection of Aβo and Aβp in the hippocampus and cerebral cortex of dogs affected with CCD.

1.2. Immunodetection of phosphorylated Tau (p-Tau) in the hippocampus and cerebral cortex of dogs affected with CCD.

2. Characterising human AD related pathologies in the retina of young, middle aged and old cognitively normal dogs:

2.1. Immunodetection of retinal Aβo and Aβp in dogs.

2.2. Immunodetection of retinal p-Tau in dogs.

2.3. Influence of demographics criteria on retinal depositions of Aβo, Aβp and p-Tau.

Chapter 2

Materials and methods

2.1. Materials

All equipment, chemicals, antibodies, and software used in this thesis are in **Tables 1-5**.

Table 1. List of equipment

Equipment	Company	Country
AAS- Advanced Anaesthesia Specialists	Darvall Vet	Gladesville, New South Wales, Australia
Peri-StarTM pro pump	Marshall Scientific	Hampton, USA
P^H meter	Rowe scientific	Sydney, NSW, Australia
Orbital shaker	Ratek Instruments Pty. Ltd.	Victoria, Australia
Vortex	Ratek Instruments Pty. Ltd.	Victoria, Australia
Powerpac^{tm} universal power supply	Bio-Rad	California, USA
Precellys evolution homogenizer with cryolys cooling option	Bertin Instruments	Montigny-le-Bretonneux, France
BMG plate reader	BMG Labtech	Ortenberg, Germany
iBright FL1500 imaging system	ThermoFisher Scientific	Massachusetts, USA
2100 antigen retriever	Aptum Biologics Ltd	Southampton, UK
Microtome	ThermoFisher Scientific	Massachusetts, USA
Poly-L-lysine coated glass slides	Agilent	California, USA
Cover slip	Agilent	California, USA
Olympus CX 43 light microscopy	Olympus corporation	Tokyo, Japan
Olympus CX 43 Polarised microscopy	Olympus corporation	Tokyo, Japan
Olympus VS 120 fluorescence microscopy	Olympus corporation	Tokyo, Japan
Confocal	Carl Zeiss Pty Ltd	Oberkochen, Germany

Table 2. List of chemicals

Chemicals	Company	Country
Isoflurane	Sigma-Aldrich	Missouri, USA
Saline	Reclens	Australia
10% neutral buffer formalin	Sigma-Aldrich	Missouri, USA
EDTA anticoagulant	Sigma-Aldrich	Missouri, USA
Dynabeads pre-coated with anti-Rabbit IgG	Invitrogen	California, USA
Ammonium chloride	Sigma-Aldrich	Missouri, USA
Formic acid	Sigma-Aldrich	Missouri, USA
Triton X	Astral scientific pty ltd	Taren Point, NSW, Australia
Protease inhibitors	Thermo-Fisher Scientific	Massachusetts, USA
Laemmli buffer	Bio-Rad	California, USA
Phosphate buffer saline (PBS)	Thermo-Fisher Scientific	Massachusetts, USA
Tris	Sigma-Aldrich	Missouri, USA
Sodium Chloride	Sigma-Aldrich	Missouri, USA
Pre-cast gels	Bio-Rad	California, USA
PVDF membranes	Bio-Rad	California, USA
Pierce™ BCA Protein Assay Kit	Thermo-Fisher Scientific	Massachusetts, USA
Clarity™ Western ECL Substrate	Bio-Rad	California, USA
Hematoxylin and Eosin	Amber scientific	Midvale WA 6056, Australia
Congo red	Leica biosystems	Wetzlar, Germany
Thioflavin T (ThT) staining	Sigma-Aldrich	Missouri, USA
Xylene	ChemSupply	Bedford Street Gillman, South Australia, Australia
Ethanol	ChemSupply	Bedford Street Gillman, South Australia, Australia
Paraffin	Thermo-Fisher Scientific	Massachusetts, USA
1× citrate buffer	Agilent	California, USA
0.3% H2O2	Agilent	California, USA
Protein Block Serum-Free	Agilent	California, USA
DAB substrate chromogen system	Agilent	California, USA
Fluorescence mounting media	Agilent	California, USA

Table 3: Antibodies used for western blot analysis

Primary antibodies					Secondary antibodies		
Target antigen	**Antibody**	**Company**	**Species**	**Dilution**	**Antibody**	**Company**	**Dilution**
Aβo	Anti-Aβo (A11)	Merck Millipore, Massachusetts, USA	Rabbit polyclonal	1:1000	anti-rabbit-IgG, HRP conjugated	Sigma-Aldrich, Missouri, USA	1:10,000
$A\beta o_{1-40}$	Single domain anti-Aβo (PrioAD12)	*David et al;2014*	Single domain camelid	1:500	anti-llama, HRP conjugated	Bethyl Laboratories, Texas, USA	1:10,000
$A\beta o_{1-42}$	Single domain anti-Aβo (PrioAD13)	*David et al;2014*	Single domain camelid	1:500	anti-llama, HRP conjugated	Bethyl Laboratories, Texas, USA	1:10,000
Aβp	Anti-β-Amyloid, 17-24 (4G8)	Bio legend, California, USA	Mouse monoclonal	1:1000	anti-mouse IgG, HRP conjugated	Sigma-Aldrich, Missouri, USA	1:10,000
Beta actin (β-actin)	anti-β-actin (SP124)	Thermo-Fisher scientific, Massachusetts, USA	Rabbit monoclonal	1:1000	anti-rabbit-IgG, HRP conjugated	Sigma-Aldrich, Missouri, USA	1:10,000

Table 4: Antibodies used for histopathological analysis

Primary antibodies					Secondary antibodies for IHC			Secondary antibodies for IF		
Target antigen	**Antibody**	**Company**	**Species**	**Dilution**	**Antibody**	**Company**	**Dilution**	**Antibody**	**Company**	**Dilution**
Aβo	Anti-Aβo (A11)	Merck Millipore, Massachusetts, USA	Rabbit polyclonal	1:250	anti-rabbit-IgG, HRP conjugated	Sigma-Aldrich, Missouri, USA	1:1000	anti-rabbit IgG conjugated to FITC	Sigma-Aldrich, Missouri, USA	1:1000
$A\beta o_{1\text{-}40}$	Single domain anti-Aβo (PrioAD12)	*David et al;2014*	Single domain camelid	1:500	anti-llama, HRP conjugated	Bethyl Laboratories, Montgomery, USA	1:1000	anti-llama IgG conjugated to FITC	Bethyl Laboratories, Texas, USA	1:500
$A\beta o_{1\text{-}42}$	Single domain anti-Aβo (PrioAD13)	*David et al;2014*	Single domain camelid	1:500	anti-llama, HRP conjugated	Bethyl Laboratories, Montgomery, USA	1:1000	anti-llama IgG conjugated to FITC	Bethyl Laboratories, Texas, USA	1:500
Aβp	Anti-β-Amyloid, 17-24 (4G8)	Bio legend, California, USA	Mouse monoclonal	1:500	anti-mouse IgG, HRP conjugated	Sigma-Aldrich, Missouri, USA	1:1000	anti-mouse IgG conjugated to Texas red	Sigma-Aldrich, Missouri, USA	1:500
p-Tau (Ser202/Thr205)	AT8	Thermo-Fisher Scientific, Massachusetts, USA	Mouse monoclonal	1:500	anti-mouse IgG, HRP conjugated	Sigma-Aldrich, Missouri, USA	1:1000	anti-mouse IgG conjugated to Texas red	Sigma-Aldrich, Missouri, USA	1:500
Glial Fibrillary Acidic Protein (GFAP)	Anti-GFAP	Thermo-Fisher Scientific, Massachusetts, USA	Mouse monoclonal	1:500	ND	ND	ND	anti-mouse IgG conjugated to Texas red	Sigma-Aldrich, Missouri, USA	1:1000
Ionized calcium binding adaptor molecule 1 (Iba1)	Anti-Iba1	Thermo-Fisher Scientific, Massachusetts, USA	Mouse monoclonal	1:500	ND	ND	ND	anti-mouse IgG conjugated to Texas red	Sigma-Aldrich, Missouri, USA	1:1000

Neuronal nuclear protein (NeuN)	Anti-NeuN (A60)	Merck Millipore, Massachusetts, USA	Mouse monoclonal	1:500	ND	ND	ND	anti-mouse IgG conjugated to Texas red	Sigma-Aldrich, Missouri, USA	1:1000
Lysosomal-associated membrane protein 2 (LAMP2)	Anti-Lamp2	Stressgen Bio reagents Corp, Canada	Mouse monoclonal	1:500	ND	ND	ND	anti-mouse IgG conjugated to Texas red	Sigma-Aldrich, Missouri, USA	1:1000

Table 5. List of software

Software	Company
Image-J' processing program	National Institutes of Health and Laboratory for Optical and Computational Instrumentation (LOCI), University of Wisconsin
Olympus OlyVIA' software	Olympus, Shinjuku, Tokyo, Japan
cellSense	Olympus, Shinjuku, Tokyo, Japan
GraphPad Prism version 7.00	GraphPad, San Diego, USA
SAS Enterprise Guide version 8.2.	SAS institute, North Carolina State University, USA
Zen blue	Carl Zeiss Pty Ltd, Oberkochen, Germany

2.2. Methods

2.2.1. Animals

2.2.1.1. 5xFAD mouse

The 5xFAD mouse model is one of the most widely used AD models which exhibit severe amyloid pathology. This model was made by co-injecting two vectors encoding APP (with Swedish (K670N/M671L), Florida (I716V), and London (V717I) mutations and PSEN1 (with M146L and L286V mutations), each driven by the mouse Thy1 promoter[169]. In the current study a total of eighteen transgenic and sixteen wild type 5xFAD mice were used (**Table 1, chapter 3)** and all mice were housed with all the necessary procedures at the Melbourne Brain Centre (Parkville, VIC, Australia) and finally all the experimental procedures were approved by the Howard Florey Animal Ethics Committee (13-068-UM). Further details are explained in study Ⅰ; Chapter 3 [101].

2.2.1.2. APP/PS1 mouse

APP/PS1 is a double transgenic mouse made by APP Swedish mutation K595N and M596L and PSEN1 with L166P mutation controlled by the Thy1 promoter[170]. Mice were housed at Western Sydney University animal facility and all the experimental procedures were approved by the Animal Ethics Committee at Western Sydney University (ACEC no- A12905). A total of forty-eight (28 transgenic and 20 wild type) APP/PS1 mice were used in this study (**Table 1, chapter 4**). Further details are provided in study Ⅱ; Chapter 4[53].

2.2.1.3. Aged dogs

Brain tissue sections from seven aged dogs including, Papillon, Mongrel, Pomeranian, Lhasa Apso and Shiba Inu were used in this study, 5 of which were cognitively impaired (**Table 1, Chapter 5**). After routine necropsies, dog brains were collected and fixed in 10% neutral buffered formalin solution. Formalin fixed paraffin embedded blocks (FFPE) were prepared and 4μm thick brain tissue sections were then deparaffinised with xylene and rehydrated through graded alcohols and finally washed with deionized water. Sections were used for further histopathological analysis as described in study Ⅲ; Chapter 5. Tissue collection was performed at the Department of Veterinary Pathology, University of Tokyo and all the histopathological experimental procedures were performed at the Neuroimmunology Laboratory, Western Sydney University, Australia.

Finally, to identify dog retinal manifestation of AD related pathological hallmarks, I used a diverse group of thirty cognitively healthy dogs with ages from 1 year to 16 years (**Table 1, Chapter 6**). Eye sections were obtained from the Comparative Ocular Pathology Laboratory of Wisconsin (COPLOW) at the Department of Pathobiological Sciences, School of Veterinary Medicine, University of Wisconsin, Madison. Eye tissues used in this study were submitted by veterinarians as biopsies to COPLOW for routine pathological diagnosis and as such not subject to approval by institutional animal ethics. The collected paraffin embedded eye tissue sections were used for further histopathological analysis. All the procedures are explained in study Ⅳ; Chapter 6.

2.2.2. Mouse tissue and blood collections (Chapter 3 and 4)

All mice tissues and blood were collected under respective approved animal ethics protocols. Before taking the blood, mice were deeply anesthetized using isoflurane in an AAS- Advanced

Anaesthesia Specialists machine (Darvall Vet, Gladesville, NSW, Australia). After longitudinal cutting of skin at the midline thoracic cage, the heart was exposed, and blood was immediately collected in an anti-coagulant coated tube. Prior to tissue collection, perfusion was performed using a Peri-Star^{TM} Pro pump (Marshall Scientific, Hampton, USA) to control the flow. At first, ice-cold saline, then 10% neutral buffer formalin, was injected into the left ventricle through a perfusion needle The flow rate of the perfusate was controlled by the pump, with the perfusion continuing until all the blood was pumped from the circulation. Finally, the brain and eyes were collected from the mice. Brain was cut longitudinally, and half of the brain was snap frozen and stored at -80˚c for further protein quantification studies, and the other half of the brain and both eyes were stored in fixative solution (10% neutral buffer formalin) until used.

2.2.3. Immunoprecipitation of amyloid beta oligomers in blood derived from APP/PS1 mice (Chapter 4)

APP/PS1 mice and wild type littermates (total of 20 wild type and 28 APP/PS1 mice) were first euthanized (AAS- Advanced Anesthesia Specialists) before blood samples were collected by cardiac puncture. Tubes coated with anti-coagulant were used to collect the blood samples, that were then used for subsequent immunoprecipitation. In order to measure levels of Aβo in APP/PS1 mouse, we performed immunoprecipitation to enrich/isolate Aβ from whole blood of 3-4- and 17-month-old mice as described previously[171]. Briefly, 1×10^6 Dynabeads pre-coated with anti-Rabbit IgG (Invitrogen) were rinsed with PBS before adding 1µg/ml of rabbit anti-Aβo A11 antibody (Merck Millipore, Massachusetts, USA) and incubated overnight at 4˚C, with rotation. The *Dynabeads-A11* complexes were then washed four times with PBS and stored at 4˚C until further use. The blood samples were collected in EDTA-coated tubes and mixed at 1:1 ratio with blood lysis buffer (200 ml Ammonium chloride lysis solution with 70% formic acid, 0.1% triton X and 1X protease inhibitors). The solution was incubated for 15 minutes at room temperature, with gentle rotation before addition of the *Dynabeads-A11* complexes and the mixture was incubated overnight with rotation at 4˚C. Next day, the *Dynabeads-A11-Aβo* complexes were washed four times in PBS and resuspended in laemmli buffer before heating to 95˚C for 5 min. Finally, the solutions were left to cool down then used for the subsequent western blotting.

2.2.4. Western blot analysis (Chapter 4)

2.2.4.1. Principle

In molecular biology western blot analysis is one of the fundamental techniques to identify target proteins from a complex mixture of total extracted protein. This method helps to separate proteins according to their electrophoretic mobility, charge and molecular weight by gel electrophoresis. Sodium dodecyl sulphate polyacrylamide gel electrophoresis (SDS-PAGE) is one of the common gel electrophoresis methods used in western blot analysis. SDS is a detergent which denatures the folded protein into linear structure, uniformly distribute negative charge and sperate protein according to their molecular mass range between 5-250 kDa. After running, total proteins are transferred to a membrane (PVDF) which is then incubated with specific antibody to target a protein of interest whereas unbound proteins are washed off. Finally the targeted protein is visible as a band, according to various molecular weight, and density of each band corresponds to the protein concentration[172].

2.2.4.2. Protein extraction:

The collected brain tissue from mice was weighed to make a stock solution of 10 % w/v right after taking it out from -80˚c. For homogenisation, lysis buffer was prepared with 100mM Tris, 150mM Nacl and 1X protease inhibitor (Thermofisher scientific, Massachusetts, USA) and pH was adjusted to 7.4. Then tissues in ice-cold lysis buffer were homogenised in the precellys evolution homogenizer with cryolys cooling option [maintaining temperature condition (0-4˚c)] (Bertin Instruments, Montigny-le-Bretonneux, France). The cycle was run at 6000rpm x

2 x 30seconds. Right after homogenisation was completed, samples were stored in ice and aliquot some amount to prepare a working stock (2 % w/v) and the rest stored at -80˚c. No detergent or heat were used to extract total protein.

2.2.4.3. Protein estimation

Protein concentration of each sample was estimated according to the manufacturer's instructions using Pierce™ BCA Protein Assay Kit (Thermofisher scientific, Massachusetts, United States). Bicinchoninic acid (BCA) protein assay is a colorimetric detection and quantitation of total protein. In an alkaline environment bicinchoninic acid forms a purple colour after the protein interaction with cuprous ion (Cu+2 to Cu+1) and total protein concentration is quantified according to the proportional changes of colour. In microplate procedure of BCA protein assay kit Bovine serum albumin (BSA) was used as standard and prepared in a working dilution of 20-2000 ug/ml and experimental samples were diluted to 0.5% w/v from 10% w/v stock solution in tris buffer saline (TBS). Then triplicates of each standard and experimental sample were pipetted out into a 96 well microplate and finally the intensity of total protein concentration was determined with the absorbance at 562 nm using a BMG plate reader (BMG Labtech, Ortenberg, Germany).

2.2.4.4. Sample preparation, running and transfer

After immunoprecipitation and protein estimation, samples were denatured by boiling in laemmli buffer at 95˚C for 5 min. Then samples were loaded on pre-cast gels (Bio-Rad, California, USA) and electrophoresed at a constant voltage of 100 V for 1.5 hours. Following electrophoresis, gels were blotted onto PVDF membranes (Bio-Rad, California, USA) at 18V for 2 hours. The membranes were rinsed in TBS-tween (0.05%) (TBST) and transferred to blocking solution (5% nonfat dried milk diluted in TBST) for 60 min at room temperature. The membranes were rinsed once in TBS-tween (0.05%) to remove the blocking solution, before adding 1µg/ml of camelid-derived single domain $A\beta_{1-40}$ (PrioAD12), $A\beta_{1-42}$ (PrioAD13) anti-oligomer antibodies[173] or A11 rabbit-anti-Aβo antibody (Merck Millipore, Massachusetts, USA) overnight at 4˚C. A rabbit-anti-β-actin antibody (Thermofisher Scientific, Massachusetts, USA) was also used as a loading control. Following 4 washes of 5 min each with TBS-tween (0.05%), the membranes were then incubated with anti-llama (Bethyl Laboratories, Inc, Texas, USA) or anti-rabbit IgG (Sigma-Aldrich, Missouri, USA) HRP conjugated antibody (1:10,000) at room temperature for 1 h. The membranes were washed then developed using the Clarity™ Western ECL Substrate (Bio-Rad, California, USA), according to the manufacturer's instructions before visualizing with iBright FL1500 imaging system (Thermofisher Scientific, Massachusetts, USA). Finally, the resulting digital images were analyzed with 'Image-J' processing program for the densitometry analysis and the values were compared between the transgenic mice and wild type controls (Chapter 4).

2.2.5. Immunostaining

2.2.5.1. Optimization of the antibodies used in immunostaining

For immunostaining including immunohistochemistry and immunofluorescence all the antibodies were optimised before final experimental procedure. Antibody concentration was optimised by testing different dilutions (low to high) of primary and secondary antibodies. Incubation time of each antibody corresponding to tissue type, including brain and eye, and species type, including mouse and dog, were also optimised. For instance, A11 or camelid derived nanobodies dilution were optimised from 1:100, 1:250, 1:500, 1:1000 up to 1:2000. Similarly, other primary antibodies were also tested for the optimal antigen-antibody interaction and binding. In addition, secondary antibodies for both immunohistochemistry and immunofluorescence were also diluted at 1:250, 1:500, 1:1000 and 1:2000; to minimize the nonspecific binding and background. The incubation time with primary and secondary antibodies were optimised from 1 hour, 2 hours and overnight. Results were varied according to the species, for example, mouse tissue exhibited nice staining with 1 hour of primary antibody incubation and 1 hour of secondary antibody incubation in immunohistochemistry, and overnight with primary antibody in immunofluorescence. In contrast dog tissue sections displayed very specific staining with overnight primary and 2 hours of secondary antibodies in both immunohistochemistry and immunofluorescence. All the antibodies used in immunostaining are listed in **Table 4**.

2.2.5.2. Optimization of the antigen retrieval method used in immunostaining:

During histological sample preparation different fixatives are usually used to preserve and fix tissues, including formalin or paraformaldehyde. However, tissue fixation can lead to masking of the epitopes and inhibit the antibody and antigen binding. So, an antigen retrieval step is very important to unmask the epitopes and enable the antibody to bind to the target antigen and improve staining expression. There are various antigen retrieval methods available, including enzymatic or heat induced. In this study I used a heat induced retrieval method which includes microwave, water bath, autoclave and 2100 antigen retriever. Different types of tissues such as mouse brain and eye sections and dogs' brain and eye sections were optimised with each method. Antigen retrieval buffer was also optimised for each antibody used in this study (**Table 4**). Among all the heating approaches I found that, with water bath method mouse eye tissue sections were morphologically intact and displayed strong staining expressions, whereas autoclave and microwave methods were causing tissue breakage and creating air bubbles. In addition, mouse brain, dog brain and eye sections were exhibiting conclusive staining with 2100 antigen retriever (Aptum biologics Ltd, Southampton, United Kingdom) incubated for 1 hour. This method is a unique approach to expose the antigen and increase the binding affinity. There are several advantages of using the 2100 antigen retriever, including maintaining optimum pressure and temperature, avoid creating air bubbles and retain tissue morphology. Furthermore, two different antigen retrieval buffers were optimised for different types of antibodies. For instance, citrate buffer was used for all the antibodies used in this thesis except p-Tau antibodies. For p-Tau antibodies 0.05% tween 20 in deionized water was used to perform 2100 antigen retriever method.

Chapter 3

Results (Paper 1)

3. Age-Specific Retinal and Cerebral Immunodetection of Amyloid-β Plaques and Oligomers in a Rodent Model of Alzheimer's Disease

Umma Habiba[a], Sam Merlin[b], Jeremiah K.H. Lim[c], Vickie H.Y. Wong[c], Christine T.O. Nguyen[c], John W. Morley[a], Bang V. Bui[c] and Mourad Tayebi[a, *]

[a]School of Medicine, Western Sydney University, Campbelltown, NSW, Australia; [b]School of Science & Health, Western Sydney University, Campbelltown, NSW, Australia; [c]Department of Optometry and Vision Sciences, University of Melbourne, Victoria, Australia

Journal: Journal of Alzheimer's Disease, vol. 76, no. 3, pp. 1135-1150, 2020
Accepted 18 May 2020 | Published: 04 August 2020

3.1. Abstract

Background: Amyloid-β soluble oligomers (Aβo) are believed to be the cause of the pathophysiology underlying Alzheimer's disease (AD) and are normally detected some two decades before clinical onset of the disease. Retinal pathology associated with AD pathogenesis has previously been reported, including ganglion cell loss, accumulation of Aβ deposits in the retina, reduction of nerve fiber layer thickness as well as abnormalities of the microvasculature.

Objective: This study's aim is to better understand the relationship between brain and retinal Aβo deposition and in particular to quantify levels of the toxic Aβo as a function of age in the retina of a rodent model of AD.

Methods: Retinas and brain tissue from 5xFAD mice were stained with Congo red, Thioflavin-T (Th-T) as well Aβ plaque-specific and Aβo-specific antibodies.

Results: We show that retinas displayed an age-dependent increase of Th-T-specific amyloid fibrils. Staining with anti-Aβ antibody confirmed the presence of the Aβ plaques in all 5xFAD retinas tested. In contrast, staining with anti-Aβo antibody showed an age-dependent decrease of retinal Aβo. Of note, Aβo was observed mainly in the retinal nuclear layers. Finally, we

confirmed the localization of Aβo to neurons, typically accumulating in late endosomes, indicating possible impairment of the endocytic pathway.

Conclusion: Our results demonstrate the presence of intra-neuronal Aβo in the retina and its accumulation inversely correlated with retinal Aβ plaque deposition, indicating an age-related conversion in this animal model. These results support the development of an early AD diagnostic test targeting Aβo in the eye.

3.2. Introduction

Alzheimer's disease (AD) is a progressive neurodegenerative disorder associated with a gradual decline in cognitive function, memory loss, abnormal behaviour and reduction of brain volume[21,22,174,175]. The neuropathological lesions observed in the brain of AD patients include extracellular deposition of amyloid-β (Aβ) plaques; intracellular deposition of hyper phosphorylated Tau (p-Tau) protein in the form of neurofibrillary tangles (NFTs), ubiquitin, cerebral amyloid angiopathy (CAA), severe synaptic loss and neuronal death [20-22,176]. Brain accumulation of misfolded/aggregated Aβ is believed to be one of the major pathological constituents for the development of the disease. Aβ peptide is derived from a larger protein, namely the amyloid-β protein precursor (AβPP) [176]. AβPP is enzymatically cleaved into amyloidogenic and non-amyloidogenic entities. In AD, the β and γ secretase sequentially cleave AβPP and produce the Aβ peptide fragments (36–43 amino acids) [177-179], that aggregate and lead to accumulation of brain deposits or plaques [20,39,180]. Enzymatic cleavage leads to the formation of two major isoforms of Aβ; $Aβ_{40}$ (~80–90%) and $Aβ_{42}$ (~5–10%) [176,181,182]. In sporadic and familial AD, 3 major assemblies of Aβ have been reported [39,183,184], including monomeric Aβ composed of low molecular weight dimers and trimers; soluble oligomers, containing 12-24 monomers which become elongated to form protofibrils; and insoluble fibrils [185,186]. Aβ soluble oligomers (Aβo) are neurotoxic and responsible for triggering the pathophysiology of AD [45,64,187,188]. Experimental detection of Aβo in peripheral tissues and/or blood precedes its central accumulation in the brain by some two decades [50,189], highlighting Aβo as a potential early diagnostic marker.

Various diagnostic approaches have been used for the detection of AD, which include neuro-clinical and neuropsychological examinations, blood, and cerebrospinal fluid (CSF) screening and brain imaging. However, most of these approaches are non-specific, some are invasive, expensive, and time-consuming. Thus, there is an urgent need for a non-invasive and cost-effective diagnostic screen to identify AD-affected subjects in the preclinical or early clinical stages. Visual disturbances are often an early complaint reported by AD patients [190,191], and have been linked to abnormalities of ocular physiology [81,85,111,192-195]. Patients experience altered colour vision [196,197], peripheral vision loss [198-200] and modified sensitivity to contrast and sometimes visual acuity [196,201]. Alteration of retinal morphology has been reported in AD patients and include changes to the vasculature [85], optic nerve head [89], ganglion cell and axon loss [88,202] and thinning of the retinal nerve fibre layer (RNFL) [82,86-88,192,202-208]. A study by O'Bryhim and colleagues using Optical Coherence Tomography and Angiography (OCT and OCTA) demonstrated that individuals with preclinical AD displayed early retinal architecture and vascular changes [97]. Another study demonstrated the feasibility to noninvasively detect and quantify, using a clinical scanning laser ophthalmoscope (SLO), amyloid deposits in the retina of human subjects given an oral solid lipid curcumin fluorochrome [206]. Koronyo *et al*, show in some cases that Aβ deposits in the retina was associated with blood vessels similar to cerebral vascular amyloid pathology [206] supporting other studies which indicate alteration to retinal vasculature [107,108,209]. Whilst Aβ deposits have been reported in the retina, how such levels change with age is not well documented. Furthermore, the relationship between retinal and brain soluble Aβo and insoluble oligomers is not well understood.

In this report, we assess in the 5xFAD mouse model age-related Aβo and Aβ plaque burden in the retina and brain of 6 to 17-month-old animals. Oakley and colleagues developed the

5xFAD, a transgenic rodent model that co-expresses five mutations [AβPP K670N/M671L (Swedish) + I716V (Florida) + V717I (London) and PS1 M146L+ L286V] that displays intraneuronal accumulation of $A\beta_{42}$ before plaque formation[210]. We show that retinal accumulation of Aβo was similar to brain in the early stage of the disease and their levels were inversely proportional to the age-related increased in Aβ plaque increase.

We showed that Aβo was colocalized to late-endosomal compartments in retinal neurons, indicating impairment in their ability to process and degrade this oligomeric species. Our study highlights the possibility of targeting Aβo in the eye a preclinical diagnostic test for AD.

3.3. Materials and Methods

3.3.1. Animals: The 5xFAD transgenic mice were made by co-injecting two vectors encoding AβPP (with Swedish (K670N/M671L), Florida (I716V), and London (V717I) mutations and PSEN1 (with M146L and L286V mutations), each driven by the mouse Thy1 promoter. This strain does not carry the retinal degeneration allele *Pde6b^{rd1}*. The 5xFAD mouse model rapidly develops severe amyloid pathology. Plaques spread throughout the hippocampus and cortex by six months of age. Synapse degeneration, neuronal loss and deficits in spatial learning are observed at approximately four months [210]. Age-matched wild type littermates were used as controls (**Table 1**).

3.3.2. Tissue collection and histological assessment of brains and eyes: All mice (**Table 1**) were perfused with saline and 10% neutral buffered formalin. Mouse brains and eyes were then fixed in 10% neutral buffered formalin, dehydrated using graded ethanol, washed with xylene, and finally embedded in paraffin. 3 x 6µm sections of each brain and retinal tissue were cut with a microtome (Thermofisher Scientific, Massachusetts, United States) and then processed for routine Haematoxylin and Eosin, Congo red and Thioflavin T staining as well as immunohistochemistry and immunofluorescence. Sections were deparaffinised with xylene and rehydrated through graded alcohols and finally deionized water.

3.3.3. Congo red amyloid-β staining: Sections were placed in Congo red (Leica biosystems, Wetzlar, Germany) working solution for 20 minutes then rinsed in 5-8 changes of deionized water. This was followed by staining in Gill ll Haematoxylin (Leica biosystems, Wetzlar, Germany) for 1-3 minutes and rinsing in 3 changes of deionized water. Sections were dehydrated in two changes of 95% alcohol and three changes of absolute alcohol for one minute each. Finally, sections were cleared in two changes of xylene and mounted in a xylene miscible medium. Amyloid fibrils appeared as dull to brick red under light microscopy (Olympus CX 43, Shinjuku, Tokyo, Japan) and apple green birefringence under polarized light (Olympus CX 43, Shinjuku, Tokyo, Japan).

3.3.4. Thioflavin-T staining of amyloid-β plaques: Following deparaffinisation with xylene and ethanol, tissue sections were incubated in filtered 1% aqueous Thioflavin-T (Sigma-Aldrich, St. Louis, Missouri, United States) for 8 minutes at room temperature. Sections were then rinsed in 3 changes of deionized water and mounted in aqueous mounting media (Agilent, Santa Clara, California, United States). Finally, slides were sealed with clear nail polish and stored in a cold and dark place. Generally, Thioflavin-T binds to the side chain channels along the long axis of amyloid fibrils. Upon binding to amyloid fibrils, Thioflavin-T has a strong signal at excitation and emission maxima of 450 and 482 nm, respectively under fluorescence microscopy (Olympus VS 120).

3.3.5. Immunohistochemical assessment of amyloid-β plaques and soluble oligomers: Sections were pre-treated with antigen retrieval method (1x citrate buffer for 20 min in a water bath; *pH* 6) to expose the target antigen. Sections were then treated with 90% formic acid for 5 minutes at room temperature followed with cell membrane permeabilization which was achieved using 1% triton X for 1 min prior to addition of 0.3% H_2O_2 for 15 minutes to inactivate endogenous peroxidases. Sections were then blocked with Protein Block Serum-Free (Agilent, Santa Clara, California, United States) for 15 minutes. Sections were then stained for 1h with the following primary antibodies in PBS: mouse purified *4G8* anti-Aβ against 17-24 of Aβ peptide (1:500; Bio legend, San Diego, California, United States) or *A11* rabbit anti-Aβo Antibody (1:250; Merck Millipore, Burlington, Massachusetts, United States) respectively. Sections were also stained with IgG1 isotype control (BRIC 222 recognizing CD44 [211] or IgG2b isotype control (BRIC 126 recognizing CD47 [212] antibodies to confirm specificity and selectivity of both A11 and 4G8 antibodies. Next, sections were incubated for 1h at RT with secondary antibodies in PBS: HRP-conjugated anti-mouse IgG (Sigma-Aldrich, St. Louis, Missouri, United States) or anti-rabbit IgG (Sigma-Aldrich, St. Louis, Missouri, United States) respectively. After washing three times with PBS, sections were covered with DAB solution and incubated for 5–10 minutes. Slides were then counterstained with haematoxylin for 1 min then imaged using the Olympus VS 120 Slide Scanner and were analysed using 'Olympus Oly VIA' software.

3.3.6. Immunofluorescence co-localisation studies: Double immuno-labelling was achieved by two different fluorescent labels, each having a separate emission wavelength. Sections were incubated overnight with both *A11* and *4G8* at 4°C. Further, and in other experiments, sections were incubated with *A11* and mouse Anti-*NeuN* mAb, clone A60 (Merck Millipore, Massachusetts, United States) to demonstrate neuronal homing of the oligomers. Additionally, sections were incubated with *A11* and mouse anti-lysosomal-associated membrane protein 2 (*LAMP2,* Stressgen Bio reagents Corp, Victoria, British Columbia, Canada) antibody to assess whether Aβo localize to lysosomes/ late endosomes. In both cases sections were incubated overnight at 4°C. Sections were then incubated with goat anti-rabbit IgG conjugated to FITC (Sigma-Aldrich, St. Louis, Missouri, United States) and donkey anti-mouse IgG conjugated to Texas red (Sigma-Aldrich, St. Louis, Missouri, United States) respectively for 2h at 4°C. Sections were then mounted using fluorescence mounting media (Agilent, Santa Clara, California, United States). Finally, the mounted sections were imaged using Olympus VS 120 Slide Scanner with a standard FITC / Texas Red double band-pass filter set.

3.3.7. Image quantification: 3 sections from different 5XFAD and wild type mice were used for image quantification (**Table 1**). 3 different areas of hippocampus, cerebral cortex and retina were analysed. Immunofluorescence signal intensity was visualized by capturing red and green fluorescent field images using the Olympus VS 120 Slide Scanner. Images were analysed using 'Olympus OlyVIA' software. Age-dependent accumulation of Aβ plaques and Aβo in 5xFAD was quantified using image processing software, *cellSense* (Olympus, Shinjuku, Tokyo, Japan). The mean colour threshold of fluorescent particles (red particles for plaques and green particles for oligomers) was calculated in several brain regions and eyes for each age group and the final result was presented as percentage fluorescence intensity and expressed as mean ± S.E.M.

3.3.8. Statistical analysis: One-way ANOVA with Dunnett's post-test was performed using GraphPad Prism version 7.00 for Windows (GraphPad, San Diego, CA, USA), for statistical analysis.

Table 1. List of 5xFAD mice for histopathological analysis

5xFAD mice used for H&E, Congo red, Thioflavin T & IHC				
Subject code	**Animal ID**	**Strain**	**Genotype**	**Age**
JC12RE6	FAD 6	5xFAD	WT	6 months
JC12RE7	FAD 7	5xFAD	WT	6 months
JC12RE10	FAD 10	5xFAD	WT	6 months
JC12RE1	FAD 1	5xFAD	WT	7 months
JC12RE5	FAD 5	5xFAD	WT	7 months
JC12RE9	FAD 9	5xFAD	HEMI	6 months
JC12RE11	FAD 11	5xFAD	HEMI	6 months
JC12RE12	FAD 12	5xFAD	HEMI	6 months
JC12RE2	FAD 2	5xFAD	HEMI	7 months
JC12RE4	FAD 4	5xFAD	HEMI	7 months
JC16B1RE	B1	5xFAD	WT	12 months
JC16B3RE	B3	5xFAD	WT	12 months
JC16B9	B9	5xFAD	WT	12 months
JC16B11	B11	5xFAD	WT	12 months
JC16B16	B16	5xFAD	WT	12 months
JC16B17	B17	5xFAD	WT	12 months

JC16B18	B18	5xFAD	HEMI	12 months
JC16B2RE	B2	5xFAD	HEMI	12 months
JC16B4RE	B4	5xFAD	HEMI	12 months
JC16B5RE	B5	5xFAD	HEMI	12 months
JC16B6RE	B6	5xFAD	HEMI	12 months
JC16B14	B14	5xFAD	HEMI	12 months
JC13A32	A32	5xFAD	WT	15 months
JC13A33	A33	5xFAD	WT	15 months
JC13A34	A34	5xFAD	WT	15 months
JC13A38	A38	5xFAD	WT	15 months
JC17FADA65L	A65	5xFAD	WT	17 months
JC12A49	A49	5xFAD	HEMI	14 months
JC12A53	A53	5xFAD	HEMI	14 months
JC17FADA36L	A36	5xFAD	HEMI	17 months
JC17FADA63R	A63	5xFAD	HEMI	17 months
JC17FADA64L	A64	5xFAD	HEMI	17 months
JC17FADA67L	A67	5xFAD	HEMI	17 months
JC17FADA75/73L	A73	5xFAD	HEMI	17 months

3.4. Results

3.4.1. Histological assessment of retinal and cerebral lesions in 5xFAD mice: We first performed an initial assessment to confirm the presence of the typical neuropathological lesions associated with AD in the brain and retina of the 6-7-month-old 5xFAD mice (**Figure 1**). H&E stain displayed widespread vacuolations, neuronal death and presence of eosinophilic structures in the cortical and hippocampal region of the brain (**Figure 1A, B, D, E**), in contrast with the retina which at the same age did not display the above structural changes (**Figure 1C &F**).

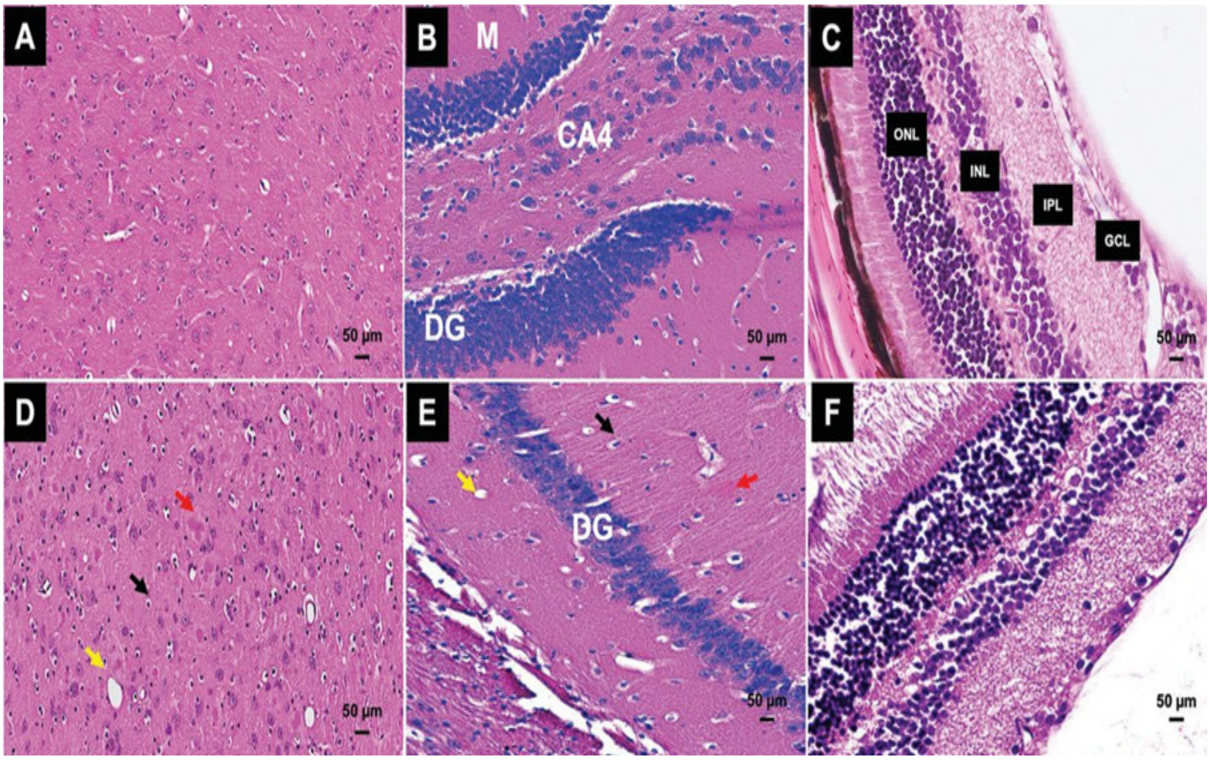

Figure 1. Photomicrographs of the microscopic lesions in the brains and retinas of 6-month-old 5xFAD mice. A) Normal appearance of the cerebral cortex in a healthy wild type mouse following staining with H & E. B) Normal appearance of the hippocampus in a healthy wild type mouse following staining with H & E (M, molecular layer; CA4, Cornu Ammonis 4; DG, dentate gyrus). C) Normal appearance of the retina in a healthy wild type mouse following staining with H & E. The photomicrograph was derived from peripheral region of the retina, away from the optic disc. Widespread vacuolations, neuronal death, and presence of eosinophilic structures in a 6-month-old 5xFAD mouse brain. Vacuolations (yellow arrow), neuronal death (black arrow), and eosinophilic structures (red arrows) are observed in the D) cortical and E) hippocampal region of the brain following staining with H & E (DG, dentate gyrus). F) Normal appearance of the retina in a 6-month-old 5xFAD mouse brain following staining with H&E. The photomicrograph was derived from peripheral region of the retina, away from the optic disc. Representative of all affected mice in this age group.

3.4.2. Retinal and cerebral detection of Congophilic and Thioflavin T-specific amyloid-β fibrils in 5xFAD mice: One of the distinctive neuropathological features associated with human AD brains is the presence of extracellular Aβ plaques [20,175,213]. We initially used Congo red (CR) and Thioflavin T staining (ThT) [214] to assess age-dependent accumulation of amyloid fibrils and compare amyloid burden in the retinas and brains derived from 6, 7, 12, 14 and 17 month of age 5xFAD and WT mice (**Figure 2**). Here, we show the distinctive Congophilic red-brick coloration confirming the presence of amyloid fibrils in the brain and retina starting from 6 month (**Figure 2A &B**) of age, respectively. This was confirmed by the presence of apple-green birefringence when examined under cross-polarized light (**Figure 2C & D**). However, retinal apple-green birefringence was less intense compared to the brain. This pattern of amyloid fibrils distribution in retina and brain in these different age groups was confirmed with ThT staining, which displayed more pronounced staining in all age groups tested starting from 6 months onward (**Figure 2E & F**). Congophilic- and ThT-specific retinal amyloid fibrils were clearly visible in the inner nuclear layer (INL), inner plexiform layer (IPL) and the ganglion cell layer (GCL) of all age groups (**Figure 2F**). These results confirm that the retina of the 5xFAD mice show signs of AD pathogenesis [200]. Of note, Congophilic- and ThT-specific amyloid fibrils were not visible in the brains and retinas of the age-matched 6-month-old wild type littermates (**data not shown**).

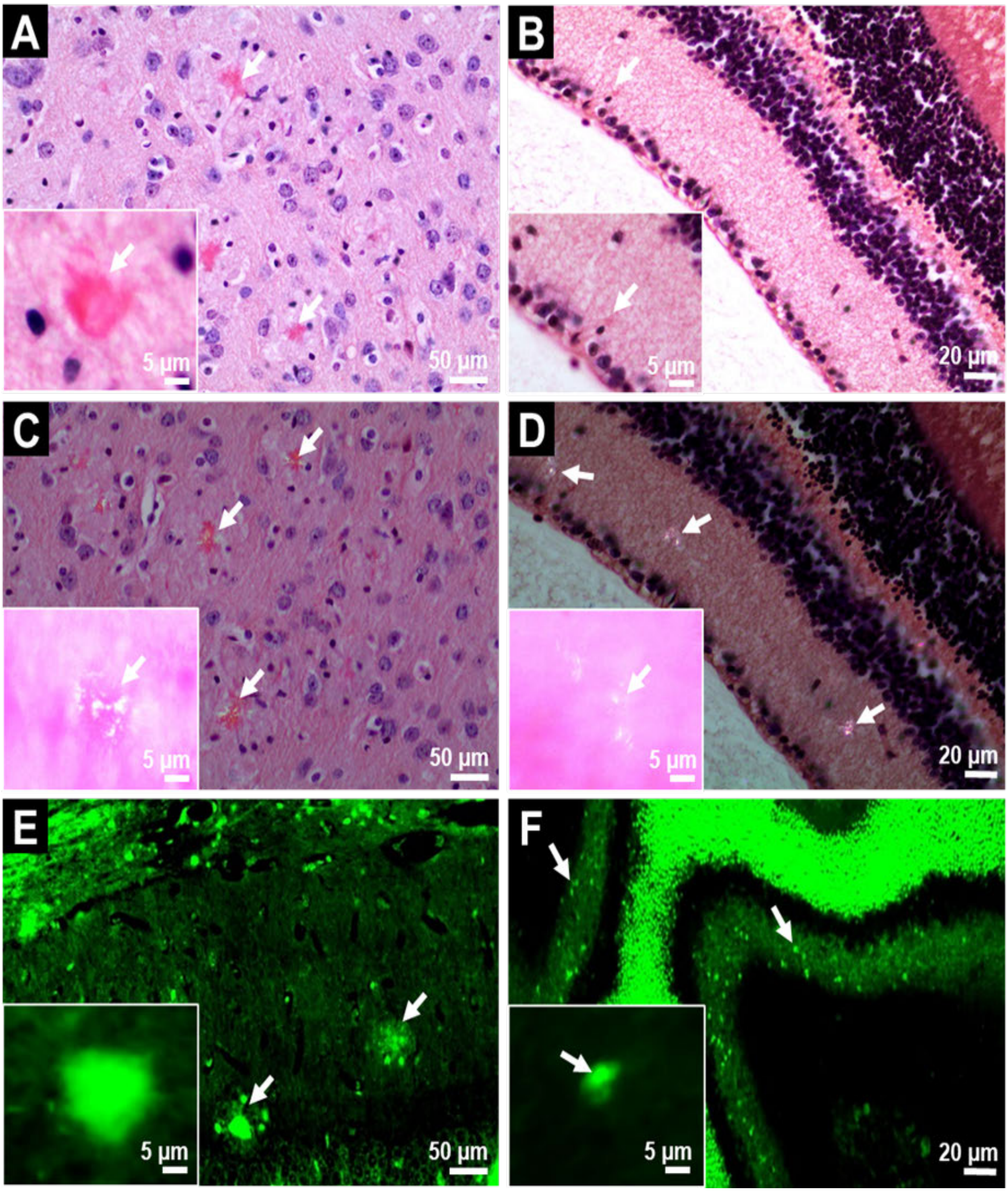

Figure 2. Photomicrographs of Congo red- and Thioflavin T-specific amyloid-β fibrils in the brains and retinas of six-month-old 5xFAD mice. A) Distinctive red-brick staining of amyloid fibrils with Congo red in the brain and B) GCL and ONL of the retina of a 6-month-old 5xFAD mouse. The photomicrograph was derived from peripheral region of the retina, away from the optic disc. The presence of the amyloid fibrils was confirmed with the presence of apple-green birefringence in the C) brain and D) retina under polarized light. Thioflavin T staining displayed presence of amyloid fibrils in the E) hippocampus and in the F) INL, IPL, and GCL of the retina (blue arrows). Representative of all affected mice in this age group.

3.4.3. Retinal and cerebral immuno-detection of amyloid-β plaques and amyloid-β soluble oligomers in 5xFAD mice: 5xFAD mice are known to exhibit cerebral accumulation of intracellular Aβo and extracellular Aβ plaques[210]. Although, amyloid fibrils are a neuropathological hallmark of human AD, there is strong evidence that oligomers are the most toxic species and appear to be the main causative agent of neurological deficits [64,215]. Moreover, it is now recognized that Aβo accumulation in serum of AD patients and experimental models can occur years before plaque build-up in the brain[216-218]. We hypothesized that Aβo accumulation in the retina might also precede cerebral plaque build-up in 5xFAD mice in an age-dependent manner. We initially examined brains and retinas for the presence of Aβo and Aβ plaques by immunohistochemistry using *A11* and *4G8,* respectively (**Figures 3-5**). 6-month-old 5xFAD mice displayed abundant intraneuronal Aβo deposits in the cerebral cortex, hippocampus, retinal nuclear layers (INL & ONL) and ganglion cell layer (GCL) (**Figure 3A-C**) as well as few extracellular Aβ plaques (**Figure 3D-F**). Interestingly, 12-month-old 5xFAD mice exhibited more pronounced extracellular cortical and hippocampal Aβ plaques but lower levels of intracellular Aβo compared to the 6-month-old age group (**Figure 4A-F**). Nonetheless, levels of intracellular Aβo appeared lower in these brain structures compared to the 6-month-old age group (**Figure 4A & B**). Similarly, retinal Aβo which could be seen in the GCL, INL and ONL appeared less abundant in this age group compared to the 6-month-old mice (**Figure 4C**). Occasional Aβ plaques were also evident in the retinal layers of 12-month-old 5xFAD mice, and their levels appeared lower than the 6-month-old age group (**Figure 4F**). As the age of the 5xFAD mice progressed, fewer intracellular Aβo deposits were observed as opposed to the abundant accumulation of Aβ plaques in the cerebrum of 14- and 17-months old mice (**Figure 5**). Retinal Aβ plaques were also conspicuous in the ganglion layer but Aβo appeared to be absent in the 14 and 17-month-old 5xFAD mice (**Figure 5C & F**). No Aβo and Aβ plaques deposits were seen in age-matched wild type littermates (**data not shown**). These results support previous findings that Aβ plaque burden increased over the course of the disease in both brain and retina, whereas Aβo levels appear to decrease in an age-dependent manner [219].

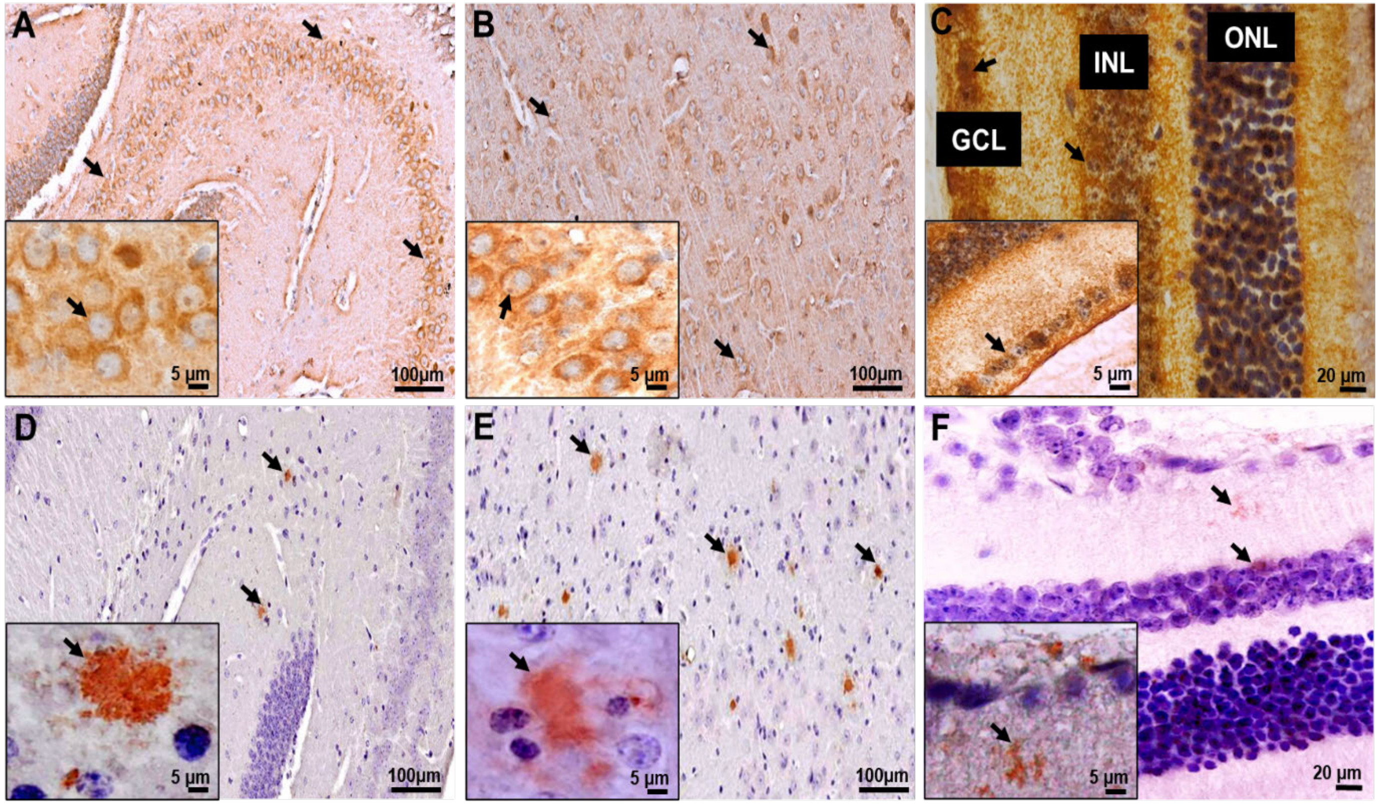

Figure 3. Photomicrographs of the amyloid-β oligomers and plaques in the brain and retina of a 6-month-old 5xFAD mouse. A) Immunohistochemical staining with A11 rabbit anti-Aβo polyclonal IgG antibody of a 6-month-old 5xFAD mouse which shows intraneuronal stained structures in the A) hippocampus, in the B) cerebral cortex and in the C) GCL, INL, and ONL of the retina. The photomicrograph was derived from peripheral region of the retina, away from the optic disc. D) Immunohistochemical staining with 4G8 murine anti-Aβ monoclonal IgG antibody of a 6-month-old 5xFAD mouse which shows characteristic extracellular AD Aβ plaques in the D) hippocampus, in the E) cerebral cortex and in the F) GCL and ONL of the retina. CA4, DG, and M refers to hippocampal cornu ammonis, dentate gyrus, and the molecular layer, respectively. Representative of all affected mice in this age group.

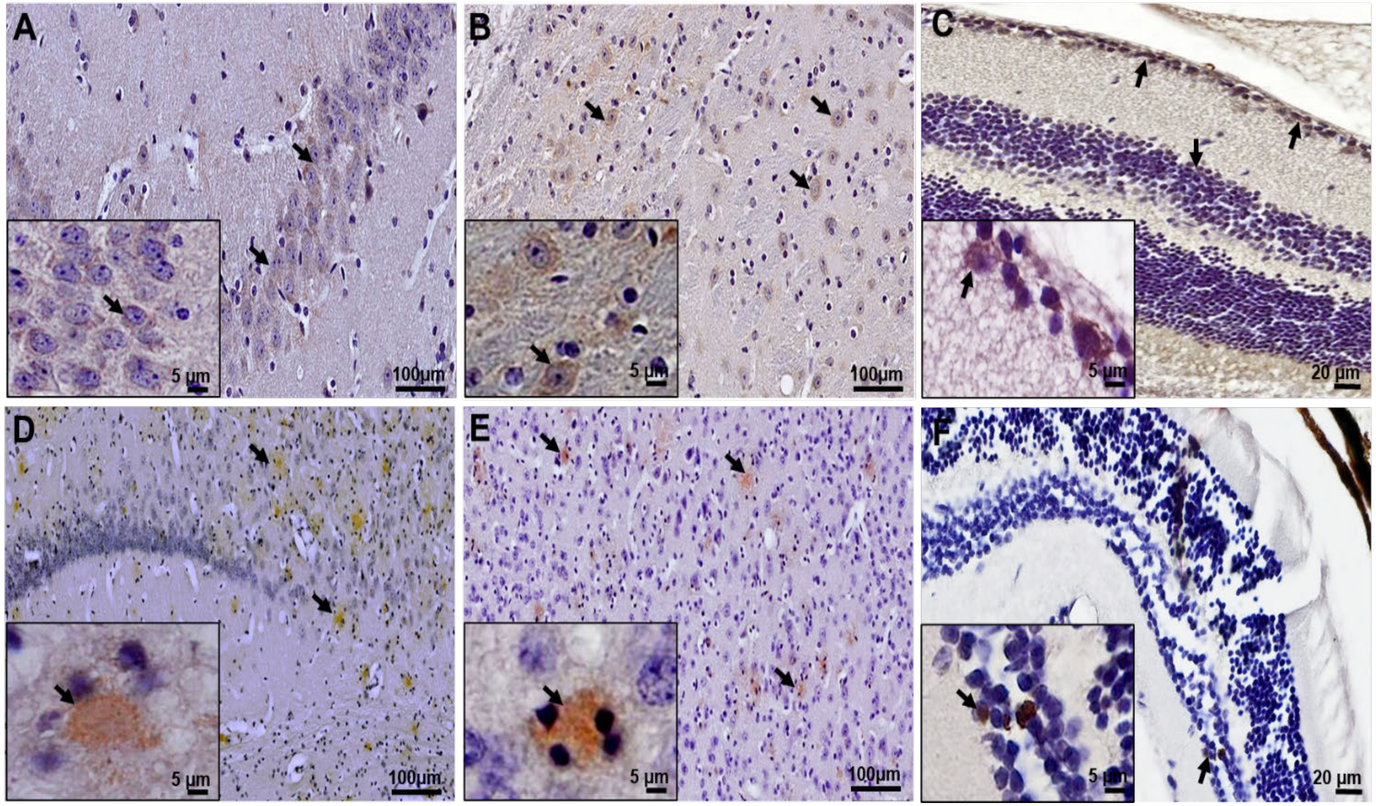

Figure 4. Photomicrographs of the amyloid-β oligomers and plaques in the brain and retina of a 12-month-old 5xFAD mouse. A) Immunohistochemical staining with A11 rabbit anti-Aβo polyclonal IgG antibody of a 12-month-old 5xFAD mouse which shows less intense intraneuronal stained structures in the A) hippocampus, in the B) cerebral cortex and in the C) GCL of the retina (arrows). The photomicrograph was derived from peripheral region of the retina, away from the optic disc. Immunohistochemical staining with 4G8 murine anti-Aβ monoclonal IgG antibody of a 12-month-old 5xFAD mouse which shows widespread and intense staining of the extracellular AD Aβ plaques in the D) hippocampus, and in the E) cerebral cortex (arrows). F) Very few plaques were observed in the retina (arrows). CA3, DG, and M refers to hippocampal cornu ammonis, dentate gyrus, and the molecular layer, respectively. Representative of all affected mice in this age group.

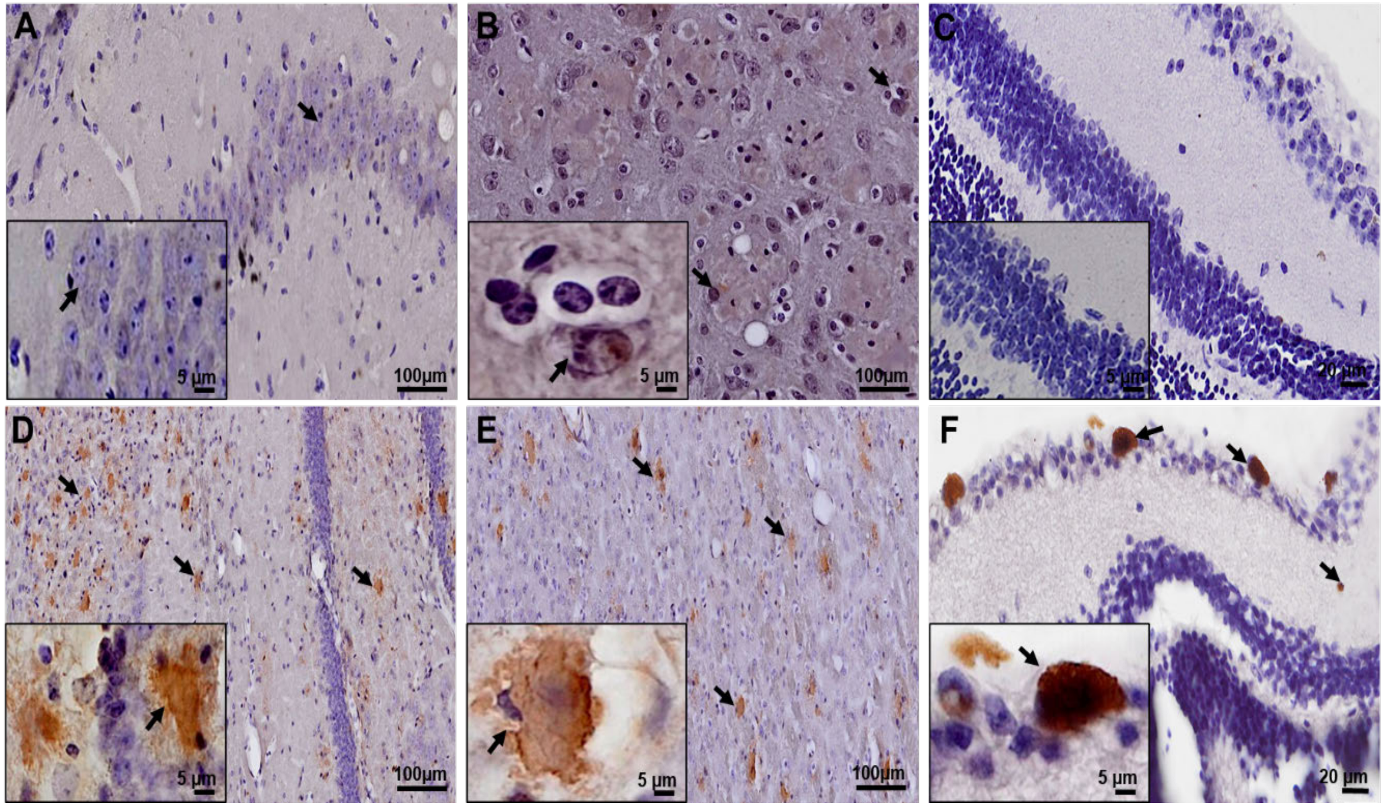

Figure 5. Photomicrographs of the amyloid-β oligomers and plaques in the brain and retina of a seventeen-month-old 5xFAD mouse. A) Immunohistochemical staining with A11 rabbit anti-Aβo polyclonal IgG antibody of a 17-month-old 5xFAD mouse which shows scarce intraneuronal stained structures in the hippocampus, and in the B) cerebral cortex (arrows). C) Aβo were absent in the retina in this age group. The photomicrograph was derived from peripheral region of the retina, away from the optic disc. D) Immunohistochemical staining with 4G8 murine anti-Aβ monoclonal IgG antibody of a 17-month-old 5xFAD mouse which shows widespread and intense staining of the extracellular AD Aβ plaques in the hippocampus, and in the E) cerebral cortex (arrows). F) Plaques were observed in the GCL of the retina (arrows). CA1, DG, and M refers to hippocampal cornu ammonis, dentate gyrus, and the molecular layer, respectively. Representative of all affected mice in this age group.

3.4.4. Amyloid-β oligomers co-accumulate with amyloid-β plaques and co-localise with an endosomal marker in neurones of 5xFAD mice: Our immunostaining results confirmed that accumulation of intracellular Aβo and Aβ plaques in the retinal layers parallels their brain build-up. We then investigated whether Aβo and Aβ plaques co-localise/accumulate in different regions and structures of the retina and brain of the various age groups tested using *A11* and *4G8* (**Figure 6 & 7**). This immunofluorescence study confirmed the presence of intracellular Aβo and Aβ plaques in the retina of the 6-month-old 5xFAD mice (**Figure 6**). Here, retinal Aβo was more prominent in the GCL and INL, and to a lesser extent in the IPL and ONL (**Figure 6**). While present, retinal Aβ plaques were less prominent in this age group (**Figure 6**). Remarkably, both Aβo and Aβ plaques were widespread in hippocampus and cerebral cortex of the 6-month old 5xFAD mice (**Figure 7**). At 12-month-old, retinal oligomers and plaques co-localised in the GCL, INL, IPL, ONL (**Figure 6**) and co-accumulated and displayed very strong staining in the cerebral cortical region and hippocampus (**Figure 7**). The immunofluorescence studies appeared to be more sensitive than immunohistochemistry as the latter allowed stronger detection of retinal Aβ plaques in the 12-month-old 5xFAD mice. Surprisingly, Aβo were detected in the retina and cerebrum of the 17-month-old 5xFAD mice (**Figure 6 & 7**). Finally, and as expected, the 17-month-old 5xFAD mice displayed conspicuous widespread accumulation of cerebral Aβ plaques, which were also observed in the retinas of these animals (**Figure 6 & 7**). No staining for both Aβo and Aβ plaques was seen in all brain and retinas of wild type age group (**data not shown**).

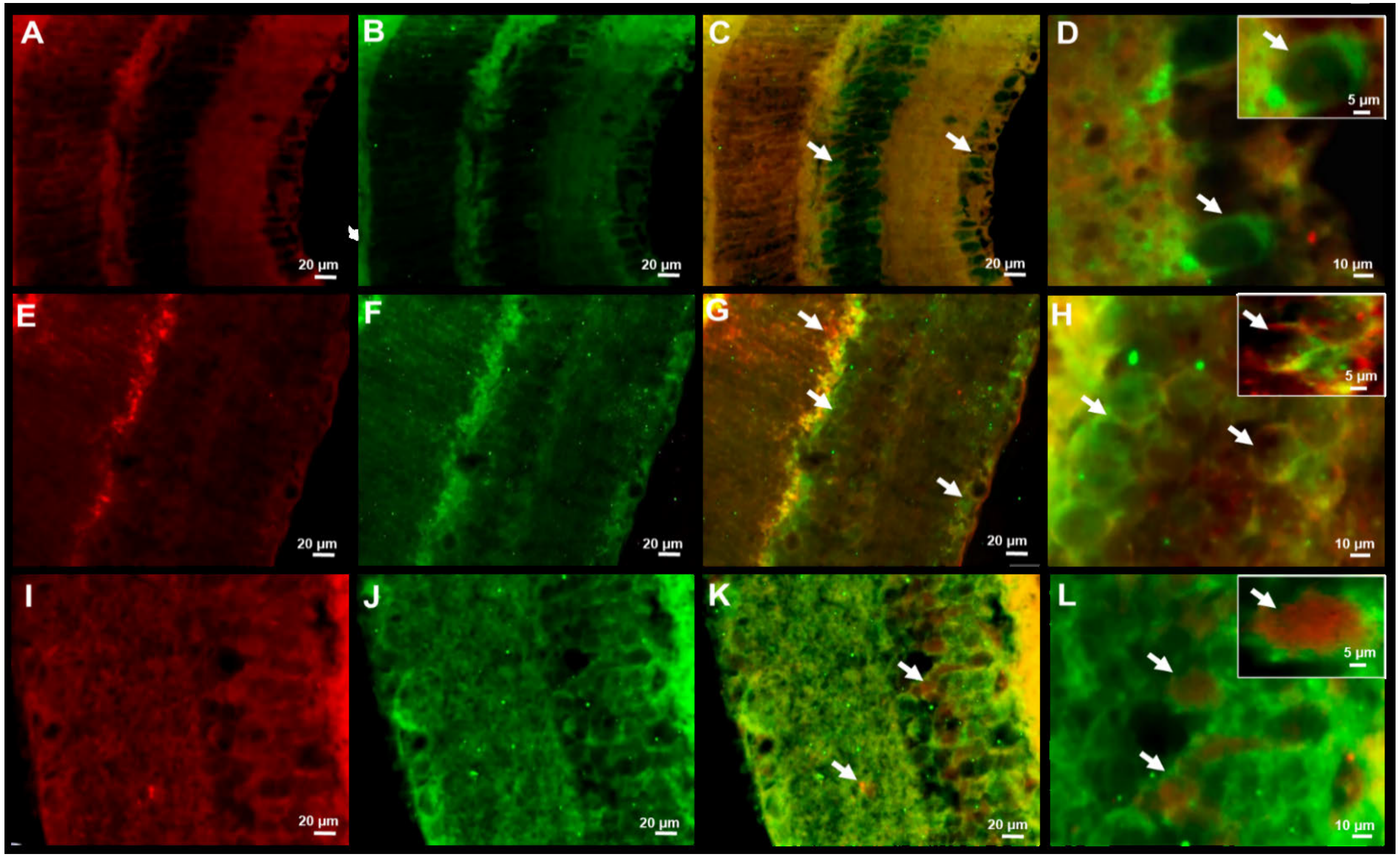

Figure 6. Immunofluorescence co-localisation of retinal beta amyloid oligomers and beta amyloid plaques in the six, twelve and eighteen-month-old 5xFAD age groups. Retinal co-staining with A11 rabbit anti-Aβo polyclonal IgG antibody (**GREEN**) and 4G8 murine anti-Aβ monoclonal IgG antibody (**RED**) of a 6, 12 and 18 months old 5XFAD mouse. In 6-month old mouse, oligomers co-localised with plaques (c and d) in the INL and GCL of the retina (arrows). High levels of oligomers co-localised with plaques in the ONL, INL, IPL and GCL of the retina in 12- month-old mice (g and h; arrows). High amounts of oligomers co-localised with plaques in the ONL, OPL, INL and IPL, GCL of the retina in the 18-month-old mouse (k and l; arrows). Representative of all affected mice in all age groups.

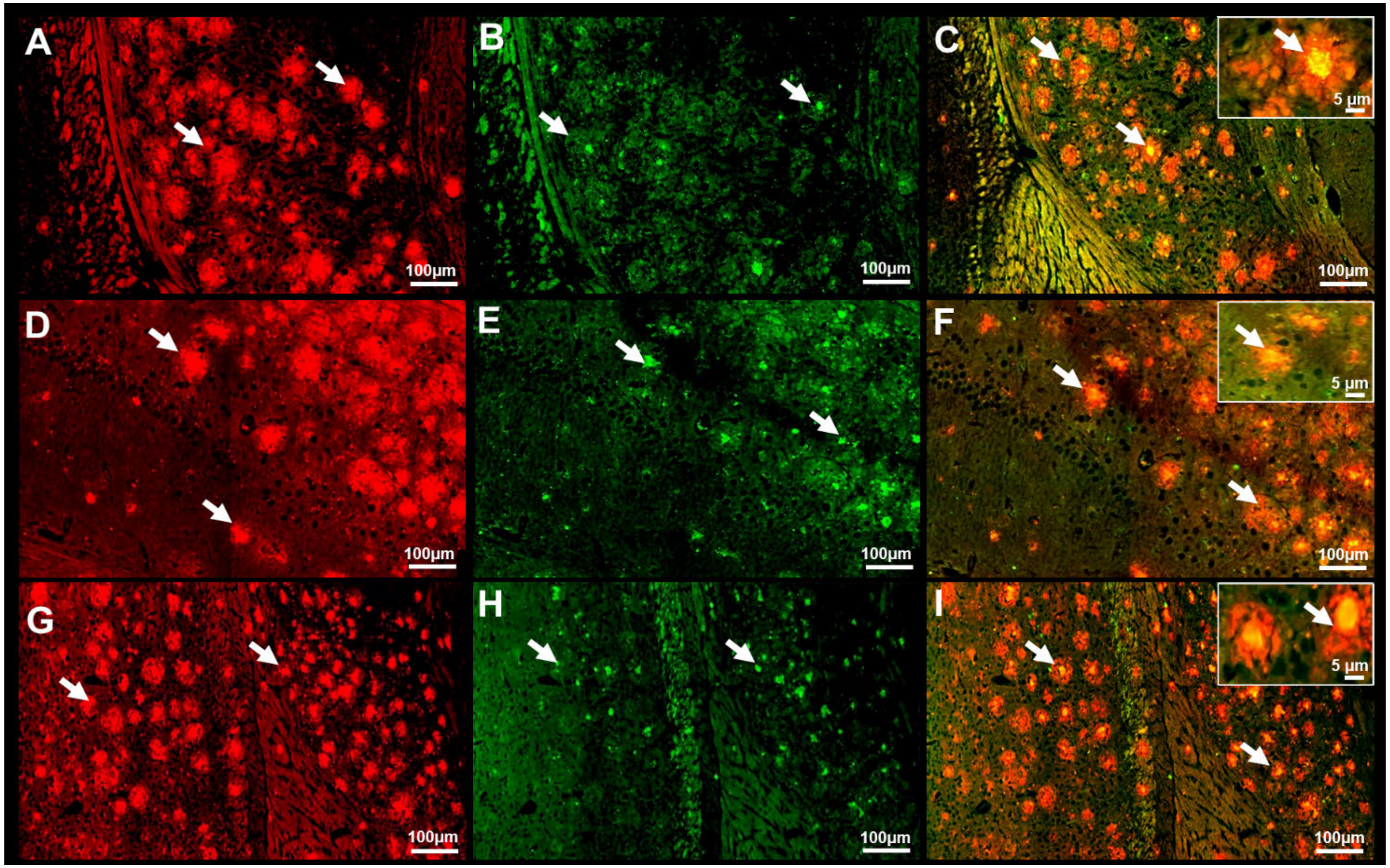

Figure 7. Immunofluorescence co-localisation of cerebral beta amyloid oligomers and beta amyloid plaques in the six, twelve and eighteen-month-old 5xFAD age groups. Cerebral co-staining with A11 rabbit anti-Aβo polyclonal IgG antibody (**GREEN**) and 4G8 murine anti-Aβ monoclonal IgG antibody (**RED**) of a 6, 12 and 18 months old 5xFAD mouse. High levels of oligomers co-localised with plaques in the hippocampus (arrows) in the 6 (e); 12 (h) and 18 (k) month old mice. Representative of all affected mice in all age groups.

Immunofluorescence signal intensity of both Aβ plaques and oligomers were quantified by an image processing software, *cellSense* (**Figure 9**) in the retina, hippocampus and cortex of the 6 months (n=5), 12 months (n=5) and ≥14 months (n=7) month old age 5xFAD groups and compared with wild type littermates 6-7 months (n=5), 12 months (n=6) and 14 months (n=5). Of note, 3 different areas of each section were analysed. Aβ plaque loads significantly increased from 6 months and onward ($p<0.001$) in the retina (**Figure 9 G & I**), hippocampus (**Figure 9 D & F**) and cortex (**Figure 9 A & C**) of the 6-7, 12 and ≥14-month-old age 5xFAD groups. In contrast, Aβ oligomers levels significantly decreased between 6-7 months and 12 months ($p<0.001$) in the retina (**Figure 9 H & I**), hippocampus (**Figure 9 E & F**) and cortex (**Figure 9 B & C**) of the 6-7 months, 12 months and ≥14 months old age 5xFAD groups.

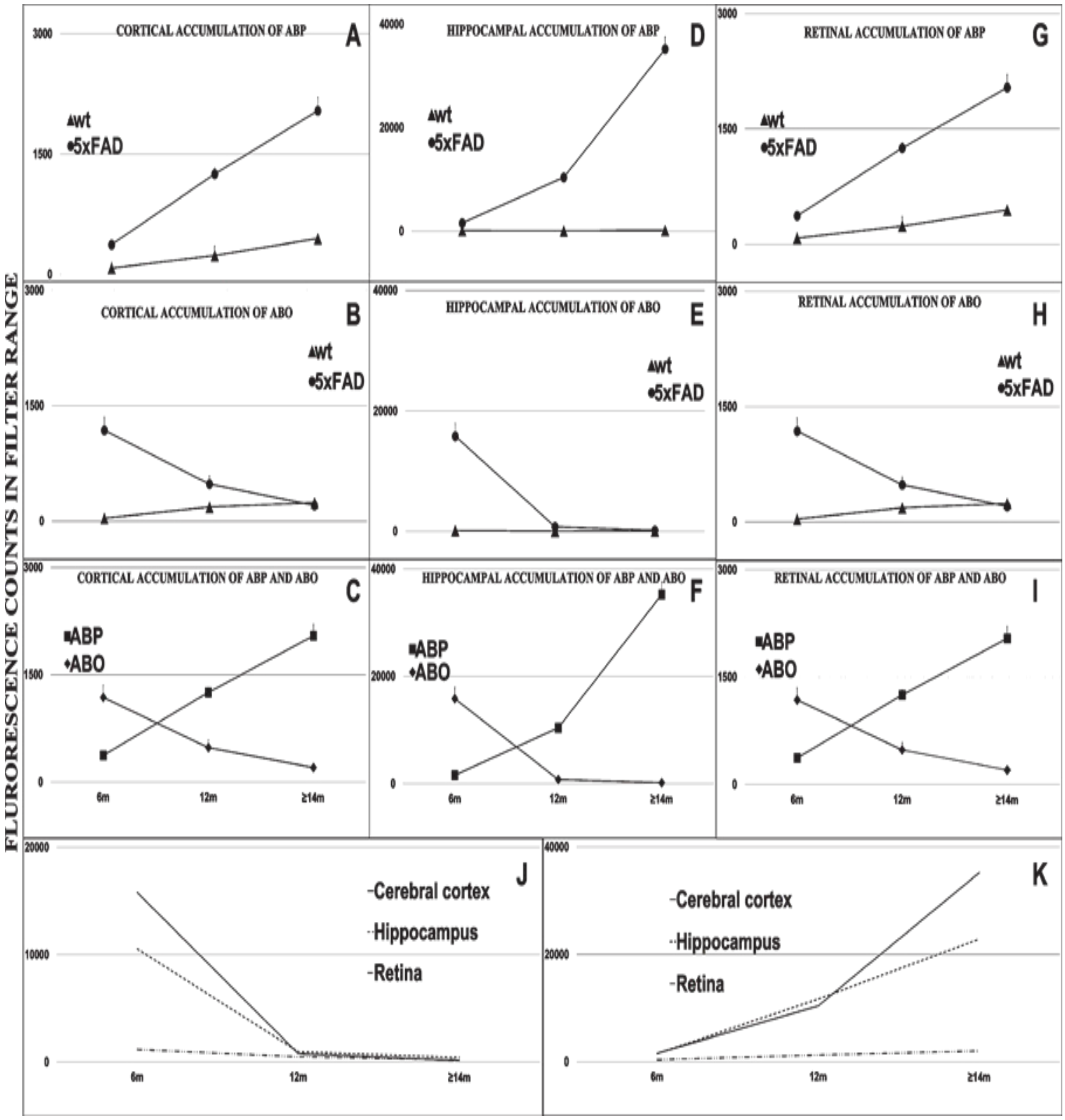

Figure 9. Quantification of amyloid-β plaque burden and amyloid-β oligomers with CellSense image processing software. Total Aβ plaque burden (Aβp) in the cerebral cortex (A, C, K), hippocampus (D, F, K), and retina (G, I, J) was quantified in 6–7-month-old (5×FAD = 5; wild type = 5); 12-month-old (5×FAD = 6; wild type = 6); and ≥14-month-old (5×FAD = 7; wild type = 5). Total Aβ oligomer load (Aβo) in the cerebral cortex (B, C, J), hippocampus (E, F, J), and retina (H, I, J) was quantified in 6-month-old (5×FAD = 5; wild type = 5); 12-month-old (5×FAD = 6; wild type = 6); and ≥14-month-old (5×FAD = 7; wild type = 5). Data represents mean ± SEM.

Disturbances of the endosomal/lysosomal system is thought to be involved in neuronal toxicity and Aβ accumulation [220]. Inhibition of Aβ secretion can lead to intra-neuronal Aβ accumulation in the endosomal/lysosomal compartment, which destabilizes its membrane leading to Aβ deposition in the cytosolic compartment [221-223]. To verify the presence of Aβo deposits in the brain and retinal endosomal/lysosomal, we co-stained *A11* and *LAMP2*, a marker against late endosome and lysosomes (**Figure 10**). Our data showed that Aβo co-localised with the lysosomal marker in the hippocampus, cortex and in the ONL, OPL, INL of the retina in all age groups (**Figure 10 A - F**). Our results strongly indicate binding of *A11* antibody in these organelles where clearance of Aβo is believed to occur. Finally, we confirmed that Aβo accumulation was in fact occurring in cerebral and retinal neurons as evident by co-staining with *NeuN* in all age groups (**Figure 10 G & H**). Moreover, Aβo deposits were more prominent in the retinal GCL and INL in the retina in the 6-month-old age group (**Figure 10 H**).

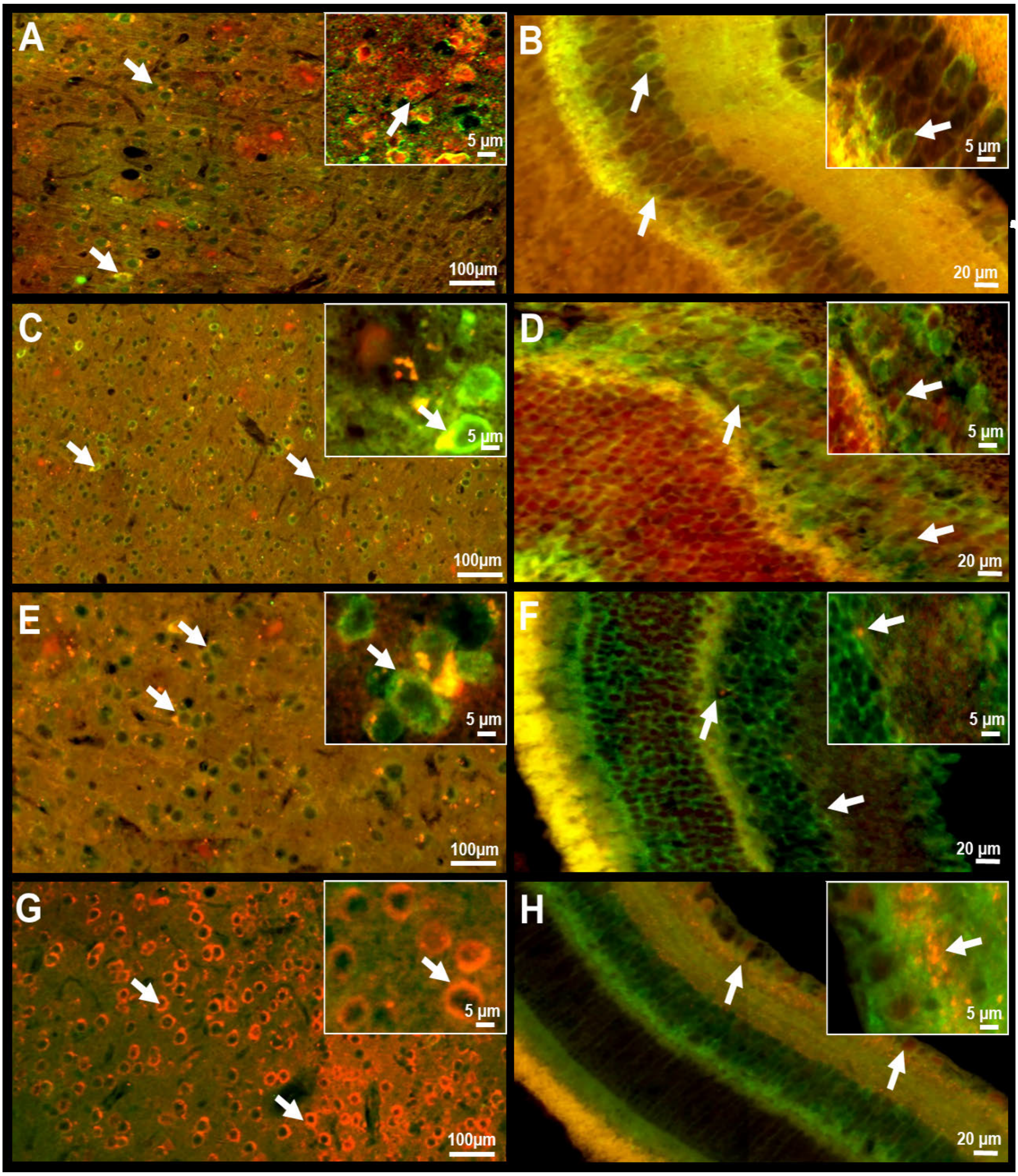

Figure10. Immunofluorescence co-localisation of retinal and cerebral amyloid-β oligomers with lysosomal-associated membrane protein 2 (LAMP2) or neuron-specific nuclear protein (NeuN). Retinal and cerebral co-staining with A11 rabbit anti-Aβo polyclonal IgG antibody (GREEN) and anti-mouse LAMP2 monoclonal IgG antibody (RED) of a 6, 12 and 17-month-old 5xFAD mice or anti-mouse NeuN monoclonal IgG antibody (RED) of a 6-month-old 5xFAD mouse. LAMP2 co-localised with Aβo in the (A, C and E) cerebral cortex and (B, D and F) in the GCL, IPL, INL, OPL and ONL of the retina in all age groups (arrows). Aβo localized to NeuN in the (G) hippocampus, and in the (H) GCL, IPL, INL and OPL of the retina in the 6-month-old age group (arrows). Representative of all affected mice in all age groups.

3.5. Discussion

One of the principal neuropathological lesions associated with Alzheimer's disease is the extracellular deposition of Aβ plaques [20]. Amongst the three major assemblies of Aβ, soluble oligomers are considered the most neurotoxic form and is the intermediary conformation recognized in early pathogenesis [39]. Soluble oligomers can lead to synaptic dysfunction, whereas large, insoluble deposits are believed to function as reservoirs of the bioactive oligomers [45]. In AD, Aβo are believed to form in the early phase of the disease and are present in blood and other tissues [74,224,225]. Current strategies for AD detection include measurement of CSF-borne $A\beta_{42}$ levels and amyloid positron emission tomography (PET) imaging [74]. However, these approaches are considered to be invasive, display a high degree of multicentre variability and are costly. A blood-based biomarker approach is gaining momentum as several groups have demonstrated its potential value, albeit work remains at experimental phase [226,227]. Since Aβo is considered the toxic species and accumulates in preclinical stage of the disease [52,228-230] several reports have demonstrated its potential as an early marker of the disease [231-233]. A recent study by Nakamura and colleagues has identified high-performance plasma Aβ biomarkers using a combination of immunoprecipitation and mass spectrometry [234]. These authors measured and compared $A\beta PP_{669-711}/A\beta_{1-41}$ and $A\beta_{1-40}/A\beta_{1-41}$ ratios in order to predict Aβ-PET imaging status in cognitively normal, mild cognitive impaired and Alzheimer's disease individuals and shown that this test was highly predictive of brain Aβ burden.

In this study, we set out to provide proof-of-concept for early retinal detection of AD through identifying and quantifying levels of retinal Aβo in an AD mouse model. The eye is not considered as a hermetic anatomical structure and the barriers that separate the eye from the periphery are not completely sealed [235]. The blood-ocular barriers comprise the blood-retinal and blood-aqueous barrier; the latter is formed by tight junctions of the inner non-pigmented ciliary epithelium and the non-fenestrated endothelial cells of the iris blood vessels [235]. In contrast and because of the fenestrated structure of the ciliary body blood vessels, plasma proteins and molecules can enter the stroma as part of aqueous humor production [235]. Therefore, there is a distinct possibility that blood borne-Aβo might reach different structures of the eye, including the retina, and this provides a great potential to develop a non-invasive retinal eye test for AD. Of note, eye inflammation leads to blood-ocular barrier disruption, which also results in increased vascular permeability, potentially allowing higher levels of Aβo to spread in all structures of the eye.

Visual disturbances are part of early complaints reported by AD patients [236]. These disturbances include reduced blood vessel diameter and venous blood flow. Studies by Berisha and colleagues [85] and Feke and colleagues [107] suggested that alterations in retinal blood flow can distinguish mild cognitive impairment and AD. Furthermore, a study by Hadoux and colleagues demonstrated significance differences in the retinal reflectance spectra when comparing PET-specific Aβ burden in mild cognitively impaired individuals with age-matched PET-negative control individuals [237]. The authors show a direct correlation between retinal imaging scores and cerebral Aβ plaque burden [237].

In this study, we used 5xFAD mice brain and retinal tissues for pathological assessment and immune-detection of age-dependent Aβo accumulation. H&E staining revealed vacuolations, neuronal loss and presence of eosinophilic aggregates in the neocortex and hippocampus of the brain but no obvious lesions were observed in the GCL and INL of the retina. We then used Congo red and ThT staining to demonstrate age-dependent accumulation of amyloid fibrils in the retina and brain of 5xFAD mice. We show that Congophilic-amyloid fibrils increased with age in the cortex and to a lesser extent in the retina. We wanted to verify whether the staining method was sensitive enough for the detection of retinal amyloid fibrils, hence we stained with ThT. This fluorescence reaction revealed staining of retinal amyloid fibrils in the GCL & INL of 5xFAD mice. Amyloid fibrils were observed in the neocortex and the inferior layer of the hippocampus of 6-month-old 5xFAD mice. In older 5xFAD mice amyloid fibrils were widely distributed throughout the cortex, hippocampus, brain stem and cerebellum. Furthermore, we used lesion specific markers for Immunodetection of Aβo and Aβ plaques. In young mice (6 months), we found high levels of Aβo in the hippocampus and neocortex and in retinal layers such as the GCL and INL, and to a lesser extent the IPL and ONL. Occasional Aβ plaques were also seen in the brain and retina of this age. The middle age group (12 months) displayed both Aβo and Aβ plaques in the brain. Retinal Aβo and to lesser extent Aβ plaques were observed in this age group, indicating that the retinal microenvironment is less efficient in sustaining plaque build-up. Finally, older 5xFAD mice (17 months) displayed widespread and extensive plaque burden in both brain and retina but only traces of Aβo. Taken together, these results strongly support the Aβo conversion to plaque paradigm in the brain. Studies by Kawarabayashi and colleagues [238] using the Tg2576 AD mouse model, showed that full-length unmodified Aβ was present in the brain of young littermates which then turned into soluble Aβo at 6-10 month of age, followed by insoluble forms of Aβ which increased exponentially and converted into diffuse plaques from 12 to 23 months. Similar findings were reported for the $A\beta PP^{sw}$-tau^{vlw} mouse model which displayed an age-dependent exponential increase of Aβo deposition followed by plaque build-up [239].

We extend previous experimental studies to show that Aβo strongly co-localizes with Aβ plaques in both brain and retina of 5xFAD mice. A similar pattern of age-related changes in Aβo and Aβ plaques was evident between the brain and retina of 5xFAD mice. Specifically, both show an initial accumulation of the toxic soluble Aβo entities that are converted into Aβ plaques with age.

In the 6-month-old 5xFAD mice, Aβo localised predominantly to the retinal inner and middle nuclear layers. This is an important finding as it provides a rationale for the development of imaging approaches for detecting AD manifestation in the retina. Liu and colleagues have shown that the majority of Aβ plaques were present in the GCL and IPL with some plaques found in the ONL, photoreceptor outer segment, and optic nerve in 14 month old Tg2576 mice [240]. That ours and other preclinical studies demonstrate a propensity for Aβo and Aβ plaques to localize to the inner retina is consistent with clinical observations of GCL and nerve fibre layer thinning and optic nerve degeneration in AD patients [241].

Koronyo-Hamaoui and colleagues [102] confirmed the presence of retinal Aβ plaques by systemic administration of curcumin in AβPP (SWE)/PS1 (ΔE9) mice. They confirmed presence of curcumin positive retinal Aβ plaques in the RNFL, GCL, IPL and OPL, and INL of the retina. The authors showed that plaques were detected as early as at 2.5 months of age which indicate that Aβ plaques in the retina precede brain plaques build-up. In our study, we detected both Aβo and Aβ plaques in the retinal layers of 6-month-old 5xFAD mice. Specifically, we found that Aβo was similar in the retinal layers when compared to levels in the brain of young mice. This suggest that detection of Aβo in the retina may be a sensitive marker for early diagnosis of AD. More work is required to understand the molecular 'behaviour' of both Aβo and Aβ plaques in the retina.

We confirmed that Aβo was found in neurons as evident by co-staining with NeuN [242,243]. It was previously reported that Aβ build-up is initiated in the intracellular compartments (reviewed by Bayer and colleagues [244]). This is consistent with other reports that $Aβ_{42}$ accumulates intraneuronally before being converted into extracellular plaques in human AD [242,245,246]. Our findings clearly show that Aβo localized to neurons in the hippocampus, neocortex and in various retinal layers, especially in the ONL, INL and GCL in 5xFAD mice across all ages. Aβ has been found in four intraneuronal compartments associated with the lysosomal system such as rab5-positive endosomes [221], autophagic vacuoles [247], lysosomes [248,249] and multivesicular bodies (MVBs) [250]. Inhibition of Aβ secretion can lead to accumulation of intra-neuronal Aβ in the lysosomal compartment and destabilizes its membrane and also deposits in the cytosolic compartment in the early AD pathogenesis [68]. In agreement, we show that Aβo co-localises to late endosomes in retinal cells, indicating that disturbance of the endocytic pathway leads to its accumulation [69,70].

3.6. Conclusion:

Our study demonstrated an age-dependent inversely proportional accumulation of Aβo versus Aβ plaques in the retina of a transgenic AD animal model. The presence of these toxic Aβ soluble oligomers was detected as early as 6 months of age in this animal model, probably mimicking prodromal human Alzheimer pathogenesis. More work is needed in earlier age groups perhaps using a less 'aggressive' animal model in order to prove that the toxic assemblies can be detected in the retina before identification of cognitive deficiencies. Studies are currently underway to establish this before the use of fluorescence confocal scanning laser ophthalmoscopy for the non-invasive detection of retinal Aβo preceding their accumulation in the brain.

Chapter 4

Results (Paper 2)

4- Detection of retinal and blood Aβ oligomers with nanobodies

Umma Habiba[1], Joseph Descallar[2,3] Fabian Kreilaus[1], Utpal K. Adhikari[1], Sachin Kumar[1], John W Morley[1], Bang V Bui[4], Maya K. Hamaoui[5], Mourad Tayebi[1]*

[1]School of Medicine, Western Sydney University, Campbelltown, New South Wales, Australia; [2]South Western Sydney Clinical School, Faculty of Medicine, UNSW, Liverpool Hospital, Liverpool, New South Wales, Australia; [3]Ingham Institute of Applied Medical Research, Liverpool, New South Wales, Australia; [4]Department of Optometry and Vision Sciences, University of Melbourne, Victoria, Australia; [5] Department of Neurosurgery, Maxine Dunitz Neurosurgical Research Institute and Department of Biomedical Sciences, Cedars-Sinai Medical Center, Los Angeles, California, USA

Journal: Alzheimer's & Dementia: Diagnosis, Assessment & Disease Monitoring
Received: 6 January 2021 | Revised: 13 April 2021| Accepted: 13 April 2021| Published online: 06 May 2021

4.1. Abstract

Introduction: Abnormal retinal changes are increasingly recognized as an early pathological change in Alzheimer's disease (AD). Although, amyloid beta oligomers (Aβo) have been shown to accumulate in the blood and retina of AD patients and animals, it is not known whether the early Aβo deposition precede their accumulation in brain.

Methods and results: Here, we report that using nanobodies targeting $A\beta_{1-40}$ and $A\beta_{1-42}$ oligomers we were able to detect Aβ oligomers in the retina and blood but not in the brain of 3-month old APP/PS1 mice. Furthermore, Aβ plaques were detected in the brain but not the retina of 3-month old APP/PS1 mice.

Conclusion: These results suggest that retinal accumulation of Aβ oligomers originates from peripheral blood and precedes cognitive decline and Aβ oligomer deposition in the brain. This provides a very strong basis to develop and implement an 'eye test' for early detection of AD disease using nanobodies targeting retinal Aβ.

Key words: Alzheimer's disease; Aβ oligomers; nanobodies; retinal immunodetection; blood immunodetection; early AD diagnosis; APP/PS1 mice

4.2. Introduction

The importance of Aβ oligomers (Aβo) detection has gained momentum and experimental studies using human AD samples have shown that this form can be detected as much as two decades before clinical onset of AD [41,251-253]. Aβo can potentially become a strong biomarker for early Alzheimer's disease (AD) detection and could provide accurate biochemical information about various preclinical stages of AD. Several investigators have shown experimentally that blood borne Aβo is a viable biomarker for human AD. A study by Nakamura and colleagues [234] has identified high-performance plasma Aβ biomarkers using a combination of immunoprecipitation and mass spectrometry and suggested that plasma Aβ ratio can predict brain Aβ burden. Plasma Aβ precursor protein $(APP)_{669–711}$/amyloid-β $(Aβ)_{1–42}$ and $Aβ_{1–40}/Aβ_{1–42}$ was correlated with brain Aβ levels determined by Aβ-PET imaging.

Ocular disturbances are early complaint in AD patients [190,191,193] with reported changes in color vision, contrast sensitivity, visual memory and perception [199,254,255], nerve damage and loss of nerve fibers [89], ganglion cell loss [203] and thinning of the retinal nerve fiber layer (RNFL) [82,256] have also been reported. A recent study by Coppola and colleagues [257] reported that RNFL thinning was associated with neurodegenerative progressions in mild cognitive impaired (MCI) and AD patients when compared to cognitively healthy individuals . Similar color vision and contrast sensitivity deficits were shown in a murine model of AD. In addition to neuronal changes in the retina, alteration of retinal blood flow and morphology have also been noted [85]. Importantly, Aβ deposits in the retina of AD patients were identified by histology [102] and *in vivo* imaging of MCI and AD patients [206]. Subsequent studies have corroborated these findings and showed accumulation of Aβ and hyperphosphorylated Tau (p-Tau) in the retina of AD patients [110,207,258] and animal models [259].

Nanobodies are camelid-derived antibody fragments with unique biological features, including lack of light chains, smaller size (more diffusible in tissues), hydrophilic (soluble in aqueous solution), highly stable, and more resistant against chemical denaturation [260]. Previous studies reported that nanobodies targeting Aβ and neurofibrillary tangles in mice brain parenchyma are able to cross the blood-brain barrier (BBB) [261]. Another study demonstrated that nanobodies specific for Aβ oligomers prevent neurotoxicity and fibril formation[262]. Moreover, Vandesquille and colleagues showed that nanobodies were able to detect cerebral Aβ plaque deposits via magnetic resonance imaging (MRI) following intravenous injection [263].

In the current study, we used nanobody anti-$A\beta_{1-40}$ (PrioAD12) and anti-$A\beta_{1-42}$ (PrioAD13) oligomer antibodies [173] to measure the levels of Aβo in the brain and retina of the APP/PS1 mice [261] at 3-4-month of age with immunohistochemistry (IHC), before behavioral changes and appearance of cognitive deficits. We showed that retinal $A\beta_{1-40}$ and $A\beta_{1-42}$ oligomer levels were significantly higher in APP/PS1 mice compared to age-matched WT controls. Furthermore, immunofluorescence (FL) analysis confirmed our IHC results and surprisingly resulted in the detection of large amounts of Aβo in the 18-month-old APP/PS1 age group. We also confirmed the localization of both $A\beta_{1-40}$ and $A\beta_{1-42}$ oligomers to neuronal late-endosomal compartments in the retina and brain [68] which was associated with activated astrocytes and microglia in APP/PS1 mice. Of importance, $A\beta_{1-40}$ and $A\beta_{1-42}$ levels in whole blood was quantified by Western blotting with the nanobodies were elevated in 3 and 18-month-old APP/PS1 mice compared with WT controls. The observation that Aβo was detectable in the retina and blood but not in the brain of young APP/PS1 mice suggests that deposition of retinal Aβo might originate from the blood. Taken together, our results provide an important milestone in achieving an ‘eye’ and /or blood-based screening test for AD.

4.3. Methods

4.3.1. Animals and Ethics Statement

All procedures followed the requirements of the National Health and Medical Research Council of Australia statement for the use of animals in research and were approved by the Western Sydney University Animal Ethics Committee (ACEC # A12905). Mice were housed with free access to water and standard rodent chow (Gordon's Specialty Stock Feeds; Yanderra, NSW Australia). APP/PS1 mice have the APP Swedish mutation K595N and M596L [264] and PSEN1 with L166P mutation controlled by the Thy1 promoter (ww.alzforum.org). Cognitive impairment is usually observed after seven months [265,266]. The APP/PS1 mouse model has high brain levels of $A\beta_{1-42}$ over $A\beta_{1-40}$ which increases with age [267,268]. Age-matched wild type (WT) littermates were used as a control.

4.3.2. Tissue collection and histological assessment

Mice were perfused with saline and followed with 10% neutral buffered formalin. Formalin fixed paraffin embedded blocks (FFPE) were prepared using 10% neutral buffered formalin as a fixative followed by graded ethanol and xylene. 6μm thick brain and eye tissue sections were cut using a microtome (Thermo-fisher Scientific, Massachusetts, United States). Sections were then deparaffinised with xylene and rehydrated through graded alcohols and finally washed with deionized water. Sections were finally stained with Haematoxylin & Eosin, Congo Red or Thioflavin-T.

4.3.2.1. Hematoxylin & Eosin staining

Hematoxylin & Eosin staining is used to assess the general morphological changes of tissue under the light microscope. Paraffin sections were dewaxed by two changes of xylene (5 minutes each), which was followed by the gradient alcohol dehydration. H&E stain was then performed by staining the specimen with Gill ll Haematoxylin stain (Leica bio systems, Wetzlar, Germany) followed by 1% acid alcohol and subsequently Eosin stain (Leica bio systems, Wetzlar, Germany). Finally, dehydrated with gradient alcohol, dewaxed by two changes of xylene and finally mounted with xylene based mounting media [269].

4.3.2.2. Congo Red staining

Congo Red (CR) is one of the general histological technique used to identify amyloid fibrils. Sections were placed in Congo red (Leica bio systems, Wetzlar, Germany) working solution for 20 minutes then rinsed in 5-8 changes of deionized water. This was followed by staining with Gill ll Haematoxylin (Leica bio systems, Wetzlar, Germany) for 1-3 minutes and rinsing in 3 changes of deionized water. Sections were dehydrated in two changes of 95% alcohol followed by three changes of absolute alcohol for one minute each. Finally, sections were cleared in two changes of xylene and mounted in a xylene miscible medium. Amyloid fibrils appeared as dull to red brick under light microscopy (Olympus CX 43, Shinjuku, Tokyo, Japan) and apple green birefringence under polarized light (Olympus CX 43, Shinjuku, Tokyo, Japan).

4.3.2.3. Thioflavin-T staining

Following deparaffinisation with xylene and ethanol, tissue sections were incubated with filtered 1% aqueous Thioflavin-T (Sigma-Aldrich, St. Louis, Missouri, United States) for 8 minutes at room temperature. Sections were then rinsed with 3 changes of deionized water and mounted in aqueous mounting media (Agilent, Santa Clara, California, United States). Finally, slides were sealed with clear nail polish and stored in a cold and dark area. Generally, Thioflavin-T binds to the side chain channels along the long axis of amyloid fibrils. Upon binding to amyloid fibrils, Thioflavin-T has a strong signal at excitation and emission maxima of 450 and 482 nm respectively under fluorescence microscopy (Olympus VS 120, virtual slide microscope).

4.3.3. Immunohistochemistry

APP/PS1 mice (n=28) and WT littermates (n=20) were first euthanized (Advanced Anesthesia Specialists, DarvallVet, Gladesville, NSW, Australia) before perfusion with saline followed with 10% neutral buffered formalin. Formalin fixed paraffin embedded blocks (FFPE) were prepared using 10% neutral buffered formalin as a fixative followed by graded ethanol and xylene. 6μm thick brain and eye tissue sections were cut using a microtome (Thermo-fisher Scientific, Massachusetts, USA). Sections were then deparaffinised with xylene and rehydrated through graded alcohols and finally washed with deionized water.

Sections were pre-treated using the 2100 antigen retriever (Aptum biologics Ltd, Southampton, United Kingdom) to expose the target epitopes. Sections were then treated with 90% formic acid for 5 minutes at room temperature followed by cell membrane permeabilization which was achieved by using 1% triton X for 1 min prior to addition of 0.3% H_2O_2 for 15 minutes to inactivate endogenous peroxidases. Sections were then blocked with Protein Block Serum-Free (Agilent, Santa Clara, California, United States) for 15 minutes. Sections were then stained for 1h with the following primary antibodies in PBS: anti-Aβ_{1-40} (PrioAD12), anti-Aβ_{1-42} (PrioAD13) antibodies (1: 500) [173] or mouse anti-Aβ purified *4G8* antibody (1:500; Bio legend, San Diego, California, USA). After washing with PBS, sections were incubated for 1h at RT with secondary antibodies in PBS: HRP-conjugated anti-llama IgG (Bethyl Laboratories, Inc, Texas, USA) or anti-mouse IgG (Sigma-Aldrich, St. Louis, Missouri, United States), Sections were then washed in PBS (x3) before addition of DAB substrate chromogen system and incubated for 5–10 minutes. Slides were then counterstained with hematoxylin for 1 min. The Olympus VS 120 Slide Scanner was used to visualize images and the Olympus *OlyVIA* and Olympus *cellSens* Imaging Software (Olympus, Shinjuku, Tokyo, Japan) was used for analysis.

4.3.4. Immunofluorescence co-localization studies

Double immuno-labelling was achieved by two different fluorescent labels, each having a separate emission wavelength. Sections were incubated overnight with anti-Aβ_{1-40} (PrioAD12), anti-Aβ_{1-42} (PrioAD13) or *4G8* antibody at 4°C. Furthermore, sections were also incubated with camelid antibodies and mouse anti-lysosomal-associated membrane protein 2 (*LAMP2,* Stressgen Bio reagents Corp, Victoria, British Columbia, Canada) antibody to assess whether Aβo localizes to lysosomes/ late endosomes. Sections derived from the 3-4-month old group were incubated with camelid antibodies and *GFAP* or Iba1 (Thermo-fisher Scientific). Finally, sections were incubated with camelid-derived antibodies and anti-NeuN mAb, clone *A60* (Merck Millipore, Massachusetts, United States) to confirm the intra-neuronal localization of the Aβ oligomers. All the sections were incubated overnight at 4°C. After washing with PBS, sections were then incubated with goat anti-llama IgG conjugated to FITC (Bethyl Laboratories, Inc, Texas, USA) and donkey-anti-mouse IgG conjugated to Texas red (Sigma-Aldrich) for 2h at 4°C. Sections were then mounted using fluorescence mounting media (Agilent, Santa Clara, California, United States) then visualised using Olympus VS 120 Slide Scanner with a standard FITC / Texas Red double band-pass filter set.

4.3.5. Image quantification

For the quantification of the age dependent accumulation of Aβp and Aβo, we used three sections derived from the 3-4 months old APP/PS1 (n=8) and WT (n=8) mice as well as the 17-18 months old APP/PS1 (n=8) and WT (n=8) mice. Three different areas of hippocampus, cerebral cortex and retinal sections were analyzed. Immunohistochemical signal intensity was visualized by capturing bright field images using the Olympus VS 120 Slide Scanner. Images were analyzed using '*Olympus OlyVIA'* software [270,271]. Age-dependent accumulation of Aβp and Aβo in APP/PS1 mice was quantified using image processing software, *cellSense* (Olympus, Shinjuku, Tokyo, Japan). The mean intensity of particles was calculated in several brain and retinal regions from each age group and the result was presented as percentage intensity and expressed as mean ± S.E.M.

4.3.6. Immunoprecipitation and Western blot analysis of beta-amyloid oligomers in whole blood

In order to measure blood levels of Aβo in APP/PS1 mice, we performed immunoprecipitation to enrich/isolate Aβ from 3-4 and 17-18 month old mice as described [171]. Samples were loaded on pre-cast gels (Bio-Rad, California, United States) and electrophoresed and 1μg/ml of nanobody $A\beta_{1-40}$ (PrioAD12), $A\beta_{1-42}$ (PrioAD13) anti-oligomer antibodies [173] or A11 rabbit-anti-Aβo antibody (Merck Millipore, Massachusetts, United States) was added followed by anti-llama (Bethyl Laboratories, Montgomery, Texas, USA) or anti-rabbit IgG (Sigma-Aldrich St. Louis, Missouri, USA) HRP conjugated antibody. The resulting digital images were analysed with 'Image-J' processing program for the densitometry analysis and the values were compared between the transgenic APP/PS1 and WT controls.

4.3.6.1. Immunoprecipitation of Aβo in whole blood

APP/PS1 mice and wild type littermates (total of 20 wild type and 28 APP/PS1 mice) were first euthanized (AAS- Advanced Anesthesia Specialists) before blood samples were collected by cardiac puncture. Tubes coated with anti-coagulant were used to collect the blood samples used for subsequent immunoprecipitation. In order to measure levels of Aβo in APP/PS1 mice, we performed immunoprecipitation to enrich/isolate Aβ from blood of 3-4- and 17-month-old mice as described previously [171]. Briefly, 1×10^6 Dynabeads pre-coated with anti-Rabbit IgG (Invitrogen, Massachusetts, United States) were rinsed with PBS before adding 1mg/ml of rabbit anti-Aβo *A11* antibody (Merck Millipore, Massachusetts, United States) and incubated overnight at 4˚C, with rotation. The *Dynabeads-A11* complexes were then washed four times with PBS and stored at 4˚C until further use. The blood samples were collected in EDTA-coated tubes and mixed at 1:1 ratio with blood lysis buffer (200 ml Ammonium chloride lysis solution with 70% formic acid, 0.1% triton X and protease inhibitors). The solution was incubated for 15 minutes at room temperature, with gentle rotation before addition of the *Dynabeads-A11* complexes and the mixture was incubated overnight with rotation at 4˚C. Next day, the *Dynabeads-A11- Aβo* complexes were washed four times in PBS and resuspended in laemmli buffer before heating to 95˚C for 5 min. Finally, the solutions were left to cool down then used for the subsequent western blotting.

4.3.6.2. Western blot analysis of Aβo in whole blood

Samples were loaded on pre-cast gels (Bio-Rad, California, United States) and electrophoresed at a constant voltage of 100 V for 1.30 hours. Following electrophoresis, gels were blotted onto PVDF membranes (Bio-Rad, California, United States) at 18V for 2 hours. The membranes were rinsed in TBS-tween (0.05%) (TBST) and transferred to blocking solution (5% nonfat dried milk diluted in TBST for 60 min at room temperature. The membranes were rinsed once in TBS-tween (0.05%) to remove the blocking solution, before adding 1mg/ml of nanobody $A\beta_{1-40}$ (PrioAD12), $A\beta_{1-42}$ (PrioAD13) anti-oligomer antibodies [173] or *A11* rabbit-anti-Aβo antibody (Merck Millipore, Massachusetts, United States) overnight at 4˚C. A rabbit-anti-β-actin antibody (Thermo-Fisher Scientific, Massachusetts, USA) was also used as a loading control. Following 4 washes of 5 min each with TBS-tween (0.05%), the membranes were then incubated with anti-llama (Bethyl Laboratories, Inc, Texas, USA) or anti-rabbit IgG (Sigma-Aldrich St. Louis, Missouri, USA) HRP conjugated antibody (1: 10,000) at room temperature for 1 h. The membranes were washed then developed using the Clarity™ Western ECL Substrate (Bio-Rad, California, United States), according to the manufacturer's instructions before visualizing with iBright FL1500 imaging system (Thermo-Fisher Scientific, Massachusetts, USA). Finally, the resulting digital images were analysed with 'Image-J' processing program for the densitometry analysis and the values were compared between the transgenic APP/PS1 and wild type controls.

4.3.7. Statistical Analysis

Statistical analyses were performed using SAS Enterprise Guide Version 8.2. A natural logarithm transformation was applied to the measurements. Shapiro-Wilk's test was used to determine normality. Group differences were analyzed by Wilcoxon-Mann-Whitney test due to non-normality. The blood borne Aβo performance at 3-4 months when predicting Aβp at 17-18 months in both brain and eye was not performed since these data weren't measured on the same animal over time. There were 36 comparisons overall so a Bonferroni correction of 0.05

/ 36 = 0.0014 was applied, meaning p-values less than this value were considered statistically significant.

Table 1. Age-dependent accumulation of Aβ oligomers and plaques in the blood, retina, and brain of APP/PS1 mice

Age groups (months)	PRIOAD12 ($A\beta_{1-40}$) or PRIOAD13 ($A\beta_{1-42}$)				4G8 (Aβ plaques)		
	Blood	Retinal Layers	Brain		Retinal Layers	Brain	
			Cerebral cortex	Hippocampus		Cerebral cortex	Hippocampus
3-4 (n=16)	present	present	absent	absent	absent	absent	absent
8-11 (n=16)	Nd *	present	present	present	present	present	present
17-18 (n=16)	present	absent	absent	absent	present	present	present

Abbreviations: Aβ, amyloid beta; Nd, Not determined.

4.4. Results

4.4.1. Histological assessment of retinal and cerebral lesions in APP/PS1 mice

H&E staining was used to observe microscopical neuropathological lesions associated with AD [272], including neuronal loss, vacuolations and eosinophilic deposits. No lesions were observed in the 3-4-month-old APP/PS1 age group **(Figure 1 A & B)**. However, neuropathological lesions were first observed in the cerebral cortex and hippocampal region of the brain at 8-month-old in APP/PS1 mice (data not shown) and as disease progressed, the neuropathology becomes more conspicuous and widespread in the 18-month-old APP/PS1 age group as reflected by the presence of extensive neuronal loss, vacuolations and eosinophilic deposits in the brain **(Figure 1 D & E)**. Moreover, these types of lesions were not seen in the retina of all age groups of APP/PS1 tested **(Figure 1 C & F)**. Wild type mice littermate also failed to display neuropathological lesions in the brain and retina in all age groups of APP/PS1 mice tested **(Figure 1 G, H & I).**

4.4.2. Detection of retinal and cerebral beta amyloid fibrils with Congo red and Thioflavin-T staining

Extracellular deposition of Aβ plaques is a major distinctive neuropathological feature associated with AD [20,175]. Congo red (CR) and Thioflavin-T (Th-T) staining were used to assess the age-dependent accumulation of amyloid fibrils in the brain and retina of APP/PS1 mice and wild type littermates, starting from 3- to 18-month-old **(Figure 2 and 3)** [272]. We have also compared the fibrillary amyloid load in the brain and retina of different age groups of mice **(Figure 2 & 3).** We show that amyloid fibril deposits were absent in the brain and retina of the 3-4-month-old APP/PS1 mice following staining with CR (**Figure 2 A, B & C).** Absence of the Congophilic depositions were also confirmed by cross-polarized light in this age group that normally appear appeared as apple-green birefringence **(Figure 2 D, E and F**). Congophilic red-brick deposits were present in the cerebral cortex and hippocampus **(Figure 2 G & H)** as well as retinal inner plexiform layer (IPL), inner nuclear layer (INL) and outer plexiform layer (OPL) **(Figure 2 I)** of 18-month-old APP/PS1 mice respectively. The Congophilic depositions were also confirmed by cross-polarized light and appeared as apple-green birefringence **(Figure 2 J, K & L)**. Furthermore, ThT staining was more pronounced in the brain neocortex, hippocampus **(Figure 3A & B)** and in the GCL, IPL, INL, OPL of the retina of 18-month old APP/PS1 mice when compared to CR staining **(Figure 3 C).** However, no ThT-specific amyloid fibrils were detected in the brain and retina of 3-4-month-old APP/PS1 age group (**Figure 3 D, E & F**). Wild type littermates did not display any ThT-specific deposits (Data not shown).

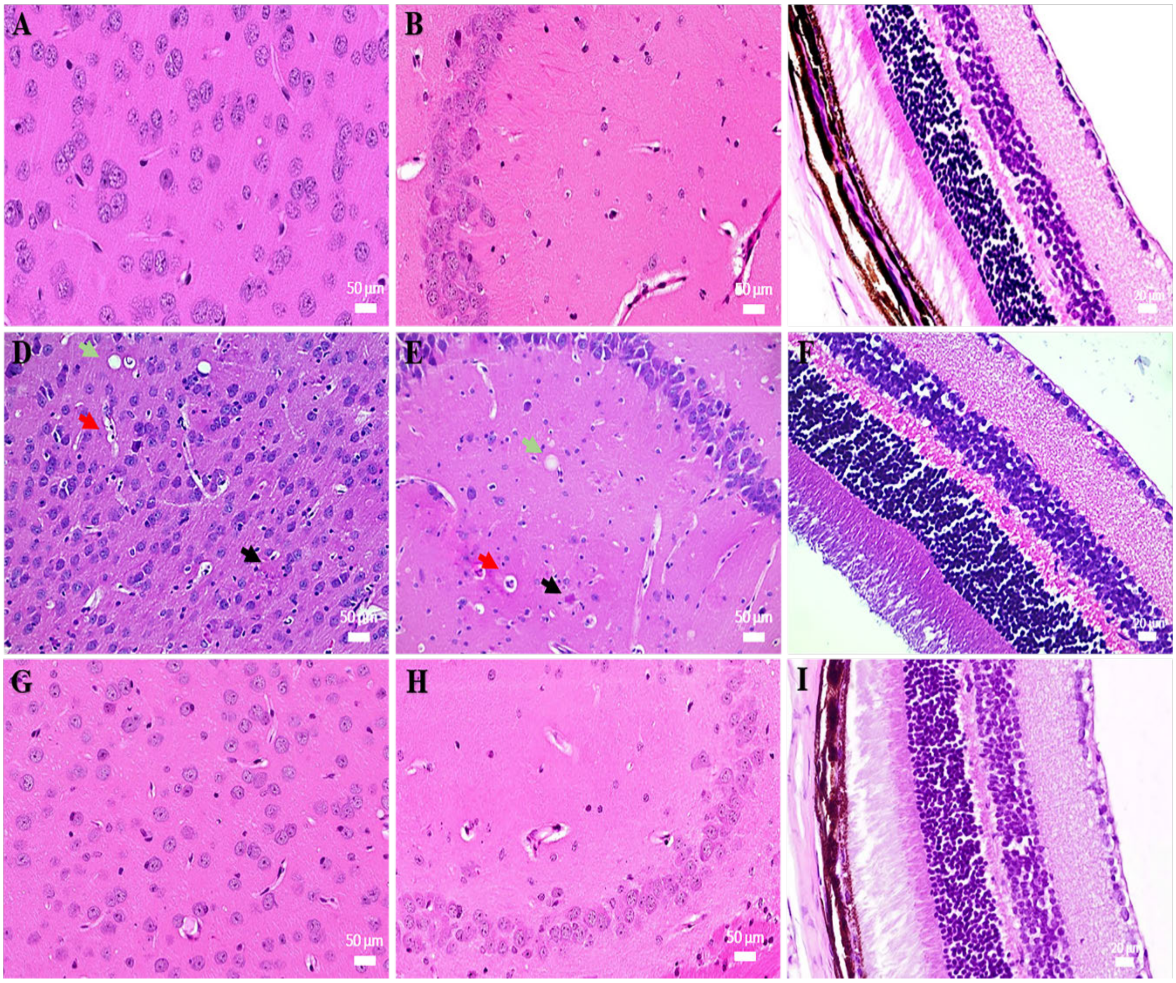

Figure 1. Photomicrographs of the microscopic lesions in the brain and retina of APP/PS1 and wild type mice. Normal appearance of the A) brain cerebral cortex; B) hippocampus and C) retina in the 3-month-old APP/PS1 age group following H&E staining. No histological lesions were observed in this age group following staining with H&E. The photomicrograph was derived from peripheral region of the retina away from the optic disc. Widespread vacuolations (green arrow), neuronal death (red arrow) and eosinophilic structures (black arrows) were observed in the D) cortical and E) hippocampal region of the brain of the 18-month-old APP/PS1 mouse following staining with H&E. F) Normal appearance of the retina of the 18-month-old APP/PS1 mouse following staining with H&E. The photomicrograph was derived from peripheral region of the retina - away from the optic disc. Normal appearance of the G) brain cerebral cortex; H) hippocampus and I) retina in the 3-month-old wild type mouse following H&E staining. The photomicrograph was derived from peripheral region of the retina away from the optic disc. Representative of all affected mice in this age group.

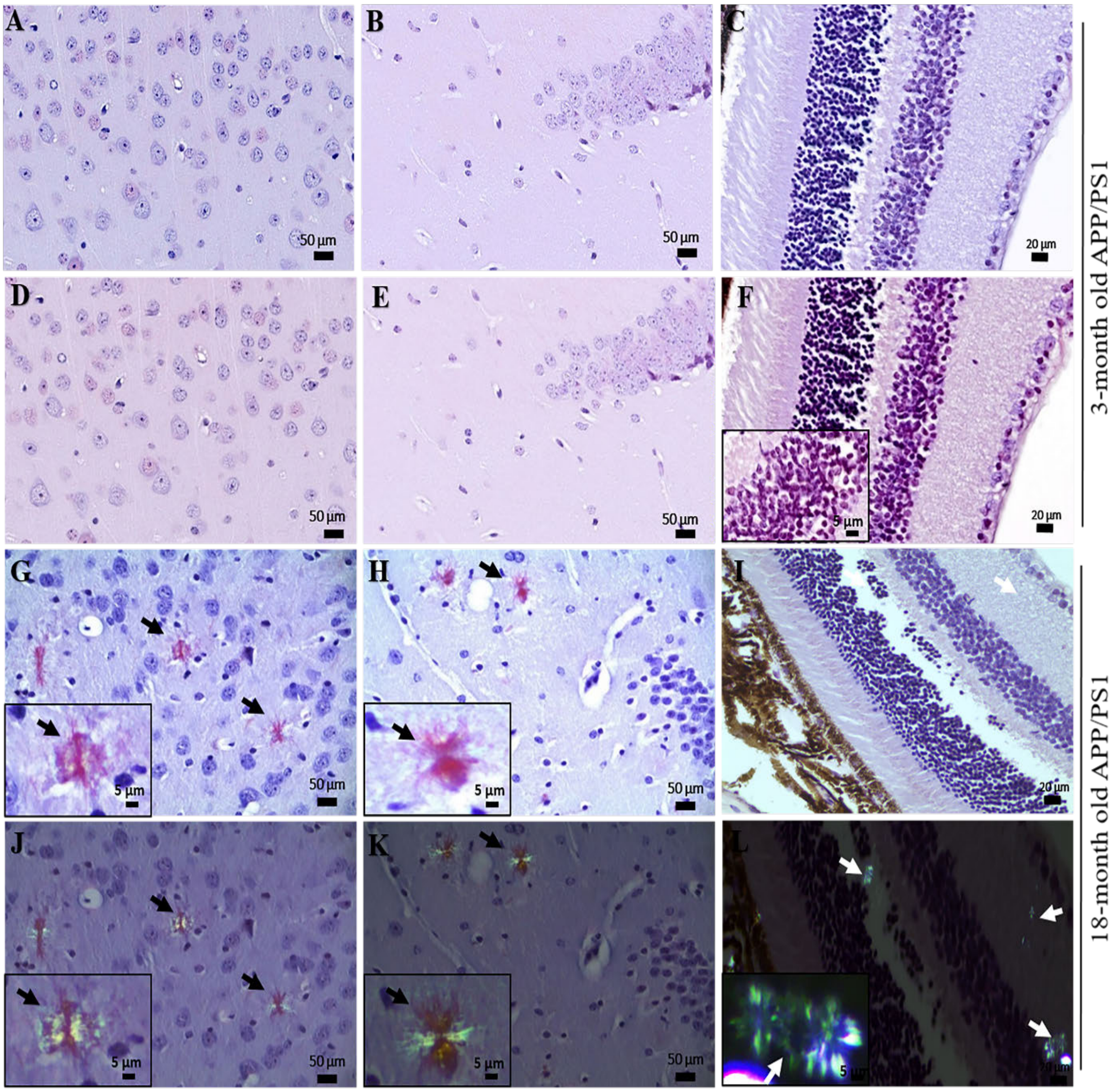

Figure 2. Photomicrographs of Congo red specific amyloid fibrils in the brain and retina of APP/PS1 mice. No distinctive red-brick staining of amyloid fibrils and apple-green birefringence with Congo red staining were observed in the brain A, D) cortical region, B, E) hippocampus and C, F) the retina of a 3-month-old APP/PS1 mice. Distinctive red-brick staining of amyloid fibrils with Congo red staining in the brain (black arrows) G) cortical region, H) hippocampus and I) IPL and INL of the retina (white arrows) of 18-month-old APP/PS1 mice. The photomicrograph was derived from peripheral region of the retina - away from the optic disc. The presence of the amyloid fibrils was confirmed with the presence of apple-green birefringence in the brain (black arrows) J) cortical region, K) hippocampus and L) retina (white arrows) under polarized light. Representative of all affected mice in this age group.

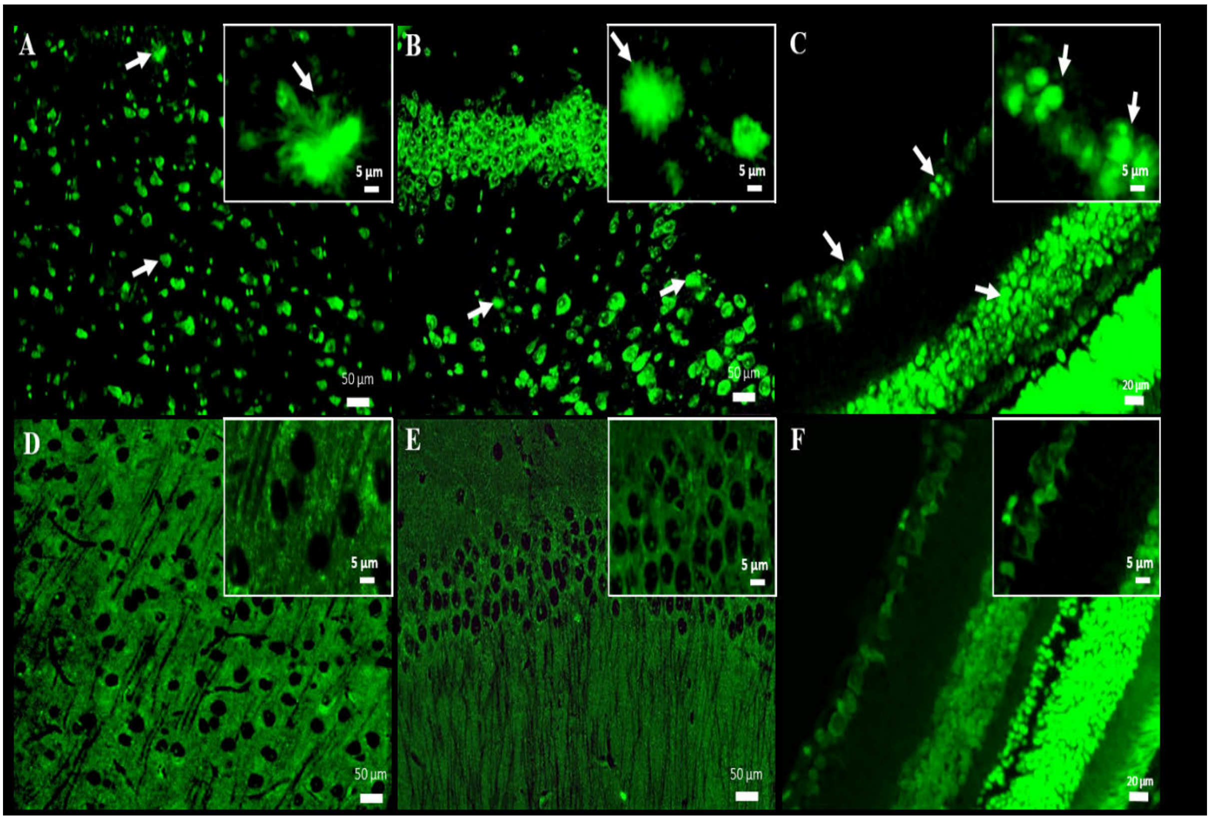

Figure 3. Photomicrographs of Thioflavin-T specific amyloid-β fibrils in the brain and retina of APP/PS1 mice. Distinctive amyloid fibrils with Thioflavin T staining in the brain (arrows) A) cortical region, B) hippocampus and C) INL and GCL of the retina (arrows) of 18-month-old APP/PS1 mice. The photomicrograph was derived from peripheral region of the retina away from the optic disc. No distinctive ThT-specific amyloid fibrils were observed in the brain D) cortical region, E) hippocampus and F) the retina of 3-month-old APP/PS1 mice. Representative of all affected mice in this age group**.**

4.4.3. Immunodetection of beta amyloid plaques and oligomers in the brain and retina of APP/PS1 mice using single-domain antibodies

In this study, we wanted to test the hypothesis that retinal Aβo accumulation precedes neurobehavioral deficits but also predates brain deposition of both Aβo and Aβp in young APP/PS1 mice using single-domain camelid derived anti-Aβo antibody fragments and the 4G8 anti-Aβp antibody (**Table 1 & Figure 4-7**). Of note, the single-domain antibody fragments, called PrioAD12 and PrioAD13 were previously shown to bind to $A\beta_{1-40}$ and $A\beta_{1-42}$ respectively [173]. Here, we showed widespread intra-neuronal $A\beta_{1-40}$ and $A\beta_{1-42}$ oligomers in the retinal inner nuclear layer (INL), outer nuclear layer (ONL) and ganglion cell layer (GCL) of the 3-month old APP/PS1 mice (**Figure 4 C & F**); in contrast, no Aβo depositions were seen in the brains at the same age (**Figure 4 A, B, D & E**), indicating that retinal Aβo accumulation precedes its appearance in the brain. Furthermore, no 4G8-specific Aβp was found in the brain and retina of the 3-month old APP/PS1 mice (**Figure 4 G, H & I**). Interestingly, both $A\beta_{1-40}$ and $A\beta_{1-42}$ were detected at 8-month of age in the cerebral cortex and hippocampus of APP/PS1 mice (**Figure 5 A, B, D & E**) as well as in the retina similar to 3-month old APP/PS1 mice (**Figure 5 C & F**). 4G8-specific Aβp was also observed in the cerebral cortex, hippocampus and INL of the retina at 8-month (**Figure 5 G, H & I**). Both Aβo and Aβp were detectable in the cerebral cortex, hippocampus and retinal layers of 11-month old APP/PS1 mice (**Figure 6**). Finally, no Aβo were detected in 18-month old APP/PS1 mice (**Figure 7 A, B, C, D, E & F**), whereas extensive, widespread and conspicuous Aβp was observed in the cerebral cortex, hippocampus (**Figure 7 G & H**) and retinal INL (**Figure 7 I**). No Aβo or Aβp deposits were seen in age-matched WT littermates (data not shown). Overall or data confirms that Aβo deposits first appear in the retina months before they are detectable in the brain and support the proposition that the retinal oligomers probably originate from the blood [112]. These results also validate our previous findings that showed Aβp burden increased over the course of the disease in both brain and retina, whereas Aβo levels appeared to decrease in an age-dependent manner [272].

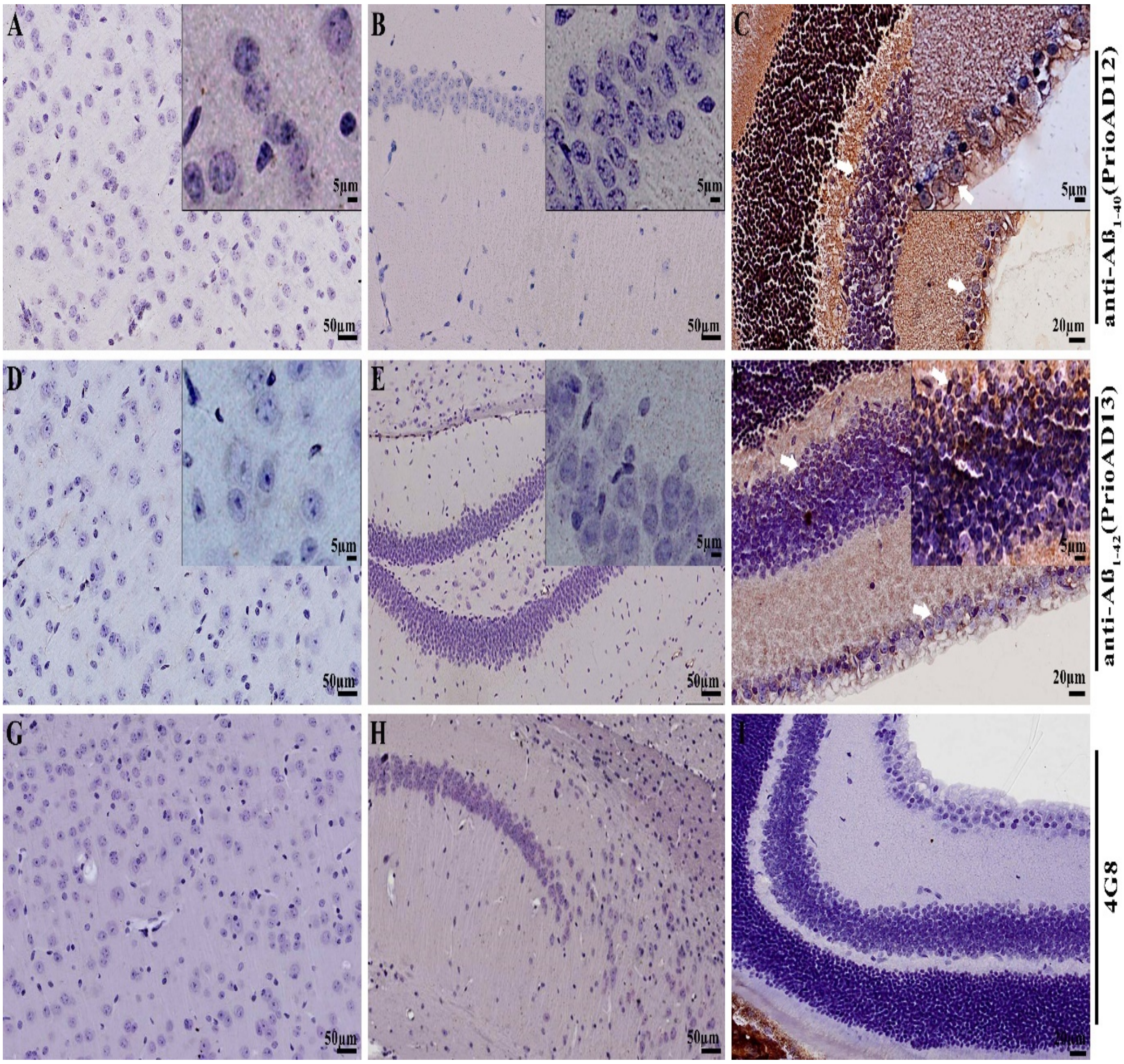

Figure 4. Immunohistochemical staining of amyloid beta (Aβ) in the brain and retina of 3-month-old APP/PS1 mice. Immunohistochemical staining with anti-$A\beta_{1\text{-}40}$ and anti-$A\beta_{1\text{-}42}$ oligomer nanobodies and 4G8 anti-Aβ plaque antibody of 3-month-old APP/PS1 mice. Immunohistochemical staining with anti-$A\beta_{1\text{-}40}$ (PrioAD12) and anti-$A\beta_{1\text{-}42}$ (PrioAD13) nanobodies of a 3-month-old APP/PS1 mice did not demonstrate $A\beta_{1\text{-}40}$ depositions in the (A) cerebral cortex and (B) hippocampus as well as $A\beta_{1\text{-}42}$ depositions in the (D) cerebral cortex and (E) hippocampus. Aβ1-40 and $A\beta_{1\text{-}42}$ depositions were observed in the (C, F) ganglion cell layer (GCL), inner nuclear layer (INL), and outer nuclear layer (ONL) of the retina. The photomicrograph was derived from peripheral region of the retina away from the optic disc. Immunohistochemical staining with 4G8 antibody of 3-month-old APP/PS1 mice did not display characteristic extracellular Aβ plaques in the (G) hippocampus, (H) cerebral cortex, and (I) retina. Representative of all affected mice in this age group

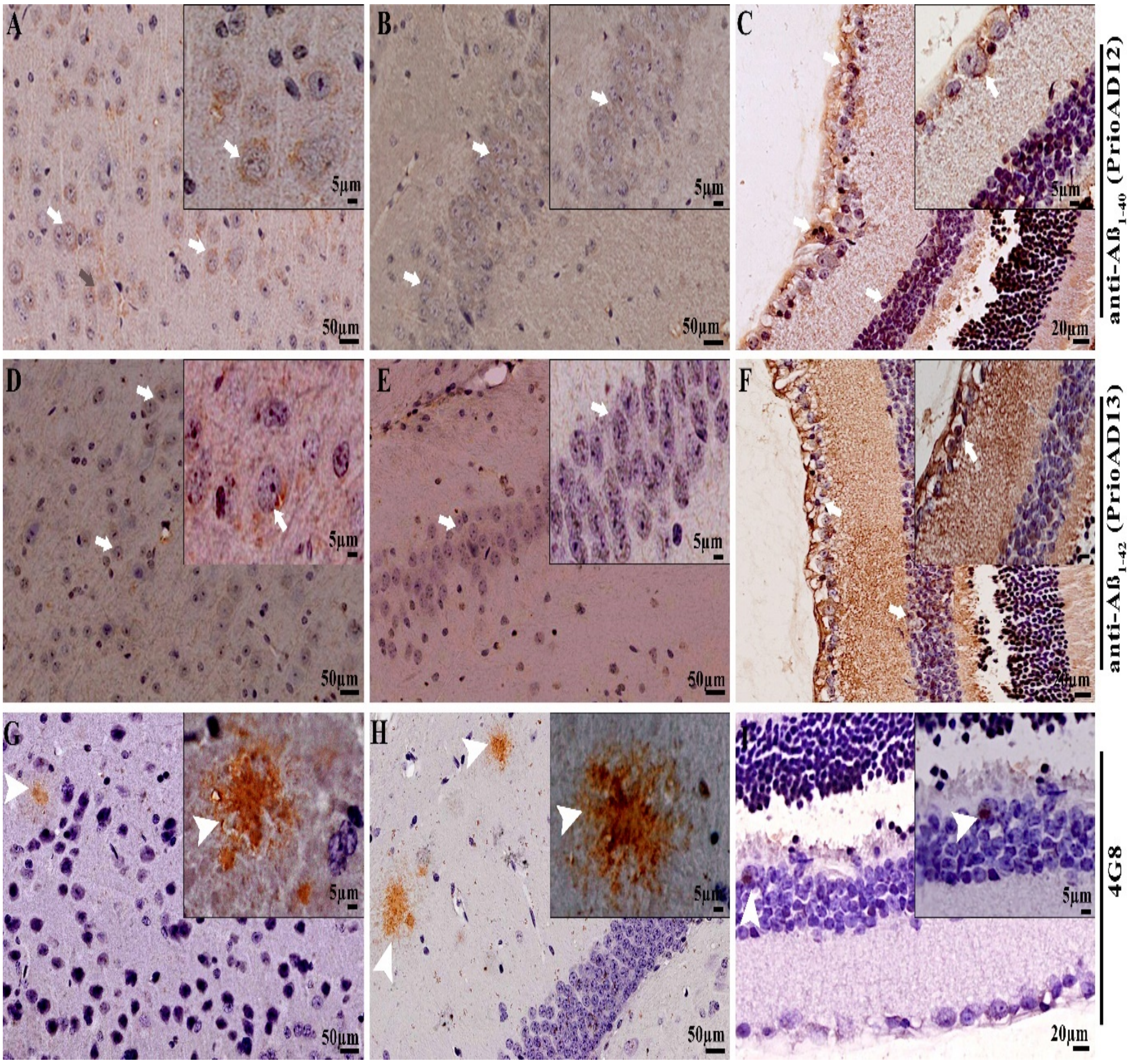

Figure 5. Immunohistochemical staining of amyloid beta (Aβ) in the brain and retina of 8-month-old APP/PS1 mice. Immunohistochemical staining with anti-$A\beta_{1-40}$ and anti-$A\beta_{1-42}$ oligomer nanobodies and 4G8 anti-Aβ plaque antibody of 8-month-old APP/PS1 mice. Immunohistochemical staining with anti-$A\beta_{1-40}$ (PrioAD12) and anti-$A\beta_{1-42}$ (PrioAD13) nanobodies of 8-month-old APP/PS1 mice showed presence of $A\beta_{1-40}$ depositions in the (A) cerebral cortex and (B) hippocampus as well as $A\beta_{1-42}$ depositions in the (D) cerebral cortex and (E) hippocampus. $A\beta_{1-40}$ and $A\beta_{1-42}$ depositions were observed in the (C, F) ganglion cell layer (GCL), inner nuclear layer (INL), and outer nuclear layer (ONL) of the retina. The photomicrograph was derived from peripheral region of the retina away from the optic disc. Immunohistochemical staining with 4G8 antibody of 8-month-old APP/PS1 mice displayed extensive extracellular Aβ plaque staining in the (G) hippocampus, (H) cerebral cortex, and (I) retina. Representative of all affected mice in this age group

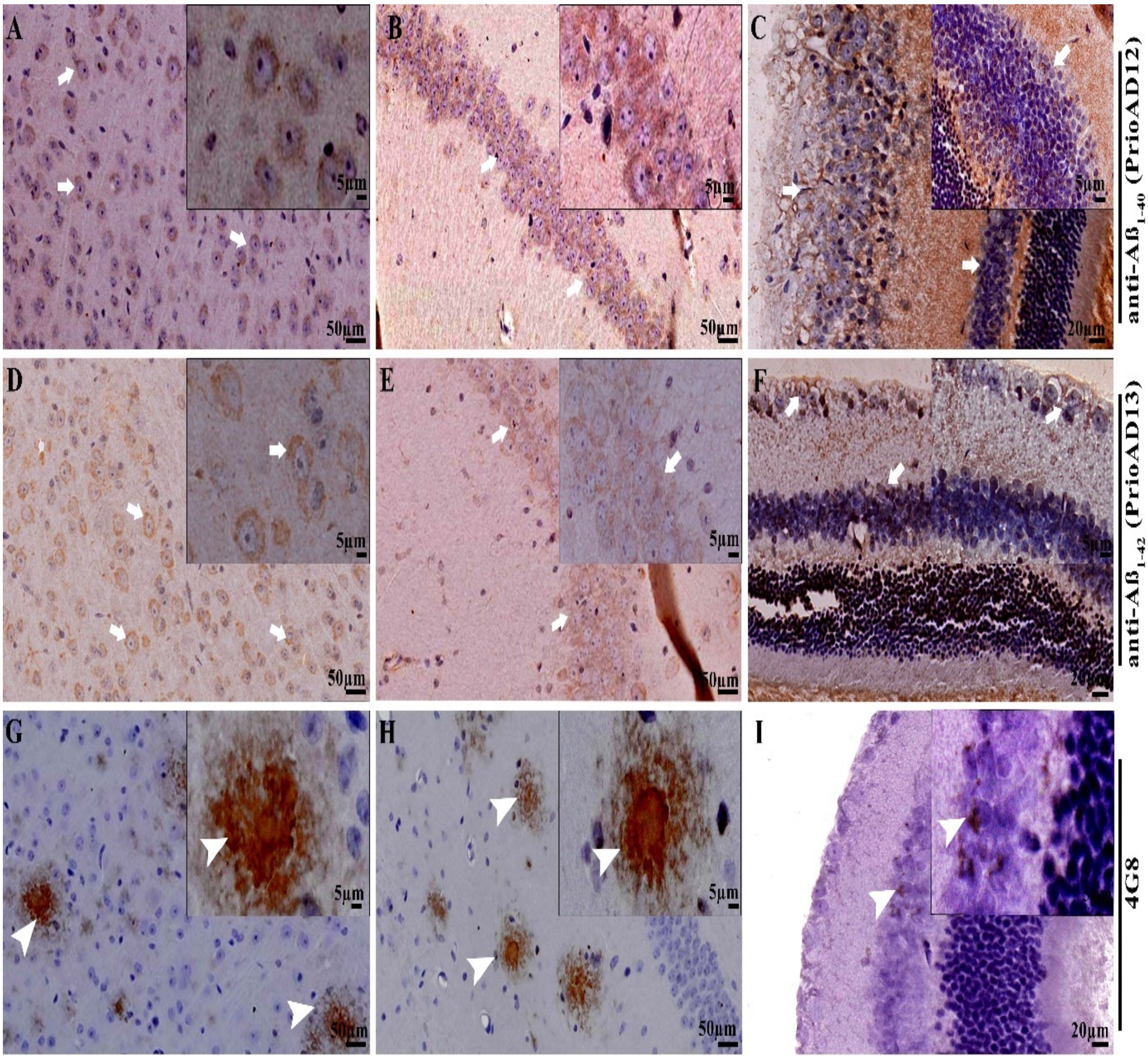

Figure 6. Immunohistochemical staining of amyloid beta (Aβ) in the brain and retina of 11-month-old APP/PS1 mice. Immunohistochemical staining with anti-$A\beta_{1\text{-}40}$ and anti-$A\beta_{1\text{-}42}$ oligomer nanobodies and 4G8 anti-Aβ plaque antibody of 11-month-old APP/PS1 mice. Immunohistochemical staining with anti-$A\beta_{1\text{-}40}$ (PrioAD12) and anti-$A\beta_{1\text{-}42}$ (PrioAD13) nanobodies of 11-month-old APP/PS1 mice showed presence of $A\beta_{1\text{-}40}$ oligomer depositions in the (A) cerebral cortex and (B) hippocampus as well as $A\beta_{1\text{-}42}$ oligomer depositions in the (D) cerebral cortex and (E) hippocampus. $A\beta_{1\text{-}40}$ and $A\beta_{1\text{-}42}$ depositions were observed in the (C, F) ganglion cell layer (GCL), inner nuclear layer (INL), and outer nuclear layer (ONL) of the retina. The photomicrograph was derived from peripheral region of the retina—away from the optic disc. Immunohistochemical staining with 4G8 antibody of 11-month-old APP/PS1 mice displayed extensive extracellular Aβ plaque staining in the (G) hippocampus, (H) cerebral cortex, and (I) retina. Representative of all affected mice in this age group.

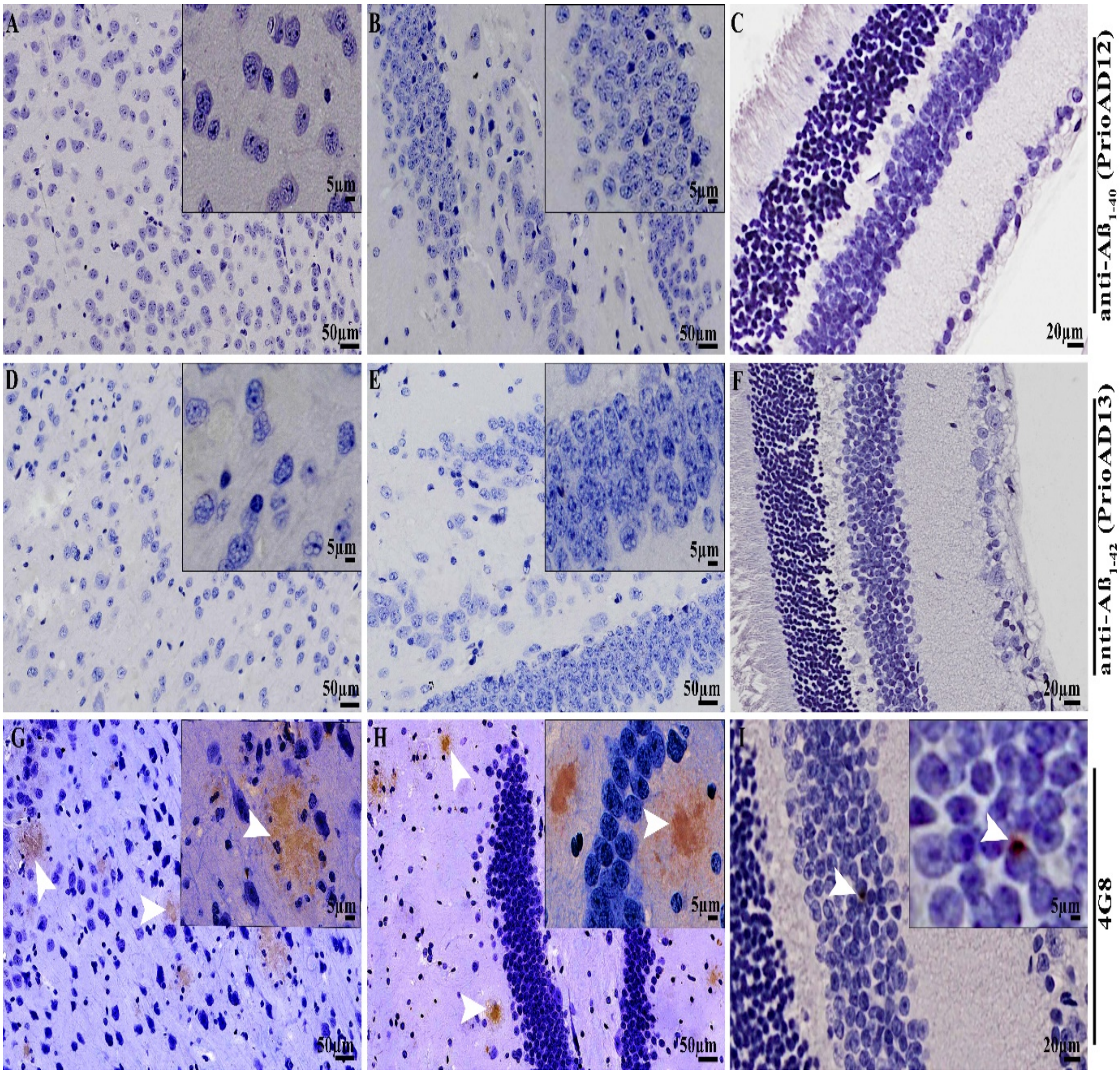

Figure 7. Immunohistochemical staining of amyloid beta (Aβ) in the brain and retina of 18-month-old APP/PS1 mice. Immunohistochemical staining with anti-$A\beta_{1-40}$ and anti-$A\beta_{1-42}$ oligomer nanobodies and 4G8 anti-Aβ plaque antibody of 18-month-old APP/PS1 mice. Immunohistochemical staining with anti-$A\beta_{1-40}$ (PrioAD12) and anti-$A\beta_{1-42}$ (PrioAD13) nanobodies of 18-month-old APP/PS1 mice did not show presence of $A\beta_{1-40}$ depositions in the (A) cerebral cortex and (B) hippocampus as well as $A\beta_{1-42}$ in the (D) cerebral cortex and (E) hippocampus. $A\beta_{1-40}$ and $A\beta_{1-42}$ depositions were not observed (C, F) in the ganglion cell layer (GCL), inner nuclear layer (INL), and outer nuclear layer (ONL) of the retina. The photomicrograph was derived from peripheral region of the retina away from the optic disc. Immunohistochemical staining with 4G8 antibody of 18-month-old APP/PS1 mice displayed extensive extracellular Aβ plaque staining in the (G) hippocampus and (H) cerebral cortex and (I) plaques were observed in the retina (white arrows). Representative of all affected mice in this age group.

4.4.4. Quantitative analysis of beta amyloid plaques and oligomers in the brain, retina, and whole blood of APP/PS1 mice using single-domain antibodies

Age-dependent retinal and brain accumulation of Aβp and Aβo in the 3-4-month old APP/PS1 mice (n=8) and wild type littermates (n=8) was quantified and compared with Aβp and Aβo levels in the 17-18-month old APP/PS1 mice (n=8) and wild type littermate (n=8) **(Table 2, Table 3 & Figure 8).** A total of three different areas of retina, hippocampus and cerebral cortex of each section (32 x 3 sections) were analyzed. **Figure 8** shows the normalized intensity of retinal and brain Aβ as measured by the *cellSense* image processing software and the values for $A\beta_{1-40}$ (PRIOAD12 antibody), $A\beta_{1-42}$ (PRIOAD13 antibody) and total Aβ (4G8 antibody). We found that the normalized intensity of retinal $A\beta_{1-40}$ and $A\beta_{1-42}$ oligomers were significantly higher in 3-4-month old when compared to the 17-18-month old APP/PS1 mice (P = 0.0002) **(Table 2 & 3),** whereas normalized intensity of brain Aβp were significantly higher in the retina and brain of 17-18-month old when compared to the 3-4-month old APP/PS1 mice (P = 0.0002) **(Table 2 & 3; Figure 8).**

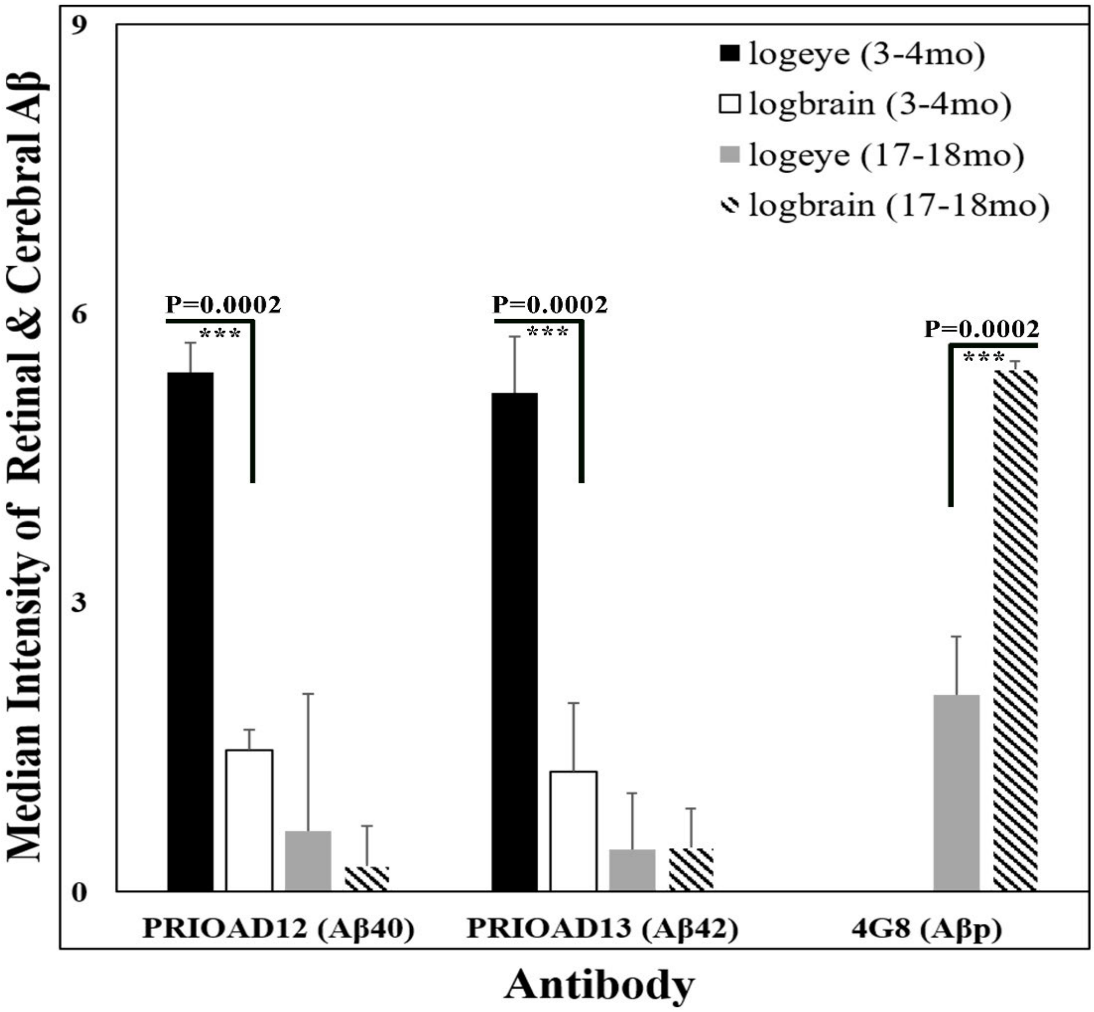

Figure 8. Quantification of the age dependent accumulation of cerebral and retinal Aβ oligomers and Aβ plaques with nanobodies: Immunodetection and quantification of retinal and cerebral $A\beta_{1-40}$ and $A\beta_{1-42}$ with PrioAD12 and PrioAD13 nanobodies in the cerebral cortex and hippocampus and retina of 3- to 4-month-old (n= 8) and 17- to 18-month-old (n= 8) APP/PS1 mice using *Cellsens* software image analysis after immunohistochemical staining. Total Aβ plaque burden (AβP) was quantified in the cerebral cortex and hippocampus and retina of 3- to 4-month-old (n= 8) and 17- to 18-month old (n= 8) APP/PS1 mice. Wilcoxon-Mann-Whitney test was performed and found that normalized intensity of both $A\beta_{1-40}$ and $A\beta_{1-42}$ oligomers were significantly higher in the retina of 3- to 4-month-old when compared to the 17- to 18-month-old age group APP/PS1 mice (P = 0.0002) whereas Aβp load was significantly higher in brain and retina of the 17- to 18-month-old age group when compared with the 3- to 4-month-old age group (P = 0.0002). Error bars represent interquartile range.

Table 2. Statistical analysis of the age-dependent retinal, brain and blood accumulation of Aβp and Aβo in the 3- to 4-month and 17- to 18-month-old APP/PS1 mice and compared to wild type littermates. Bonferroni correction of 0.05 / 36 = 0.0014 was applied, meaning p-values less than this value were considered statistically significant.

Antibody	**Age**	**Predictor**	**APP/PS1**					**Wild type**					**Difference**	
			n	Median	Lower Quartile	Upper Quartile	IQR	n	Median	Lower Quartile	Upper Quartile	IQR	z	P-value
PRIOAD12	3-4 Months	logeye	8	8.67	8.53	8.84	0.32	8	3.28	2.51	4.04	1.53	-3.3082	0.0002
PRIOAD12		logbrain	8	4.00	3.82	4.04	0.22	8	2.55	2.43	2.63	0.20	-3.3082	0.0002
PRIOAD12		logblood	8	3.94	3.78	4.28	0.51	8	2.30	2.30	2.56	0.25	-2.2185	0.0286
PRIOAD13		logeye	8	8.34	7.99	8.57	0.58	8	3.01	2.43	3.97	1.53	-3.3106	0.0002
PRIOAD13		logbrain	8	3.83	3.40	4.11	0.71	8	2.50	2.33	2.88	0.55	-3.3106	0.0002
PRIOAD13		logblood	8	4.08	3.96	4.12	0.16	8	2.30	2.30	2.30	0.00	-2.3067	0.0286
4G8		logeye	8	2.30	2.30	2.30	0.00	8	2.30	2.30	2.30	0.00	0	1
4G8		logbrain	8	2.30	2.30	2.30	0.00	8	2.30	2.30	2.30	0.00	0	1
PRIOAD12	17-18 months	logeye	8	2.93	2.33	3.77	1.43	8	2.30	2.30	2.30	0.00	2.8359	0.007
PRIOAD12		logbrain	8	2.57	2.38	2.80	0.42	8	2.30	2.30	2.30	0.00	3.1854	0.0014
PRIOAD12		logblood	8	4.43	4.28	4.47	0.19	8	2.30	2.30	2.30	0.00	2.3067	0.0286
PRIOAD13		logeye	8	2.74	2.35	2.93	0.58	8	2.30	2.30	2.30	0.00	2.8359	0.007
PRIOAD13		logbrain	8	2.76	2.57	2.98	0.41	8	2.30	2.30	2.30	0.00	3.1825	0.0014
PRIOAD13		logblood	8	2.83	2.72	3.22	0.50	8	2.30	2.30	2.30	0.00	2.3067	0.0286
4G8		logeye	8	4.35	4.06	4.66	0.60	8	2.30	2.30	2.30	0.00	3.5336	0.0002
4G8		logbrain	8	7.73	7.68	7.77	0.09	8	2.30	2.30	2.30	0.00	3.5366	0.0002

Table 3. Age-dependent retinal and brain accumulation of Aβp and Aβo in the 3- to 4-month-old APP/PS1 mice were quantified and compared to Aβp and Aβo levels in the 17- to 18-month-old APP/PS1 mice. Bonferroni correction of 0.05 / 36 = 0.0014 was applied, meaning p-values less than this value were considered statistically significant.

Antibody	Group	Log	n	Age (month)	Difference	
					z	p-value
PRIOAD12	APP/PS1	EYE	8	3-4 vs 17-18	-3.3106	0.0002
PRIOAD13		EYE			-3.3106	
4G8		EYE			3.5336	
4G8		BRAIN			3.5366	

Several studies have demonstrated the presence of Aβo in plasma of patients with mild cognitive impairment (MCI) and Alzheimer's disease (AD) [114,234,273], plasma levels may also predict the brain amyloid-β burden. In this study, we hypothesized that Aβo accumulation in blood might also precede retinal accumulation or at least occur simultaneously with retinal accumulation. Here, we used fresh whole blood in blood lysis buffer to enrich Aβo. Initially and after lysing whole blood derived from APP/PS1 mice, anti-oligomer-A11-coated immunomagnetic microbeads were used to isolate Aβ from APP/PS1 mice and wild type littermates (APP/PS1, n=16 and WT, n=16). Following Western blotting, anti-$A\beta_{1-40}$ (PrioAD12) or anti-$A\beta_{1-42}$ (PrioAD13) oligomer single-domain antibodies were used to immunodetect Aβ oligomer isoforms in 3 and 18-month old APP/PS1 and wild type mice. Anti-$A\beta_{1-40}$ PrioAD12 displayed a two-band pattern ranging between 10-15 kDa in the 3-month old APP/PS1 mice, whereas only one band at 10-15 kDa was seen in the 18-month old APP/PS1 age group **(Figure 9 A & B)**. In contrast, anti-$A\beta_{1-42}$ PrioAD13 showed only one band at 10-15 KDa in both the 3-month and 18-month old APP/PS1 age groups **(Figure 9 A & B)**. Furthermore, we also used A11 rabbit anti-Aβo antibody to immuno-compare $A\beta_{1-40}$ and $A\beta_{1-}$

$_{42}$ levels detected with PrioAD12 and PrioAD13. In both age groups A11 displayed a different band pattern compared with the single-domain antibodies and ranged between 70-80 kDa **(Figure 9 A& B)**. We then performed densitometric analysis of scanned western blot membranes[274]. **Table 2** also shows the normalized intensity of whole-blood Aβ as measured by the *ImageJ* software and the values for $A\beta_{1-40}$ (PRIOAD12 antibody) and $A\beta_{1-42}$ (PRIOAD13 antibody). Levels of both $A\beta_{1-40}$ and $A\beta_{1-42}$ oligomers were not significantly higher when compared with the wild type levels in the 3-month age group ($P = 0.0286$) when a Bonferroni correction was applied. However, when the statistical analysis was performed using paired t-tests (p-values below 0.05 were deemed significant in this case) to compare levels of both $A\beta_{1-40}$ and $A\beta_{1-42}$ oligomers in APP/PS1 versus wild type, these were significant ($P < 0.05$) **(Figure 10).** Levels of $A\beta_{1-40}$ increased significantly from 3 to 18-month while $A\beta_{1-42}$ decreased by at least 3-fold in the 18-month-old APP/PS1 mice **(Figure 10).** These results also highlight the high binding affinity of the camelid-derived single domain antibodies for detection of $A\beta_{1-40}$ and $A\beta_{1-42}$ oligomers in whole blood.

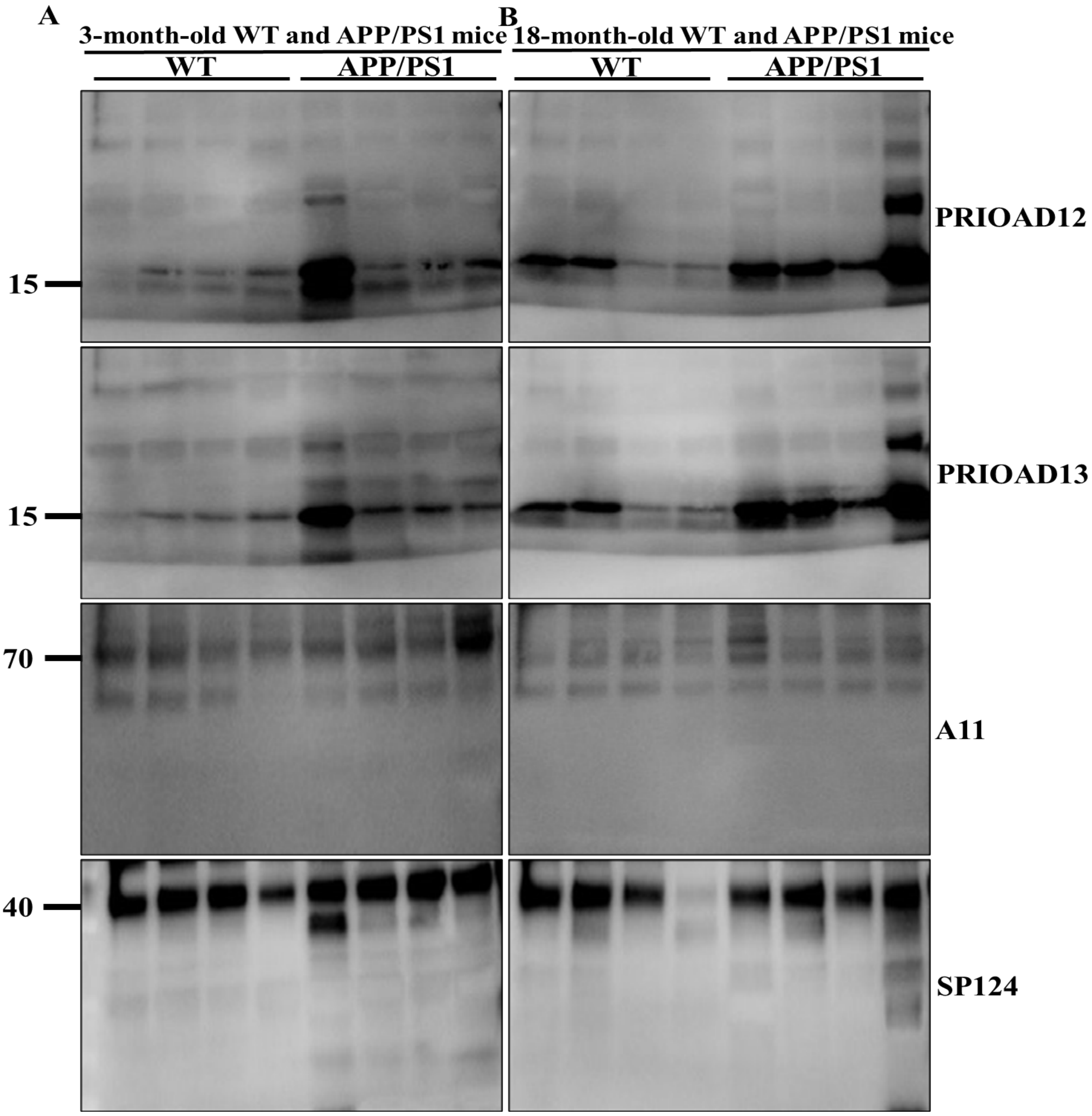

Figure 9. Immunodetection of Aβ soluble oligomers: Western blot data showing that anti-Aβ_{1-40} (PrioAD12) and anti-Aβ_{1-42} (PrioAD13) camelid-derived single domain IgG antibody strongly bind to Aβ oligomers in the blood sample, both at 15 KDa in (A) 3-month age group and (B)18-month age group. First 4 lanes are wild type mice and next 4 lanes indicating APP/PS1 mice. *A11* conventional antibody used to compare with our single domain VHHs and band found at 70 KDa.

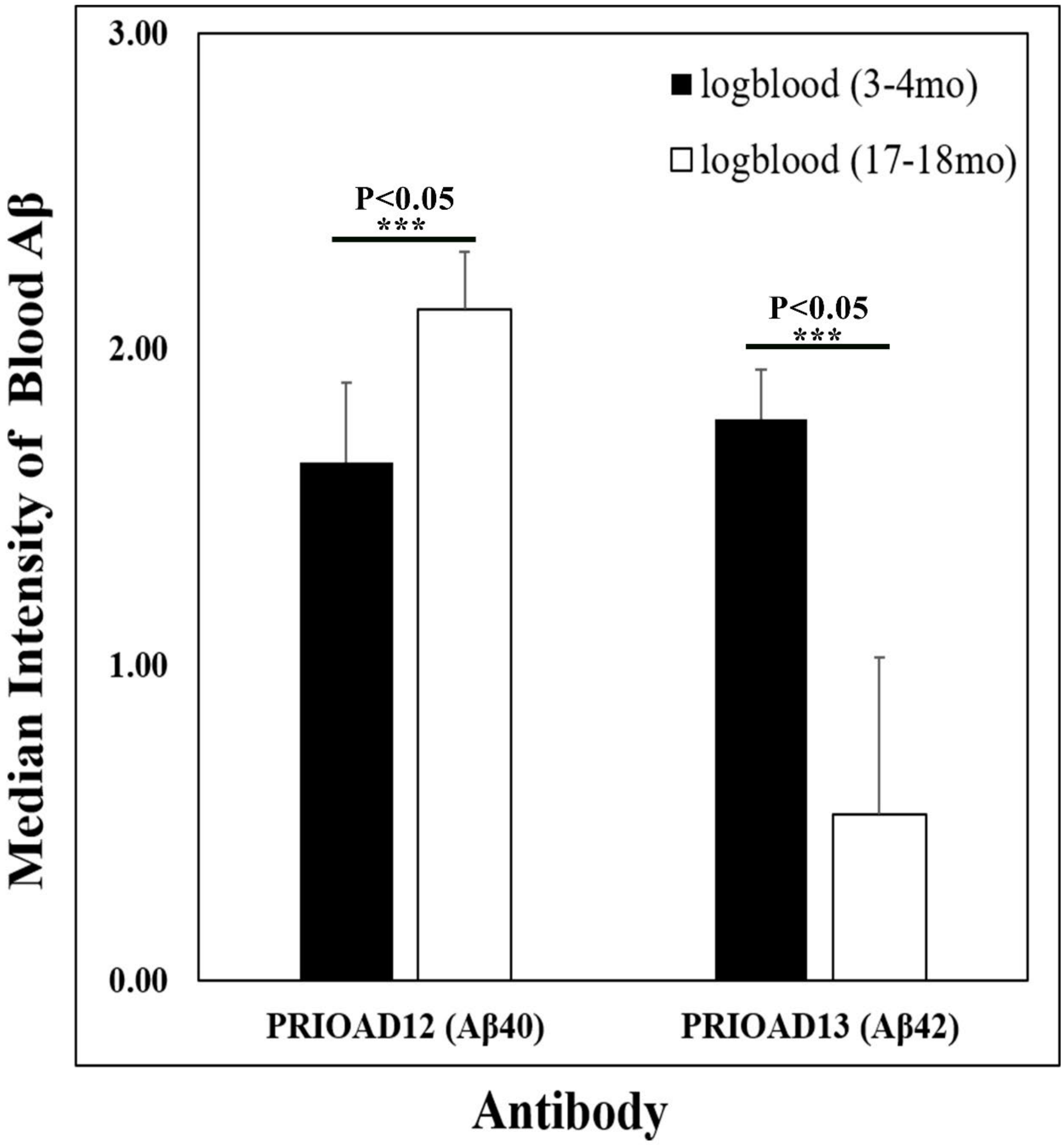

Figure 10. Quantification of the age dependent accumulation of blood-borne Aβ oligomers with nanobodies: Immunodetection and quantification of blood-borne $A\beta_{1\text{-}40}$ and $A\beta_{1\text{-}42}$ with PrioAD12 and PrioAD13 nanobodies in whole blood of 3- to 4-month-old (n=8) and 17- to 18-month-old (n= 8) APP/PS1 mice using *ImageJ* software analysis following Western blotting. The normalised intensity was calculated in three independent experiments for each age group and the final result was presented as median intensity. Paired t-tests were performed and p-values below 0.05 were considered significant. Levels of both $A\beta_{1\text{–}40}$ and $A\beta_{1\text{–}42}$ oligomers were significantly higher in the 3- to 4-month age group. $A\beta_{1\text{-}40}$ oligomer level increased significantly from 3 to 4 to 17 to 18-month whereas $A\beta_{1\text{-}42}$ oligomer level decreased by at least three-fold in the 17- to 18-month-old APP/PS1 mice. Error bars represent interquartile range.

4.4.5. Co-localization of beta amyloid oligomers and plaques in the retina and brain of APP/PS1 mice

In order to determine whether $A\beta_{1-40}$ or $A\beta_{1-42}$ oligomers co-localized with Aβp in different anatomical regions and structures of the retina and brain, we co-stained brain and retinal sections with 4G8 antibody with either anti-$A\beta_{1-40}$ (PrioAD12) or anti-$A\beta_{1-42}$ (PrioAD13) oligomer single-domain antibodies (**Figure 11**). We did not observe any co-localization in the brain and retina of the 3-month old APP/PS1 mice (**Figure 11 A-F**) but confirmed the presence of $A\beta_{1-40}$ or $A\beta_{1-42}$ oligomer in the retinal layers (**Figure 11 C and F**). However, both retinal Aβp and $A\beta_{1-40}$ or Aβp and $A\beta_{1-42}$ were shown to co-localize in the GCL, IPL & INL of the 8-month old APP/PS1 age group (**Figure 11 I and L**). Furthermore, co-accumulation of Aβp and $A\beta_{1-40}$ or Aβp and $A\beta_{1-42}$ was also seen in the cerebral cortex and hippocampus (**Figure 11 G, H, J & K**), noticeably higher levels of Aβo in this age group when compared to plaques. Aβp in 11-month old APP/PS1 mice was markedly increased while $A\beta_{1-40}$ and $A\beta_{1-42}$ oligomers decreased in the brain (**Figure 11 M, N, P and Q**). High levels of $A\beta_{1-40}$ and $A\beta_{1-42}$ oligomers were consistently found in the retina (**Figure 11 O and R**). Finally, 18-month old APP/PS1 mice showed that both $A\beta_{1-40}$ and $A\beta_{1-42}$ co-localized with Aβp in the cerebral cortex, hippocampus and in the retinal GCL, INL and ONL (**Figure 11 S-X**). Surprisingly, high levels of $A\beta_{1-40}$ and $A\beta_{1-42}$ oligomers were observed in the retina and brain of 18-month old APP/PS1 mice (**Figure 11 S-X**), perhaps confirming the hypothesis that plaques act as a reservoir for the toxic Aβo [45]. WT age-matched littermates did not show any co-localization of Aβp with $Aβ_{1-40}$ or $Aβ_{1-42}$ (data not shown).

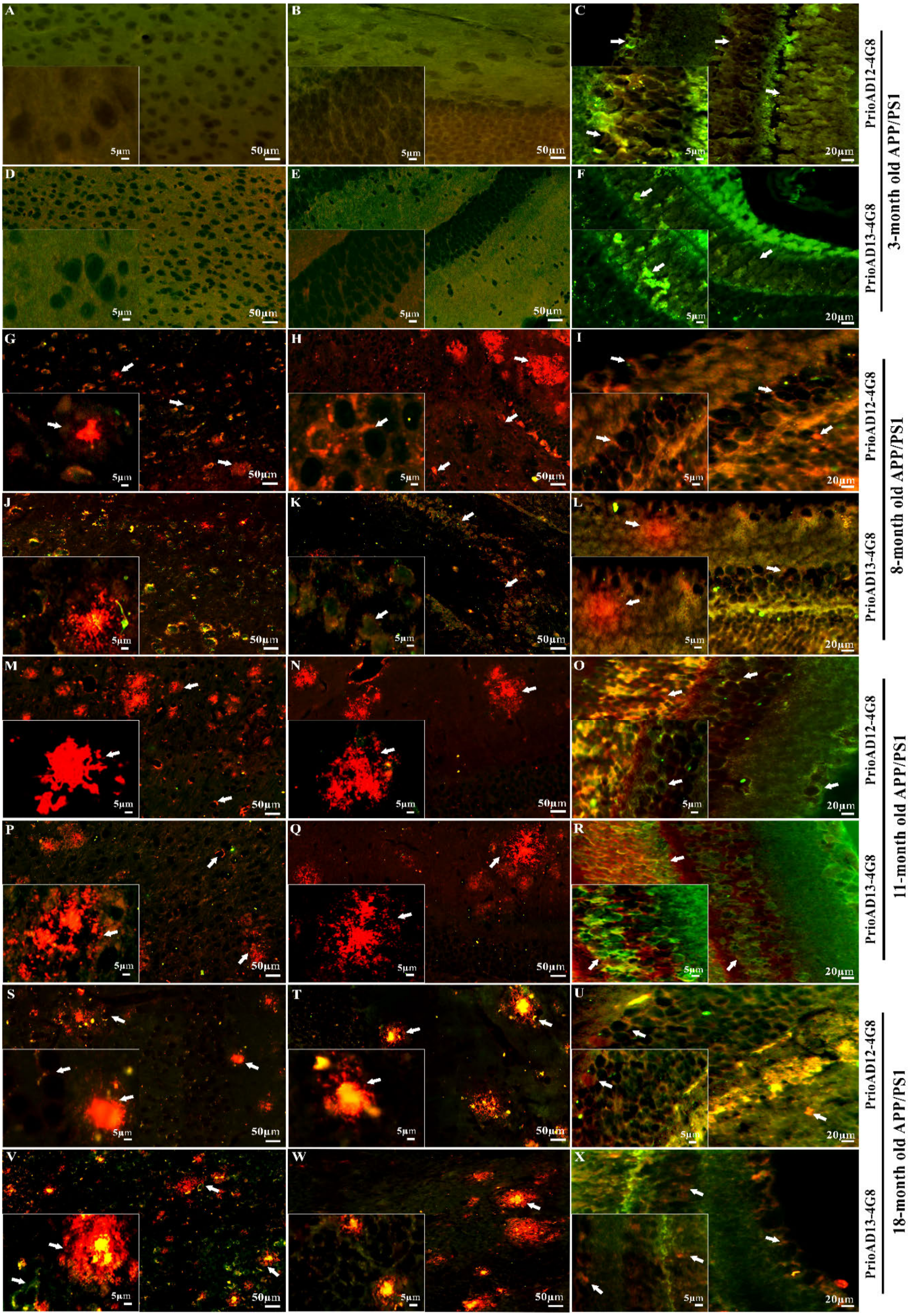

Figure 11. Co-localization of amyloid beta (Aβ) oligomers and plaques. Immunofluorescence co-localization of cerebral and retinal Aβ oligomers and Aβ plaques in different APP/PS1 age groups. Cerebral and retinal co-staining with anti-$A\beta_{1-40}$ (PrioAD12) and anti-$A\beta_{1-42}$ (PrioAD13) nanobodies (GREEN) and 4G8 antibody (RED) of 3- (A-F), 8- (G-L), 11- (M-R), and 18-month-old (S-X) APP/PS1 mice. No distinctive oligomers co-localized with plaques in the brain cortical region (A, D) and in the hippocampus (B, E). Large number of oligomers found in the (C, F) retinal ganglion cell layer (GCL), inner nuclear layer (INL), and outer nuclear layer (ONL) but no co-localization observed in the 3-month-old mice (white arrows). Then $A\beta_{1-40}$ (G, H) and $A\beta_{1-42}$ (J, K) oligomers co-localized with plaques in the brain cortical region and hippocampus, respectively, and in the retinal GCL and INL (I, L) of the 8-month-old mice (white arrows), respectively. With age progression, $A\beta_{1-40}$ (M, N) and $A\beta_{1-42}$ (P, Q) oligomers co-localized with plaques in the brain cortical region and hippocampus, respectively, and in the retinal INL (O, R) of the 11-month-old mice (white arrows). Finally, in 18-month-old APP/PS1 mice, Aβ oligomers co-localized with plaques in the brain cortical region (S, V) and in the hippocampus (T, W) and also in the retinal GCL, INL, and ONL (U, X) of the 18-month-old mice, respectively (white arrows). Representative of all affected mice in all age groups.

4.4.6. Homing of Aβ oligomer to neuronal endosomes in the retina and brain of APP/PS1 mice

Endocytic dysfunction has previously been linked with the primary stage of AD [221]. Furthermore, inhibition of Aβ clearance can lead to its intra-neuronal accumulation in the endosomal/lysosomal compartment leading deposition in the cytosolic compartment [222]. In order to assess whether $A\beta_{1-40}$ and $A\beta_{1-42}$ localise to the endosomes/lysosomes (**Figure 12 A-F**), sections derived from brain and retina of APP/PS1 mice were co-stained with anti-either $A\beta_{1-40}$ PrioAD12 or anti-$A\beta_{1-42}$ PrioAD13 single domain antibodies and anti-LAMP2 antibody [222]. We show that both $A\beta_{1-40}$ and $A\beta_{1-42}$ co-localised with the lysosomal marker in the retinal GCL, INL and ONL of the 3-month-old APP/PS1 mice (**Figure 12 C & F**). Excessive glial cell activation leads to neuronal death, brain atrophy and cognitive impairment [275,276]. Previous studies have shown that activated microglial cells 'encircled' Aβp in AD [277,278]. In our study we wanted to confirm whether activated microglia formed cognate interaction with $A\beta_{1-40}$ and $A\beta_{1-42.}$ We co-labelled anti-$A\beta_{1-40}$ PrioAD12 and anti-$A\beta_{1-42}$ PrioAD13 oligomer antibody and a microglial marker in the brain and retina of 3-month-old APP/PS1 mice respectively **(Figure 13 A-L**). Our results did not find any reactive astrocytes around the anti-$A\beta_{1-40}$ and anti-$A\beta_{1-}$

42 oligomers (F**igure 13 A, B, D & E**) but we show that few reactive microglia 'engulfed' and / or closely 'surrounded' $A\beta_{1-40}$ and $A\beta_{1-42}$ in the brain hippocampus and cortex (**Figure 13 G, H, J &** K) . However, in this age group, the retina displayed extensive and widespread staining for reactive astrocytes and microglia in the GCL, INL and ONL (**Figure 13 C, F, I & L**). Because absence of amyloid beta oligomer depositions in the brain of earlier age group leads to a moderate glial cell reactivity in the brain. Whereas in the retinal layers we found excessive microglial activation co-localized with the $A\beta_{1-40}$ and $A\beta_{1-42}$ oligomers. Finally, we also confirmed that Aβo deposits were more prominent in the retinal GCL and INL and co-localize with neuron specific marker NeuN (**Figure 14 C & F**) whereas in the cerebral cortex and hippocampus in the 3-month old APP/PS1 mice very less amount of co-staining was found **(Figure 14 A, B, D & E).**

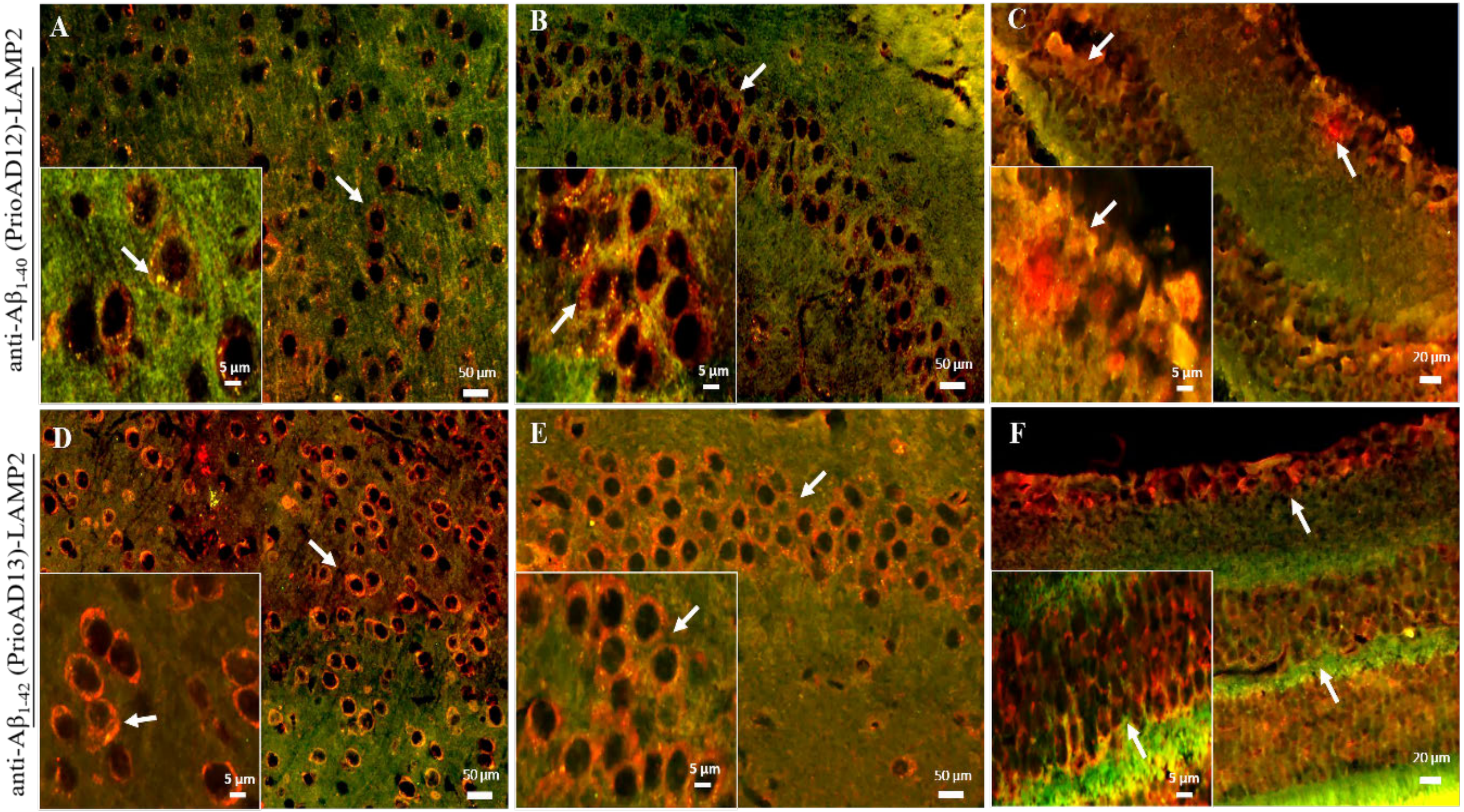

Figure 12. Immunofluorescence co-localization of retinal and cerebral amyloid β oligomers with lysosomal-associated membrane protein 2. Cerebral and retinal co-staining with anti-A$\beta_{1\text{-}40}$ (PrioAD12) and anti-A$\beta_{1\text{-}42}$ (PrioAD13) camelid-derived single domain antibody (GREEN) and anti-mouse LAMP2 monoclonal antibody (RED) of 3-month-old APP/PS1 mice. LAMP2 co-localised with Aβo in the brain cortical region (A, D) and in the hippocampus (B, E) and in the retina (C, F) of the 3-month-old mice respectively (white arrows). Representative of all affected mice in all age groups.

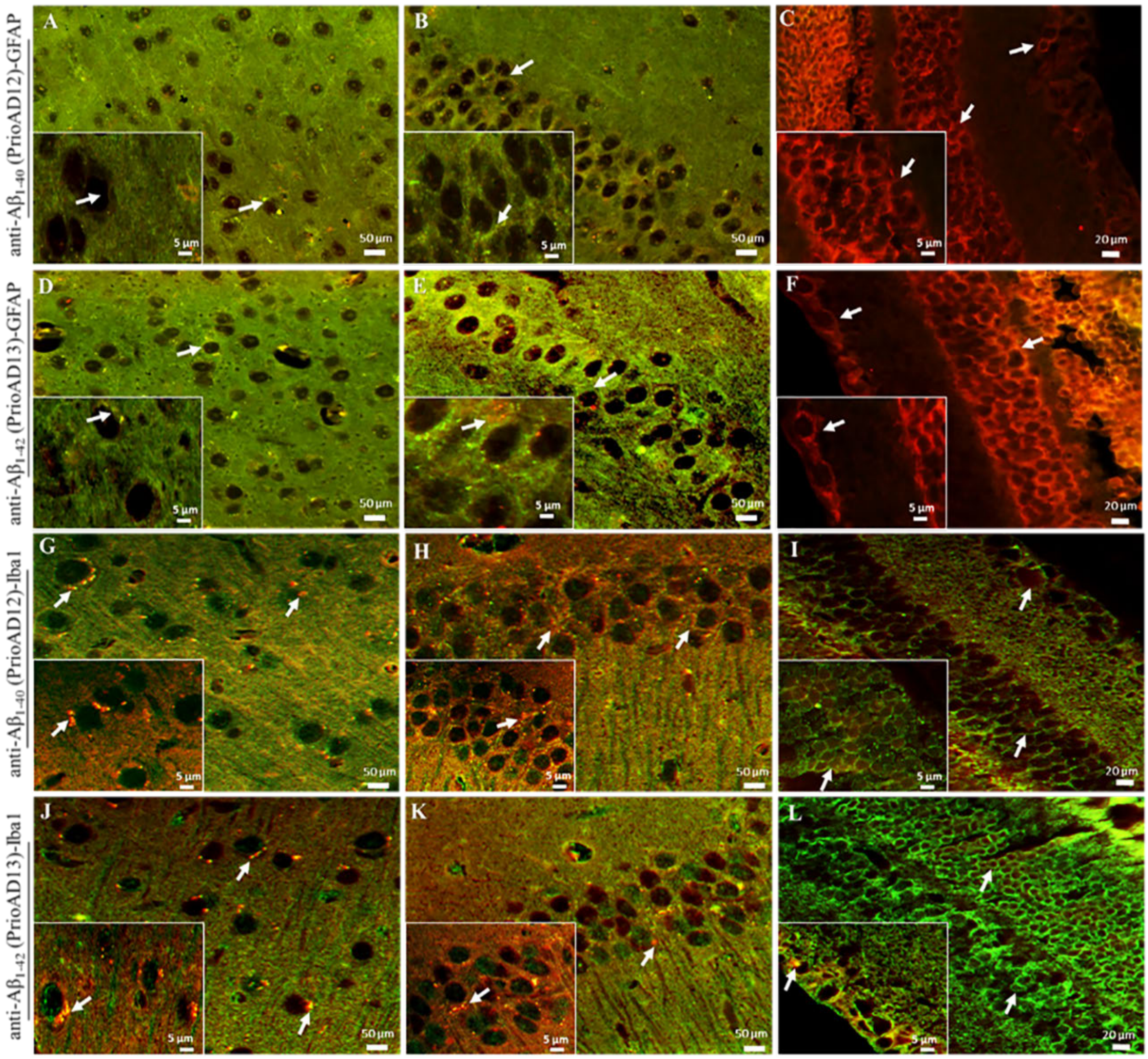

Figure 13. Immunofluorescence co-localization of retinal and cerebral amyloid β oligomers with Anti-Glial Fibrillary Acidic Protein (GFAP). Cerebral and retinal co-staining with anti-A$\beta_{1\text{-}40}$ (PrioAD12) and anti-A$\beta_{1\text{-}42}$ (PrioAD13) camelid-derived single domain antibody (GREEN) and anti-mouse GFAP monoclonal antibody (RED) of 3-month-old APP/PS1 mice. Aβo poorly co-localized with GFAP in the brain cortical region (A, D) and in the hippocampus (B, E) of the 3-month-old mice respectively (white arrows). Retinal layers (C, F) displayed high levels of co-localization (white arrows). Representative of all affected mice in all age groups.

G-L) Immunofluorescence co-localization of retinal and cerebral amyloid β oligomers with Anti-Ionized calcium binding adaptor molecule 1 (Iba1). Cerebral and retinal co-staining with anti-A$\beta_{1\text{-}40}$ (PrioAD12) and anti-A$\beta_{1\text{-}42}$ (PrioAD13) camelid-derived single domain antibody (GREEN) and anti-goat Iba1 polyclonal antibody (RED) of 3-month-old APP/PS1 mice. Aβo poorly co-localized with Iba1 in the brain cortical region (G, J) and in the hippocampus (H, K) of the 3-month-old mice respectively (white arrows). Retinal layers (I, L) displayed high levels of co-localization (white arrows). Representative of all affected mice in all age groups.

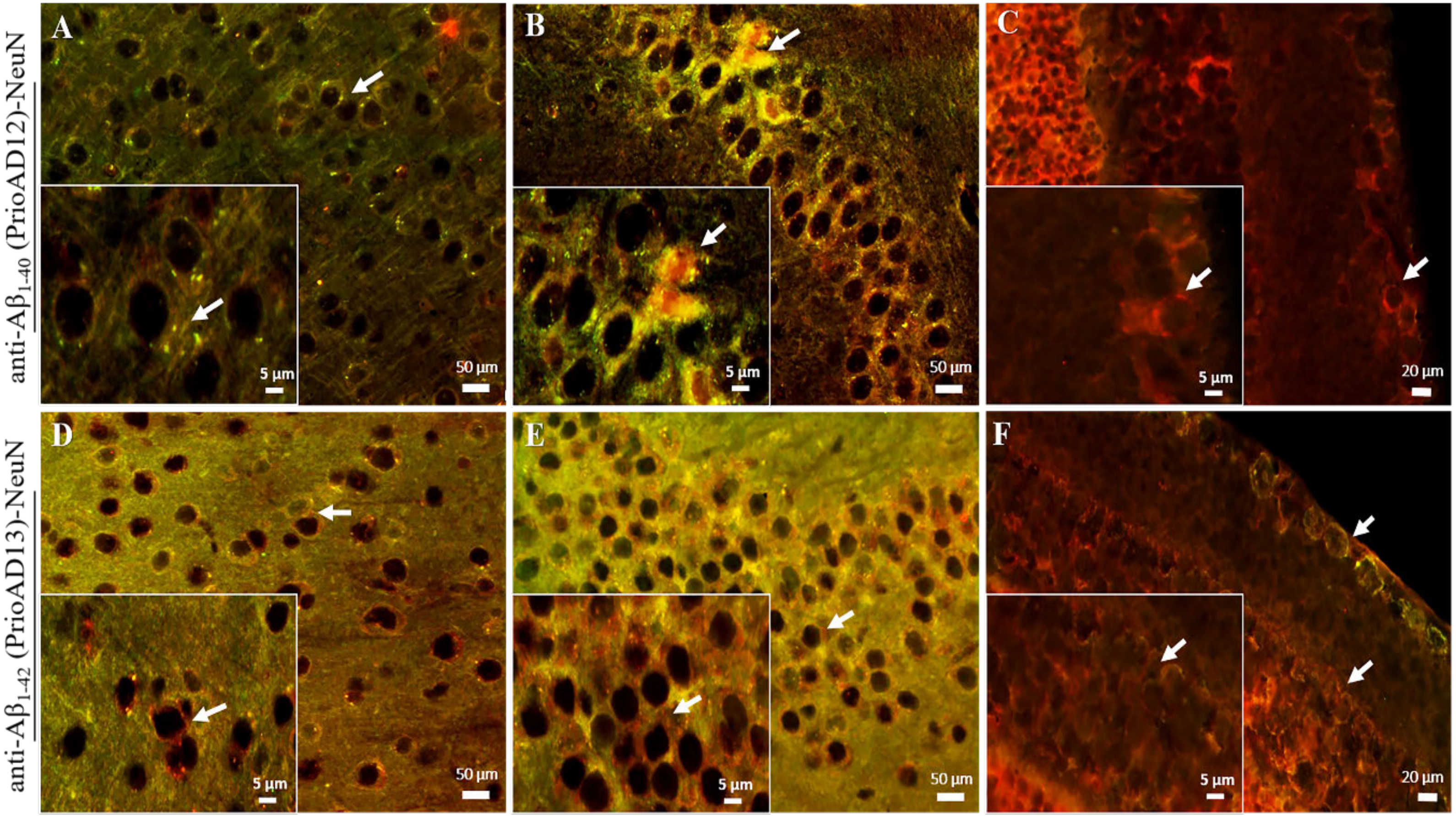

Figure 14. Immunofluorescence co-localization of retinal and cerebral amyloid β oligomers with neuron-specific nuclear protein. Cerebral and retinal co-staining with anti-A$\beta_{1\text{-}40}$ (PrioAD12) and anti-A$\beta_{1\text{-}42}$ (PrioAD13) camelid-derived single domain antibody (GREEN) and anti-mouse NeuN monoclonal antibody (RED) of 3-month-old APP/PS1 mice. Aβo localized with NeuN in the brain cortical region (A, D) and in the hippocampus (B, E) of the 3-month-old mice respectively (white arrows). Retinal layers (C, F) displayed high levels of co-localization (white arrows). Representative of all affected mice in all age groups.

4.5. Discussion

Behavioural assessment of the APP/PS1 AD mouse model, demonstrated that memory decline and cognitive deficits start after 7-month of age [266]. Although, our study did not include behavioural assessments, mice appeared healthy until 10-month of age. Of importance, we show that increased Aβo in blood and retinal accumulation of Aβo was observed at 3-month-old in APP/PS1 mice in the absence of Aβp accumulation in the retina and before appearance of both Aβo and Aβp in brain. The accumulation of blood and retinal Aβo occur at a very early age, likely months before the expected memory and cognitive deficits in APP/PS1 mice. These data indicate that these assemblies are likely to be responsible for the toxic effects associated with AD [39,279], can be detected before AD onset [52] and might originate from the blood [112]. Several diagnostic strategies have been developed for early AD detection, including systems for the detection of Aβo in plasma [273] and in the CSF [280]. The experimental value of detecting blood-borne Aβ biomarkers has gained considerable momentum [226,227], however, a decade of research efforts in this area has not yet led to a clinical diagnostic due to the complexity and lack of reproducibility of these approaches [281]. Nonetheless, pursuing a blood-detection approach might have great diagnostic [217]. A recent study combining immunoprecipitation and mass spectrometry led to the identification of high-performance blood borne Aβs derived from human MCI and AD [234]. Similarly, using our unique camelid single domain anti-$Aβ_{1-40}$ or anti-$Aβ_{1-42}$ oligomer antibody, we were able to detect both $Aβ_{1-40}$ and $Aβ_{1-42}$ oligomer in whole blood derived from 3- and 18-month-old APP/PS1 mice via immunoprecipitation followed by Western blotting.

In my previous study using 5xFAD mice (chapter 3), *A11* anti-oligomer conventional antibody was used to detect Aβo in the brain and retinal layers. Widespread distribution of *A11* positive intraneuronal Aβo was observed in the cerebral cortex, hippocampus, retinal nuclear layers (INL & ONL), and ganglion cell layer (GCL). However, in this current study and in addition to *A11*, camelid-derived single domain nanobodies were also used to target $A\beta_{1-40}$ and $A\beta_{1-42}$ oligomers in the brain and retina of APP/PS1 mice. Extensive intra-neuronal $A\beta_{1-40}$ and $A\beta_{1-42}$ oligomers were also found in the brain cerebral cortex and hippocampus and retinal nuclear layers (INL & ONL) and ganglion cell layer (GCL).

A11 was previously shown to bind to different epitopes of Aβo but also reacts with oligomeric aggregates found in different amyloidogenic proteins, including prion proteins, α-synuclein, copper/zinc superoxide dismutase[64]. However, *A11* was not able to discriminate between Aβo isoforms namely $A\beta_{1-40}$ and $A\beta_{1-42}$ oligomers.

In contrast, nanobodies are heavy chain only IgG (VHH). They are smaller in size than the conventional antibodies, a feature that enables them to diffuse in tissues and specifically bind to the target antigen. Also, nanobodies are soluble in aqueous solution, extremely stable, fully functional at high temperature (90°C), and resistant to chemical denaturation. Most importantly, the specific nanobodies used against $A\beta_{1-40}$ and $A\beta_{1-42}$ oligomers were able to detect separate isoforms. When comparing the data in chapter 3 and chapter 4, I found that conventional *A11* antibody showed excessive-high background and few non-conformational bindings which could arise from its polyclonal nature, whereas nanobodies showed specific binding to $A\beta_{1-40}$ and $A\beta_{1-42}$ oligomers respectively with the minimum background.

Previous studies reported an inverse interrelationship between neurotoxicity and the size of Aβo. The toxic effect of Aβo decreases with the increase of its size. The general molecular weight (MW) of Aβo was found to be around 10-100 kDa in AD brain, ranging from dimer to dodecamer[282]. A study by Lambert and colleagues first described the cytotoxic effect of the small diffusible Aβo on the hippocampal neurons[283]. The small Aβo referred to as ADDLs toxicity was tested in organotypic mouse brain slice cultures. The authors found that 17 and 22 kDa molecular weight small oligomers were lethal to hippocampal neurons at nanomolar concentration[283]. In addition, a study by Cizas and colleagues proved that oligomers larger than

30 KDa have a less toxic effect on the inhibition of long-term potentiation[284]. The authors also suggested the transition of sizes from small to large correlate with the high to a low toxic effect of Aβo. *A11* specifically binds to the prefibrillar oligomers[285]. However, studies suggested that the specificity of *A11* to AD-related oligomers might vary as it recognized prefibrillar oligomers from various proteins that share a common structure including α-synuclein, islet amyloid polypeptide, polyglutamine (PolyQ), lysozyme, and prion peptide[64,230]. Glabe and colleagues reported the ideal band size of prefibrillar oligomer-specific antibody *A11* of approximately ~75 kDa tetramer[185]. In this study, western blot data showed *A11*-specific bands at ~70kDa which indicates binding to prefibrillar oligomer in APP/PS1 mice. In comparison, camelid-derived single domain nanobodies revealed ~15KDa-specific bands confirming its specificity to smaller highly toxic oligomers. In line with previous reports, my data suggested that nanobodies were able to detect the toxic small diffusible oligomers specific to AD whereas *A11* binds to the larger oligomers which are believed to be less toxic to the neurons.

$A\beta_{1\text{-}40}$ and $A\beta_{1\text{-}42}$ oligomer levels were significantly higher when compared with WT mice in the 3-month-old age group, while their levels were elevated for $A\beta_{1\text{-}40}$ oligomers and reduced for $A\beta_{1\text{-}42}$ oligomers in the 18-month old age group when compared with the 3-month old age group. The reduction of $A\beta_{1\text{-}42}$ in the older age group mirrors the biological behaviour of this assembly in human AD where plasma $A\beta_{1\text{-}42}$ or total $A\beta_{1\text{-}42}$/ $A\beta_{1\text{-}40}$ ratio is used as a strong predictor of amyloid-PET status [153,217]. Although the levels of blood borne Aβ levels were significantly higher in APP/PS1 when compared to the levels in the wild type littermates, the Western blot technique has its limitations and might generally lead to false positives[286].

We have previously shown a strong inverse correlation between retinal Aβo and brain Aβp deposition [272]. This previous study provided the rationale for assessing and comparing age-dependent accumulation of Aβo in the retina, whole blood and brain. In this current study, the 3- to 4-month-old APP/PS1 age group displayed extensive accumulation of Aβo deposits in the outer nuclear layer (ONL), inner nuclear layer (INL) and ganglion cell layer (GCL) of the retina, whereas the brain remained free of Aβo deposition. In addition, Aβ plaques were completely absent in both brain and retina in this age group. Retinal Aβo deposition was lower with age and was no longer detected in the 17- to 18-month-old age group using immunohistochemistry. In contrast, cerebral Aβo was first detected at 8-month of age in our APP/PS1 mice and remained unchanged in 11-month-old mice but was undetectable in 18-month-old APP/PS1 mice. Consistent with our previous study [272], retinal Aβp was first detected in 8 to11-month-old APP/PS1 and increased in the 18-month age group. Taken together, and acknowledging the limitations of the study in relation to the lack of data related to animal behaviour in our current study, these results suggest that retinal Aβo accumulation precedes its cerebral deposition and that its simultaneous presence in the blood at high levels strongly suggests that retinal Aβo originate from the blood [102,287], albeit a lymphatic and/or a CSF origin cannot be ruled out [288].Of note, fluorescence assessment also showed presence of cerebral Aβo depositions forming the dense core of the Aβp plaques in the 18-month age group. This data strengthens the hypothesis of Haass and colleagues[45] suggesting that Aβ plaques might act as a reservoir for Aβ oligomers.

In this study, we established that Aβo could be detected simultaneously in the blood and retina of APP/PS1 mice before their appearance in the brain. Aβo neuroinvasion appears to originate from blood before reaching the retina probably via 'leaky' blood-ocular barriers [289]. A study by Morin and colleagues [241] reported that beta-amyloid precursor protein (APP) is synthesized in retinal ganglion cells (RGC) and transported to the optic nerve in small transport vesicles. It can be speculated that blood borne Aβo deposition in the retina might initiate a seeding reaction leading to aggregation and spread to the brain [112]. The ability to detect Aβo concurrently in the blood and retina using nanobodies that specifically bind $A\beta_{1\text{-}40}$ and $A\beta_{1\text{-}42}$ oligomers before cognitive decline and neuropathology are evident offers a real possibility to establish a screening platform (retinal imaging of Aβo) and a reference diagnostic testing platform (blood testing of Aβo).

Chapter 5

Results (Paper 3)

4. Neuronal deposition of amyloid beta oligomers and hyperphosphorylated tau is closely connected with cognitive dysfunction in aged dogs

Umma Habiba[1], Makiko Ozawa[2], James K. Chambers[2], Kazuyuki Uchida[2], Joseph Descallar[3], Hiroyuki Nakayama[2], Brian A. Summers[4], John W Morley[1], Mourad Tayebi[1]*

[1]School of Medicine, Western Sydney University, Campbelltown, NSW, Australia; [2]Department of Veterinary Pathology, the University of Tokyo, Japan; [3]Ingham Institute of Applied Medical Research, Liverpool, NSW 2170; [4]School of Veterinary Medicine, Melbourne University, Werribee, Victoria, Australia.

Received: 03 August 2021 | Revised: 28 August 2021| Accepted: 03 September 2021

5.1. Abstract

Background: Canine cognitive dysfunction (CCD) is a progressive syndrome recognized in mature to aged dogs with a variety of neuropathological changes similar to human Alzheimer's disease (AD), for which it is thought to be a good natural model. However, the presence of hyperphosphorylated tau protein (p-Tau) in dogs with CCD has only been demonstrated infrequently.

Objective: The aim of the present study was to investigate the presence of p-Tau and amyloid beta oligomer (Aβo) in cerebral cortex and hippocampus of dogs with CCD, with focus on an epitope retrieval protocol to unmask p-Tau.

Method: Immunohistochemical and immunofluorescence analysis of the cortical and hippocampal regions of five CCD-affected and two nondemented aged dogs using 4G8 anti-Aβp, anti-$A\beta_{1-42}$ nanobody (PrioAD13) and AT8 anti-p-Tau (Ser202, Thr205) antibody were used to demonstrate the presence of amyloid beta plaques (Aβp) and $A\beta_{1-42}$ oligomers and p-Tau deposits, respectively.

Results: The extracellular Aβ senile plaques were of the diffuse type which lack the dense core normally seen in human AD. While p-Tau deposits displayed a widespread pattern and closely resembled the typical human neuropathology, they did not co-localise with the Aβp. Of considerable interest however, widespread intraneuronal deposition of $A\beta_{1-42}$ oligomers was exhibited in the frontal cortex and hippocampal region that co-localised with p-Tau.

Conclusion: Taken together, these findings reveal further shared neuropathologic features of AD and CCD, supporting the case that aged dogs afflicted with CCD offer a relevant model for investigating human AD.

Keywords: Canine cognitive dysfunction, Alzheimer's disease, $A\beta_{1-42}$ oligomers, Amyloid beta plaques, Hyperphosphorylated Tau.

5.2. Introduction

The human life expectancy is increasing with the advancement of medicine, nutrition and technology, health, and social care. According to the World Health Organisation (WHO), the number of people aged over 60 years reached 1 billion in 2020 and is expected to increase to 2.1 billion by 2050 [290]. One of the most common neurological disorders in the aging population is Alzheimer's disease (AD) and advancing age is the single most important risk factor. The worldwide prevalence of AD is currently at 50 million and will likely triple to 150 million people by 2050 [7]. AD is a progressive neurodegenerative disorder causing gradual decline in cognitive functions believed to begin at least two decades before any obvious cognitive symptoms [50,52]. Thus far, the most commonly used animal model to investigate human AD employs rodents. The common strategy to generate these models is by overexpressing mutant human APP and/or PS1 genes [159,160]. Although the importance of such transgenic models is undisputed, most cases of AD are sporadic, and these models do not fully recapitulate key clinical and pathological aspects. Sarasa and colleagues reported that human transgenes such as APP, PS1 or PS2 encode variable Aβ peptides which might be impeded by mouse endogenous APP and APP processing enzymes [160]. In addition, transgenic animal models currently used to investigate human AD, only replicate a particular aspect of the disease (amyloidogenic VS tauopathic) and often fail to reproduce all the associated pathological features. Significantly, favourable immunotherapeutic outcomes using AD transgenic animal models [120,121] have failed to translate into effective human therapy, which raises serious doubts as to the validity of these amyloid-focused experimental models.

To understand the multifactorial nature of human AD pathogenesis, it has become vital to characterise a non-transgenic natural disease model. In this context, aged dogs have been proposed as a preclinical and clinical model for AD, because they naturally develop considerable human like AD neuropathology associated with cognitive deficits [136,291].

Advancement of veterinary medical prophylaxis, interventions and nutrition has helped increase the life expectancy of pet dogs, which in parallel with man has increased the age-related disease burden [129]. Human AD neuropathology is characterised by the presence of extracellular Aβp, intracellular NFTs composed of p-Tau protein and ubiquitin; CAA and also severe synaptic loss and neuronal death [20]. Aged dogs with cognitive decline have already been shown to display human-like AD neuropathological features with the exception of intracellular p-Tau, the evidence for which has infrequently been found in this species [137,142,143]. To that end, we investigated the deposition and accumulation of p-Tau in seven aged dogs using an improved and refined protocol. Our study demonstrated intracellular p-Tau depositions in the hippocampus and frontal cortex of these seven dogs [31]. The overall aim of this study is to further characterise aged dogs as a translational model for human AD and validate p-Tau as a hallmark of CCD or 'Dog-zheimer'.

5.3. Materials and Methods

5.3.1. Case presentation

Detailed information about the dogs used in this study is found in a previously published clinical report by Ozawa and colleagues [149]. Briefly, 37 brains were removed following routine necropsies performed at the Department of Veterinary Pathology, University of Tokyo. The brains of seven out of the 37 dogs were used in the current study following confirmation and scoring of canine cognitive dysfunction (CCD) [139]. We included small and medium size breeds according to the American Kennel Club breed size division such as Papillon, Pomeranian, Lhasa Apso and Shiba Inu and their ages were 14 (n=1), 15 (n=1), 16 (n=1) and 17 (n=1) years respectively (Table 1). The size of the mongrels was determined according to their weight as <15 kg is considered small, 15–25 kg medium and >25 kg large. In the current study one small size Mongrel aged 16 years and two medium size Mongrels aged 14 and 17 years were used [149]. CCD scores were calculated from an established questionnaire [139] that was completed by the dogs' owners and dogs that scored ≥ 50 were considered as suffering from CCD [149]. Five dogs were diagnosed with CCD (CCD score ≥ 50) and two dogs were considered nondemented (CCD score <50), including a 16-year-old small size Lhasa Apso and 14-year-old small size Papillion with CCD scores of 38 and 44 respectively (**Table 1**).

5.3.2. Dog brain samples

Following fixation in a 10% phosphate-buffered formalin solution and routine processing [149], congo red (CR) staining, immunohistochemistry (IHC) and immunofluorescence (IF) were performed using 4-μm-thick Paraffin-embedded tissue sections of brains of the seven aged dogs. Two regions of these brains, the hippocampus and frontal cortex, were used in this study.

5.3.3. Congo red staining (CR)

Initially, we performed CR staining to identify amyloid fibrils as described previously [53,272]. Briefly, deparaffinized sections were placed in CR working solution for 20 minutes then rinsed in 5-8 changes of deionized water. This was followed by staining with Gill ll Haematoxylin (Leica bio systems, Wetzlar, Germany) for 1-3 minutes and rinsing in 3 changes of deionized water. Sections were then dehydrated in two changes of 95% alcohol followed by three changes of absolute alcohol for one minute each. Finally, sections were cleared in two changes of xylene and mounted in a xylene miscible medium. Sections were then visualized under bright and polarized light microscopy (Olympus CX 43, Shinjuku, Tokyo, Japan).

5.3.4. Immunohistochemical staining of amyloid beta and hyperphosphorylated Tau

Brain hippocampal and cortical sections were pre-treated for one hour using the 2100 antigen retriever (Aptum biologics Ltd, Southampton, United Kingdom) followed by 90% formic acid then 0.1% triton-X treatment for 5 minutes and 1 minute, respectively. Sections were then blocked with 0.3% H_2O_2 for 15 minutes to inactivate endogenous peroxidases and with Protein Block Serum-Free (Agilent, Santa Clara, California, United States) for 15 minutes before adding the primary antibodies. Sections were then stained with the following primary antibodies: 4G8 anti-Aβp (1:500; Bio legend, San Diego, California, United States) and AT8 anti-p-Tau (Ser202, Thr205) antibody (1:500; Thermo-fisher Scientific, Massachusetts, United States) respectively for 1h at room temperature (RT). After washing three times with Tris buffered saline/0.05% Tween (TBST), sections were stained with secondary antibodies in TBS: HRP-conjugated anti-mouse IgG (1:500; Sigma-Aldrich, Missouri, United States) or anti-rabbit IgG (1:500; Sigma-Aldrich, Missouri, United States) respectively for 1h at RT. Sections were again washed three times with TBST before addition of 3,3'-Diaminobenzidine (DAB) substrate chromogen system and incubated for 5–10 minutes. Slides were then counterstained with hematoxylin for 1 min. After mounting, slides were finally imaged using the Olympus CX 43 light microscope (Shinjuku, Tokyo, Japan) [53].

5.3.5. Immunofluorescence co-localization study

Double immunofluorescence labelling was performed to determine whether $A\beta_{1-42}$ oligomers co-localized with Aβp in the cortex and hippocampus. Sections were co-stained with 4G8 antibody (1:500; Bio legend, San Diego, California, United States) and anti-$A\beta_{1-42}$ oligomer nanobody (PrioAD13; 1:500) [173]. Double immunofluorescence labelling was also performed to determine whether $A\beta_{1-42}$ oligomers co-localized with p-Tau in the cortex and hippocampus using anti-$A\beta_{1-42}$ oligomer nanobody (PrioAD13; 1: 500) and AT8 anti-p-Tau (Ser202, Thr205) antibody (Thermo-fisher Scientific, Massachusetts, United States). Sections were incubated with primary antibodies overnight at 4˚C. Sections were washed three times with TBST then incubated with secondary antibodies: goat anti-llama IgG conjugated to FITC (Bethyl Laboratories, Inc, Texas, USA) and donkey-anti-mouse IgG conjugated to Texas red (Sigma-Aldrich, Missouri, USA) at a dilution of 1:500 for 2 hours at RT. For IHC and IF studies, duplicate sections were also stained with secondary antibodies with omission of primary antibodies as negative control **(Figure 9)**. After washing with TBST sections were cover slipped with paramount aqueous mounting medium (Dako, Agilent, Santa Clara, California, USA), sealed and dried overnight. Finally, images were acquired using the LSM800 Confocal microscope with a standard FITC / Texas Red double band-pass filter set.

5.3.6. Neuropathological scoring of beta-amyloid and hyperphosphorylated tau

Counting the number of positively stained cells in 10 consecutive high-power fields (40 x) resulted in a score ("Ten Field Score"– TFS) for $A\beta_{1-42}$, Aβp and p-Tau in the hippocampus and cortex. Our scoring system was calculated by quantifying neurons and plaques showing intracellular immunofluorescence stain of $A\beta_{1-42}$ oligomers/p-Tau and extracellular deposits (plaques). For both $A\beta_{1-42}$ oligomers and p-Tau scoring, we first counted the number of positively stained cells in 10 consecutive high-power fields (40 x) which resulted in a TFS. After calculating the mean TFS values (mTFS) of Aβ oligomers or p-Tau intensity count from the 10 consecutive high-power fields, they were categorised as low, moderate, or high mTFS. For Aβ oligomers, a mTFS < 42 was considered as low, 42-52 as moderate and > 52 as high in the hippocampus and in the frontal cortex. For p-Tau, a mTFS < 40 was considered as low, 40-50 as moderate and > 50 as high in the hippocampus and in the frontal cortex. Finally, for Aβp scoring, as the number of plaques was scarce, we instead counted the total number of plaques (PC) per section. A PC <10 was considered as low, 10-20 as moderate and >20 as high in the hippocampus and in the frontal cortex. The extent to which both mTFS and PC scores were compared with CCD scores (**Table 1**) was determined [139].

Table 1. List of demographics, clinical and pathological information of seven aged dogs affected with Canine Cognitive Dysfunction

Animal No	Age (Years)	Breed	Size	Sex	CCD Score	Pathological Score		
						Hippocampus (H) and Frontal cortex (Fc)		
						mTFS-Aβo	mTFS-p-Tau	PC-Aβp
1	14	Papillion	Small	Castrated male	44	37.2 (H) 41.5 (Fc)	36.4 (H) 36.3 (Fc)	21(H) 15 (Fc)
2	14	Mongrel	Medium	Castrated male	58	53.6 (H) 46.3 (Fc)	47.2 (H) 45.1 (Fc)	20 (H) 22 (Fc)
3	15	Pomeranian	Small	Male	58	55.1 (H) 63.5 (Fc)	64.2 (H) 67.2 (Fc)	30 (H) 32 (Fc)
4	16	Lhasa Apso	Small	Male	38	52 (H) 57 (Fc)	45.9 (H) 66.5 (Fc)	16 (H) 20 (Fc)
5	16	Mongrel	Small	Female	50	11.9 (H) 41.1 (Fc)	56 (H) 15.3 (Fc)	15 (H) 10 (Fc)
6	17	Shiba Inu	Medium	Spayed female	64	44.8 (H) 41.3 (Fc)	62.1 (H) 25.9 (Fc)	5 (H) 14 (Fc)
7	17	Mongrel	Medium	Spayed female	60	60 (H) 54.1 (Fc)	53.9 (H) 68.6 (Fc)	23 (H) 18 (Fc)

Table 1. Aβo indicates amyloid beta ($A\beta_{1\text{-}42}$) oligomers, p-Tau indicates hyperphosphorylated tau and Aβp indicates amyloid beta plaques. TFS (Ten Field Score) refers to positively stained cells in 10 consecutive high-power fields (40 x) which resulted in a score. mTFS is the mean value of the 10 high-power fields. PC is plaque count. mTFS of Amyloid β oligomers (Aβo) in the hippocampus and frontal cortex: <42 considered as low, 42-52 as moderate, >52 as high. mTFS of p-Tau <40 considered as low, 40-50 as moderate, >50 as high in the hippocampus and frontal cortex. Plaque count (PC) of amyloid β plaques: <10 considered as low, 10-20 as moderate and >20 as high in the hippocampus and frontal cortex.

5.4. Results

5.4.1. Aged dogs with canine cognitive dysfunction display similar neuropathology to human Alzheimer's disease

CAA is one of the histological hallmarks observed in the brains of AD patients and is characterised by the accumulation of Aβ in cerebral blood vessels [20,31]. In this study, we used CR staining to identify amyloid fibrils and CAA deposits in the cortex and hippocampus of the aged dogs affected with CCD. Congophilic deposits were detected in CR-hematoxylin-stained sections and substantiated by cross-polarized light and appeared as apple-green birefringence in the brain hippocampal and cortical region confirming the presence of CAA (**Figure 1**). However, as anticipated, CR positivity was not observed in the diffuse plaques in the hippocampal and cortical regions of the aged dogs (**Figure 2**), indicating lack of the β pleated-sheet conformations [136]. Further, the hippocampus and cortex displayed widespread deposition of diffuse Aβp following IHC and IF staining with 4G8 antibody (**Figure 3, 4 and 5**).

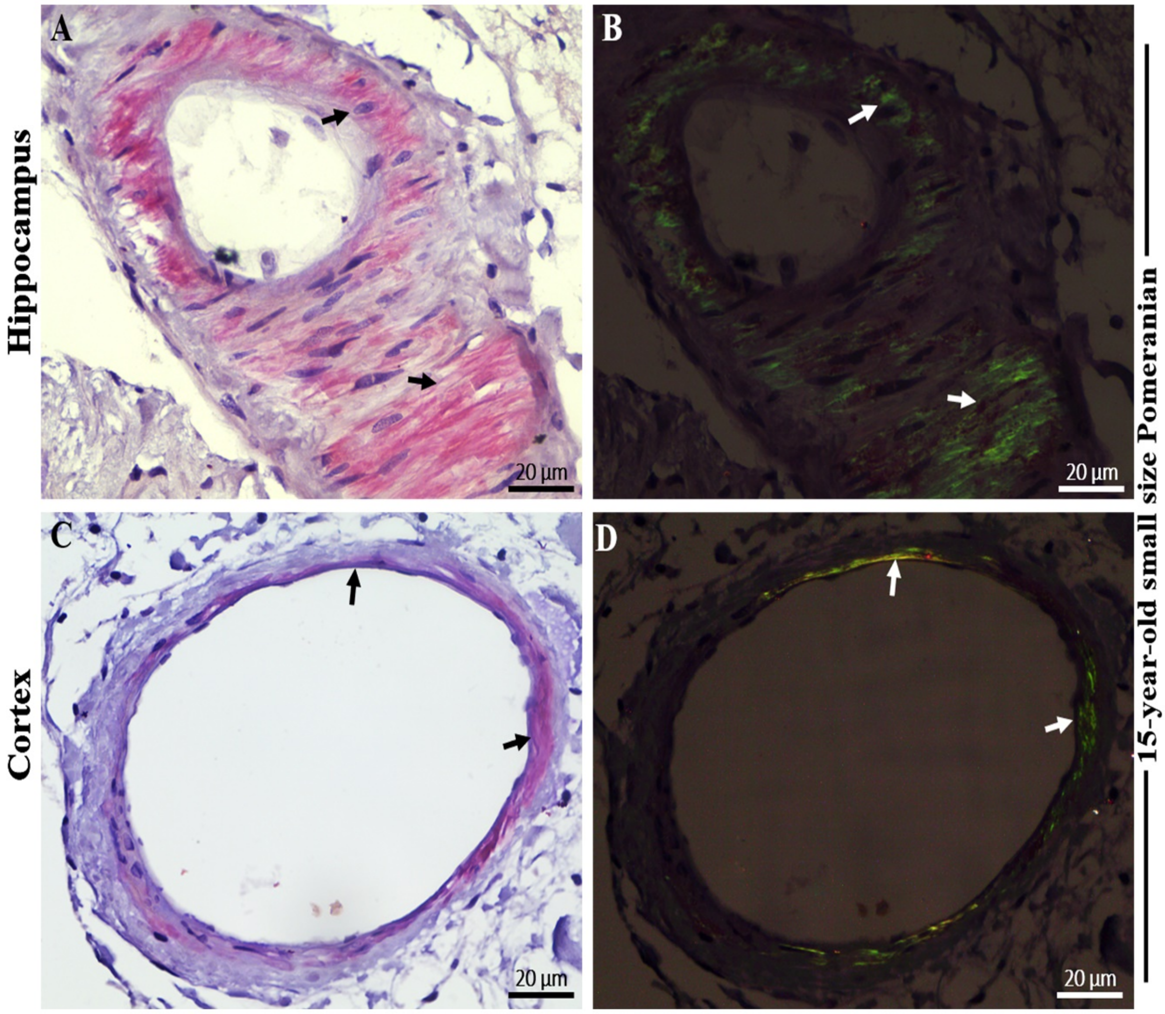

Figure 1. Photomicrographs of Congo red (CR) staining in cerebral amyloid angiopathy (CAA) in the brain hippocampal and cortical region of an aged dog. Distinctive red brick staining of cerebral blood vessels (largely the tunica media) (A) in the hippocampus and (C) in the frontal cortex (black arrows) of a 15-year-old small size Pomeranian following CR-hematoxylin staining. Vascular amyloid, confirming CAA, with the presence of apple-green birefringence (B) in the hippocampus and (D) in the frontal cortex (white arrows) of a 15-year-old small size Pomeranian under polarized light. Representative of all aged dogs. Scale bar = 20µm.

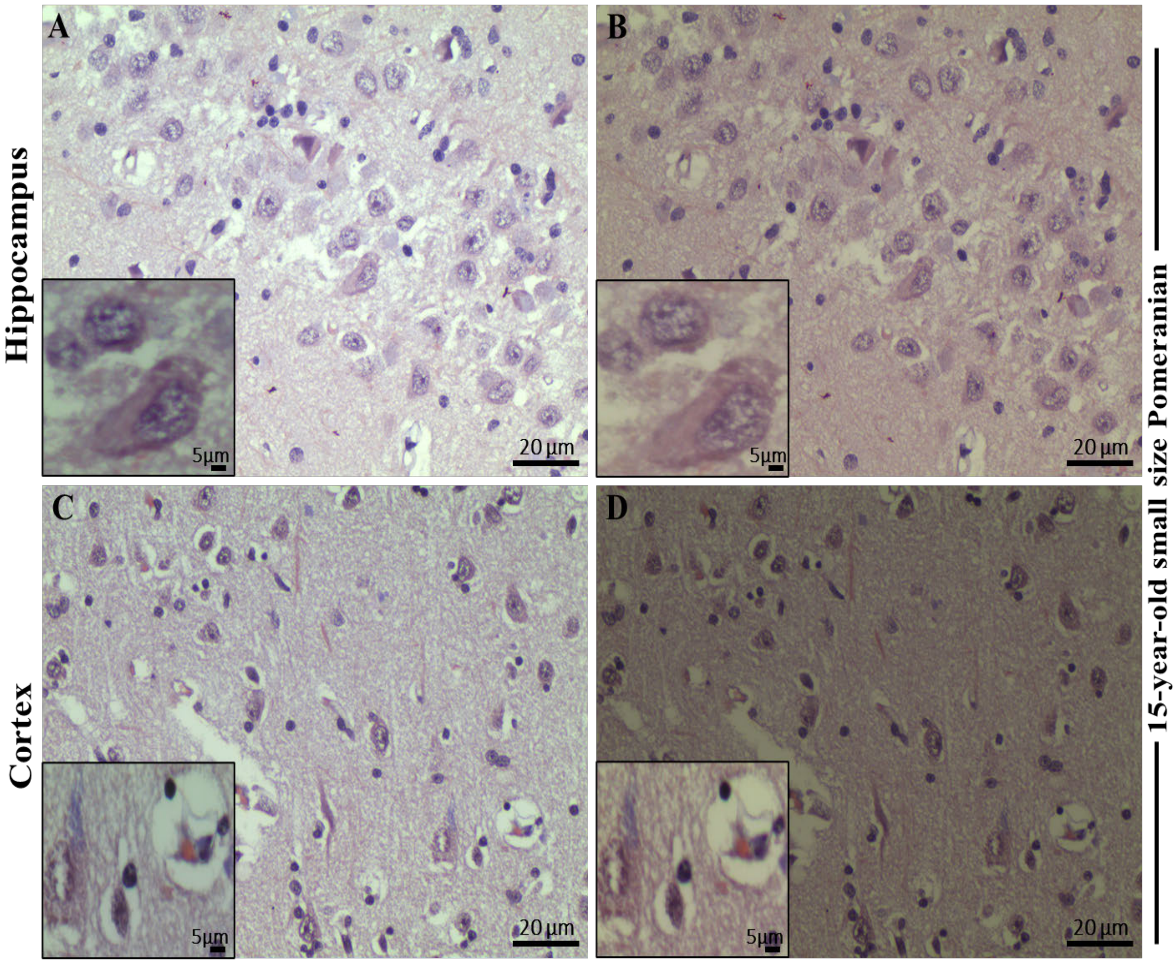

Figure 2. Photomicrographs of Congo red (CR) staining in the brain hippocampal and cortical region of a 15-year-old small size Pomeranian. No distinctive red-brick staining of amyloid fibrils and apple-green birefringence with Congo red staining were observed in the brain A, B) hippocampus C, D) frontal cortex of a 15-year-old small size Pomeranian (scale bar = 20µm and inserts scale bar = 5 µm). Representative of all aged dogs.

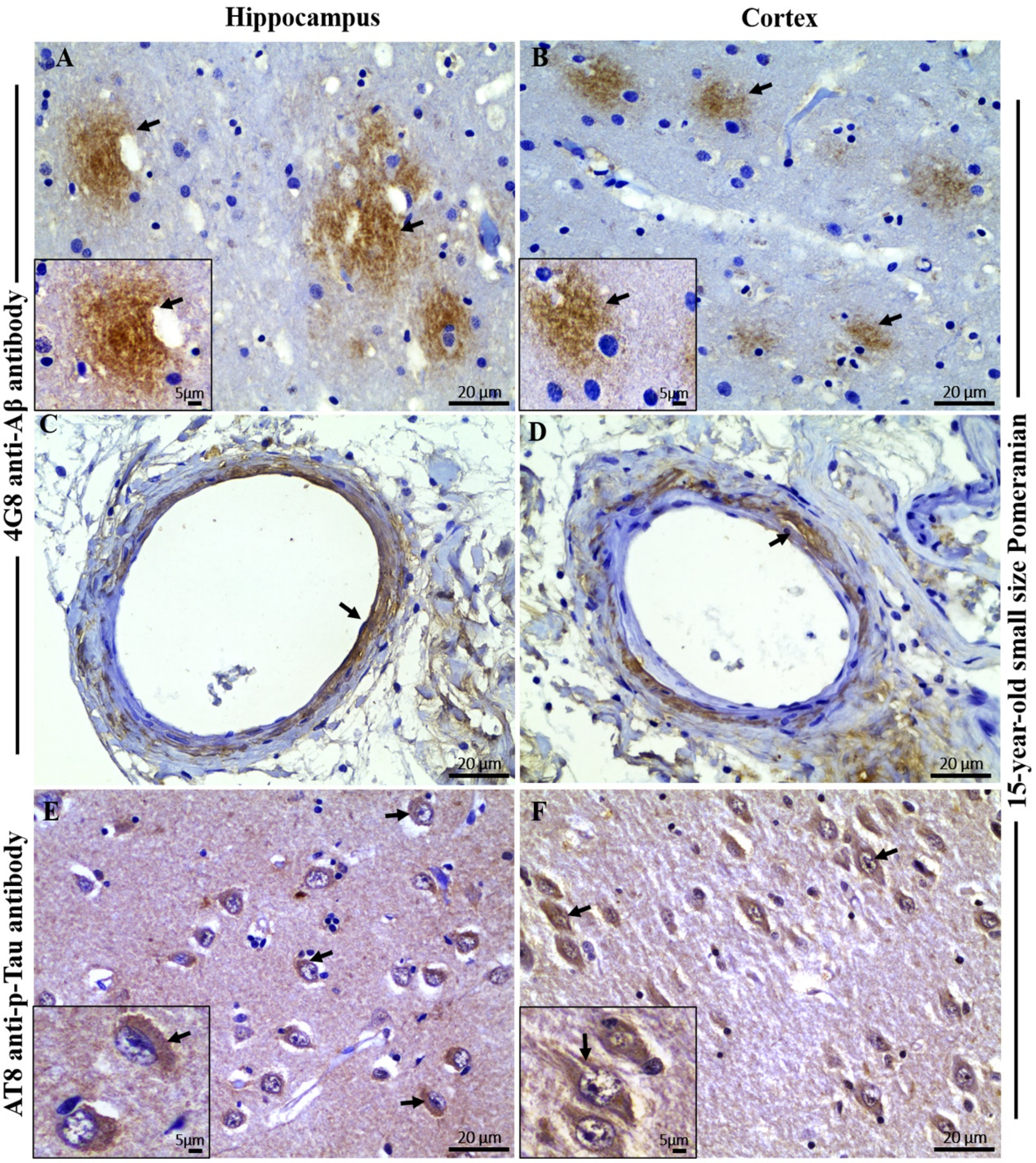

Figure 3. Immunohistochemical staining with 4G8 anti-Aβ and AT8 anti-pTau antibody in the brain hippocampal and cortical region of an aged dog. Immunohistochemical staining showed extensive extracellular Aβ plaques in the A) hippocampus and & B) frontal cortex (black arrows) of a 15-year-old small size Pomeranian. Staining of vascular amyloid (cerebral amyloid angiopathy) was prominent in the C) hippocampus and D) frontal cortex of a 15-year-old small size Pomeranian respectively (black arrows). Immunohistochemical staining showed extensive intracellular hyperphosphorylated tau (p-Tau) staining in the E) hippocampus and F) frontal cortex respectively (black arrows) of a 15-year-old small size Pomeranian. Representative of all aged dogs. Scale bar = 20μm and inserts scale bar = 5μm.

We then compared the PC among the seven aged dogs including five affected with CCD (**Figure 7, Table 1**). In general, dogs with the higher CCD scores also had among the higher PC-Aβp counts (dogs number 2, 3 and 7) but dog number 6 with the highest CCD score of 64 showed the lowest plaque count with a PC =5 in the hippocampal region and a moderate PC =14 in the cortex **(Figure 7, Table 1**), indicating that the senile plaques may not be responsible for the cognitive deficits in these aged dogs as demonstrated for human AD [20,138]. Amyloid β formation progresses from monomers to oligomers to fibrils and then to plaques. In order to identify the earlier assembly and most toxic isoform of Aβ, namely $A\beta_{1-42}$ oligomers and determine whether $A\beta_{1-42}$ oligomers co-localised with Aβp, we co-stained the hippocampal and cortical regions with both 4G8 and PrioAD13 anti-$A\beta_{1-42}$ nanobody [173]. Of importance, intraneuronal $A\beta_{1-42}$ oligomers deposition was widespread but did not co-localise with Aβp (**Figure 4 and 5**). Highest mTFS of $A\beta_{1-42}$ oligomers (hippocampus = 55.1; cortex = 63.5) were observed in a 15-year-old small size male Pomeranian with a CCD score of 58 and a 17-year-old medium size spayed female Mongrel (hippocampus = 60; cortex = 54.1) with a CCD score 60 (**Figure 8, Table 1**). Moderate to high $A\beta_{1-42}$ oligomers mTFS were observed in a 16-year-old small size Lhasa Apso (hippocampus = 52; cortex = 57) with a CCD score of 38 and a 14-year-old medium size castrated male Mongrel (hippocampus = 53.6; cortex = 46.3) with a CCD score of 58 respectively (**Figure 8, Table 1**). A 14-year old castrated male Papillion with a CCD score of 44 displayed low mTFS (hippocampus = 37.2; cortex =41.5) and finally a 16-year-old female Mongrel with a CCD score of 50 exhibited the lowest mTFS (hippocampus = 11.9; cortex =41.1) (**Figure 8, Table 1**).

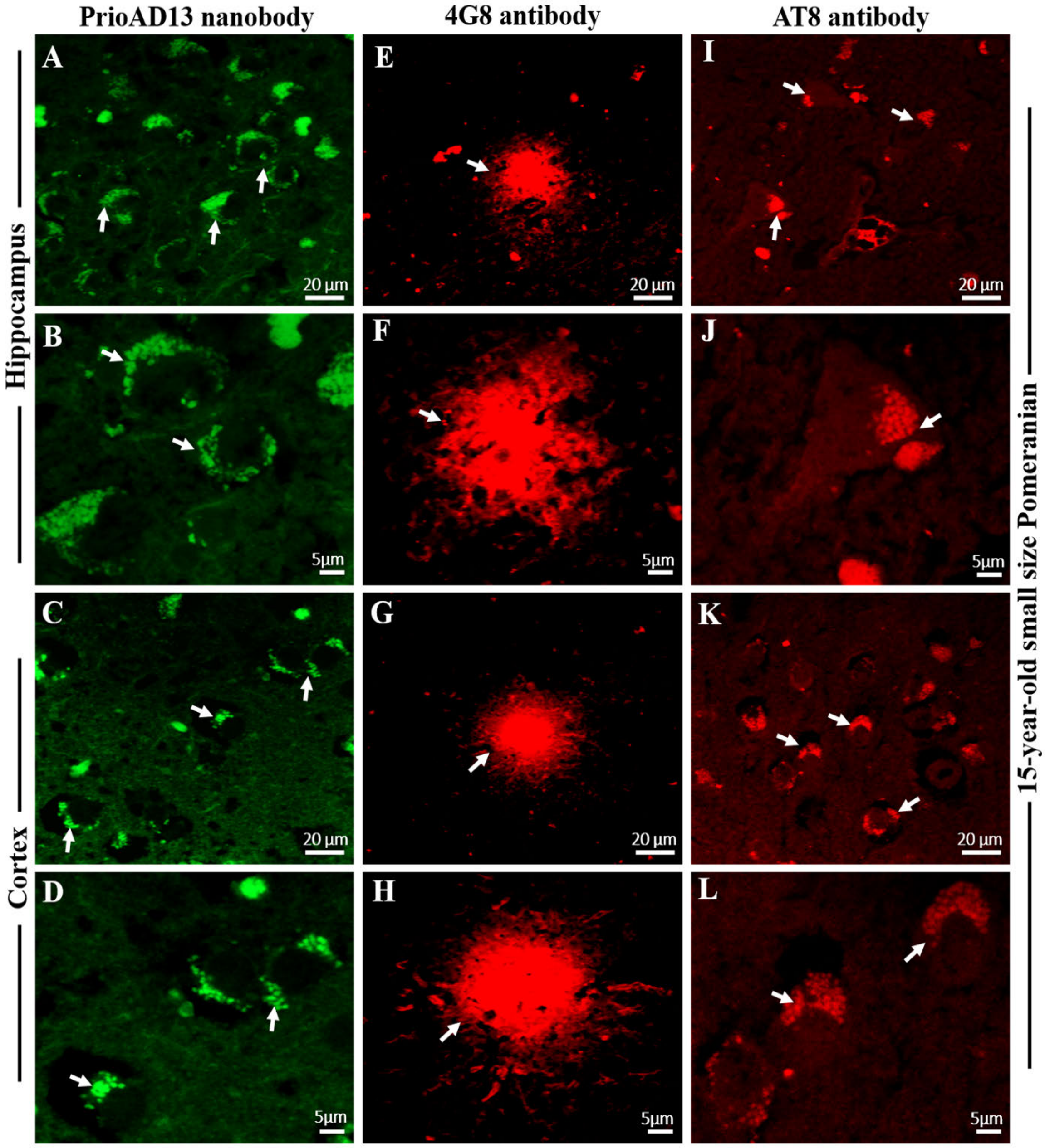

Figure 4. Immunofluorescence staining with PrioAD13 anti-Aβ$_{1-42}$ oligomer nanobody, 4G8 anti-Aβ and AT8 anti phospho-Tau (Ser202, Thr205) antibody in brain hippocampal and cortical region of an aged dog. LSM800 confocal images were taken at 40x and 100x respectively for each tissue section with a standard FITC / Texas Red double band-pass filter set. Staining with anti-Aβ$_{1-42}$ (PrioAD13) nanobody (GREEN) demonstrated extensive intracellular deposition of Aβ$_{1-42}$ oligomers (white arrows) in the hippocampus at A) 40x magnification, scale bar = 20µm and B) higher magnification at 100x, scale bar = 5µm and also in the frontal cortex at C) 40x magnification, scale bar = 20µm and D) higher magnification at 100x, scale bar = 5µm of a 15-year-old small size Pomeranian; Staining with 4G8 anti-Aβ antibody (RED) displayed extracellular diffuse plaque (white arrows) in the hippocampus both at E) 40x magnification, scale bar = 20µm and F) higher magnification at 100x, scale bar = 5µm and in the frontal cortex at G) 40x magnification, scale bar = 20µm and H) higher

magnification at 100x, scale bar = 5µm of a 15-year-old small size Pomeranian; Staining with AT8 anti-p-Tau antibody (RED) exhibited widespread intracellular p-Tau (white arrows) in the hippocampus both at I) 40x magnification, scale bar = 20µm and J) higher magnification at 100x, scale bar = 5µm and in the frontal cortex both at K) 40x magnification, scale bar = 20µm and L) higher magnification at 100x, scale bar = 5µm of a 15-year-old small size Pomeranian. Representative of all aged dogs.

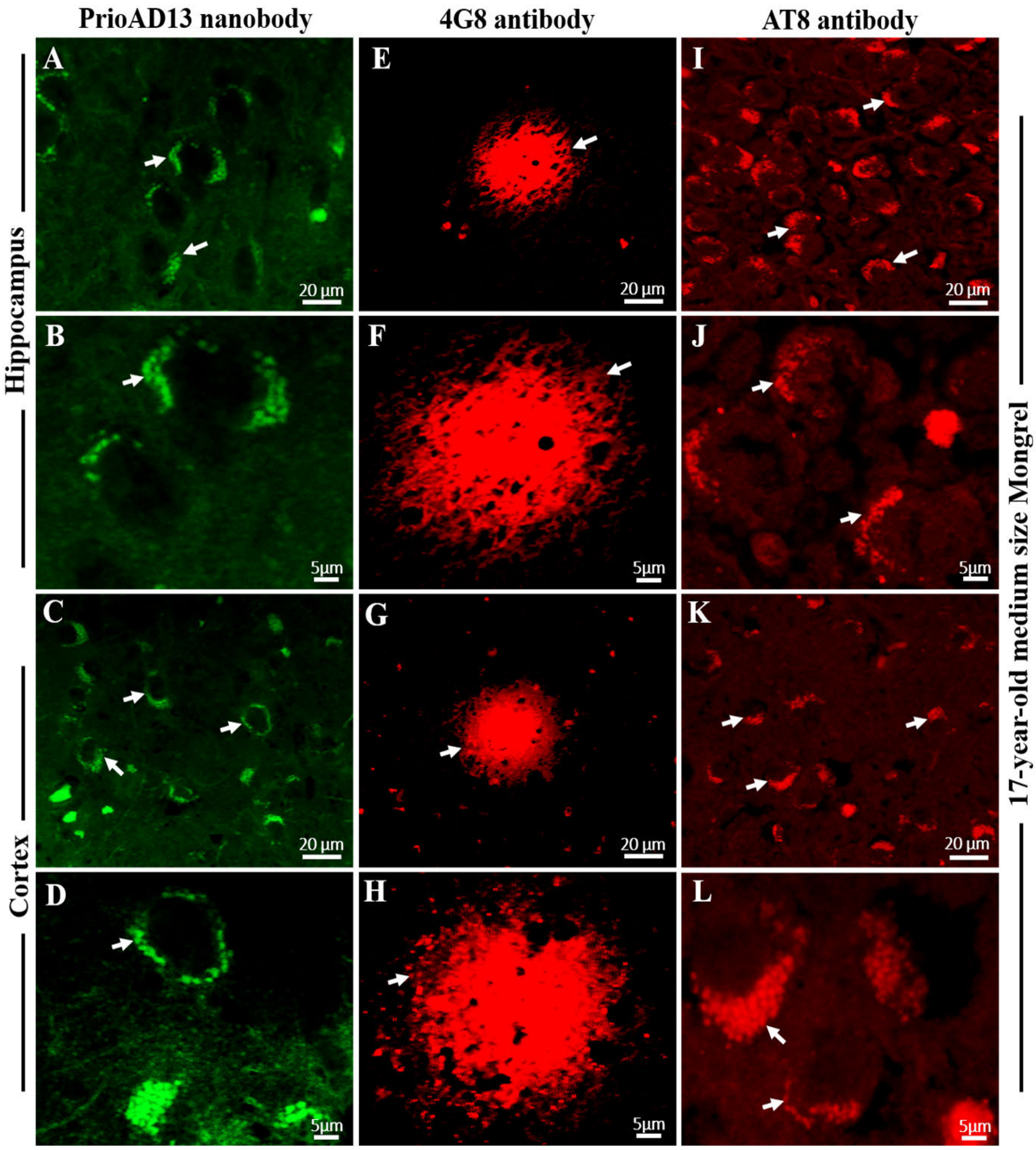

Figure 5. Immunofluorescence staining with PrioAD13 anti-Aβ$_{1-42}$ oligomer nanobody, 4G8 anti-Aβ and AT8 anti phospho-Tau (Ser202, Thr205) antibody in brain hippocampal and cortical region of an aged dog. LSM800 confocal images were taken at 40x and 100x respectively for each tissue section with a standard FITC / Texas Red double band-pass filter set. Staining with anti-Aβ$_{1-42}$ (PrioAD13) nanobody (GREEN) demonstrated widespread

intracellular deposition of $A\beta_{1\text{-}42}$ oligomers (white arrows) in the hippocampus at A) 40x magnification, scale bar = 20µm and B) higher magnification at 100x, scale bar = 5µm and also in the frontal cortex at C) 40x magnification, scale bar = 20µm and D) higher magnification at 100x, scale bar = 5µm of a 17-year-old medium size Mongrel; Staining with 4G8 anti-Aβ antibody (RED) displayed extracellular diffuse plaque (white arrows) in the hippocampus both at E) 40x magnification, scale bar = 20µm and F) higher magnification at 100x, scale bar = 5µm and in the frontal cortex at G) 40x magnification, scale bar = 20µm and H) higher magnification at 100x, scale bar = 5µm of a 17-year-old medium size Mongrel; Staining with AT8 anti-p-Tau antibody (RED) exhibited extensive intracellular p-Tau (white arrows) in the hippocampus both at I) 40x magnification, scale bar = 20µm and J) higher magnification at 100x, scale bar = 5µm and in the frontal cortex both at K) 40x magnification, scale bar = 20µm and L) higher magnification at 100x, scale bar = 5µm of a 17-year-old medium size Mongrel. Representative of all aged dogs.

Finally, AT8 anti-p-Tau (Ser202, Thr205) monoclonal antibody strongly bound to p-Tau in the hippocampal and cortical regions following staining using IHC (**Figure 2**) and IF (**Figure 4 and 5**) and displayed intracellular structures [21,31]. Highest mTFS of p-Tau were seen in a 15-year-old small size Pomeranian (hippocampus = 64.2; cortex = 67.2) with a CCD score 58 and in a 17-year-old medium size Mongrel (hippocampus = 53.9; cortex = 68.6) with a CCD score of 60 (**Figure 8, Table 1**). Moderate to high mTFS of p-Tau were displayed in a 16-year-old small size Lhasa Apso (hippocampus = 45.9; cortex = 66.5) with a CCD score of 38 and a 14-year-old medium size Mongrel (hippocampus = 47.2; cortex = 45.1) with a CCD score of 58. Finally, lowest mTFS of p-Tau were seen in a 14-year-old small size Papillion (hippocampus = 36.4; cortex = 36.3) with a CCD score of 44. Interestingly a 17-year-old medium size Shiba Inu with a CCD score of 64 and a 16-year-old small size female Mongrel with a CCD score of 50 exhibited high mTFS for p-Tau in the hippocampus (62.1 and 56 respectively) and low mTFS for p-Tau in the cortex (25.9 and 15.3 respectively) (**Figure 8, Table 1**)

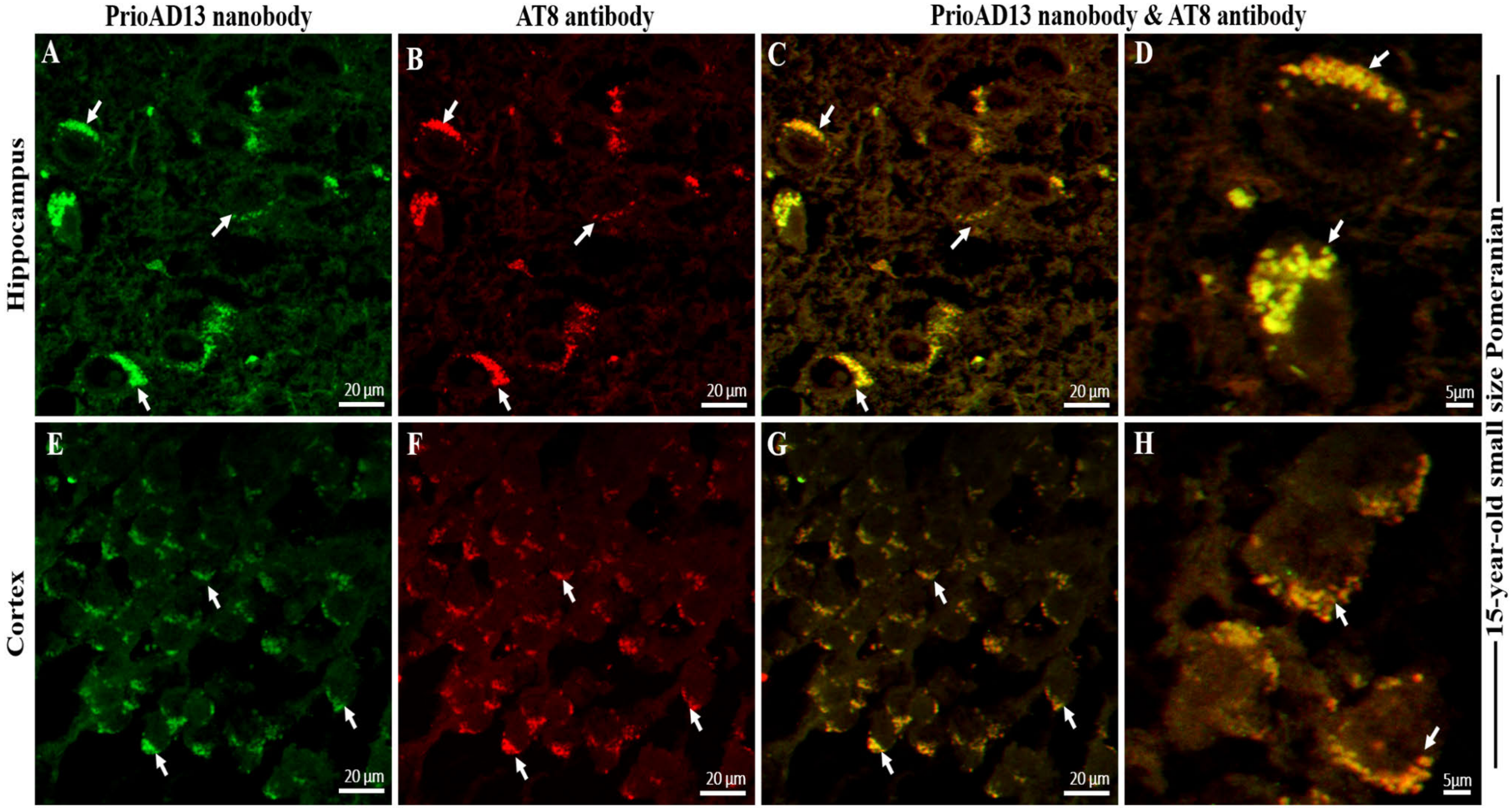

Figure 6. Co-localisation Aβ oligomers and phosphorylated Tau (p-Tau) in the hippocampus and frontal cortex of an aged dog. LSM800 confocal images were taken at 40x and 100x respectively with a standard FITC / Texas Red double band-pass filter set. Staining with anti-$A\beta_{1\text{-}42}$ (PrioAD13) nanobody (GREEN) exhibited intracellular deposition of $A\beta_{1\text{-}42}$ oligomers (white arrows) in the A) hippocampus and in the E) frontal

cortex of a 15-year-old small Pomeranian, Scale bar = 20µm. Staining with AT8 anti-p-Tau antibody (RED) displayed widespread intracellular p-Tau (white arrows) in the B) hippocampus and in the F) frontal cortex of a 15-year-old small Pomeranian respectively, Scale bar = 20µm. Co-localisation, such as indicated by arrows, of anti-Aβ_{1-42} (PrioAD13) nanobody and AT8 anti-p-Tau antibody demonstrated the intracellular co-accumulation of Aβ_{1-42} oligomers and p-Tau in the hippocampus at C) 40x magnification, scale bar = 20µm and D) higher magnification at 100x, scale bar = 5µm and in the frontal cortex at G) 40x magnification, scale bar = 20µm and H) higher magnification at 100x, scale bar = 5µm respectively. Representative of all aged dogs.

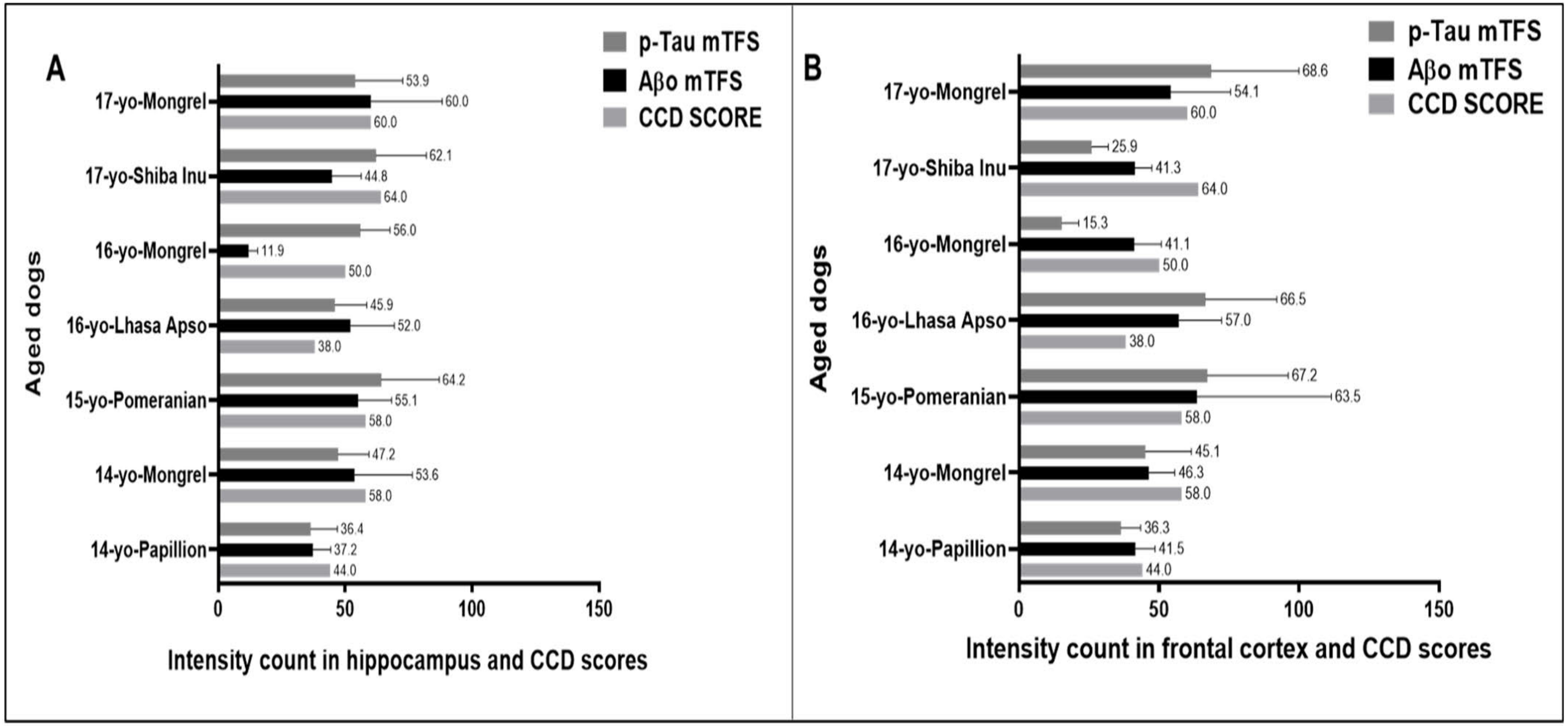

Figure 7. Comparing the CCD Scores with hippocampal and cortical Aβ plaque count (PC) in seven aged dogs. CCD score of ≥ 50 were considered as CCD or dog dementia. Aβ plaque count (PC) was calculated from whole tissue sections at high power fields (40x). Plaque count (PC) of amyloid β plaques: <10 considered as low,10-20 as moderate and >20 as high in the hippocampus and frontal cortex. A small size male Pomeranian with CCD score of 58 displayed the highest PC in the (A) hippocampus, PC=30 and in the (B) frontal cortex, PC=32. In contrast, a medium size spayed female Shiba Inu with highest CCD score of 64 exhibited the lowest PC in the (A) hippocampus, PC=5 and a 16-year-old small size female Mongrel with CCD score of 50 showed the lowest PC in the (B) frontal cortex, PC=10.

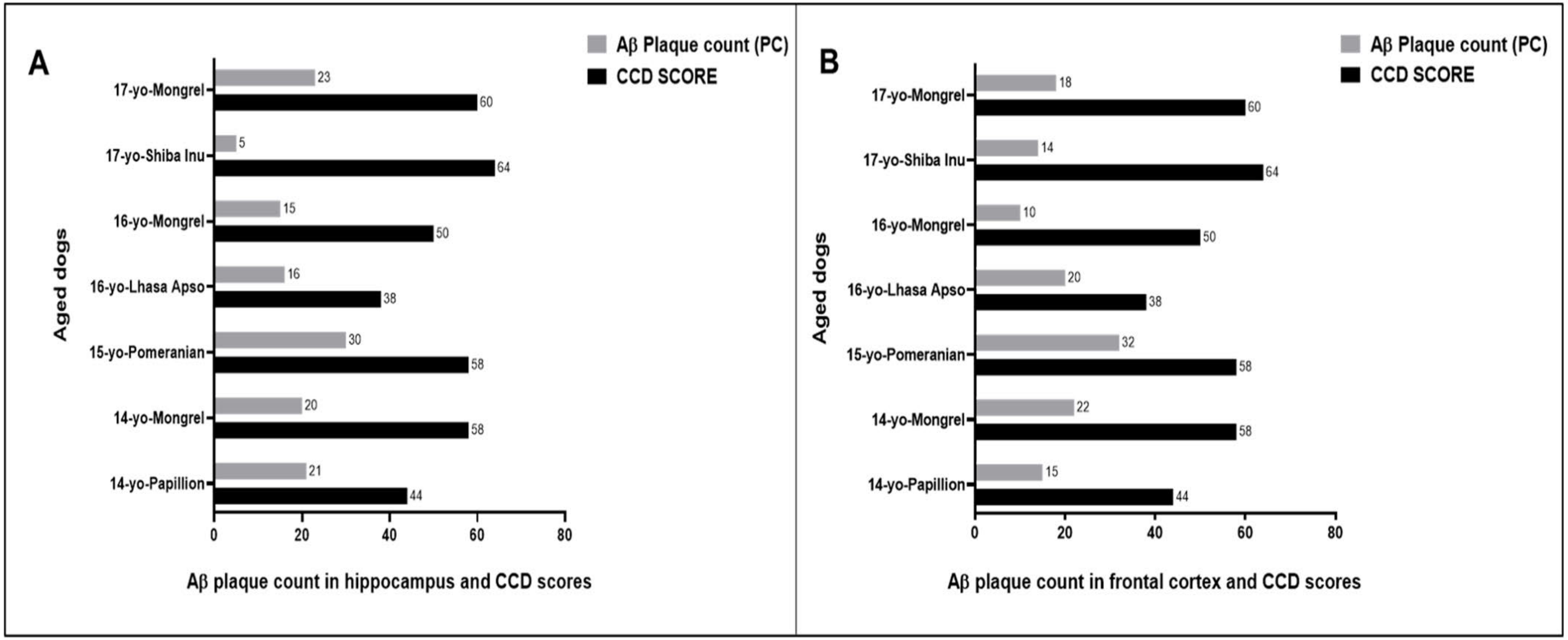

Figure 8. Comparing the CCD Scores with hippocampal and cortical $A\beta_{1-42}$ oligomers (Aβo), hyperphosphorylated tau (p-Tau) mean Ten Field Score (mTFS) in seven aged dogs. CCD score of ≥ 50 were considered as CCD or dog dementia. mTFS is the mean value calculated from 10 consecutive high-power fields (40x). mTFS of Amyloid β oligomers (Aβo) in the hippocampus and frontal cortex: <42 considered as low, 42-52 as moderate, >52 as high and mTFS of p-Tau <40 considered as low, 40-50 as moderate, >50 as high in the hippocampus and frontal cortex respectively. A small size male Pomeranian with CCD score of 58 has the highest Aβo mTFS = 55.1 and 63.5 and p-Tau mTFS=64.2 and 67.2 in the (A) hippocampus and in the (B) frontal cortex respectively. In the (A) hippocampus a 16-year-old small size female Mongrel with CCD score of 50 exhibited the lowest Aβo mTFS = 11.9 and a 14-year-old small size castrated male Papillion with CCD score of 44 showed the lowest p-Tau mTFS = 36.4 whereas, in the (B) frontal cortex a 16-year-old small size female Mongrel with CCD score of 50 showed the lowest Aβo mTFS= 41.1 and p-Tau mTFS = 15.3 respectively.

We then investigated whether the toxic $A\beta_{1-42}$ oligomers and p-Tau co-localised to the same cellular compartments by double labelling of $A\beta_{1-42}$ oligomers (PrioAD13) and p-Tau (AT8) in the hippocampal and cortical regions of the aged dog brains. We found widespread intracellular co-localisation of oligomers with p-Tau deposits in the hippocampus and cortex (**Figure 6**). High levels of $A\beta_{1-42}$ oligomers and p-Tau which co-localised in a large number of neurons were found in a 15-year-old small size Pomeranian. Of note, this particular dog displayed the highest mTFS for both $A\beta_{1-42}$ oligomer and p-Tau (**Figure 8, Table 1**). This concurrent accumulation of both $A\beta_{1-42}$ oligomer and p-Tau [63,65], independent of Aβp co-localisation**,** suggests that they may act synergistically to enhance synaptic dysfunction and neuronal death as shown in human AD [45,64].

5.4.2. Clinical and demographic predictors of neuropathology in aged dogs with canine cognitive dysfunction

Details of the demographics of the aged dogs in this study reveal ages of 14 to 17 years with two castrated males, two males, one female and two sprayed females. There were four small size and three medium size dogs (**Table 1**). Previous studies showed that small size dogs usually have a longer life span than the larger dogs and are more prone to have age related disorder [292] [293]. In our study, a 15-year-old small size male Pomeranian and a 17-year-old medium size sprayed female Mongrel displayed the highest Aβp count (**Figure 7, Table 1**) as well as mTFS for_$A\beta_{1-42}$ oligomer and p-Tau (**Figure 8, Table 1**). However, while a 14-year-old Papillion displayed one of the lowest pathological scores we also found that a 16-year-old small size female Mongrel also had many low scores (**Figure 7 and 8, Table 1**). In addition, a medium size breed Shiba Inu is one of the oldest dogs included in our study and showed the highest CCD score of 64 but exhibited the lowest number of plaques and moderate levels of $A\beta_{1-42}$ oligomers and p-Tau (**Figure 7 and 8, Table 1**), which suggests that CCD score might be triggered by the age and pathological scores including $A\beta_{1-42}$ oligomers and p-Tau depositions but not with Aβp deposition [138].

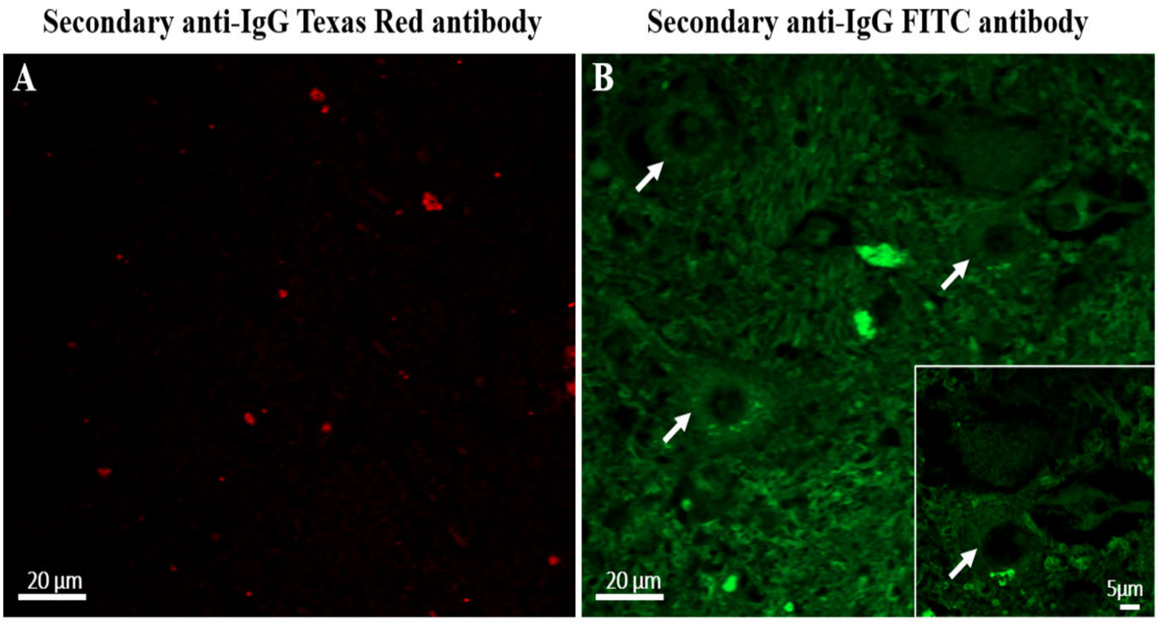

Figure 9. Immunofluorescence staining of hippocampal region of an aged dog. Secondary antibody with the omission of the primary antibody was used as a negative control. Secondary anti-IgG Texas Red (RED) or FITC (GREEN) antibodies were used in the hippocampus (A & B) of a 15-year-old small size Pomeranian, scale bar = 20µm, insert scale bar = 5µm. Representative of all aged dogs.

5.5. Discussion

In the present study we investigated the presence of neuropathological hallmarks normally associated with human AD in a few breeds of aged dogs affected with a syndrome called canine cognitive dysfunction (CCD) [138,291]. Transgenic mice, used extensively to investigate human AD [159], have provided crucial information related to AD pathogenesis but their translational use has been inadequate. Therapeutic successes in treating AD in mice models have failed in numerous human AD clinical trials [118]. Dogs with CCD appear to replicate many neuropathological hallmarks of human AD, including accumulation of Aβ oligomers and plaques as well as CAA [129,145,291]. However, dogs with CCD are not universally accepted as a valid natural disease model of AD because the presence of a fundamental lesion, namely p-

Tau, has been demonstrated in only a minority of cases and thus its association with this syndrome remains controversial [129,136,137,142,143]. To that end, we used a refined antigen retrieval protocol that enabled us to conclusively identify p-Tau in the hippocampal and cortical regions of aged dogs. The newly refined protocol for both immunohistochemical and immunofluorescence p-Tau staining relied on the use of the 2100 antigen retriever [294], which helped maintain optimal temperature, pressure and cycle time automatically controlled by an in-built sensor. The p-Tau are composed of microtubule-associated hyperphosphorylated tau protein. In human AD, p-Tau are deposited within the neurons and their morphology may vary according to the type of neurons [21,31]. Braak and Braak proposed six distinct stages for the progression of p-Tau [148,295] which include Braak and Braak stage III/IV where NFTs is present in the hippocampus [20,148,295]. In the current study, aged dogs exhibited extensive deposition of intracellular AT8 positive p-Tau in the hippocampal and frontal cortex region, therefore replicating morphological and regional distribution similar to human AD pathology [20]. Aged dogs also exhibited widespread distribution of both $A\beta_{1\text{-}42}$ oligomers [296] and diffuse Aβp in the frontal cortex and hippocampal region [142,149]. In human AD brain, regional distribution of Aβp is less predictable as compared to p-Tau distribution [20] . According to the Braak and Braak staging of amyloid accumulation, Aβp first deposits in the basal portions of the frontal, temporal and occipital lobes (stage A) and then expand towards the hippocampal region (stage B) [72,148]. In the canine brain, widespread Aβp deposition has been found involving prefrontal, parietal, occipital and entorhinal cortices in dogs [146]. However, Aβo have not been well characterised histopathologically in dog brains affected with CCD. A previous study by Head and colleagues demonstrated accumulation of Aβo in the CSF of aged Beagles which inversely correlated with brain total Aβ load [296]. Furthermore, Rusbridge and colleagues were able to immunodetect Aβo in blood and CSF of an aged dog affected with CCD using single domain camelid antibody fragments PrioAD12 ($A\beta_{1\text{–}40}$), or PrioAD13 ($A\beta_{1\text{–}42}$) and also reported the neurotoxic effect of dog Aβo in a human neuroblastoma cell line [297]. In the present study we identified $A\beta_{1-42}$ oligomers using single domain camelid antibody in our immunofluorescence assay. We showed extensive distribution of intracellular $A\beta_{1-42}$ oligomers in the frontal cortex and hippocampus which failed to co-localise with diffuse Aβ plaques. In contrast, co-accumulation of p-Tau and $A\beta_{1-42}$ oligomers deposits were conspicuous and closely linked. This strongly supports the hypothesis that it is the co-accumulation of both Aβ oligomers and p-Tau, and not Aβ plaques and p-Tau that are responsible for the neurotoxic effects and resultant cognitive deficits associated with AD [65] and CCD [144,297,298]. This might also indicate that Aβo may be responsible for initiating accumulation and spread of p-Tau as shown previously in human AD [299,300]. Shin and colleagues reported a synergistic interaction between Aβo and Tau aggregates [63]. The authors used different assemblies of Aβ in a Tau cell-based model, including human neuroblastoma cells and primary hippocampal neurons and showed that Tau seeding was facilitated by Aβo rather than Aβ fibrils or aggregates [63]. Interestingly, Chambers and colleagues showed for the first time that aged domestic cats develop hippocampal Aβ accumulation and NFT formation [301]. The authors demonstrated that Aβo accumulate in the cytosol of hippocampal pyramidal cells and suggested that these lead to p-Tau and NFT development [301,302]. Moreover, we developed a new scheme that allowed us to count the number of positively stained cells in 10 consecutive high-power fields (40 x) resulted in a score, similar to the "mitotic index" widely used for assessing cancer pathology [303], to quantify $A\beta_{1-42}$ oligomers and p-Tau (mTFS); we also quantified the total number of plaques (PC) in the hippocampal and cortical regions of the seven aged dogs. We then compared the quantified brain pathologies (mTFS vs PC) with cognitive performance (CCD scores). The cognitive scores were determined by a reference study by Salvin and colleagues who had developed a comprehensive questionnaire consisting of 13 questions to enable dog owners to rate cognitive function/dysfunction in aged dogs with 98.9% diagnostic accuracy. This questionnaire was used to score CCD (CCD score) in the seven dogs investigated in this study [21]. Among the seven aged dogs, five dogs were diagnosed with CCD (score ≥50) and two dogs were nondemented (CCD score <50) which included a 16-year-old small size Lhasa Apso with a CCD score of 38 and a 14-year-old small size Papillion with a CCD scores of 44.

In AD, both neuritic and diffuse plaques are usually found in human brain where the former are believed to be associated with synaptic loss and glial cell reactivity and the latter related to ageing. The effects of neuritic and/or diffuse plaques was previously investigated in cognitively unimpaired individuals and dogs [20,129,149,304]. Ahmadi and colleagues [305] assessed the link between cognitive performance and diffuse as well as neuritic plaque depositions in cognitively unimpaired individuals. The authors showed that cognitively unimpaired individuals with neuritic plaques exhibited low cognitive performance whereas diffuse plaques were shown to not influence cognition. Moreover, this study demonstrated that while diffuse plaques were not involved in cognitive deficits, increased neuritic plaques deposition paralleled a decrease in cognitive performance [305]. Similarly, Rofina and colleagues [138] performed a semiquantitative analysis of diffuse Aβ plaque deposition in a group of 30 dogs aged between 1 month to 19 years. The authors showed that diffuse plaques deposition was significantly higher in dogs older than 11 years. Furthermore, the authors demonstrated that this increased diffuse plaque burden did not influence the cognitive ability of the dogs[138]. Similarly, our study also confirmed that aged non-demented dogs (14-year-old Papillion and 16-year-old Lhasa Apso) with low CCD scores (< 50) also displayed high PC scores reflecting a high burden of diffuse Aβp. Our study supports the hypothesis that diffuse plaques might be the part of normal ageing process, however, larger cohorts of dogs should be investigated in order to reach a conclusive outcome.

5.6. Conclusion

In conclusion, aged dogs affected with CCD display neuropathological features resembling those observed in human AD, such as intracellular Aβ oligomers, Aβp, CAA and p-Tau as well as cognitive dysfunction [20]. To date no studies have conclusively demonstrated this extensive accumulation of p-Tau in dog brains; our study achieved this goal through the crucial use of an improved antigen retrieval methodology. Remarkably, early middle-aged dogs (6-10 years), equivalent to humans age 40-60 years [166], displayed cognitive decline and neurobehavioral changes which worsened with age, similar to human mild cognitive impairment (MCI) [129,306]. The ability to characterise aged dogs as a strong translational model for hAD offers a real possibility to efficiently investigate molecular determinants underlying AD pathogenesis, and to develop and test molecules for effective detection and treatment of AD. However, the use of imaging modalities, such as PET and MRI, currently used to aid in the diagnosis of hAD, is limited in aged dogs affected with CCD[307,308]. There are substantial advantages of incorporating PET/MRI neuroimaging platforms to study/monitor AD in a large animal model such as dogs and will certainly inform on disease status, correlate blood and eye biomarkers with brain pathology and predict treatment outcomes. Taken together, our results confirm the presence of the major neuropathological hallmarks of human AD associated with cognitive decline and argue for the use of this natural model to investigate AD.

Chapter 6

Results (Paper 4)

6. Amyloid Beta Oligomers and Phosphorylated Tau Deposition in the Retina of Cognitively Unimpaired Dogs (in preparation)

Umma Habiba[1], Leandro Teixeira[2], John Morley[1], Mark Krockenberger[3], Brian Summers[4], Richard Dubielzig[2], Mourad Tayebi[1*]

[1]School of Medicine, Western Sydney University, Campbelltown, NSW, Australia; [2]School of Veterinary Medicine, University of Wisconsin-Madison, Madison, United States; [3]Faculty of science, University of Sydney NSW, Australia; [4]School of Veterinary Medicine, Melbourne University, Werribee, Victoria, Australia.

6.1. Abstract

Human and companion animals' life expectancy has increased substantially due to progresses of modern medicine, nutrition and technology and health. According to the World Health Organisation (WHO), the number of people aged over 60 years is expected to increase to 2.1 billion by 2050. Similarly, dogs have experienced a similar trend as their life span increased substantially in the past two decades. Cognitively unimpaired people and dogs have been shown to accumulate senile amyloid beta (Aβ) plaques and phosphorylated Tau in an age-dependent manner, starting from a very young age. The significance of these neuropathological lesions normally found in the brains of cognitively impaired individuals is poorly understood, however, it has been proposed that their identification in young people and dogs might help predict Alzheimer's disease (AD). Therefore, investigating AD-related pathologies in the preclinical phase might help identify individuals and dogs at risk of developing the disease.

The retina is considered as part of the CNS connected to the brain via the optic nerve. In human AD, retinal changes are recognised as an early pathological occurrence. The common morphological changes include impairment of retinal blood flow, ganglion cell loss and thinning of retinal nerve fibre layer, optic nerve damage, optic nerve fibre loss, and pyramidal cell loss in the visual cortex. Previous studies have demonstrated the deposition of Aβp and p-Tau in the retina of AD rodent models.

In the present study our aim was to provide an insight on Aβ and p-Tau retinal accumulation in a diverse group of thirty cognitively unimpaired dogs. The animals were subdivided into three different age groups, young (1-5 years old), middle (6-10 years old) and old (≥11 years old) age groups. Following immunostaining with nanobodies against $A\beta_{1-40}$ and $A\beta_{1-42}$ oligomers, and antibodies against Aβp and p-Tau, we showed that accumulation of $A\beta_{1-40}$ and $A\beta_{1-42}$ oligomers was widespread and localised to the ganglion cell layer (GCL), inner nuclear layer (INL) and outer nuclear layer (ONL) in all age groups, whereas Aβp were detected in the middle and old age groups but not in the young age group in the GCL, inner plexiform layer (IPL), INL and outer plexiform layer (OPL). Furthermore, p-Tau staining was observed in the GCL, IPL, INL and OPL of four old dogs only, while other dogs were p-Tau free. We also co-localize the Aβo with Aβp and with p-Tau in order to determine their interaction and whether they co-localise in different regions and structures of the retina. Interestingly, both Aβo and Aβp co-localized in the middle and old age groups of dogs in GCL, IPL and OPL. Moreover, diffuse granular p-Tau co-localized with intracellular Aβo in the old age group in GCL, IPL, INL and OPL. Finally, we also observed co-localisation of Aβo and Aβp in the retinal vasculature which might be similar to brain cerebral amyloid angiopathy associated with AD. This study highlights the importance of early detection of Aβo and p-Tau in young and middle-aged dogs to predict AD later in life. Moreover, we argue for use of retinal detection of Aβo and p-Tau in human and dogs to achieve effective and early diagnosis of AD.

Keywords: Cognitively unimpaired dogs, Alzheimer’s disease, Retinal layers, Early diagnosis, Aβo, Aβp, p-Tau.

6.2. Introduction

Dementia is a group of neurodegenerative disorders in which human Alzheimer's disease (hAD) accounts for 60-80 % of all cases[2,215]. hAD is a progressive brain disorder that gradually impairs cognitive functions [21,50,52] and its pathologic changes are recognized decades before the clinical manifestation[41,252,253]. The principal neuropathological lesions observed in hAD brains include extracellular neuritic and/or diffuse plaques containing amyloid beta (Aβ), intracellular Tau protein (p-Tau) in the form of neurofibrillary tangles (NFTs) in addition to cerebral amyloid angiopathy (CAA), ubiquitin, severe synaptic loss and neuronal death[1,29,309,310]. Deposition of Aβ in the human brain is a major hallmark of hAD[215], however, its accumulation is also observed in about 20% of cognitively unimpaired aged individuals[311,312]. The significance and impact of Aβ accumulation in healthy individuals are poorly understood[313] and previous studies did not establish a clear correlation with memory loss[314-316]. Previous reports highlighted the importance of the accumulation of both Aβ plaques (Aβp) in the brain[317,318] and Aβ oligomers (Aβo) in the brain and periphery of cognitively unimpaired individuals[52,319]. A study by Lesne *et al* measured the levels of three Aβo 'species', including Aβ trimers, Aβ*56 and Aβ dimers in brain tissues derived from 75 cognitively unimpaired individuals, including young children and adolescents[52]. The authors showed that Aβ trimers were present in children and adolescents and their levels increased progressively with age, suggesting that this particular Aβo could be used to track hAD progression from a very young age. Another study investigated the relationship between amyloid levels and memory performance in young unimpaired adults[319]. This study, which included 147 participants divided into young (30-49 years), middle-old (50-69 years), and older adults (70-89 years) groups, established a clear relationship between episodic memory performance and amyloid accumulation in the young group[319]. A longitudinal study by Hanseeuw *et al* demonstrated a correlation between Aβ/p-Tau and cognition in 60 clinically normal individuals aged between 65-85 years. The authors concluded that there was a positive correlation between Aβ/p-Tau PET outcome and cognition, where participants with high Aβ and Tau were at higher risk of developing Mild Cognitive Impairment (MCI)[320]. These studies highlight the importance of investigating normal aging in cognitively unimpaired younger individuals to identify those at risk of progressive increase of hAD pathology and cognitive impairment and establish a time frame for early diagnostic and therapeutic intervention. However, such studies are difficult to implement in human subjects and will take decades to deliver any meaningful outcome[313,321]. Currently available transgenic animal models of hAD do not replicate the subtle clinical and pathological features of the disease as demonstrated by their lack of reproducible therapeutic outcomes[118,159]. However, aged dogs naturally develop progressive cognitive decline and memory loss in parallel with accumulation of Aβ and p-Tau associated with a syndrome, named Canine Cognitive Dysfunction (CCD) or 'Dog'zheimer' (dAD)[129,136,145,146,296,322], similar to the neuropathological hallmarks characteristic of hAD [304,323-325]. Amyloid Precursor Protein (APP) is sequentially cleaved by β and γ secretase leading to the production of Aβ peptide fragments (36–43 amino acids), which then aggregate and deposit as plaques[26,29,326]. The canine APP and Aβ peptides are 98% and 100% identical to their human counterparts[129]. In dogs affected with dAD, Aβ deposits as diffuse plaques while the dense core of the plaques is very rare or absent[136,145,146,154]. There are two major isoforms of Aβ, $A\beta_{1-40}$ (~80–90%) and $A\beta_{1-42}$ (~5–10%) and three major assemblies [36-39], including monomeric Aβ, Aβo containing 12-24 monomers which become elongated to form protofibrils and finally insoluble fibrils[28,40]. Among these three stages, Aβo is thought to be the most toxic to neurons and responsible for the pathophysiology associated with hAD[42,45-47]. Likewise, a previous study reported that cognitive decline occurs prior to the accumulation of Aβp in dAD, suggesting that earlier assembly states of Aβ may be the toxic species[327]. In addition, CAA, ubiquitin and severe synaptic loss have also been reported in dAD[136,137,142-144]. Another cardinal pathological hallmark of hAD is the accumulation of p-Tau[20,21]. Several phosphorylation sites were identified on Tau in aged dogs including Thr181[142], Ser422[143], Ser202/Thr205[143,144], Ser396[143,144,154], Ser189 and Ser207[155], however the presence of NFTs remains inconclusive. A study by Schmidt and colleagues, in which the authors used anti-pT205, AT8, AT100, PHF-1 and anti-pT422 antibodies to confirm the presence of Tau pathology in 24 dogs aged between 2 and 19 years, showed that three 13-15 year old dogs displayed p-Tau and only one 15 year old Pekingese dog displayed NFT-like appearance[143].

In hAD, visual disturbances are one of the early complaints and include loss of color vision, impairment of peripheral vision and object recognition, contrast sensitivity, decreased visual memory and perception[90,328,329]. A recent human longitudinal study of 1,349 older adults showed that poor visual acuity paralleled the development of dementia[330], suggesting that ocular disturbances can be used as an early predictor of dementia risk in the older population[330]. Moreover, post-mortem studies of hAD and animal models of AD demonstrated a strong association between retinal accumulation of Aβo[110,272], Aβ plaques[102,331], p-Tau[103,105] and brain depositions and cognitive decline, where retinal Aβo was shown to deposit earlier than the brain and before deficits in cognition. Although, to our knowledge, age-dependent retinal deposition of Aβo and/or Aβp has not been investigated in hAD and cognitively unimpaired individuals, including children and adolescents, our recent studies in AD mouse models confirmed the conversion of cerebral and retinal Aβo to Aβp in an age-dependent manner, where retinal Aβo was detected as early as 3-month old APP/PS1 mice, before brain pathology and cognitive decline were observed[53,101].

In this study, we investigated the retinal accumulation of Aβo, Aβp and p-Tau in three age groups of genetically diverse and cognitively unimpaired population of dogs. Furthermore, we aimed to demonstrate whether Aβ and/or p-Tau accumulation was associated with a pre-existing condition or co-morbidity affecting these dogs. Here, following immunohistochemistry and immunofluorescence analysis, we confirmed the presence of retinal $A\beta_{40}$ and $A\beta_{42}$ oligomers, Aβp and p-Tau. Retinal $A\beta_{40}$ and $A\beta_{42}$ oligomers deposition was conspicuous and widespread and observed in all age groups, including the young 1-5-year-old cognitively unimpaired group. Moreover, retinal co-localization of $A\beta_{40}/A\beta_{42}$ oligomers and Aβp was observed in a few middle-aged dogs and most dogs in the old cognitively unimpaired age group, while retinal co-localization of $A\beta_{40}/A\beta_{42}$ oligomers and p-Tau was only seen in the old cognitively unimpaired age group of dogs. Morphologically, extracellular Aβp deposits appeared as small and dot-like rounded deposits while intracellular p-Tau deposits adopted a diffuse appearance in the retinal layers[105]. No NFTs or neuropil threads were observed in these dogs. Taken together, these results highlight the importance of further investigations of AD-related pathology in the retina of cognitively unimpaired young children and adolescents to gain insight about disease timeline, potentially identify early at-risk individuals to help implementation of speedy therapeutic interventions.

6.3. Materials and Methods

6.3.1. Dog eye samples and animal ethics

The study was conducted on formalin-fixed paraffin-embedded retina tissue sections isolated from eyes of 30 genetically diverse and cognitively unimpaired dogs ranging from 1year to 16 years old (Table 1 and 2). Eye sections were obtained from the Comparative Ocular Pathology Laboratory of Wisconsin (COPLOW) at the Department of Pathobiological Sciences, School of Veterinary Medicine, University of Wisconsin, Madison. Eye tissues used in this study were submitted by veterinarians as biopsies to COPLOW for routine pathological diagnosis and as such not subject to approval by institutional animal ethic.

6.3.2. Tissue preparation

Complete eyes or eye biopsies were fixed in 10% neutral buffered formalin and processed overnight using a Leica ASP300S tissue processor (Leica biosytem, Wetzlar, Germany). Eye tissues and biopsies were then embedded in paraffin blocks and sectioned at 4µm thickness using a Leica RM2235 microtome (Leica biosytem, Wetzlar, Germany) and placed on charged slides. Sections were then stained with Haematoxylin & Eosin (H&E) and Congo Red (CR). Sections were also used for immunohistochemistry (IHC) and immunofluorescence (IF) staining.

6.3.3. Hematoxylin & Eosin (H&E) staining

H&E staining was used to assess the general morphological changes of the retinal sections. Paraffin sections were dewaxed by two changes of absolute xylene for 5 minutes each. Sections were rehydrated using two changes of 100% ethanol for 2 minutes each, 95% ethanol for 3 minutes and 70% ethanol for 2 minutes and finally rinsed in deionised water for 2 minutes. H&E staining was then performed by adding Gill ll Haematoxylin solution (Leica bio systems, Wetzlar, Germany) followed by 1% acid alcohol and subsequently Eosin stain (Leica bio systems, Wetzlar, Germany). Finally, the sections were dehydrated with increasing concentrations of ethanol, from 70%, 95% to 100%, then dewaxed by two changes of xylene and finally mounted with xylene based mounting media (Sigma Aldrich, Missouri, United States) [269].

6.3.4. Congo red (CR) staining

Initially, CR working solution was prepared by mixing 50 ml Congo red solution and 0.5 ml potassium hydroxide solution supplied in the Congo red amyloid special stain kit (Leica bio systems, Wetzlar, Germany). Retinal sections were placed in the working solution for 20 minutes then rinsed in 5-8 changes of deionized water. This was followed by staining with Gill ll Haematoxylin (Leica bio systems, Wetzlar, Germany) for 1-3 minutes and rinsing in 3 changes of deionized water. Sections were then dehydrated in two changes of 95% alcohol followed by three changes of absolute alcohol for one minute each. Finally, the sections were cleared in two changes of xylene and mounted in a xylene miscible medium. Amyloid fibrils appeared as dull to red brick under light microscopy (Olympus CX 43, Shinjuku, Tokyo, Japan) and apple green birefringent under polarized light (Olympus CX 43, Shinjuku, Tokyo, Japan).

6.3.5. Immunohistochemical staining of amyloid beta plaques and amyloid beta oligomers

Retinal sections were pre-treated using the 2100 antigen retriever (Aptum biologics Ltd, Southampton, United Kingdom) to expose the target epitopes. The sections were then treated with 90% formic acid for 5 minutes at room temperature (RT) followed by cell membrane permeabilization, achieved by using 0.1% triton X for 1 min prior to addition of 0.3% H_2O_2 for 15 minutes to inactivate endogenous peroxidases. Sections were then blocked with protein block serum-free (Agilent, California, United States) for 15 minutes. The sections were then stained for 1hour with the following primary antibodies in phosphate buffered saline (PBS): mouse purified 4G8 anti-$A\beta_{17–24}$ (1: 500; Bio legend, California, United States) or A11 rabbit anti-Aβo (1: 250; Merck Millipore, Burlington, MA, USA) antibodies. After washing with PBS, sections were incubated for 1hour at RT with the following secondary antibodies in PBS: HRP-conjugated anti-mouse IgG (Sigma-Aldrich, Missouri, United States) or anti-rabbit IgG (Sigma-Aldrich, Missouri, United States). The sections were then washed three times with PBS before addition of 3,3'-Diaminobenzidine (DAB) substrate chromogen system and incubated for 5–10 minutes. The sections were then counterstained with hematoxylin for 1 minute before mounting. Sections were finally imaged using the Olympus CX 43 light microscope (Shinjuku, Tokyo, Japan).

6.3.6. Immunofluorescence co-localization studies

To investigate whether Aβo co-localized with Aβp or with p-Tau, we performed immunofluorescence double labelling using camelid-derived single domain anti-$A\beta_{40}$ (PRIOAD12) or anti-$A\beta_{42}$ (PRIOAD13) oligomer antibodies with 4G8 anti-Aβp antibody (Bio legend, San Diego, California, United States) or anti-phosphorylated Tau AT8 antibody targeting amino acid residues Ser202/Thr205 (Thermo-fisher Scientific, Massachusetts, United

States). Retinal sections were processed as described above before addition of the primary antibodies. The sections were double stained with either PrioAD12 (1:500) or PrioAD13 (1: 500)[173] and 4G8 antibody overnight (1:500) or AT8 (1:500) and either PrioAD12 (1:500) or PrioAD13 (1:500). Sections were then washed in Tris buffered saline with 0.05% Tween 20 (TBST) and incubated with secondary antibodies at a dilution of 1:500, including goat anti-llama IgG conjugated to FITC (Bethyl Laboratories, Inc, Texas, USA) or donkey-anti-mouse IgG conjugated to Texas red (Sigma-Aldrich, Missouri, United States) for 2 hours at room temperature. Other sections were used as negative control and stained with secondary antibodies with omission of the primary antibodies. Retinal sections derived from an APP/PS1 and TAU58/2 transgenic mice models [268,332] were used as positive control and stained with anti-Aβ and anti-P-Tau antibodies respectively. The sections were cover slipped with paramount aqueous mounting medium (Dako, Agilent, Santa Clara, California, United States), sealed and dried overnight. Finally, the sections were visualized with a LSM800 confocal microscope with a standard FITC / Texas Red double band-pass filter set (Zeiss, Oberkochen, Germany).

Table 1. Comparison of demographic criteria of the cognitively unimpaired dogs and Aβ oligomers and plaques immunohistochemical scores

Age groups	**Age (year)**	**Sex**	**Breed**	**Size**	**AD related pathological findings in the dog retina**	
					A11 - Aβ oligomers	**4G8 - Aβ plaques**
Young (1-5 years)	1	SF	Staffordshire terrier	Medium	+	-
	1.4	M	Siberian husky	Medium	-	-
	1.8	SF	Mixed breed	ND*	+++	-
	1.10	SF	Siberian husky	Medium	++	-
	2	F	Chihuahua mix.	Toy	+++	-
	2	M	Bichon Frise Mix	Small	+	-
	2	NM	Shih Tzu	Small	+	-

	3	NM	German shepherd	Large	+++	-
	3	F	Giant Schnauzer	Large	+	-
	3.6	M	Siberian husky	Medium	+	-
Middle age (6-10 years)	7	NM	Hound mixed	Medium	-	-
	8	SF	Bedlington terrier	Small	-	-
	8	SF	Cocker Spaniel	Medium	-	-
	8	M	Mixed breed	ND*	-	-
	8	M	Cocker Spaniel	Medium	+	-
	8	F	German shepherd mix	Large	-	-
	8	SF	Great Dane dog.	Giant	-	-
	9	M	Jack Russell terrier dog	Small	-	-
	9.5	SF	Boxer dog	Large	-	-
	9.9	SF	Cocker Spaniel	Medium	-	-
Older (≥11 years)	11	NM	Mixed breed	ND*	-	-
	11	NM	Beagle	Small	-	-
	11.9	SF	Bouvier des Flanders	Large	+	-
	12	SF	German Shepherd	Large	-	++
	12	SF	German Shepherd mix	Large	-	-
	12	NM	Husky mix	Medium	-	-
	12.8	NM	Shih-tzu	Small	-	++
	13	NM	Border Collie	Medium	-	-
	15	SF	Basset hound	Medium	-	+
	16	SF	Shih Tzu	Small	-	-

Sizes were determined according to the American Kennel club (AKC)[166]. Size range between 34 – ≥54 kg is considered ‘giant’, 24 – 38 kg is considered ‘large’, 15 – 29 kg is considered ‘medium’, 3 – 15 kg is considered ‘small’ and 0.9 – 4 kg is considered ‘toy’. Aβ oligomers and Aβ plaques staining intensity were semi-quantitatively analysed and scored across the retinal layers under the brightfield microscope (Olympus CX 43, Shinjuku, Tokyo, Japan). Total area was examined at 40 magnification and categorized into no immunostaining “–”; low immunoreactivity found only in limited areas of the retinal layers “+”, moderate immunoreactivity where Aβ deposits were more apparent “++” and finally strong immunoreactivity with widespread A11 and 4G8 positive Aβ labelling were exhibited "+++".

ND*: Not determined

SF: Spayed female; F: Female; NM: Neutered male; M: Male

6.4. Results

6.4.1. Histological assessment of retinal lesions in cognitively unimpaired dogs

We performed H&E staining of the retinal layers to assess the general morphological appearances and identify abnormal microscopical changes such as vacuolation, neuronal death and eosinophilic aggregate[53,101]. No specific lesions were observed in the retinal layers of the young and middle age groups (data not shown). However, scattered eosinophilic deposits in the ganglion cell layer (GCL) and inner nuclear layer (INL) of the retina were noticeable in five dogs in the older age group (11-16 years old), including an 11 year-old Beagle, a 12 year-old German shepherd, a 12-year-old Husky mix, a 12.8-year-old Shih-tzu and a 15 year-old Basset hound **(Figure 1 A and B**). Furthermore, CR staining was used to detect amyloid fibrils and CAA in retinal sections of the cognitively unimpaired dogs. CR did not display any staining in the retina tissues derived from all age groups (data not shown).

6.4.2. Immunohistochemical detection of retinal Aβ oligomers and plaques in cognitively unimpaired dogs

Dogs have shown to develop human type Aβ deposition at a very young age when compared to other aged animals including cats, bears [129,333]. In the present study, we investigated the presence of Aβ in the retinal tissues of all age groups of dogs using A11 anti-Aβo and 4G8 anti-Aβp antibody (**Figure 1 C-F**). The staining intensity was semi quantitatively analyzed and scored across the retinal layers. Each bright field was examined at 40x magnification and categorized into no immunostaining "–"; low immunoreactivity, found in limited areas of the retinal layers "+"; moderate immunoreactivity where Aβ deposits were more apparent "++" and finally strong immunoreactivity with widespread A11 and 4G8 positive Aβ labelling

“+++” (**Table 1**). Retinal tissues stained with A11 exhibited intracellular Aβo depositions in the outer nuclear layer (ONL), INL and GCL (**Figure 1 C and D**). The intraneuronal Aβo intensity following A11 staining ranged from low (+), moderate (++) to strong (+++) in all dogs in the young age group except a 1.4 years old male Siberian husky that did not display any A11 positive stain (**Table 1**). A spayed female mixed breed aged 1.8 years, a female Chihuahua aged 2 years and a neutered male German shepherd aged 3 years showed strong (+++) accumulation of A11 positive Aβo (**Figure 1 C and D**). Two dogs displayed a low amount (+) of A11 positive Aβo in the retinal layers in the middle and old age groups, including an 8-year-old male Cocker spaniel and a 11.9-year-old spayed female Bouvier des flanders (**Table 1**). In addition, 4G8-positive small rounded and dot like extracellular deposits were observed in the INL, inner plexiform layer (IPL) and GCL (**Figure 1 E and F**) of the retina, and were structurally different from the typical large diffuse plaques normally observed in dog brains with dAD[146,154,334]. The extracellular Aβp intensity following 4G8 staining ranged from low (+) to moderate (++) in some dogs in the old age group, including a 15 year-old spayed female Basset hound, a 12.8 year-old neutered male Shih-Tzu and a 12 year-old spayed female German shepherd. Other dogs in this age group were all negative for 4G8 staining (**Table 1, Figure 1 E and F).**

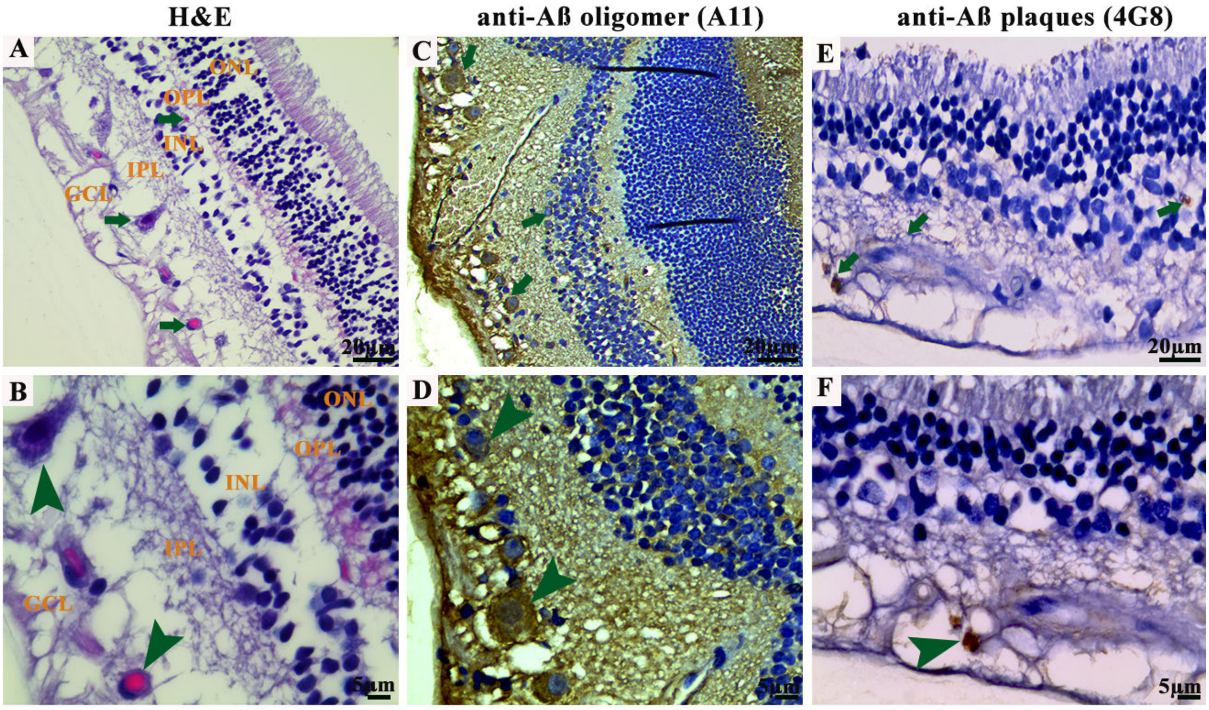

Figure 1. Photomicrographs of the microscopic lesions in the dog retina.
A) Eosinophilic deposits (green arrows; 40X) were observed in the ganglion cell layer (GCL) and inner nuclear layer (INL) of the retina in a 12-year-old German shepherd dog following staining with Hematoxylin and Eosin (H&E). Representative of 10 cases of old age group.
B) Higher magnification of image-A (green arrowhead; 100X) in the GCL.
C) Immunohistochemical staining with A11 anti-Aβo IgG antibody of a 3-year-old German shepherd dog. Staining exhibited Aβo depositions in the GCL and INL of the retina (green arrows; 40X). Representative of 10 cases of young age group.
D) Higher magnification of image-C (green arrowhead; 100X) in the GCL.
E) Immunohistochemical staining with 4G8 anti-Aβp IgG antibody of a 12-year-old German shepherd mix dog. Staining exhibited extracellular Aβ aggregates in the GCL and INL of the retina (green arrows; 40X).
F) Higher magnification of image-E (green arrowhead; 100X) in the GCL.
The photomicrographs were taken from peripheral region of the retina - away from the optic disc. Representative of all 30 dogs examined.

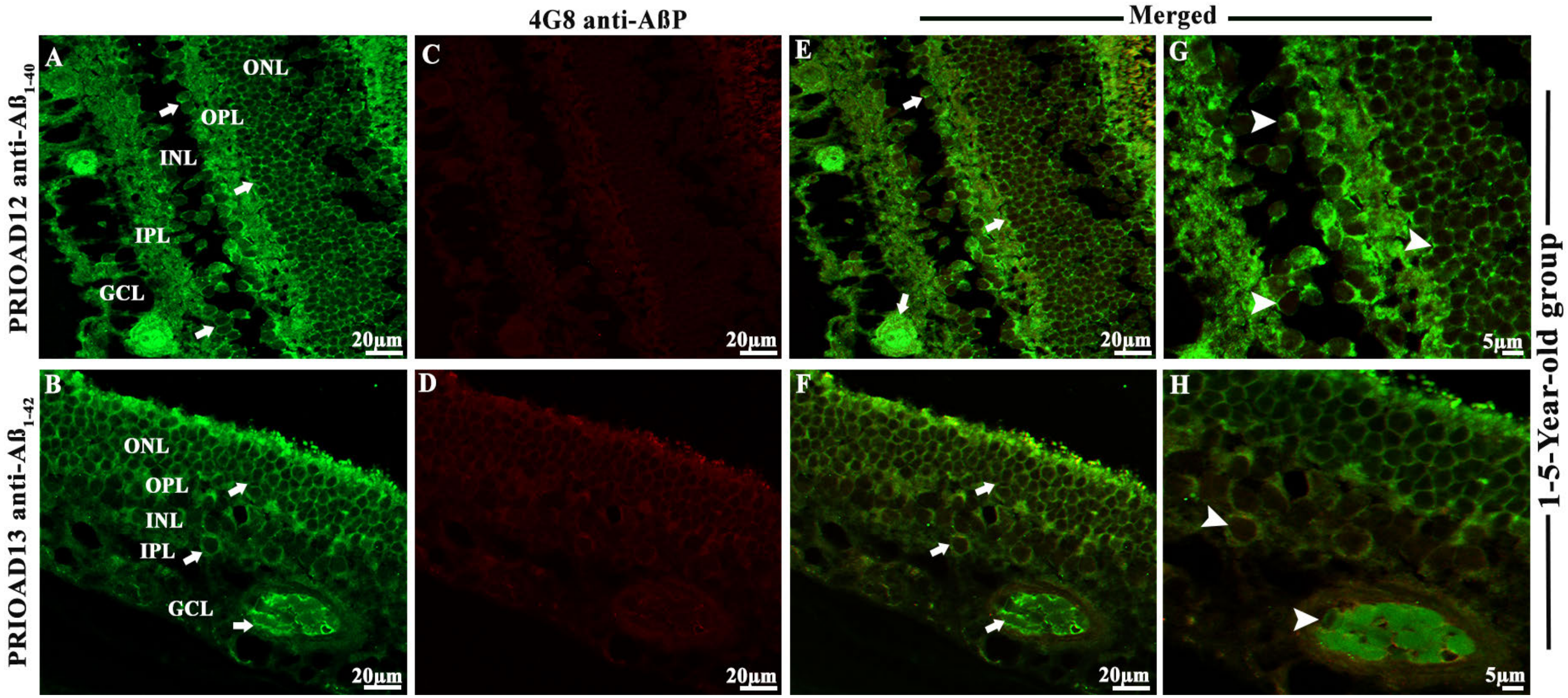

Figure 2. Immunofluorescence co-localization of retinal amyloid beta oligomers and amyloid beta plaques in the dogs of the 1-5-year-old group. Retinal co-staining with anti-Aβ_{40} (PrioAD12), anti-Aβ_{42} (PrioAD13) camelid-derived single domain antibodies (green) or anti-Aβ (4G8) antibody (red) of a 3-year-old German shepherd dog (A-H).

*GCL - ganglion cell layer, IPL- inner plexiform layer INL- inner nuclear layer, OPL- outer plexiform layer and ONL - outer nuclear layer.

A) and B) show widespread accumulation of Aβ_{40} and Aβ_{42} oligomers in the GCL, INL and ONL (white arrows) and retinal vasculature, respectively.

C, D) no Aβp was detected in the retinal layers of this animal.

E, F) Co-localisation of Aβo and Aβp was not observed in the retinal layers of this animal (Aβo was present - white arrows).

G) and H) are higher magnification (100X) of images-A and B in the GCL and INL, ONL and retinal vasculature respectively of the same 3-year-old German shepherd dog. The photomicrographs were taken from the peripheral region of the retina - away from the optic disc. Representative of 10 dogs in the younger age group (1-5 years).

6.4.3. Fluorescence co-localization of retinal Aβ_{40}, Aβ_{42} oligomers and Aβ plaques in cognitively unimpaired dogs

To confirm the presence of retinal Aβ_{40}, Aβ_{42} oligomers and to determine whether Aβ_{40} and/or Aβ_{42} oligomers co-localized with Aβp in the retinas of different age groups and breeds of cognitively unimpaired dogs, we performed immunofluorescence double staining using PRIOAD12 (Aβ_{40} oligomers), PRIOAD13 (Aβ_{42} oligomers) camelid-derived single domain anti-Aβ oligomer and 4G8 anti-Aβp antibodies. Morphologically, Aβo appeared as globular and annular in shape[53,335] and deposited intracellularly in the ONL, INL and GCL (**Figure 2, 3 & 4**). 4G8 positive Aβ plaques appeared morphologically as dot like and small rounded extracellular deposits[105,110] in the OPL, IPL and GCL (**Figure 2, 3 & 4**). We found that both Aβ_{40} and Aβ_{42} oligomers staining was widespread in the majority of dogs in the young (**Table 2, Figure 2 A&B**), middle (**Table 2, Figure 3 A&E**) and old age groups (**Table 2, Figure 4 A&E**) except four dogs including an 1.4-years-old male Siberian husky, a 7-years-old neutered male Hound mixed, a 8-years-old spayed female Bedlington terrier and an 11-years-old mixed breed. In comparison, Aβp was absent in young dogs (**Table 2, Figure 2 C&D**), but it's presence in the middle age group was moderate (**Table 2, Figure 3 D&E**) and conspicuous in the old age group (**Table 2, Figure 4 D&E**). Therefore, no co-localization of Aβo and Aβp was noticed in the retinal layers of the young age group (**Figure 2 E-H**). However, retinal Aβp was shown to co-localize with Aβ_{40} or Aβ_{42} in the GCL, IPL & INL of the middle (**Figure 3 C, G, D and H)** and old (**Figure 4 C, G, D and H**) cognitively unimpaired age groups. Co-localisation of Aβ oligomers and 4G8 positive Aβ plaques was also exhibited in the retinal vessel wall, where young dogs didn't exhibit any co-localisation, middle age group showed scarce co-localisation **(Figure 3 K and L)** and older age group exhibited conspicuous co-localisation in the vessel wall (**Figure 4 K and L**). In the middle age group, two Cocker spaniels aged 8 years male and 9.9 years female respectively exhibited widespread co-localization of Aβo and Aβp and in the old age group, a neutered male Beagle aged 11 years, two spayed female German shepherd aged 12 years, a neutered male Border collie aged 13 years and a spayed female Basset hound aged 15 years displayed strong and widespread co-localization of Aβo and Aβp. This co-localization study revealed an age dependent distribution and co-accumulation of Aβo and Aβp in the retina of the cognitively unimpaired dogs. We found that the young dogs exhibited widespread accumulation of $A\beta_{40}$ and $A\beta_{42}$ oligomers without any plaque deposits; in the middle age group, $A\beta_{40}$ and $A\beta_{42}$ oligomers accumulation was less conspicuous and, in some cases, co-localized with Aβp; and in the old age group, there was widespread and strong co-localization of Aβo and Aβp strongly distributed in most dogs. Representative retinal sections derived from dogs of all age groups stained with secondary antibodies with omission of the primary antibody did not show any co-localization (data not shown). Retinal sections derived from an APP/PS1 mouse were used as positive control and confirmed the presence of $A\beta_{40}$ and $A\beta_{42}$ oligomers (**Figure 8 A and B**) and Aβp (**Figure 8 C**)[53,101]

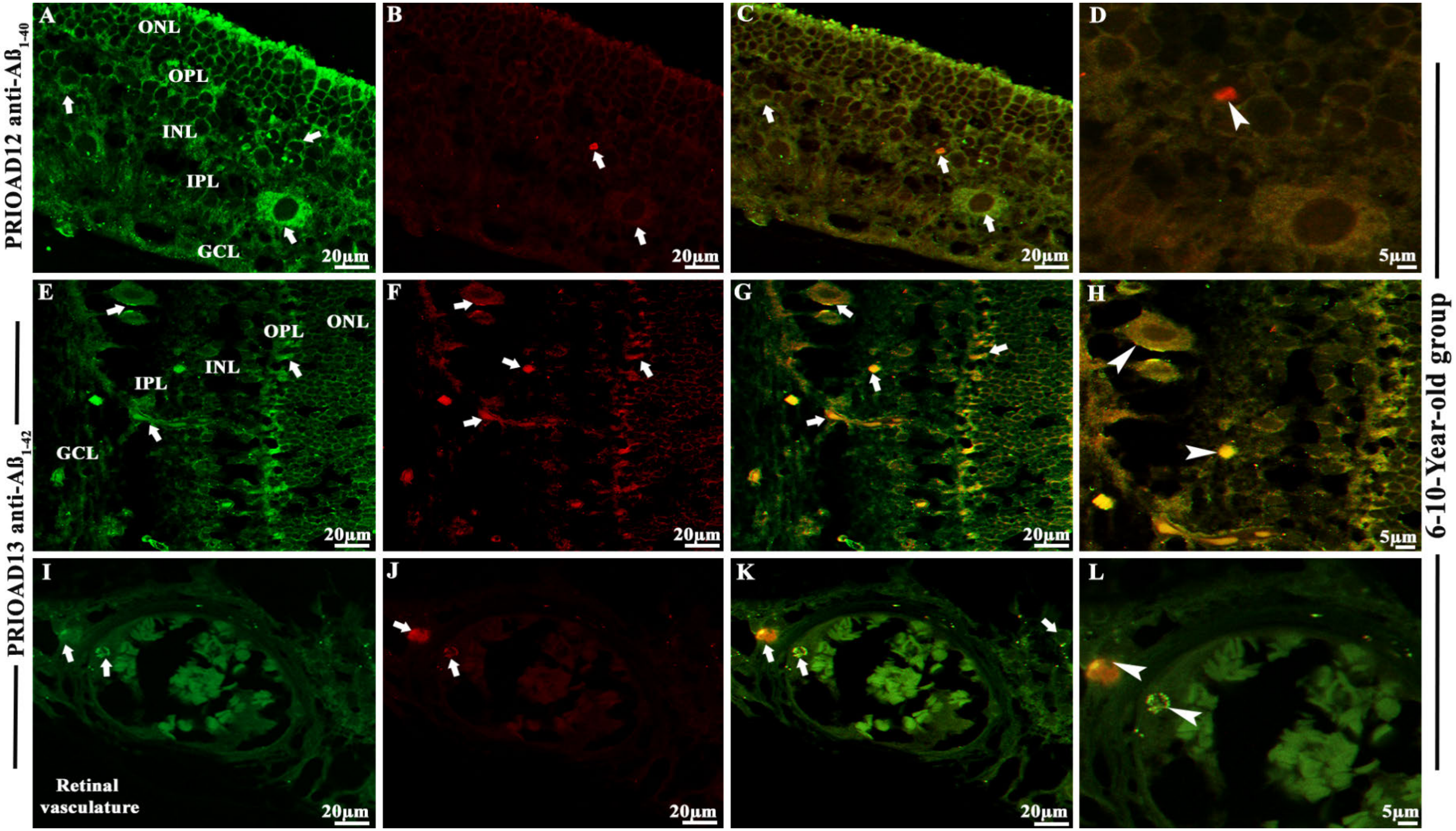

Figure 3. Immunofluorescence co-localization of retinal amyloid beta oligomers and amyloid beta plaques in dogs of the 6-10-year-old group. Retinal co-staining with anti-$A\beta_{40}$ (PrioAD12) and anti-$A\beta_{42}$ (PrioAD13) camelid-derived single domain antibody (GREEN) and 4G8 antibody (RED) of a 9-year-old Cocker spaniel dog (A-L).

*GCL - ganglion cell layer, IPL- inner plexiform layer INL- inner nuclear layer, OPL- outer plexiform layer and ONL - outer nuclear layer.

Large number of A) $A\beta_{40}$ and E) $A\beta_{42}$ oligomers found in the GCL, INL and ONL (white arrows,40X). 4G8 positive Aβ plaque like deposits were observed in the B, F) GCL, IPL, INL and OPL of the retina (white arrows, 40X). Widespread co-localisation observed in the C, G) retinal layers (white arrows, 40X). Co-localisation of 4G8 positive Aβ plaque with D) $Aβ_{40}$ and H) $Aβ_{42}$ depositions (white arrowhead) showed with higher magnification (100X) in the GCL and INL of the same 9-year-old Cocker spaniel dog retinal section. I) Aβ oligomers and J) 4G8 positive Aβ plaques were observed in the retinal vasculature (white arrows). K, L) Co-localisation of Aβ oligomers and 4G8 positive Aβ plaques were exhibited with 40X and also with higher 100X magnification in the retinal vessel wall respectively (white arrowhead). The photomicrograph was derived from peripheral region of the retina - away from the optic disc. Representative of 10 dogs examined from middle age group (6-10 years).

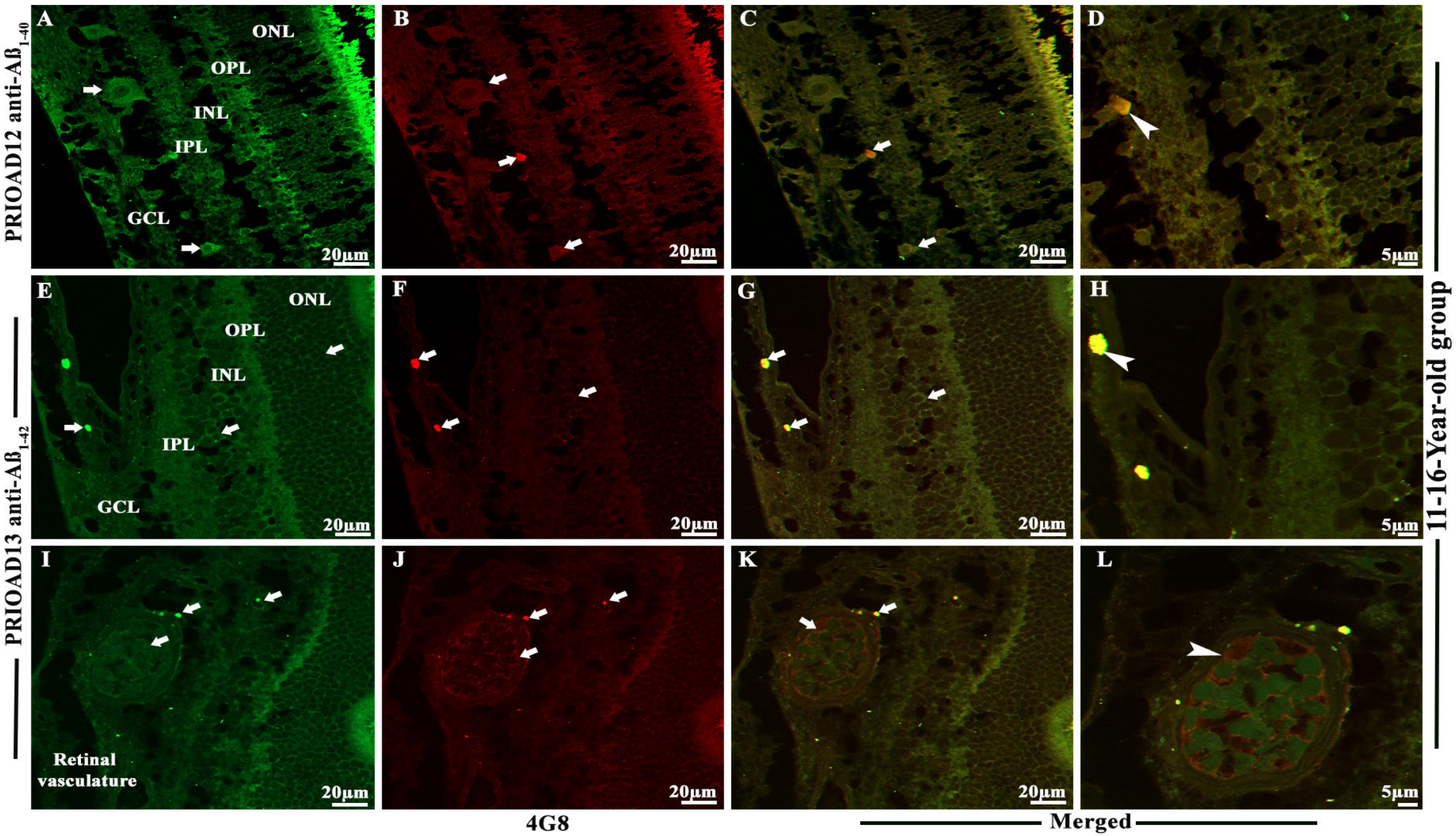

Figure 4. Immunofluorescence co-localization of retinal amyloid beta oligomers and amyloid beta plaques in dogs of 11-16-year-old group. Retinal co-staining with anti-Aβ_{40} (PrioAD12) and anti-Aβ_{42} (PrioAD13) camelid-derived single domain antibody (GREEN) and 4G8 antibody (RED) of a 12-year-old German shepherd dog (A-L).

*GCL - ganglion cell layer, IPL- inner plexiform layer INL- inner nuclear layer, OPL- outer plexiform layer and ONL - outer nuclear layer.

Large number of A) Aβ_{40} and E) Aβ_{42} oligomers found in the GC, INL and ONL (white arrows, 40X). 4G8 positive Aβ plaque like deposits were observed in the B, F) GCL of the retina (white arrows, 40X). Widespread co-localisation observed in the C, G) retinal layers (white arrows, 40X). Co-localisation of 4G8 positive Aβ plaque with D) Aβ_{40} and H) Aβ_{42} depositions (white arrowhead) showed with higher magnification (100X) in the GCL of the same 12-year-old German shepherd dog retinal section. I) Aβ oligomers and J) 4G8 positive Aβ plaques were observed in the retinal vasculature (white arrows). K, L) Co-localisation of Aβ oligomers and 4G8 positive Aβ plaques were exhibited with 40X and also with higher 100X magnification in the retinal vessel wall respectively (white arrow head).The photomicrograph was derived from peripheral region of the retina - away from the optic disc. Representative of 10 dogs examined from older age group (11-16 years).

6.4.4. Fluorescence co-localization of retinal Aβ oligomers and phosphorylated Tau in cognitively unimpaired dogs

To confirm the presence of p-Tau and to investigate whether p-Tau co-localizes with Aβo, we performed fluorescence double staining of Aβo and p-Tau using PrioAD12 ($A\beta_{40}$) or PrioAD13 ($A\beta_{42}$) anti-oligomer[173] and AT8 anti-p-Tau antibody, targeting Ser202/Thr205[105]. Aβo appeared as globular and annular in shape[53,335] (**Figure 5 A and B**) and AT8 positive p-Tau appeared morphologically as diffuse and granular intracellular deposits[105] in the OPL, INL, IPL and GCL (**Figure 5 C and D**). Overall, Aβo and p-Tau did not display consistent co-localization in all age groups, as P-tau was only detected in the old age group and $A\beta_{40}$ or $A\beta_{42}$ oligomers were identified in all age groups. Among ten dogs in the old age group only four dogs displayed the presence of p-Tau, including a spayed female German shepherd and a neutered male Husky aged 12 years, a neutered male Shih-tzu aged 12.8 years and a neutered male Border collie aged 13 years exhibited strong co-localization with $A\beta_{40}$ or $A\beta_{42}$ oligomers (**Figure 5 E-H).** Representative retinal sections derived from Tau 58/2 mouse were used as positive control and confirmed the presence of AT8 positive p-Tau (**Figure 8 D)**[332].

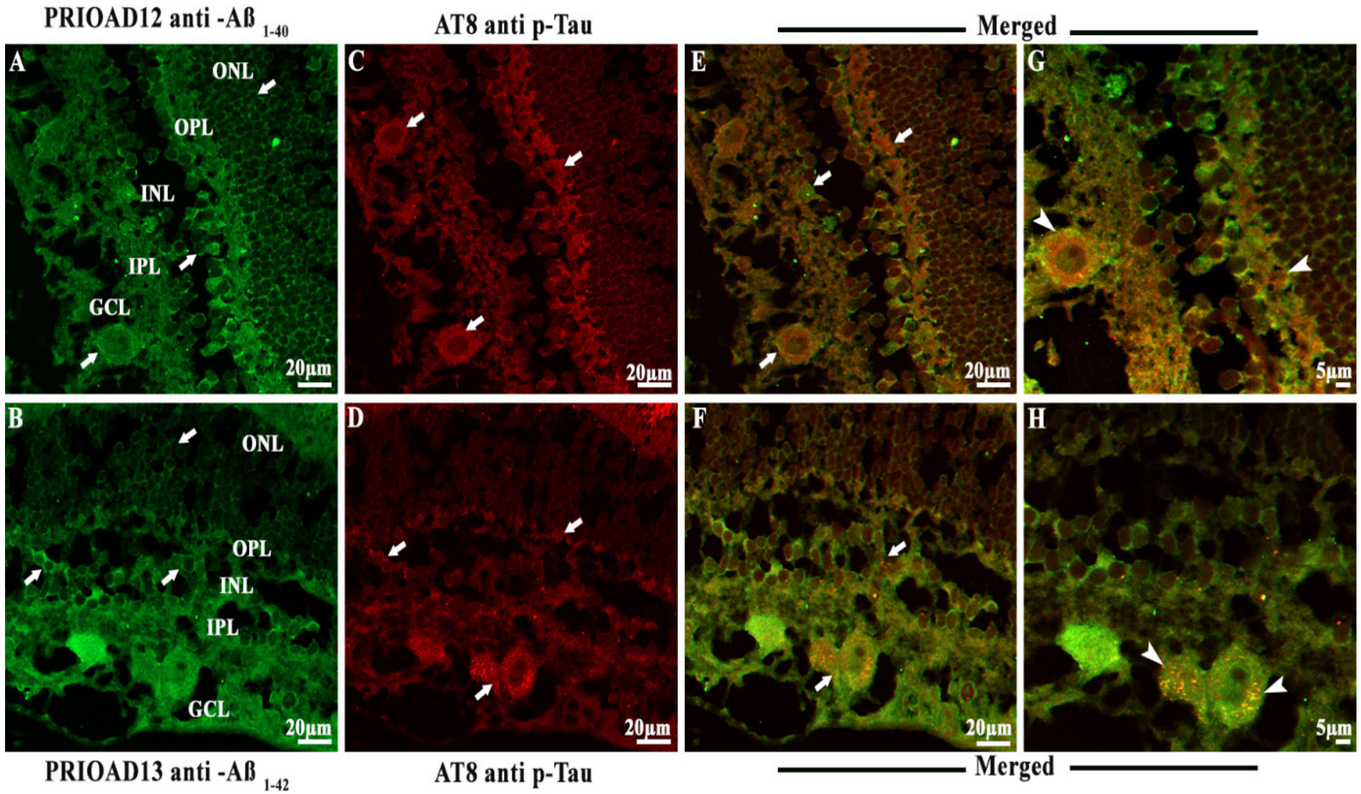

Figure 5. Immunofluorescence co-localization of retinal amyloid beta oligomers and Hyperphosphorylated Tau in dogs of 11-16-year-old group. Retinal co-staining with anti-$A\beta_{40}$ (PrioAD12) and anti-$A\beta_{42}$ (PrioAD13) camelid-derived single domain antibody (GREEN) and AT8 antibody (RED) of a 12-year-old German shepherd dog (A-H).

Large number of A) $A\beta_{40}$ and B) $A\beta_{42}$ oligomers found in the GCL, INL and ONL (white arrows, 40X). AT8 positive diffuse p-Tau like deposits were observed in the C, D) GCL, IPL, INL and OPL of the retina (white arrows, 40X). Widespread co-localization observed in the E, F) retinal layers (white arrows, 40X). Co-localization of AT8 positive p-Tau with G) $A\beta_{40}$ and H) $A\beta_{42}$ depositions (white arrowhead) showed with higher magnification (100X) in the GCL and OPL of the same 12-year-old German shepherd dog retinal section. The photomicrograph was derived from peripheral region of the retina - away from the optic disc. Representative of 10 dogs examined from older age group (≥11 years).

6.4.5. Influence of demographic factors on retinal deposition of Aβ oligomers, Aβ plaques and phosphorylated Tau in cognitively unimpaired dogs

To investigate the influence of the demographic factors on retinal Aβ and p-Tau deposition, staining intensity was compared with the age, breed, size, and sex of the cognitively unimpaired dogs (**Table 2**). $A\beta_{40}$ and $A\beta_{42}$ oligomers, Aβp and p-Tau fluorescence intensity was assessed at 40x magnification. Immunoreactivity throughout the retinal layers was semi-quantified and categorized into no immunostaining "–"; low immunoreactivity, exhibited in limited areas of the retinal layers "+"; moderate immunoreactivity where deposits were more apparent "++" and finally strong immunoreactivity with widespread Aβo, Aβp and p-Tau labelling "+++" (**Table 2**). After comparing the age of the dogs and immunofluorescence staining scores, we found that both $A\beta_{40}$ and $A\beta_{42}$ oligomers staining was high in young dogs which slightly decreased in the middle age group then finally an upward trend was noticed in older dogs **(Table 2, Figure 6**). In comparison, Aβp was absent in young dogs, but its presence in the middle age group was moderate and high in the old age group (**Table 2, Figure 6**). Finally, p-Tau deposits were not observed in the young and middle age groups whereas old dogs exhibited widespread staining for p-Tau (**Table 2, Figure 6**). This pattern of deposition strongly supports a possible age dependent progression as observed in AD mouse models[53,101]. Previous studies have shown that breed variance does not determine the pathological outcome associated with dAD in aged dogs[150,336]. In agreement, our study did not reveal any breed dependent pathological accumulation (**Table 2**). However, when the size of the dog was compared with the pathological outcome, we found that 6 medium sized dogs displayed strong Aβo staining and only 2 dogs exhibited strong p-Tau staining **(Table 2, Figure 7).** In addition, 7 dogs revealed strong Aβp staining of which 4 were medium size (**Table 2, Figure 7).**

Table 2. Comparison of demographic criteria and pre-existing conditions in the cognitively unimpaired dogs and Aβ and p-Tau immunofluorescence scores

Age groups	Age (year)	Sex	Breed	Size	Comorbidities	AD related pathological findings in the dog retina			
						$A\beta_{40}$ oligomers	$A\beta_{42}$ oligomers	Aβp	p-Tau
Young (1-5 years)	1	SF	Staffordshire terrier	Medium	Anterior segment dysgenesis	+	+	-	-
	1.4	M	Siberian husky	Medium	Anterior segment dysgenesis	-	-	-	-
	1.8	SF	Mixed breed	ND*	Anterior segment dysgenesis	+++	+++	-	-
	1.10	SF	Siberian husky	Medium	Anterior segment dysgenesis	+++	+++	-	-
	2	F	Chihuahua mix.	Toy	Anterior segment dysgenesis	+++	+++	-	-
	2	M	Bichon Frise Mix	Small	Proptosis	+++	+++	-	-
	2	NM	Shih Tzu	Small	Melanoma limbal	++	++	-	-
	3	NM	German shepherd	Large	Rhabdomyosarcoma orbital	+++	+++	-	-
	3	F	Giant Schnauzer	Large	Phthisis bulbi	++	++	-	-
	3.6	M	Siberian husky	Medium	Anterior segment dysgenesis	++	++	-	-
Middle age (6-10 years)	7	NM	Hound mixed	Medium	Hemangiosarcoma	-	-	-	-
	8	SF	Bedlington terrier	Small	Neoplasia	-	-	-	-
	8	SF	Cocker Spaniel	Medium	Conjunctivitis	+++	+++	+	-
	8	M	Mixed breed	ND*	Conjunctival melanoma	+++	+++	+	-
	8	M	Cocker Spaniel	Medium	Pre glaucoma	+++	+++	+++	-
	8	F	German shepherd mix	Large	Mast cell tumor	++	++	+	-
	8	SF	Great Dane dog.	Giant	Complex apocrine adenocarcinoma	+	+	-	-
	9	M	Jack Russell terrier dog	Small	sialoadenitis	++	++	-	-
	9.5	SF	Boxer dog	Large	Hemangioma	+	+	-	-

	9.9	SF	Cocker Spaniel	Medium	Adenocarcinoma aorbital	+++	+++	+++	-
Older (≥11 years)	11	NM	Mixed breed	ND*	Squamous cell carcinoma	-	-	-	-
	11	NM	Beagle	Small	Melanoma conjunctival	+++	+++	+++	-
	11.9	SF	Bouvier des Flanders	Large	Melanoma eyelid	+	+	-	-
	12	SF	German Shepherd	Large	Melanoma eyelid	+++	+++	+++	+++
	12	SF	German Shepherd mix	Large	Melanoma conjunctival	+++	+++	+++	-
	12	NM	Husky mix	Medium	Orbital carcinoma	+++	+++	++	+++
	12.8	NM	Shih-tzu	Small	Glaucoma	+++	+++	++	+++
	13	NM	Border Collie	Medium	Melanoma skin	+++	+++	+++	+++
	15	SF	Basset hound	Medium	Conjunctival hemangiosarcoma	+++	+++	+++	-
	16	SF	Shih Tzu	Small	Squamous cell carcinoma	+	+	-	-

Pre-existing conditions of the 30 cognitively unimpaired dogs were determined from the clinical report. Sizes were determined according to the American Kennel club (AKC)[166]. Size range between 34 – ≥54 kg is considered 'giant', 24 – 38 kg is considered 'large', 15 – 29 kg is considered 'medium', 3 – 15 kg is considered 'small' and 0.9 – 4 kg is considered 'toy'. Aβ oligomers Aβ plaques and p-Tau staining intensity were semi-quantitatively analysed and scored across the retinal layers under the confocal microscope (LSM800, Zeiss, Oberkochen, Germany). Total area was examined at 40 magnification and categorized into no immunostaining "–"; low immunoreactivity found only in limited areas of the retinal layers "+", moderate immunoreactivity where deposits were more apparent "++" and finally strong immunoreactivity with widespread Aβo, Aβp and p-Tau labelling were exhibited "+++". ND*: Not determined; SF: Spayed female; F: Female; NM: Neutered male; M: Male

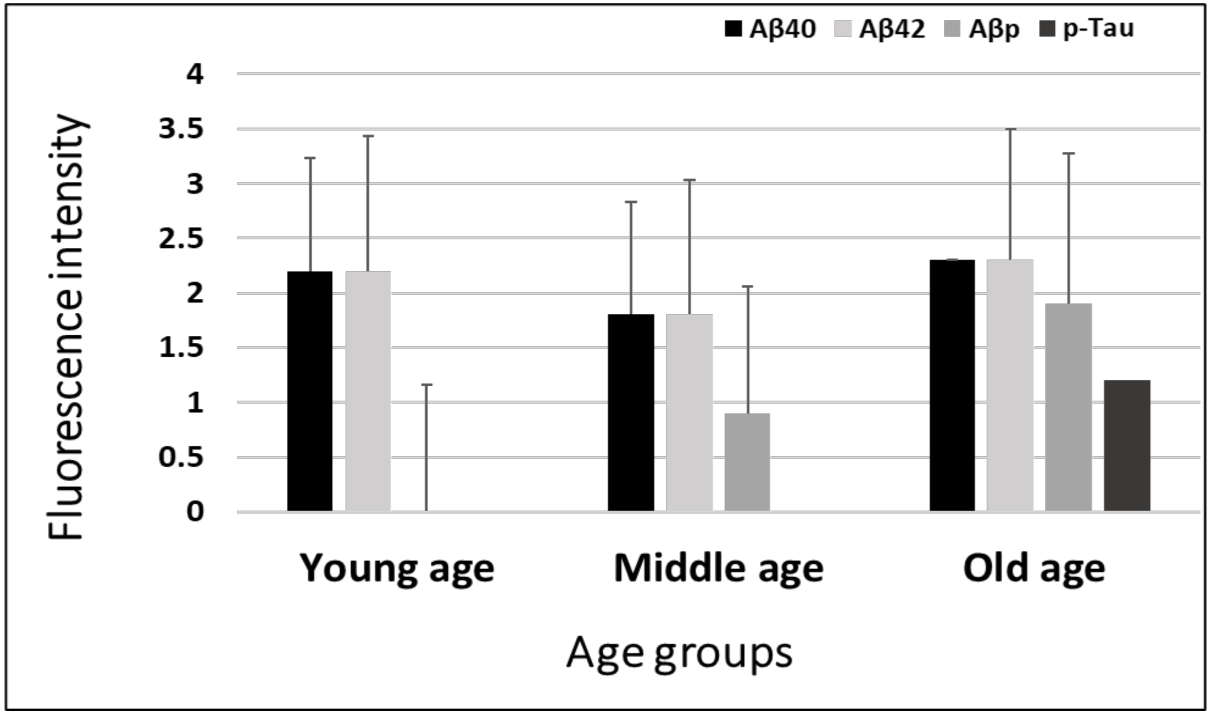

Figures 6. Semiquantitative analysis of Aβ$_{40}$ and Aβ$_{42}$ oligomers, Aβ plaques and p-Tau in cognitively unimpaired young (1-5-years), middle (6-10-years) and old (11-16-years) age group of dogs. PRIOAD12 (Aβ$_{40}$ oligomers), PRIOAD13 (Aβ$_{42}$ oligomers), 4G8 (Aβp) and AT8 (p-Tau) fluorescence immunoreactivity and intensities were examined and quantified at 40 magnification under the fluorescence microscope. Semiquantitative analysis were compared with the three different age groups. Large amount of Aβ$_{40}$ and Aβ$_{42}$ oligomers were found in young dogs which decreased in middle age group then finally an upward trend noticed in older dogs. In comparison Aβp were completely absent in young dogs then moderately found in middle and large amount in old age groups. Finally, p-Tau deposits were not found in young and middle age group of dogs whereas old dogs exhibited considerable amount of p-Tau. The error bars represent standard errors of Aβo, Aβp and p-Tau intensity between young, middle, and old age group.

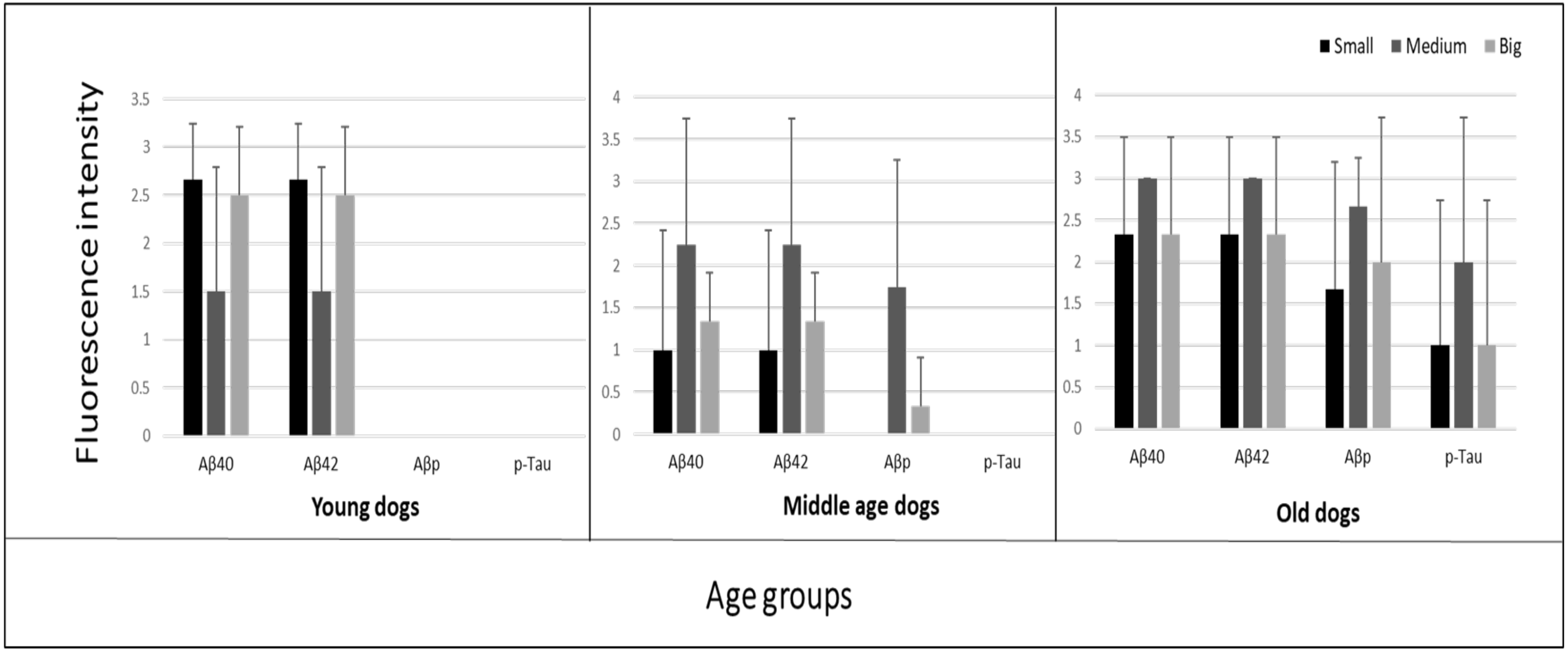

Figure 7. Influence of size of the dogs on retinal deposition of amyloid beta oligomers (Aβo), plaques (Aβp), and phosphorylated Tau (p-Tau) in cognitively unimpaired young (1-5-years), middle (6-10-years) and old (11-16-years) age group of dogs. PRIOAD12 ($A\beta_{40}$ oligomers), PRIOAD13 ($A\beta_{42}$ oligomers), 4G8 (Aβp) and AT8 (p-Tau) fluorescence immunoreactivity and intensities were examined and quantified at 40 magnification under the fluorescence microscope. In three different age groups semiquantitative analysis were compared with the size of the dogs. In young dogs' large number of oligomers displayed by the small and big size dogs. Majority of medium sized dogs displayed strong Aβo and Aβp staining intensity in the middle age dogs. Finally, among different size of old dogs' medium size breeds displayed highest amount of Aβo, Aβp and p-Tau staining intensity. The error bars represent standard errors of Aβo, Aβp and p-Tau intensity between small, medium, and big size dogs in each age group

6.4.6. Influence of pre-existent eye pathology on retinal deposition of Aβ oligomers, Aβ plaques and phosphorylated Tau in cognitively unimpaired dogs

Further, to understand whether the presence of pre-existing underlying eye pathology in the cognitively unimpaired dogs may influence retinal Aβ and p-Tau depositions, we compared their staining intensity with the reported underlying clinical eye conditions **(Table 2)**. We found that four young dogs aged 1-5 years affected with anterior segment dysgenesis, a spectrum of disorders that affect the development of the anterior segment, including the cornea, iris, ciliary body, and lens[337-339], displayed 'moderate' to 'strong' intensity staining for $A\beta_{40}$ and $A\beta_{42}$ oligomers (**Table 2**). However, another two dogs in this age group and affected with anterior segment dysgenesis showed little to no deposition of $A\beta_{40}$ and $A\beta_{42}$ oligomers (**Table 2**). Eighteen out of thirty dogs presented with eye neoplasms; including two in the young age group, seven in the middle age group and nine in the old age group (**Table 2**). There was no clear relation between neoplasms and the intensity of Aβ or p-Tau (**Table 2**). Interestingly, eye inflammation (Proptosis/ Phthisis bulbi in young dogs and Conjunctivitis in a middle-aged dog) was corresponding to $A\beta_{40}$ and $A\beta_{42}$ oligomers intensity that ranged from 'moderate' to 'strong' (**Table 2**). Finally, a case of pre-glaucoma in the middle age group and a case of glaucoma in the old age group also matched well with $A\beta_{40}$ and $A\beta_{42}$ oligomers as well as Aβp intensity. Overall, this analysis appears to indicate that no direct influence of pre-existing eye disorders on Aβ and p-Tau intensity exists, however, the small size of the cohorts used in this study did not allow us to reach a substantive conclusion and studies with much larger cohorts are needed.

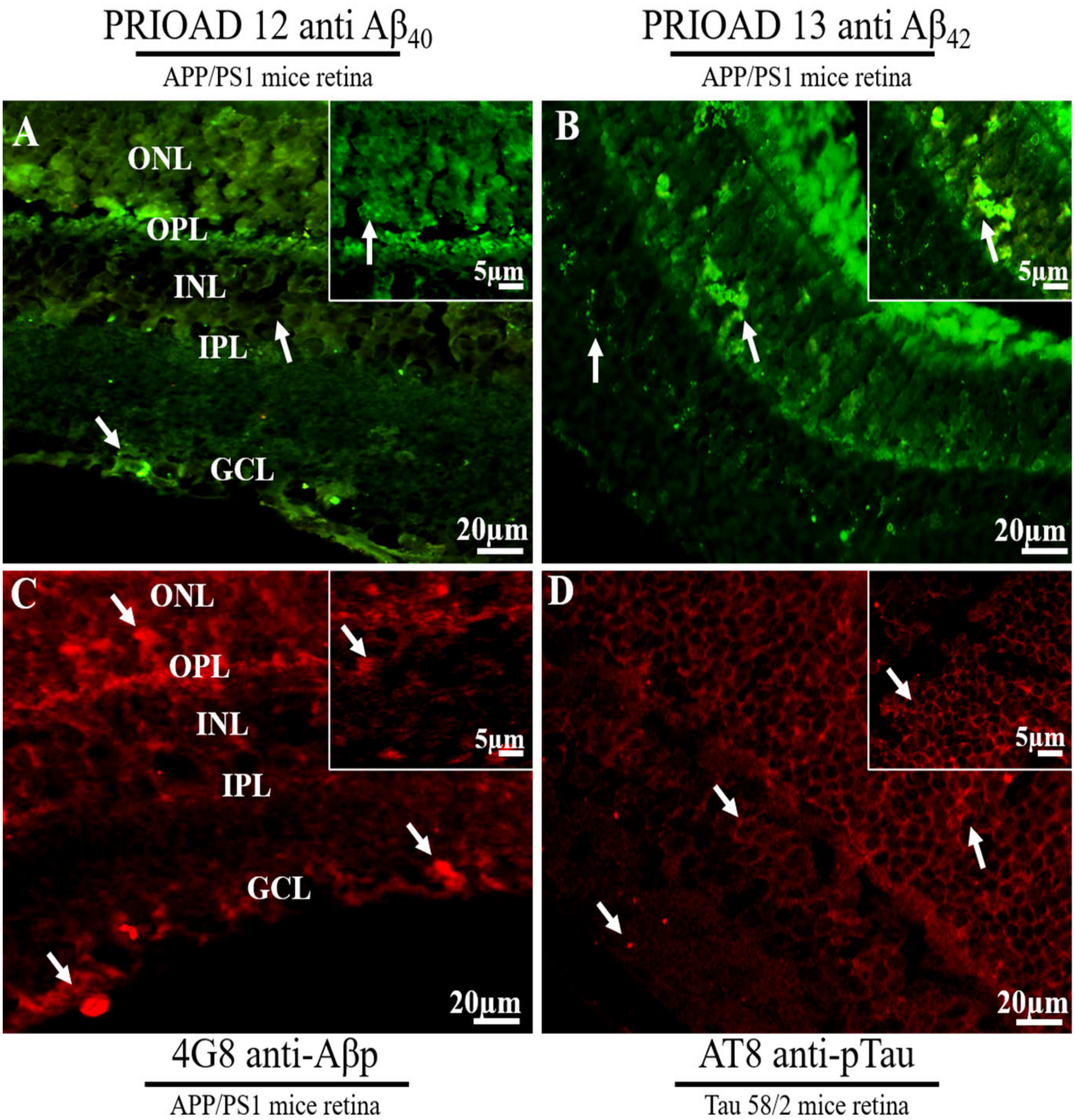

Figure 8. Immunofluorescence staining of retinal amyloid beta oligomers, amyloid beta plaques and hyperphosphorylated Tau in APP/PS1 and TAU 58/2 mice. Retinal staining with anti-$A\beta_{40}$ (PrioAD12), anti-$A\beta_{42}$ (PrioAD13) camelid-derived single domain antibody (GREEN) and anti-Aβ (4G8) antibody (RED) of a 3-month-old APP/PS1 mouse (A-C). A) and B) Widespread $A\beta_{40}$ and $A\beta_{42}$ oligomers accumulation in the retinal ganglion cell layer (GCL), inner nuclear layer (INL) and outer nuclear layer (ONL) (white arrows, 40X and insert 100X). C) Accumulation of small rounded 4G8 positive Aβ plaques in the GCL, outer plexiform layer (OPL) and outer nuclear layer (ONL) of an 8-month-old APP/PS1 mouse (white arrows, 40X and insert 100X). D) Accumulation of diffuse AT8 positive p-Tau deposits in the retinal ganglion cell layer (GCL), inner nuclear layer (INL) and outer nuclear layer (ONL) of the retina of a 17-month-old TAU 58/2 mouse (white arrows, 40X and insert 100X).

6.5. Discussion

Several human longitudinal and biomarker studies reported subtle memory changes decades before extensive cognitive impairment [156,157] and also demonstrated the presence of Aβo and p-Tau in cognitively intact individuals [52,54]. Therefore, the AD pathophysiological process may begin many years before clinical onset, providing a window of opportunity for early detection and therapeutic intervention[340]. Handoko and colleagues have highlighted the presence of Aβo species including Aβ trimer and Aβ*56 in young (mean age = 41.7 years) and old (mean age = 64.8 years) cognitively normal individuals [54]. The authors also found an age dependent CSF increase of Aβ trimers and Aβ*56 and suggest that this elevation may predict individuals at high risk of developing AD. Hanseeuw and colleagues confirmed this pattern in a longitudinal study of cognitively normal participants aged 65 to 85 years[320] and demonstrated that progressive accumulation of Aβ and Tau also predicted cognitive impairment. These studies highlighted the importance of investigating long term changes related to AD in cognitively intact individuals to identify those at high risk of developing MCI and/or AD and possibly implement disease-modifying therapeutic strategies in the early asymptomatic stage[157,341-343]. In this context, eye imaging can provide an opportunity to develop an easily accessible and point-of-care routine diagnostic testing to help predict MCI/AD early[344,345]. A study by Ko and colleagues examined the retinal nerve fiber layer (RNFL) thickness and cognitive status of individuals aged 40 to 69 years over a 3-year period [346]. The authors found that individuals with thinner RNFL showed higher incidence of cognitive decline. Despite the validation of the dog as a robust translational model for hAD[129,154,347], only very limited studies investigated AD-related changes in the young and cognitively unimpaired dogs. A study by Stylianaki and colleagues confirmed a similar pattern of behaviour following assessment of 61 dogs, subdivided into young (0-4 years-old), middle aged (4-8 years-old), aged cognitively normal (8-20 years-old) and aged cognitively impaired (8-17 years-old) dogs [161]. The authors found that young dogs displayed the highest levels of total plasma $A\beta_{42}$ and $A\beta_{42}/A\beta_{40}$ ratio and the middle-aged dogs had the highest CSF $A\beta_{40}$ and $A\beta_{42}$ when compared to cognitively impaired aged dogs.

Previous studies suggested that diversity across human ethnoracial groups have an impact on the prevalence of AD. A review by Chin and colleagues reported that whites, African Americans, and Hispanics or Latinos displayed differences in the prevalence of AD[348]. A study by Barry and colleagues have screened three ethnoracial groups including African Americans, Latinos and non-Latino whites from New York City[349]. They noticed that in Latinos and African Americans, the prevalence of dementia was higher than non-Latino whites. However, these epidemiological data are not conclusive. Due to substantial gap in the scientific literature and lack of effective recruitment of diverse communities in health research[348]. A report by Fillenbaum and colleagues did not notice any significant difference between African Americans and white individuals[350,351]. The majority of the CCD studies focused on laboratory beagles as a model of human AD[291]. Initially, beagles became a model of interest due to their availability through breeding clubs over other breeds and the observation that this breed consistently display memory impairment starting at the age of 6 years[306]. Different presentations of clinical AD in human based on echogenicity and the realization that several breeds of dogs also display signs of memory and cognitive decline at an equivalent age to the so-called mild cognitive impairment (MCI) in human provided a strong rational to study AD in a variety of dog breeds. Further, human and dogs share the same environment and can be exposed to the same environmental risk factors[291,352].

In the current study, we used thirty cognitively unimpaired and genetically diverse dogs aged between 1-16 years and divided into three age groups, including young (1-5 years old), middle (6-10 years old) and old (≥11 years old) age groups. Our initial main goal was to investigate the presence and age-related accumulation of retinal Aβo, Aβp and p-Tau in these unimpaired dogs and to understand their relationship with normal ageing. Moreover, we examined the link between Aβ/ p-Tau deposition and pre-existing eye disorders as well as demographic criteria of these dogs, to identify factors that might influence Aβ and p-Tau development in the retina. At first, we investigated the presence of both $A\beta_{40}$ and $A\beta_{42}$ oligomers to characterize their tissue distribution and morphological appearances in the retinal layers of these cognitively unimpaired dogs. Studies suggested that in the canine brain, Aβo may be the toxic species and responsible for cognitive decline and can potentially be an early biomarker for the detection of dAD[296,297]. Naaman and colleagues reported that $A\beta_{42}$ oligomers cause extensive retinal neurotoxicity in rats when compared to fibrillary $A\beta_{40}$ and $A\beta_{42}$ [113]. Our findings demonstrated extensive deposition of $A\beta_{40}$ and $A\beta_{42}$ oligomers in the retinal layers, including GCL, INL and ONL in 26 out of 30 dogs in the young, middle and old age groups, with the exception of a 1.4 year-old male Siberian husky, a 7 year-old neutered male Hound mixed, an 8 year-old spayed female Bedlington terrier and a 11 year-old neutered male mixed breed. Moreover, we did not notice any difference in the pattern of deposition or morphology between $A\beta_{40}$ and $A\beta_{42}$ oligomers in these age groups. This presentation was unlikely influenced by the breed of the animals as for instance, out of three Siberian Huskies, one dog failed to display $A\beta_{40}$ and $A\beta_{42}$ oligomers accumulation. Remarkably, the younger age group, with an age range of 1-5 years which is equivalent to human age 15-40 years according to the American kennel club[166], has displayed extensive deposition of Aβ oligomers. Of interest, a recent study by Lesne *et al* confirmed the presence of Aβ oligomers in young children and adolescents with no cognitive dysfunction[52]. The authors investigated the presence of three different types of Aβ oligomers, including Aβ trimers, Aβ*56 and Aβ dimers in 75 cognitively unimpaired individuals aged 1 to 96 years. They found an age-related accumulation of Aβ oligomers where level of amyloid-β dimer was significantly higher in subjects in their 60s and amyloid-β trimer in their 70s whereas Aβ*56 level was significantly higher in individuals in their 40s. These data suggested that Aβo specifically Aβ*56 might trigger the pathological cascade in asymptomatic phase of AD which may be possible to identify two decades before the clinical onset[52].

Furthermore, we also investigated the presence/deposition of fibrillar Aβ in the retina of all cognitively unimpaired dogs. We show that none of the young dogs' display 4G8-positive Aβ fibrils and plaques (Aβp). However, Aβp were observed in the middle age group, where three dogs exhibited 'low' staining intensity and two exhibited 'strong' staining intensity in the GCL, IPL & INL. Aβp was also observed at the old age group, where five dogs showed 'strong' signal intensity and two with 'moderate' signal intensity in the GCL, IPL & INL. Several studies have demonstrated the presence of Aβp in dogs' brains in the absence of significant correlation with the severity of cognitive dysfunction[140,149]. Trine *et al* investigated this age-dependent correlation of Aβp deposition with cognitive decline in dogs aged 9-15 years, including cognitively normal, dogs with MCI and dogs with CCD and compared with young dogs aged less than 6 years[347]. The authors reported that the levels of Aβ deposition strongly correlated with the age of the dog but not to the cognitive capacity of the animals. However, the presence of Aβp in retinal layers of dogs has not been investigated but some recent reports confirmed their presence in the retina of hAD[105,110,206]. In this study, we have demonstrated accumulation of retinal Aβp in the cognitively unimpaired dogs which supports the hypothesis that Aβp might not influence the severity of cognitive deficits but can be a predictor of AD development[316,321]. Overall, our study revealed that the Aβ deposition pattern in the retina, showed that Aβo was observed in all age groups, whereas Aβp accumulation was restricted to the middle and more intensely the old age group of dogs, regardless of demographic criteria, breed, and pre-existing eye conditions.

Interestingly, co-accumulation of both Aβo and Aβp were apparent in some middle and old age dogs. This is in agreement with our report where 17-18 months old APP/PS1 mice showed high levels of oligomers deposits in the retinal layers that co-localized with Aβp[53] . Previous studies in hAD have shown that cerebral Aβo is usually present in early disease stages and mostly responsible for neurotoxicity and synaptic dysfunction[39,224,225,353,354], whereas extracellular Aβp are believed to accumulate at later ages and may act as a reservoir for Aβo[355]. Moreover, the involvement of Aβo in retinal degeneration in hAD has also been reported[209,356,357]. In this study, we noticed widespread distribution of Aβo in the retinal layers of dogs of all age groups, indicating its involvement in retinal degeneration perhaps leading to vision impairment in dogs[358,359]. Of importance, a previous study by Ozawa and colleagues that focused on web and paper-based survey of dogs aged ≥10 years to identify physical disturbances related to CCD showed that more than 90% of dogs affected with CCD had vision impairment[141]. In addition, and similar to hAD [112], we observed the deposition of vascular Aβ depositions in the retina of young, middle and old age groups, which might imitate CAA[106,112,360]. Sharafi *et al* suggested that retinal vasculature changes captured by hyperspectral imaging can differentiate cerebral amyloid status between cognitively impaired and unimpaired individuals[361].

Some published reports have shown that there is no significant correlation between breed or sex and the onset of CCD. Fast and colleagues studied 28 CCD and 21 borderline CCD dogs of different breeds with age range from 9-17 and 8-14 years respectively[362]. The authors reported that the breed, size, and sex have no influence on the progression of CCD. However, a study by Katina and colleagues reported that medium or large size (≥15 kg) breeds aged 11-13 years have higher prevalence of CCD as compared to small size (≤15 kg) breeds[363]. However, the authors did not notice any differences between male and female dogs. In agreement, my study also showed that medium size dogs exhibited strong Aβo, Aβp and p-Tau staining compared to small and large size dogs. In comparison, a report by Azkona and colleagues found that small size (≤15 kg) breeds have higher risk of developing CCD[364]. The authors also reported that female and neutered dogs were significantly affected more than the intact male dogs. Similarly, Hart and colleagues reported that neutered male and female dogs were more likely to develop CCD than male and intact dogs[365].

Of importance, a study by Neilson and colleagues reported that age related behavioural changes are associated with CCD development[366]. The authors used 97 spayed female and 83 castrated male dogs with age range from 11 to 16 years old. Their data showed that 28% of dogs aged 11-12 years and 68% of dogs aged 15-16 years had the prevalence of age dependant progressive cognitive impairment. Similarly, a study by Salvin and colleagues also reported that the prevalence of CCD increased exponentially with age whereas breed size has no influence on CCD progression[367]. A questionnaire of six behavioural categories were used to determine the prevalence of CCD among 109 different pedigree breeds and 203 crossbred dogs aged range 8-19.8 years. In Chapter 6, I also found a possible age dependent accumulation of Aβo, Aβp and p-Tau depositions in dogs with age range from 1- 16 years old, although a larger study is needed to confirm this molecular behaviour. Moreover, other risk factors potentially associated with the development of CCD include nutrition. A study by Katina and colleagues reported that dogs under controlled diet are less likely to develop CCD as opposed to uncontrolled diet. They proposed that dogs fed controlled diet such as high quality standard commercial diet had 2.8 times lower chances of having CCD than dogs fed with kitchen waste or low quality commercial uncontrolled diet. In this investigation the authors used different breeds of 116 male and 99 female dogs age ranged 8 to 18 years. Similarly, previous reports have shown that age, physical activity, diet might influence the development of human AD related pathology. Age is a most known risk factors for AD albeit it is not to be a direct cause. Age related changes such as brain atrophy, vascular damage and inflammation are the contributing risk factors in AD. These age-related changes are also profound in aged dogs with CCD. This area remains controversial and large-scale longitudinal studies are needed to investigate whether unknown factors associated to the breed might influence the development of CCD.

Moreover, intraneuronal deposition of NFTs, composed of p-Tau, is one of the cardinal neuropathological hallmarks of AD[20,21]. In dogs with dAD, p-Tau, unlike NFTs, has been identified in the brain, but remains inconclusive. It has been speculated that, unlike hAD, NFTs and p-Tau do not systematically accumulate in dogs due to the animal's shorter lifespan (Tayebi & Habiba, personal communication). p-Tau neuropathology was shown to develop about a decade before the formation of Aβp in hAD brains and was hypothesized to trigger hAD[300,366]. In contrast, Aβo accumulation was shown to precede and drive p-Tau accumulation and synaptic spread in the parietal cortex of hAD[300].

In this study, we investigated the presence of p-Tau Ser202/Thr205 to confirm the presence of retinal p-Tau in cognitively unimpaired dogs. We revealed diffuse p-Tau distribution in the OPL, INL, IPL and GCL in four out of ten dogs of the old age group, including a spayed female German shepherd and a neutered male Husky aged 12 years old, a neutered male Shih-tzu aged 12.8 years old and a neutered male Border collie aged 13 years' old. The same dogs also showed widespread distribution of $A\beta_{40}$ and/or $A\beta_{42}$ oligomers and 4G8- positive Aβp. Similarly, Abey and colleagues have demonstrated the presence of p-Tau Ser202/Thr205 in one out of six and p-Tau Ser396 in six out of six cognitively impaired, 14-17 years aged dog brain [144]. In the retina of human AD patients, p-Tau displayed a diffuse pattern in the plexiform layers in the absence of NFTs and fibrillary Tau [105]. Schön and colleagues reported the presence of AT8-positive intracellular NFTs and diffuse p-Tau signals in five out of six retina derived from AD patients [104]. Previous studies in dogs have demonstrated the presence of Aβp and p-Tau in dogs' brain[143,154], however Pugleise *et al* showed that the diffuse Aβp and p-Tau are unrelated and form independently in the brains of aged dogs[142].

In hAD, it was shown that p-Tau and Aβo cause neuronal toxicity and may act synergistically to trigger synaptic dysfunction[45,64,66]. Manczak and colleagues showed that $A\beta_{40}$ or $A\beta_{42}$ oligomers co-localized with p-Tau in the brains of AD patient [65]. The authors also reported that the interaction between Aβo and p-Tau becomes more prominent with disease progression and was more pronounced at Braak stage V and VI compared to Braak stage III and IV[367,368]. In agreement, we also show that p-Tau co-localized with $A\beta_{40}$ or $A\beta_{42}$ oligomers in the OPL, INL, IPL and GCL of the retina of four dogs. A recent study by Lockhart *et al* demonstrated the presence of both Aβ and Tau pathology in cognitively normal older adults brain using PET imaging approach[369]. They showed significant spatial correlation with Aβ and Tau deposition in cognitively normal brain[369].

Several studies in the field of AD research highlighted the importance of diagnostic and therapeutic interventions in the asymptomatic phase while the individuals are cognitively intact[52,370]. However, it is challenging to track the disease progression in human without any accurate and cost effective early diagnostic approaches and lack of robust natural translational models. In that context, dogs can be an effective natural model for the study of ageing and AD as they share the same environment with human[371,372] , they have a short lifespan, and ease of cognitive testing helps reduce physiological stress[373]. The current study provides strong impetus for further characterizing the dog as a strong model for investigating human ageing and AD and exploring the eye in this species to track disease progression and establish a timeframe for early detection and therapeutic interventions.

This study investigated the potential effect of pre-existing eye conditions on the retinal accumulation of Aβo, Aβp, and p-Tau in three age groups of dogs. The current data showed some correlation between eye diseases including anterior dysgenesis, glaucoma, eye inflammation, and the retinal deposition of Aβ and p-Tau. However, the small cohort size didn't allow this study to provide an extensive understanding of the effect of eye comorbidities on the retinal deposition of Aβ and p-Tau. Future large cohort studies are required to investigate the eye diseases that may cause retinal physiological changes in dogs and trigger the deposition of Aβ and p-Tau in the retinal layers. Recent studies in human aging and cognition suggested that physiological changes in the retina can be an early predictor of AD[90,374]. A study by Shang and colleagues reported that in the aging human population, cataracts were found more in AD patients whereas glaucoma was most commonly present in normal aged populations. Therefore, further longitudinal, and large cohort studies in dogs are very important to translate the disease process and understand the deleterious effect of eye diseases on normal aging and cognition. Also, to characterize dogs as a translational model the *in-vivo* retinal physiological study needs to be considered.

Moreover, human AD studies have reported that approximately two-thirds of AD patients are women[375]. However, what increases the risk factor for women to develop AD is not clearly understood. Hormonal fluctuations and the longer life expectancy of women are believed to influence the risk of AD. In dogs, studies reported that female dogs were more likely to develop CCD. In the current study, data showed that spayed females had higher deposition of Aβ and p-Tau than male dogs. Therefore, future studies are also required to understand the correlation between sex and the potential effect of Aβ and p-Tau in aging and cognitive decline.

Chapter 7

General discussion

7.1. Neurodegenerative diseases are associated with the gradual degeneration of nerve cells[22,376]. Among them, Alzheimer's disease (AD) is the most devastating cause of neuronal damage, gradual memory decline and death[2]. Two misfolded proteins, including Aβ and Tau aggregates in the brain hippocampal and cortical neurons, are believed to initiate the pathophysiology of AD. However, so far, no accurate and easily accessible diagnostic technique have been developed to facilitate early and/or pre-clinical diagnosis of AD. Therefore, it is vital to develop an early and accurate diagnosis of AD in order to reduce the impact of dementia and also meet this urgent unmet medical need globally.

Extracellular deposition of Aβp is one of the cardinal neuropathological lesions in AD[20,21]. However, recent studies have proved that Aβp are the reservoir of its earlier assembly state called Aβo. In AD neuropathology, Aβp was reported to have no correlation with cognitive dysfunction[377,378], whereas Aβo have been shown to cause neurotoxicity, synaptic dysfunction and impaired long-term potentiation[39,50,64,379]. Ono and colleagues reported that some oligomers such as dimers and trimers/tetramers are 3-fold and 13-fold more toxic respectively when compared with other Aβ assemblies[380]. Another report also demonstrated that small Aβ oligomers (ADDLs) were toxic to organotypic mouse brain slice cultures[283]. The authors showed that nanomolar concentration of fibril-free synthetic small Aβo are toxic to hippocampal neurons via inhibition of long-term potentiation leading to disruption of synaptic plasticity and subsequently causing neuronal death[343]. Synaptic deficits associated with plaque-independent Aβ toxicity have also been demonstrated in other *in vivo* studies where the hAPP mice showed age-dependent synaptic deficits without any plaque deposits[381,382]. In agreement, my studies in AD mouse models, including 5xFAD (study Ⅰ; chapter 3) and double transgenic APP/PS1 (study Ⅱ; chapter 4) have exhibited accumulation of Aβo in both retina and brain before appearance of Aβp. These studies also proved that retinal Aβo can be detected before their appearance and accumulation of plaques in the brain. These data have provided a proof-of-concept that, eye can be a powerful diagnostic tool for pre-clinical AD diagnosis. Researchers have been trying to develop diagnostic platforms for AD for decades, however and so far no specific, easily accessible and cost-effective methods have been established to diagnose AD at prodromal stage before brain onset or to confirm late stage AD. Clinicians are only relying on the psychiatric and neurologic tests for the clinical assessment of AD. Further, the use of imaging approaches including positron emission tomography (PET) imaging or magnetic resonance imaging (MRI) have also been used albeit all these approaches are expensive, less accessible and require advanced laboratory procedures. However, confirmatory and deficit diagnosis of AD is to be only possible after post-mortem neuropathological examination and histopathology. Recent research efforts in retinal manifestation of AD pathology and advancement of eye imaging technology suggested that eye can be a potential diagnostic platform for AD. In AD patients, visual disturbances, including loss of colour vision, vascular degeneration and loss of retinal blood flow, loss of retinal ganglion cell, optic nerve damage and so on, are the earliest complaint. A recent study by Kwon and colleagues reported that changes in retinal thickness can be an early predictor of MCI when compared with AD and healthy individuals[383]. The authors used eyes from cognitively normal individual, MCI, and AD patients and compared the average retinal thickness using optical coherence tomography (OCT)[383]. In chapter 3, I used 6-17-month-old 5xFAD mice for histopathological assessment of age dependant accumulation of Aβo and Aβp in the brain and retina. My aim was to understand the retinal manifestation of amyloid pathology and how this correlates with brain deposits and age. I subdivided the mice according to their age, including young (6-month-old), middle (12-month-old) and old (≥14-month-old) age group. I found extensive accumulation of Aβo in the retinal ganglion cell layer (GCL) and inner nuclear layer (INL) and brain hippocampal and neocortical area of the young age group, whereas Aβp were less conspicuous. After quantifying Aβo and Aβp in all age groups, I observed an age dependant progression of

Aβp and decline of Aβo, which may also indicate an age dependant conversion of Aβo to Aβp[101]. A study by DaRocha-Souto *et al* compared the effect of different Aβ assemblies, including oligomers and plaques, on neurons, memory function and glial cell activity in APPsw - tau^{vlw} double transgenic mice aged 5-17 months[239]. The authors also observed an age dependant conversion of Aβo to Aβp and confirmed that Aβo triggers neuronal loss, memory decline and increased astrogliosis[239].

Overall, my study using 5xFAD mouse provided an insight about the age dependant retinal and brain Aβ pathological progression. However, one of the main goals of this thesis is to immunodetect Aβo before brain onset and cognitive decline take place and to identify a time frame to detect retinal Aβo as diagnostic platform. Therefore, in study Ⅱ, chapter 4, I have designed a controlled study using APP/PS1 mice that included a very young and old age groups, starting from 3-months until 17-months of age. The young 3-month old double-transgenic APP/PS1 mice were used to establish that retinal Aβo can be detected in the eye and blood before the appearance and accumulation of plaques in the brain and also to understand the mechanism(s) of retinal 'neuroinvasion'.

Detection of blood-based biomarkers has gained great momentum and researchers are trying to explore the potential link between plasma Aβo and brain deposits[218,232,233]. A recent study by Meng and colleagues investigated the relationship of plasma Aβo levels and memory function using AD patients and cognitively normal individuals[384]. To measure the plasma Aβo level, they used a multimer detection system (MDS) and memory performance was measured by different clinical cognitive tests including MMSE, CASI and ADAS-Cog. Also, to examine the episodic memory performance, the authors used common objects memory test (COMT) and found that increased levels of Aβo in plasma have a direct correlation with memory performance in AD patients and suggested that Aβo can potentially be used as a plasma-based biomarker in AD diagnosis[384]. Similarly, I explored the correlation between levels of Aβo in whole blood, retina, and brain of APP/PS1 mouse. Notably, I used our novel anti-A$\beta o_{1\text{-}40}$ and anti-A$\beta o_{1\text{-}42}$ camelid derived nanobodies to immunocapture A$\beta o_{1\text{-}40}$ and A$\beta o_{1\text{-}42}$ from whole blood via immunoprecipitation in the 3-month-old and 18-month-old APP/PS1 transgenic and wild type (WT) mice. After quantifying the level of A$\beta o_{1\text{-}40}$ and A$\beta o_{1\text{-}42}$, the 3-month-old APP/PS1 age group displayed significantly higher levels of Aβo as compared to WT mice. Similarly, the immunohistopathological data showed that significant amount of Aβo accumulated in the retinal nuclear layers and GCL of the 3-month APP/PS1 age group without the presence of Aβp and before brain Aβp deposition. Retinal Aβp and brain Aβo and Aβp started to appear from 8-month in APP/PS1 mice, which clearly indicates the time frame to diagnose AD before brain onset and cognitive impairment in this mouse model of AD[53]. Previous reports on APP/PS1 mice behavioural assessment showed that cognitive deficits start to appear after 7-months[266,385,386]. Hsiao and colleagues were the first to report that in APP/PS1 mice brain Aβp depositions and cognitive impairment starts from 9-10 months of age[387]. Another study by Webster and colleagues demonstrated the age dependent progression of memory deficits in APP/PS1 mice aged 7, 11, 15 and 24-month-old[388]. The authors showed that memory deficits started at 11-month APP/PS1 mice using the radial arm water maze (RAMW) behavioural test and the number of cognitive errors continued to progress with age[388]. Furthermore, Zhang and colleagues used 12-month-old APP/PS1 mice to correlate cognitive deficits with soluble Aβ and insoluble Aβ levels as well as plaque burden[389]. In the water maze test and step-down passive avoidance test, the authors found only significant correlation ($P < 0.0083$) between cognitive impairments and soluble Aβ levels[389] .

Together, the above data suggests that intracellular deposition of retinal Aβo is an early event in AD neuropathological cascades and that may predate the brain Aβ depositions and neuronal degeneration. However, the origin of retinal Aβo is still not well established but the correlation between blood, retinal and brain Aβo deposition indicated that Aβo might ‘travel’ through blood to deposit in the retinal layers. The outer and inner blood-retinal barrier (BRB) maintains the homeostatic environment of the retina, prevents access of blood borne proteins and balances ion and metabolic exchanges[390,391]. Blood-retinal barrier integrity can be disrupted due to inflammation, degeneration of retinal pigment epithelial (RPE) cells and impairment of tight junctions which may lead to free passage of unwanted diffusion of molecules and fluids[392,393]. Macular edema[392], diabetic retinopathy[394] and age-related macular degeneration (AMD)[395] are also the consequence of blood-retinal barrier integrity disruption. A recent study in APP/PS1 AD mice by Shi *et al* reported an age dependant degeneration of retinal capillaries and BRB disruption[396] and showed that retinal capillary disintegration started from 4 months and deficiency of PDGFRβ started from 8 month of age which were associated with BRB disruption and vascular 4G8 positive Aβp deposition. Also, in agreement with my study, I found that 4G8 positive Aβp was first observed in the retina from 8-months in APP/PS1 mice [396] (study Ⅱ; Chapter 4).

This study (study Ⅱ, Chapter 4) have provided new knowledge regarding the underlying mechanisms on the origin of retinal Aβ deposits, also supported and highlighted the importance of the retina as an early diagnostic platform and finally established the time frame for diagnostic intervention before brain onset and cognitive dysfunction[53].

AD was first discovered in 1906, and since then a large volume of research that focused on diagnostic and therapeutic approaches has been reported. However, poor outcome related to failures to develop early, and accurate diagnosis and failure of clinical trials outcomes essentially kept this area of early diagnosis as one of the highest priorities. The main reason behind these failures is the validity of animal models used in preclinical studies and their failure to mirror the subtle pathological aspects of AD[118]. The vast majority of animals used to investigate AD are transgenic mice model, albeit wild type mice Aβ sequence differs by only three amino acids from its human counterpart, wild type mice do not develop Aβp when they age. The sequence homology between human and mice APP is about 97%[397] and this sequence variations might explain failure of aged mice to develop Aβ pathology. Transgenic mice are developed by overexpressing APP, PS1 and PS2 mutations associated with FAD resulting in Aβ plaque build-up[159]. However, the phenotypic characteristics of different AD mice models depend on the type of mutation, promoter region and strain. Also, in human AD, there are significant difference between SAD and FAD, therefore conducting clinical trials on SAD patients might not necessarily reproduce successes observed in various transgenic mice models, and might lead to clinical discrepancies and major downfall[398,399].

Recent studies have suggested that the canine species may represent a strong alternative as a natural translational model for AD[398,400]. Like human MCI and AD, age dependent cognitive impairment and neurobehavioral changes are exacerbated with age in dogs[136,145,146,291]. Aged dogs have been shown to develop all the neuropathological lesions of AD including amyloid pathology, cerebral amyloid angiopathy and Tau phosphorylation albeit the presence of NFTs was observed in a limited number of studies[142-144,336,400,401]. Previous studies have demonstrated the presence of Aβp in aged dogs which usually starts to appear from 6-8 years of age[142,154]. Similar to Braak and Braak staging in human AD, Aβ deposited and distributed in dog brains following the staging scheme[21,146,347]. However, studies by Head *et al* suggested that levels of Aβo in dogs' CSF were inversely proportional to the brain total Aβ levels[296]. Also, this study suggested that Aβo might have a toxic effect on neurons replicating the neurotoxic effect of Aβo in human AD. While the canine Aβ sequence is 100% similar to the human sequence and canine Aβ pathological process mimics human AD, Tau pathology is not fully understood in this species. Several studies have assessed tauopathy in dogs[136,143,144] and confirmed a small number of phosphorylation sites [129,137,142,143], but NFTs were not clearly demonstrated in dogs' brain. Using immunohistochemical approaches, few studies have demonstrated the presence of p-Tau Thr181[142], Ser396[154], Thr205, Ser422[143] and Ser202/Thr205[143]. A study by Abey and colleagues used six different breeds of cognitively impaired dogs aged between 14-17 years old and confirmed only one dog displayed p-Tau at Ser202/Thr205 but all other dogs were positive for p-Tau at Ser396[144]. Their failed to demonstrate the presence NFTs. Another study by Schmidt *et al* examined the frontal cortex, hippocampus, and entorhinal cortex of 24 different breeds of dogs, aged between 2-19 years. The authors used anti-pT205, AT8, AT100, PHF-1 and anti-pT422 antibodies to determine the presence of p-Tau and NFTs. Out of 24 dogs, only 3 dogs aged 13 to 15 years exhibited p-Tau and only one 15 year old Pekingese dog displayed NFT-like deposits[143].

In study Ⅲ, chapter 5, I have investigated the presence of the neuropathological hallmarks of human AD in seven different breeds of aged dogs, amongst which five were affected with CCD. Small and medium size breeds such as Papillon, Mongrel, Pomeranian, Lhasa Apso and Shiba Inu aged aged between 14 -17 years were included in this study. Cognitive score was also confirmed by the comprehensive questionnaire established by Salvin and colleagues[139]. Cognitive score ≥ 50 were considered as cognitively deficient [149] and according to the scoring system, five dogs were affected with CCD (CCD score ≥ 50) and two dogs were considered nondemented (CCD score <50), including a 16-year-old small size Lhasa Apso and 14-year-old small size Papillion with CCD scores of 38 and 44 respectively. After immunospecific staining, cerebrovascular deposition $A\beta_{1\text{-}42}$ oligomer and Aβp, which resembles CAA normally associated with human AD, were identified in the brain hippocampal and frontal cortex region albeit no co-localisation of Aβo and Aβp was observed.

Previous studies have shown that diffuse plaques, generally present in aged individuals, are related to normal ageing whereas neuritic plaques are believed to be associated with synaptic loss and glial cell reactivity[20,304,305]. Similarly, diffuse plaques were reported to be influenced by the age of dogs and unrelated to the cognitive severity in dogs [138,347]. In this study (study Ⅲ; chapter 5), after comparing with CCD score, I found a positive correlation between Aβo and CCD score but not with Aβp, mimicking the studies in human AD where Aβo have been shown to trigger the plaque build-up, neurotoxicity, synaptic dysfunction and cognitive impairment[52,355,402]. Larger cohorts of dogs are required to investigate this relationship further in order to understand this pathological process in dogs affected with CCD.

Furthermore, the most important highlight of this study is the immunodetection of p-Tau in brain hippocampal and cortical regions of neurologically deficient dogs using AT8 anti-p-Tau antibody via immunohistochemical and immunofluorescence staining. Rigorous optimisation of the protocol and refined antigen retrieval methodologies were performed in the course of identifying p-Tau in the brains of dogs affected with CCD. Intraneuronal distribution of AT8 positive p-Tau deposits were identified in the frontal cortex and hippocampus of all aged dogs (study III; chapter 5). Further, co-immunolabelling of both $A\beta_{1-42}$ oligomer and p-Tau revealed extensive intracellular co-localisation in the hippocampus and frontal cortex in the brains of dogs affected with CCD. This resembles the recent findings in human AD where it was shown that Aβo and p-Tau have synergistic interaction and that to Aβo triggers Tau phosphorylation and the neurotoxic effect in observed in AD brain[403]. An *in-vivo* study by Chabrier and colleagues reported that reduction in β-site APP cleaving enzyme (BACE) decreases the levels of Aβo which directly leads to inhibiting Tau phosphorylation and improved cognition[404]. The authors developed a novel 'arctic' Tau transgenic mice model by co-injecting arctic mutant Aβ (E22G) and wild type human Tau. This study suggested that Aβo are the main causal factor that induce tauopathy and cognitive impairment in human AD[404]. Additionally, Mairet-Coello *et al* showed a direct correlation between $A\beta_{42}$ oligomers and Tau. The authors showed that inhibition of AMP-activated kinase (AMPK) and Calcium/calmodulin-dependent protein kinase (CAMKK2) Tau pathway can protect hippocampal neurons from $A\beta_{42}$ oligomers induced synaptotoxicity[405].

Overall, the aim of this study was to investigate neuropathological features in cognitively deficits aged dogs resembling those observed in human AD. To date no studies have conclusively demonstrated this extensive accumulation of p-Tau in dog brains affected with CCD. Taken together, my study has shown that aged dogs were able to mimic the AD neuropathological hallmarks including a conclusive demonstration of p-Tau in dogs with CCD. Therefore, these data propose that aged dogs can form a strong translational model for human AD and offers a real possibility to efficiently investigate molecular determinants underlying AD pathogenesis (study Ⅲ; chapter 5).

The significance and impact of Aβ and p-Tau accumulation in healthy cognitively unpaired individuals and its relation to memory functions was seldomly investigated and remained poorly understood; however, some studies have suggested that early deposition of both Aβ and p-Tau particularly in young and adolescents individuals led to poor cognitive outcomes later in life[320]. This could be useful in order to identify a time frame for early diagnostic and therapeutic intervention[157,320]. The pathophysiological process of AD reported to begin many years before clinical onset[157,340]and many longitudinal studies in human have reported the presence of Aβo and p-Tau in cognitively intact individuals with no clinical symptoms[52,54]. Handoko and colleagues have identified the presence of Aβo species including Aβ trimer and Aβ*56 in the CSF young (mean age = 41.7 years) and old (mean age = 64.8 years) cognitively normal individuals' [54]. This was confirmed by Lesne and colleagues in 75 cognitively unimpaired individuals, including young children and adolescents[52]. Both studies showed an age dependant deposition of different Aβo species where Aβ trimer was shown to be present in young individuals and Aβ*56 oligomer was found in middle aged cognitively normal individuals. The authors suggested that these Aβo species can predict individuals at high risk of developing clinical AD[52,54]. In addition, Handoko and colleagues showed a coupling between Aβo and total Tau and p-Tau Thr181 in cognitively normal older adults, which weakened in MCI and

AD patient, this also signified the importance of therapeutic intervention in asymptomatic individuals[54]. However, very limited number of studies have investigated the relationship between normal aging and age-related deposition of AD or CCD related brain biomarkers in cognitively asymptomatic dogs albeit; and no studies have been reported on the relationship between normal aging and age-related deposition of AD or CCD related retinal biomarkers in cognitively asymptomatic dogs. In study Ⅳ, chapter 6, I have studied a diverse group of 30 cognitively asymptomatic dogs to investigate whether the retina accumulates AD related biomarkers. Clinically, these dogs were not cognitively deficient, and their age ranged from 1-16 years. Of note, a dog aged 1 year is equivalent to 15 years in human age and early middle-aged dogs (6-10 years) is equivalent to humans age 40-60 years[166]. Therefore, the identification of AD related retinal biomarkers in a group of young, middle, and old aged cognitively unimpaired dogs, may help predict preclinical AD before brain onset and cognitive decline. A study by Ko and colleagues examined the retinal nerve fiber layer (RNFL) thickness and cognitive status of individuals aged 40 to 69 years over a 3-year period [346]. The authors found that individuals with thinner RNFL showed higher incidence of cognition. In this study, cognitively normal dogs demonstrated the presence of Aβo, Aβp and p-Tau in the retinal layers. Both isoform of Aβo including $A\beta_{1-40}$ and $A\beta_{1-42}$ were identified in the retinal layers of young (1-5 years old), middle (6-10 years old) and old (≥11 years old) age groups of dogs. Morphologically, similar presentation, such as globular and annular shape $A\beta_{1-40}$ and $A\beta_{1-42}$ oligomers, were detected in the ONL, INL and GCL of all age groups[53]. 26 out of 30 dogs in the young, middle and old age groups, with the exception of a 1.4-year-old male Siberian husky, a 7-year-old neutered male Hound mixed, an 8-year-old spayed female Bedlington terrier and a 11-year-old neutered male mixed breed were demonstrated $A\beta_{1-40}$ and $A\beta_{1-42}$ oligomers. Previous studies suggested that in the canine brain, Aβo may be the toxic species and responsible for cognitive decline and can potentially be an early biomarker for the detection of CCD[296,297]. Also, Naaman and colleagues reported that $A\beta_{42}$ oligomers cause extensive retinal neurotoxicity in rats when compared to fibrillary $A\beta_{40}$ and $A\beta_{42}$ [113].

Furthermore, after staining with 4G8 antibody, dot like and small rounded in shape[105,110] 4G8 positive Aβp were found extracellularly in the GCL, IPL & INL. Young dogs did not exhibit any plaque depositions, whereas in the middle age group, three dogs exhibited 'low' staining intensity and two exhibited 'strong' staining intensity and finally five dogs showed 'strong' signal intensity and two with 'moderate' signal intensity in the old age group. Of importance, Aβp accumulation was shown to have significant correlation with age but not with the severity of cognitive dysfunction[138,149,347]. Rofina *et al* and Trine *et al* investigated the correlation of Aβp with age and severity cognitive decline in dogs aged 1 month to 19 years and 9-15 years respectively[138,347]. Both studies reported that levels of Aβp deposition were significantly influenced by the age of the dog but no relationship with cognitive ability of the animals was observed. Mormino *et al* reported that deposition of Aβ plaques, usually detected by PET imaging or post-mortem histopathological identification, are commonly present in the cognitively normal aged population [406]. However, the authors stated that elevated level of Aβp can increase the level of p-Tau deposition which further increase the risk of developing progressive cognitive dysfunction, MCI and dementia[406]. In agreement with this study, Rowe *et al* demonstrated the presence of Aβ with MRI and PET imaging in 183 cognitively normal individual. From the initial imaging assessment and a 3 year follow up clinical reclassification, the authors found that 13% of healthy individuals developed MCI and dementia and suggested that individuals with positive Aβ scanning and subtle memory changes were at high risk of developing MCI and AD and that the 3 year time frame can be useful for the diagnostic and therapeutic interventions[321].

Now, how Aβ deposited in retina is not clear, albeit one hypothesis is that retinal Aβ may originate from blood[396]. My own study in a rodent model of AD predicted that retinal Aβ originates from blood (chapter 4), where Aβo co-accumulated simultaneously in eye and blood without any brain deposits in the 3-4 month age group[53]. Additionally, in human AD, several studies have demonstrated the presence of Aβ deposition in the retinal vasculature[112]. However, in the 'cognitively unimpaired dog study' (study Ⅳ; chapter 6), vascular Aβ deposited in the retinal sections derived from the young, middle and old age group, which might imitate cerebral amyloid angiopathy[106,360]. Sharafi *et al* suggested that retinal vasculature changes captured by hyperspectral imaging can differentiate cerebral amyloid status between cognitively impaired and unimpaired individuals[361]. After investigating the co-accumulation of both retinal Aβo and Aβp, I found that Aβp colocalised with Aβo in some middle and old age dogs. This is in agreement with my study in chapter 4, where 17-18 months old APP/PS1 mice showed high levels of oligomers deposits in the retinal layers that co-localized with Aβp[53]. Previous studies in hAD have shown that cerebral Aβo is usually present in early disease stages and mostly responsible for neurotoxicity and synaptic dysfunction[39,224,225,353,354], whereas extracellular Aβp are believed to accumulate at later ages and may act as a reservoir for Aβo[355].

Another hallmark of AD is p-Tau, which develops and deposits as NFTs[20,21]. Studies have reported that p-Tau neuropathology may develop about a decade before the formation of Aβp and involved in the early stage of AD[54,366]. Weigand and colleagues showed that individuals with Aβ negative and p-Tau positive PET imaging (A−/T+) have poor cognitive performance[407]. They conducted a PET Aβ and p-Tau imaging study in 301 humans without dementia and grouped them into A−/T−, A−/T+, A+/T− and A+/T+ and found that 45% of total subjects were A−/T+. Finally, this study suggested that p-Tau deposition in the temporal lobe without the presence of cortical Aβ may represent the early stage of AD[407].

However, some studies have shown that in dogs affected with CCD, p-Tau, unlike NFTs, has been identified in the brains, but remained inconclusive. It has been speculated that, unlike human AD, hyperphosphorylated Tau may not develop systematically in dogs due to their shorter lifespan (Tayebi & Habiba, personal communication). In agreement with this hypothesis, Pugleise *et al* showed that the diffuse Aβp and p-Tau are unrelated and form independently in the brains of aged dogs[142]. In chapter 6, I have investigated the presence of AT8 positive p-Tau Ser202/Thr205 to confirm the presence of retinal p-Tau in cognitively unimpaired dogs. My study revealed diffuse p-Tau distribution in the OPL, INL, IPL and GCL in four out of ten dogs of the old age group, including a spayed female German shepherd, a neutered male Husky aged 12 years old, a neutered male Shih-tzu aged 12.8 years old and a neutered male Border collie aged 13 years' old. The same dogs also showed widespread distribution of $A\beta_{40}$ and/or $A\beta_{42}$ oligomers and 4G8-positive Aβp. Likewise, retinal AT8-positive intracellular diffuse p-Tau was reported by Schön and colleagues in AD patients [104]. In study Ⅲ, chapter 5, $A\beta_{42}$ oligomers and p-Tau were shown to have a positive correlation and co-localised in the brain of dogs affected with CCD and this interaction is believed to cause neuronal toxicity and may act synergistically to trigger synaptic dysfunction[45,64,66]. In line with this observation, a histopathological study by Manczak and colleagues showed that $A\beta_{40}$ or $A\beta_{42}$ oligomers co-localised with p-Tau in AD patient brain[65]. Therefore, in this study Ⅳ, I have identified an interaction between p-Tau and Aβo in retinal layers. Interestingly, the same four dogs displayed co-localisation of p-Tau and $A\beta_{40}$ and/or $A\beta_{42}$ oligomers in the OPL, INL, IPL and GCL of retina. These data in cognitively unimpaired dogs suggested that, not only Aβo but also diffuse p-Tau might be an early predictor of AD and CCD and could be useful as an optical diagnostic platform for AD before cognitive onset. Taken together, these results provided a novel insight into AD related biomarkers in cognitively unimpaired dogs with a possible timeframe for diagnostic and therapeutic interventions. Several studies in the field of AD research highlighted the importance of diagnostic and therapeutic interventions in the asymptomatic phase while the individuals are cognitively intact[52,370]. However, it is challenging to 'track' the disease progression in human without any accurate and cost effective early diagnostic approaches and lack of robust natural translational models. Finally, an undisputable demonstration of AD related pathology naturally developed in these dogs support the usefulness of dogs as a natural translational model for investigating AD (study Ⅳ; chapter 6).

Recent advancement in eye imaging technology with high-resolution capacity can help assess subtle changes to severe abnormalities in the retina. Clinically, optical coherence tomography (OCT) is widely used for various retinal dysfunctions, including diabetic retinopathy, macular edema, macular degeneration, vascular occlusions, and also hereditary diseases[408-410]. OCT imaging platform also allow monitoring of the disease progression and treatment efficacy. A recent study by Muakkassa *et al* monitored the treatment efficacy of vascular endothelium growth factor (VEGF) therapy for choroidal neovascularization (CNV) using optical coherence tomography angiography (OCTA)[411]. This study showed OCT based metrics might be a potential tool for future. Considering that, it is important to further validate young and middle-aged dogs as a model for investigating human ageing and pre-clinical AD.

7.2. Conclusion

1. In 5xFAD AD mouse model study (study Ⅰ; chapter 3), I showed the presence of intra-neuronal Aβo in the retinal nuclear layers which started to appear extensively from 6-months of age. However, the amount of Aβo were decreased in an age dependant manner and suggested that its accumulation inversely correlated with retinal Aβp deposition, indicating an age-related Aβ conversion in this animal model. This study also confirmed the localization of Aβo to neurons, typically accumulating in late endosomes, indicating possible impairment of the endocytic pathway[101].
2. In APP/PS1 AD mouse model study (study Ⅱ; chapter 4), a unique tool, namely camelid-derived single domain antibodies were used to identify Aβo in the retinal layers, brain, and blood in early stages of the disease. Camelid-derived single domain antibodies targeting

$A\beta_{1-40}$ (PrioAD12) and $A\beta_{1-42}$ (PrioAD13) oligomers were able to detect Aβo in the retina and blood but not in the cerebrum of 3-4-months old APP/PS1 mice. Similar to my previous study (study 1, chapter 3), the age-dependent conversion of Aβo to Aβp was confirmed. This study suggested that retinal Aβo may originate from peripheral blood and precedes Aβo deposition in the brain and cognitive decline. This provides a very strong basis to develop and implement an 'eye test' for early detection of AD using camelid-derived single domain antibodies targeting retinal Aβ[53].

3. Study Ⅲ, chapter 5, proposed dogs as a natural translational model for AD. All the major neuropathological hallmarks of AD, including intracellular $A\beta_{1-42}$ oligomers, extracellular Aβ senile plaques and p-Tau were demonstrated unequivocally in the hippocampus and frontal cortex of dogs affected with CCD. $A\beta_{1-42}$ oligomers and p-Tau co-accumulation was demonstrated in this species for the first time whereas no co-localisation with Aβp was noticed. Taken together, these findings highlighted greater understanding of the strength of the 'dog CCD' as a model for AD.
4. Finally, study Ⅳ, chapter 6 proposed that identification of AD related biomarkers in cognitively normal dogs might help predict individuals at higher risk of contracting AD in old age and confirm the 'dog CCD' as a strong model to study human AD. This work provides strong impetus to develop a non-invasive, easily accessible, and point-of-care diagnostic platform for AD for initial use and testing in dogs with CCD before trialling in human AD.

7.3. Future direction

1. The study in chapter 4 provided strong evidence that Aβo could be detected simultaneously in the blood and retina of APP/PS1 mice before their appearance in the brain. It showed that nanobodies were able to bind to $A\beta_{1-40}$ and $A\beta_{1-42}$ oligomers and detect the toxic small diffusible Aβo specific to AD. Previous studies have highlighted

the anatomical and morphological similarities between the BRB and BBB and confirmed that disruption of BRB integrity leads to $A\beta_{40}$ and $A\beta_{42}$ accumulation in the retinal vasculature. Future studies are required to use larger cohorts of animals starting from 1-2 months age group of APP/PS1 mice in order to investigate the blood and retinal accumulation of Aβo before brain pathology ensues. Also, to understand the correlation between blood and retinal deposition of Aβo. Age-related progression of Aβ and how it triggers the deposition of p-Tau also needs to be addressed in the blood and retina before cognitive changes take place[413]. Finally, a longitudinal study is also required to correlate progressive cognitive decline and blood and retinal pathological progression. This study will help to determine a possible time frame for AD development.

2. Retina has a very unique and transparent structure as compared to the brain, which has a complex network. Recent advances in the development of retinal microvascular imaging using OCT angiography[112], pericyte imaging using adaptive optics scanning laser ophthalmoscope (AOSLO)[414], and also fluorescence tagged retinal amyloid imaging[206] provided a strong understanding of retinal AD-related changes and leads to the future development of non-invasive retinal AD diagnostic platform which may provide a higher chance of detecting AD at the pre-clinical stage.
3. Several studies have reported differences in retinal degeneration in MCI and AD patients[415]. However, this pathological changes in the retinal layer have never been compared with the pathological effect of Aβo deposition in the retinal layers and the differences between preclinical, MCI, and AD patients. Also, the field needs to focus on which layer of the retina is mostly affected by these changes and how it is connected to the brain, what are the possible indication of brain retinal interaction in progressive Aβo build-up, and neurodegeneration. Therefore, future extensive studies are highly

recommended to address all the structural, physiological, and pathological details of the retina for the development of a reliable and accurate diagnostic platform for AD.

4. Disturbances in the endo-lysosomal–autophagic system are believed to be one of the early neuropathological changes associated with AD. More importantly, a growing body of research suggested that excessive levels of $A\beta_{42}$ oligomer may destabilize the physical integrity of endo-lysosomal–autophagic compartments which subsequently affect the late autophagy stages, leading to inefficient clearance of Aβ causing their progressive build up and neurodegeneration[416]. In chapters 3 and 4 this work confirmed the colocalization of Aβo with endo-lysosomal system in the hippocampal region and cerebral cortex. Also, colocalization of Aβo with endo-lysosomal system in the ONL, OPL, INL of the retina indicate retinal cell impairment and their inability to process and degrade this oligomeric species. A comprehensive understanding of the autophagic process in AD are necessary for the development of therapeutic strategies. Future therapeutic studies may also aim to enhance the activity of lysosomal degradation to enhance Aβ clearance.
5. The most commonly used animal models are transgenic rodent models. In chapter 5, I confirmed the presence of the major neuropathological hallmarks of human AD, including Aβo, Aβp, and p-Tau, in the brain hippocampal and cortical region of a group of cognitively impaired dogs. The current study advocates for the use of this natural disease model to investigate AD. Further large cohort studies are necessary to extensively characterize the dog as a natural disease model of AD.
6. Lack of reproducible translational therapeutic outcomes has been a major issue in the AD field. By in large, transgenic animal models of human AD failed to replicate the subtle clinical and pathological features of the disease. Therefore, future AD therapeutic

studies should consider employing cognitively deficient dogs to determine the treatment suitability and efficacy.

7. In human AD, neuroimaging platforms, including PET and MRI scanning, are commonly used to diagnose AD. However, there is a very limited number of studies on the use of neuroimaging in dogs affected with CCD[308]. Future research may consider improving the understanding of canine cognitive processes using PET and/or MRI scanning and correlate with the behavioural deficits and cognitive status in CCD dogs which will contribute to the early diagnosis of CCD.
8. Several longitudinal studies in humans highlighted the importance of investigating normal aging in cognitively unimpaired younger individuals to identify those at risk of progressive increase of AD pathological burden and cognitive impairment and the possible time frame for early diagnostic and therapeutic intervention. However, it is impossible to track the disease progression in humans without an accurate animal model and early diagnostic platform. So, dogs can meet this requirement as a natural translational model for aging and AD research. The study in chapter 6 reported the presence of Aβ and p-Tau in the retinal layers of cognitively unimpaired dogs. This study also provided a basis to characterize dogs as a model for aging and human AD, a possible timeframe to predict AD and to develop a retinal diagnostic platform. Future studies are required to incorporate a large cohort size of dogs including young 1-5 years to 11-16 years age groups to extensively study the progressive development of AD-related pathology in dogs. This current study only addresses the histopathological changes in the retina; therefore, future studies should consider examining the dog retinal physiological changes and compare with the histopathological lesions.

Chapter 8

References

1. Perl DP. Neuropathology of Alzheimer's disease. *Mount Sinai Journal of Medicine: A Journal of Translational and Personalized Medicine: A Journal of Translational and Personalized Medicine.* 2010;77(1):32-42.
2. 2020 Alzheimer's disease facts and figures. *Alzheimer's & Dementia.* 2020;16(3):391-460.
3. 2020 Alzheimer's disease facts and figures. *Alzheimer's & dementia : the journal of the Alzheimer's Association.* 2020.
4. Jaul E, Barron J. Age-Related Diseases and Clinical and Public Health Implications for the 85 Years Old and Over Population. *Front Public Health.* 2017;5:335-335.
5. Langa KM. Is the risk of Alzheimer's disease and dementia declining? *Alzheimer's research & therapy.* 2015;7(1):34.
6. Nations U. World population ageing report. *World Popul Ageing Rep.* 2015;2015.
7. Rosenberg A, Mangialasche F, Ngandu T, Solomon A, Kivipelto M. Multidomain Interventions to Prevent Cognitive Impairment, Alzheimer's Disease, and Dementia: From FINGER to World-Wide FINGERS. *The journal of prevention of Alzheimer's disease.* 2020;7(1):29-36.
8. El-Hayek YH, Wiley RE, Khoury CP, et al. Tip of the Iceberg: Assessing the Global Socioeconomic Costs of Alzheimer's Disease and Related Dementias and Strategic Implications for Stakeholders. *J Alzheimers Dis.* 2019;70(2):323-341.
9. Wimo A, Guerchet M, Ali GC, et al. The worldwide costs of dementia 2015 and comparisons with 2010. *Alzheimer's & dementia : the journal of the Alzheimer's Association.* 2017;13(1):1-7.
10. (WHO) WHO. Dementia. 2 September 2021.
11. Dorszewska J, Prendecki M, Oczkowska A, Dezor M, Kozubski W. Molecular Basis of Familial and Sporadic Alzheimer's Disease. *Current Alzheimer research.* 2016;13(9):952-963.
12. Acosta-Baena N, Sepulveda-Falla D, Lopera-Gómez CM, et al. Pre-dementia clinical stages in presenilin 1 E280A familial early-onset Alzheimer's disease: a retrospective cohort study. *The Lancet Neurology.* 2011;10(3):213-220.
13. Bagyinszky E, Youn YC, An SS, Kim S. The genetics of Alzheimer's disease. *Clin Interv Aging.* 2014;9:535-551.
14. Lehtovirta M, Soininen H, Helisalmi S, et al. Clinical and neuropsychological characteristics in familial and sporadic Alzheimer's disease: relation to apolipoprotein E polymorphism. *Neurology.* 1996;46(2):413-419.
15. Roses AD, Saunders AM. APOE is a major susceptibility gene for Alzheimer's disease. *Current opinion in biotechnology.* 1994;5(6):663-667.
16. Santiago JA, Potashkin JA. The Impact of Disease Comorbidities in Alzheimer's Disease. *Front Aging Neurosci.* 2021;13:631770.
17. Association As. Stages of Alzheimer's. 2021.
18. Aging NIo. What Are the Signs of Alzheimer's Disease? May 16, 2017.
19. Parnetti L, Chipi E, Salvadori N, D'Andrea K, Eusebi P. Prevalence and risk of progression of preclinical Alzheimer's disease stages: a systematic review and meta-analysis. *Alzheimer's research & therapy.* 2019;11(1):7.
20. Serrano-Pozo A, Frosch MP, Masliah E, Hyman BT. Neuropathological alterations in Alzheimer disease. *Cold Spring Harb Perspect Med.* 2011;1(1):a006189.
21. Perl DP. Neuropathology of Alzheimer's disease. *The Mount Sinai journal of medicine, New York.* 2010;77(1):32-42.
22. Mott RT, Hulette CM. Neuropathology of Alzheimer's disease. *Neuroimaging clinics of North America.* 2005;15(4):755-765, ix.

23. Cai X-D, Golde TE, Younkin SG. Release of excess amyloid beta protein from a mutant amyloid beta protein precursor. *Science (New York, NY).* 1993;259(5094):514-516.
24. Suzuki N, Cheung TT, Cai X-D, et al. An increased percentage of long amyloid beta protein secreted by familial amyloid beta protein precursor (beta APP717) mutants. *Science (New York, NY).* 1994;264(5163):1336-1340.
25. Haass C, Selkoe DJ. Cellular processing of β-amyloid precursor protein and the genesis of amyloid β-peptide. *Cell.* 1993;75(6):1039-1042.
26. Chow VW, Mattson MP, Wong PC, Gleichmann M. An overview of APP processing enzymes and products. *Neuromolecular medicine.* 2010;12(1):1-12.
27. Kang J, Lemaire H-G, Unterbeck A, et al. The precursor of Alzheimer's disease amyloid A4 protein resembles a cell-surface receptor. *Nature.* 1987;325(6106):733.
28. Mroczko B, Groblewska M, Litman-Zawadzka A, Kornhuber J, Lewczuk P. Amyloid β oligomers (AβOs) in Alzheimer's disease. *Journal of Neural Transmission.* 2018;125(2):177-191.
29. Serrano-Pozo A, Frosch MP, Masliah E, Hyman BT. Neuropathological alterations in Alzheimer disease. *Cold Spring Harbor perspectives in medicine.* 2011;1(1):a006189.
30. Choudhury DA, Chakraborty I, Bhattacharjee R, et al. An update on pathological implications of enzymatic dysregulation in Alzheimer's disease. 2018;29:2215-2226.
31. DeTure MA, Dickson DW. The neuropathological diagnosis of Alzheimer's disease. *Molecular neurodegeneration.* 2019;14(1):32.
32. Yasuhara O, Kawamata T, Aimi Y, McGeer EG, McGeer PL. Two types of dystrophic neurites in senile plaques of Alzheimer disease and elderly non-demented cases. *Neurosci Lett.* 1994;171(1-2):73-76.
33. Thal DR, Capetillo-Zarate E, Del Tredici K, Braak H. The development of amyloid beta protein deposits in the aged brain. *Science of aging knowledge environment : SAGE KE.* 2006;2006(6):re1.
34. Alafuzoff I, Arzberger T, Al-Sarraj S, et al. Staging of neurofibrillary pathology in Alzheimer's disease: a study of the BrainNet Europe Consortium. *Brain pathology.* 2008;18(4):484-496.
35. Murpy M, LeVine III H. Alzheimer's disease and the β-amyloid peptide. *J Alzheimers Dis.* 2010;19(1):311-323.
36. Broersen K, Rousseau F, Schymkowitz J. The culprit behind amyloid beta peptide related neurotoxicity in Alzheimer's disease: oligomer size or conformation? *Alzheimer's research & therapy.* 2010;2(4):12.
37. Goure WF, Krafft GA, Jerecic J, Hefti F. Targeting the proper amyloid-beta neuronal toxins: a path forward for Alzheimer's disease immunotherapeutics. *Alzheimer's research & therapy.* 2014;6(4):42.
38. Morgado I, Fändrich M. Assembly of Alzheimer's Aβ peptide into nanostructured amyloid fibrils. *Current opinion in colloid & interface science.* 2011;16(6):508-514.
39. Sengupta U, Nilson AN, Kayed R. The Role of Amyloid-β Oligomers in Toxicity, Propagation, and Immunotherapy. *EBioMedicine.* 2016;6:42-49.
40. Glabe CG. Structural classification of toxic amyloid oligomers. *Journal of Biological Chemistry.* 2008;283(44):29639-29643.
41. Funke SA. Detection of Soluble Amyloid-Oligomers and Insoluble High-Molecular-Weight Particles in CSF: Development of Methods with Potential for Diagnosis and Therapy Monitoring of Alzheimer's Disease. *International Journal of Alzheimer's Disease.* 2011;2011.
42. Benilova I, Karran E, De Strooper B. The toxic Aβ oligomer and Alzheimer's disease: an emperor in need of clothes. *Nature neuroscience.* 2012;15(3):349.

43. Gandy S, Simon AJ, Steele JW, et al. Days to criterion as an indicator of toxicity associated with human Alzheimer amyloid-β oligomers. *Annals of neurology.* 2010;68(2):220-230.
44. Gong Y, Chang L, Viola KL, et al. Alzheimer's disease-affected brain: presence of oligomeric Aβ ligands (ADDLs) suggests a molecular basis for reversible memory loss. *Proceedings of the National Academy of Sciences.* 2003;100(18):10417-10422.
45. Haass C, Selkoe DJ. Soluble protein oligomers in neurodegeneration: lessons from the Alzheimer's amyloid beta-peptide. *Nature reviews Molecular cell biology.* 2007;8(2):101-112.
46. Kayed R, Head E, Thompson JL, et al. Common structure of soluble amyloid oligomers implies common mechanism of pathogenesis. *Science (New York, NY).* 2003;300(5618):486-489.
47. Zhao LN, Long HW, Mu Y, Chew LY. The toxicity of amyloid ß oligomers. *International journal of molecular sciences.* 2012;13(6):7303-7327.
48. Walsh DM, Klyubin I, Fadeeva JV, et al. Naturally secreted oligomers of amyloid beta protein potently inhibit hippocampal long-term potentiation in vivo. *Nature.* 2002;416(6880):535-539.
49. Lesné S, Kotilinek L, Ashe KH. Plaque-bearing mice with reduced levels of oligomeric amyloid-beta assemblies have intact memory function. *Neuroscience.* 2008;151(3):745-749.
50. Viola KL, Klein WL. Amyloid β oligomers in Alzheimer's disease pathogenesis, treatment, and diagnosis. *Acta Neuropathol.* 2015;129(2):183-206.
51. Hayden EY, Teplow DB. Amyloid β-protein oligomers and Alzheimer's disease. *Alzheimer's research & therapy.* 2013;5(6):60.
52. Lesné SE, Sherman MA, Grant M, et al. Brain amyloid-β oligomers in ageing and Alzheimer's disease. *Brain.* 2013;136(Pt 5):1383-1398.
53. Habiba U, Descallar J, Kreilaus F, et al. Detection of retinal and blood Aβ oligomers with nanobodies. *Alzheimers Dement (Amst).* 2021;13(1):e12193.
54. Handoko M, Grant M, Kuskowski M, et al. Correlation of specific amyloid-β oligomers with tau in cerebrospinal fluid from cognitively normal older adults. *JAMA Neurol.* 2013;70(5):594-599.
55. Tian J, Shi J, Mann DM. Cerebral amyloid angiopathy and dementia. *Panminerva Med.* 2004;46(4):253-264.
56. Yamada M. Risk factors for cerebral amyloid angiopathy in the elderly. *Ann N Y Acad Sci.* 2002;977:37-44.
57. Augustinack JC, Schneider A, Mandelkow EM, Hyman BT. Specific tau phosphorylation sites correlate with severity of neuronal cytopathology in Alzheimer's disease. *Acta Neuropathol.* 2002;103(1):26-35.
58. Braak E, Braak H, Mandelkow EM. A sequence of cytoskeleton changes related to the formation of neurofibrillary tangles and neuropil threads. *Acta Neuropathol.* 1994;87(6):554-567.
59. Wang Y, Mandelkow E. Tau in physiology and pathology. *Nature reviews Neuroscience.* 2016;17(1):5-21.
60. Iqbal K, Liu F, Gong CX, Grundke-Iqbal I. Tau in Alzheimer disease and related tauopathies. *Current Alzheimer research.* 2010;7(8):656-664.
61. Kolarova M, García-Sierra F, Bartos A, Ricny J, Ripova D. Structure and pathology of tau protein in Alzheimer disease. *Int J Alzheimers Dis.* 2012;2012:731526.
62. Li C, Götz J. Somatodendritic accumulation of Tau in Alzheimer's disease is promoted by Fyn-mediated local protein translation. *The EMBO journal.* 2017;36(21):3120-3138.

63. Shin WS, Di J, Cao Q, et al. Amyloid β-protein oligomers promote the uptake of tau fibril seeds potentiating intracellular tau aggregation. *Alzheimer's research & therapy.* 2019;11(1):86.
64. Kayed R, Head E, Thompson JL, et al. Common structure of soluble amyloid oligomers implies common mechanism of pathogenesis. *Science (New York, NY).* 2003;300(5618):486-489.
65. Manczak M, Reddy PH. Abnormal interaction of oligomeric amyloid-β with phosphorylated tau: implications to synaptic dysfunction and neuronal damage. *J Alzheimers Dis.* 2013;36(2):285-295.
66. De Felice FG, Wu D, Lambert MP, et al. Alzheimer's disease-type neuronal tau hyperphosphorylation induced by A beta oligomers. *Neurobiology of aging.* 2008;29(9):1334-1347.
67. Sakono M, Zako T. Amyloid oligomers: formation and toxicity of Aβ oligomers. *The FEBS journal.* 2010;277(6):1348-1358.
68. Yang AJ, Chandswangbhuvana D, Margol L, Glabe CG. Loss of endosomal/lysosomal membrane impermeability is an early event in amyloid Abeta1-42 pathogenesis. *J Neurosci Res.* 1998;52(6):691-698.
69. Zheng L, Cedazo-Minguez A, Hallbeck M, Jerhammar F, Marcusson J, Terman A. Intracellular distribution of amyloid beta peptide and its relationship to the lysosomal system. *Translational neurodegeneration.* 2012;1(1):19.
70. Yu C, Nwabuisi-Heath E, Laxton K, Ladu MJ. Endocytic pathways mediating oligomeric Abeta42 neurotoxicity. *Molecular neurodegeneration.* 2010;5:19.
71. Braak H, Braak E. Frequency of stages of Alzheimer-related lesions in different age categories. *Neurobiology of aging.* 1997;18(4):351-357.
72. Thal DR, Rüb U, Orantes M, Braak H. Phases of A beta-deposition in the human brain and its relevance for the development of AD. *Neurology.* 2002;58(12):1791-1800.
73. Braak H, Braak E. Staging of Alzheimer's disease-related neurofibrillary changes. *Neurobiology of aging.* 1995;16(3):271-278; discussion 278-284.
74. McKhann GM, Knopman DS, Chertkow H, et al. The diagnosis of dementia due to Alzheimer's disease: recommendations from the National Institute on Aging-Alzheimer's Association workgroups on diagnostic guidelines for Alzheimer's disease. *Alzheimer's & dementia : the journal of the Alzheimer's Association.* 2011;7(3):263-269.
75. James M. Ellison M, MPH,Alzheimer's Disease Research. Diagnostic Tests for Alzheimer's Disease. November 9, 2020.
76. Turner RS, Stubbs T, Davies DA, Albensi BC. Potential New Approaches for Diagnosis of Alzheimer's Disease and Related Dementias. *Front Neurol.* 2020;11:496.
77. Association As. Medical Tests for Diagnosing Alzheimer's. 2021.
78. Blennow K, Zetterberg H. Use of CSF biomarkers in Alzheimer's disease clinical trials. *J Nutr Health Aging.* 2009;13(4):358-361.
79. Kerr NL. HARKing: hypothesizing after the results are known. *Personality and social psychology review : an official journal of the Society for Personality and Social Psychology, Inc.* 1998;2(3):196-217.
80. Hampel H, O'Bryant SE, Molinuevo JL, et al. Blood-based biomarkers for Alzheimer disease: mapping the road to the clinic. *Nat Rev Neurol.* 2018;14(11):639-652.
81. Lim JK, Li QX, He Z, et al. The Eye As a Biomarker for Alzheimer's Disease. *Frontiers in neuroscience.* 2016;10:536.

82. Colligris P, Perez de Lara MJ, Colligris B, Pintor J. Ocular Manifestations of Alzheimer's and Other Neurodegenerative Diseases: The Prospect of the Eye as a Tool for the Early Diagnosis of Alzheimer's Disease. *Journal of ophthalmology.* 2018;2018:8538573.
83. Bassi CJ, Solomon K, Young D. Vision in aging and dementia. *Optometry and vision science : official publication of the American Academy of Optometry.* 1993;70(10):809-813.
84. Mahajan D, Votruba M. Can the retina be used to diagnose and plot the progression of Alzheimer's disease? *Acta Ophthalmol.* 2017;95(8):768-777.
85. Berisha F, Feke GT, Trempe CL, McMeel JW, Schepens CL. Retinal abnormalities in early Alzheimer's disease. *Investigative ophthalmology & visual science.* 2007;48(5):2285-2289.
86. Blanks JC, Schmidt SY, Torigoe Y, Porrello KV, Hinton DR, Blanks RH. Retinal pathology in Alzheimer's disease. II. Regional neuron loss and glial changes in GCL. *Neurobiology of aging.* 1996;17(3):385-395.
87. Iseri PK, Altinaş O, Tokay T, Yüksel N. Relationship between cognitive impairment and retinal morphological and visual functional abnormalities in Alzheimer disease. *Journal of neuro-ophthalmology : the official journal of the North American Neuro-Ophthalmology Society.* 2006;26(1):18-24.
88. Sadun AA, Bassi CJ. Optic nerve damage in Alzheimer's disease. *Ophthalmology.* 1990;97(1):9-17.
89. Danesh-Meyer HV, Birch H, Ku JY, Carroll S, Gamble G. Reduction of optic nerve fibers in patients with Alzheimer disease identified by laser imaging. *Neurology.* 2006;67(10):1852-1854.
90. Marquié M, Castilla-Martí M, Valero S, et al. Visual impairment in aging and cognitive decline: experience in a Memory Clinic. *Scientific reports.* 2019;9(1):8698.
91. Doustar J, Torbati T, Black KL, Koronyo Y, Koronyo-Hamaoui M. Optical Coherence Tomography in Alzheimer's Disease and Other Neurodegenerative Diseases. *Front Neurol.* 2017;8:701.
92. Drexler W, Fujimoto JG. State-of-the-art retinal optical coherence tomography. *Prog Retin Eye Res.* 2008;27(1):45-88.
93. Cheung CY, Ikram MK, Sabanayagam C, Wong TY. Retinal microvasculature as a model to study the manifestations of hypertension. *Hypertension.* 2012;60(5):1094-1103.
94. Garcia-Martin ES, Rojas B, Ramirez AI, et al. Macular thickness as a potential biomarker of mild Alzheimer's disease. *Ophthalmology.* 2014;121(5):1149-1151.e1143.
95. Thomson KL, Yeo JM, Waddell B, Cameron JR, Pal S. A systematic review and meta-analysis of retinal nerve fiber layer change in dementia, using optical coherence tomography. *Alzheimers Dement (Amst).* 2015;1(2):136-143.
96. Frost S, Kanagasingam Y, Sohrabi H, et al. Retinal vascular biomarkers for early detection and monitoring of Alzheimer's disease. *Translational psychiatry.* 2013;3:e233.
97. O'Bryhim BE, Apte RS, Kung N, Coble D, Van Stavern GP. Association of Preclinical Alzheimer Disease With Optical Coherence Tomographic Angiography Findings. *JAMA Ophthalmol.* 2018;136(11):1242-1248.
98. Coppola G, Di Renzo A, Ziccardi L, et al. Optical Coherence Tomography in Alzheimer's Disease: A Meta-Analysis. *PloS one.* 2015;10(8):e0134750.

99. Ascaso FJ, Cruz N, Modrego PJ, et al. Retinal alterations in mild cognitive impairment and Alzheimer's disease: an optical coherence tomography study. *J Neurol.* 2014;261(8):1522-1530.
100. London A, Benhar I, Schwartz M. The retina as a window to the brain-from eye research to CNS disorders. *Nat Rev Neurol.* 2013;9(1):44-53.
101. Habiba U, Merlin S, Lim JKH, et al. Age-Specific Retinal and Cerebral Immunodetection of Amyloid-β Plaques and Oligomers in a Rodent Model of Alzheimer's Disease. *J Alzheimers Dis.* 2020;76(3):1135-1150.
102. Koronyo-Hamaoui M, Koronyo Y, Ljubimov AV, et al. Identification of amyloid plaques in retinas from Alzheimer's patients and noninvasive in vivo optical imaging of retinal plaques in a mouse model. *Neuroimage.* 2011;54 Suppl 1:S204-217.
103. Jentsch S, Schweitzer D, Schmidtke KU, et al. Retinal fluorescence lifetime imaging ophthalmoscopy measures depend on the severity of Alzheimer's disease. *Acta Ophthalmol.* 2015;93(4):e241-247.
104. Schön C, Hoffmann NA, Ochs SM, et al. Long-term in vivo imaging of fibrillar tau in the retina of P301S transgenic mice. *PloS one.* 2012;7(12):e53547.
105. den Haan J, Morrema THJ, Verbraak FD, et al. Amyloid-beta and phosphorylated tau in post-mortem Alzheimer's disease retinas. *Acta Neuropathol Commun.* 2018;6(1):147.
106. Patton N, Aslam T, Macgillivray T, Pattie A, Deary IJ, Dhillon B. Retinal vascular image analysis as a potential screening tool for cerebrovascular disease: a rationale based on homology between cerebral and retinal microvasculatures. *J Anat.* 2005;206(4):319-348.
107. Feke GT, Hyman BT, Stern RA, Pasquale LR. Retinal blood flow in mild cognitive impairment and Alzheimer's disease. *Alzheimers Dement (Amst).* 2015;1(2):144-151.
108. Williams MA, McGowan AJ, Cardwell CR, et al. Retinal microvascular network attenuation in Alzheimer's disease. *Alzheimers Dement (Amst).* 2015;1(2):229-235.
109. Feke GT, Hyman BT, Stern RA, Pasquale LR. Retinal blood flow in mild cognitive impairment and Alzheimer's disease. *Alzheimer's & Dementia: Diagnosis, Assessment & Disease Monitoring.* 2015;1(2):144-151.
110. Lee S, Jiang K, McIlmoyle B, et al. Amyloid Beta Immunoreactivity in the Retinal Ganglion Cell Layer of the Alzheimer's Eye. *Frontiers in neuroscience.* 2020;14:758.
111. Frost S, Kanagasingam Y, Sohrabi H, et al. Retinal vascular biomarkers for early detection and monitoring of Alzheimer's disease. *Translational psychiatry.* 2013;3(2):e233.
112. Shi H, Koronyo Y, Rentsendorj A, et al. Identification of early pericyte loss and vascular amyloidosis in Alzheimer's disease retina. *Acta Neuropathol.* 2020;139(5):813-836.
113. Naaman E, Ya'ari S, Itzkovich C, et al. The retinal toxicity profile towards assemblies of Amyloid-β indicate the predominant pathophysiological activity of oligomeric species. *Scientific reports.* 2020;10(1):20954.
114. Youn YC, Lee BS, Kim GJ, et al. Blood Amyloid-β Oligomerization as a Biomarker of Alzheimer's Disease: A Blinded Validation Study. *J Alzheimers Dis.* 2020;75(2):493-499.
115. de Ruyter FJH. Early tau phosphorylation as a potential retinal biomarker for AD and other tauopathies. *Alzheimer's & Dementia.* 2020;16(S5):e040924.
116. Chiasseu M, Alarcon-Martinez L, Belforte N, et al. Tau accumulation in the retina promotes early neuronal dysfunction and precedes brain pathology in a mouse model of Alzheimer's disease. *Molecular neurodegeneration.* 2017;12(1):58.

117. Wisniewski T, Sigurdsson EM. Murine models of Alzheimer's disease and their use in developing immunotherapies. *Biochimica et biophysica acta.* 2010;1802(10):847-859.
118. Drummond E, Wisniewski T. Alzheimer's disease: experimental models and reality. *Acta Neuropathol.* 2017;133(2):155-175.
119. Holtzman DM, Fagan AM, Mackey B, et al. Apolipoprotein E facilitates neuritic and cerebrovascular plaque formation in an Alzheimer's disease model. *Annals of neurology.* 2000;47(6):739-747.
120. Banik A, Brown RE, Bamburg J, et al. Translation of Pre-Clinical Studies into Successful Clinical Trials for Alzheimer's Disease: What are the Roadblocks and How Can They Be Overcome? *J Alzheimers Dis.* 2015;47(4):815-843.
121. Cummings JL, Morstorf T, Zhong K. Alzheimer's disease drug-development pipeline: few candidates, frequent failures. *Alzheimer's research & therapy.* 2014;6(4):37.
122. Leon WC, Canneva F, Partridge V, et al. A novel transgenic rat model with a full Alzheimer's-like amyloid pathology displays pre-plaque intracellular amyloid-beta-associated cognitive impairment. *J Alzheimers Dis.* 2010;20(1):113-126.
123. Cohen RM, Rezai-Zadeh K, Weitz TM, et al. A transgenic Alzheimer rat with plaques, tau pathology, behavioral impairment, oligomeric aβ, and frank neuronal loss. *The Journal of neuroscience : the official journal of the Society for Neuroscience.* 2013;33(15):6245-6256.
124. Liu L, Orozco IJ, Planel E, et al. A transgenic rat that develops Alzheimer's disease-like amyloid pathology, deficits in synaptic plasticity and cognitive impairment. *Neurobiology of disease.* 2008;31(1):46-57.
125. Bekris LM, Yu C-E, Bird TD, Tsuang DW. Genetics of Alzheimer disease. *Journal of geriatric psychiatry and neurology.* 2010;23(4):213-227.
126. Bertram L, Tanzi RE. Alzheimer's disease: one disorder, too many genes? *Human molecular genetics.* 2004;13 Spec No 1:R135-141.
127. Braidy N, Poljak A, Jayasena T, Mansour H, Inestrosa NC, Sachdev PS. Accelerating Alzheimer's research through 'natural' animal models. *Curr Opin Psychiatry.* 2015;28(2):155-164.
128. Camus S, Ko WK, Pioli E, Bezard E. Why bother using non-human primate models of cognitive disorders in translational research? *Neurobiol Learn Mem.* 2015;124:123-129.
129. Youssef SA, Capucchio MT, Rofina JE, et al. Pathology of the Aging Brain in Domestic and Laboratory Animals, and Animal Models of Human Neurodegenerative Diseases. *Vet Pathol.* 2016;53(2):327-348.
130. Franco R, Cedazo-Minguez A. Successful therapies for Alzheimer's disease: why so many in animal models and none in humans? *Front Pharmacol.* 2014;5:146.
131. Landsberg GM, Nichol J, Araujo JA. Cognitive dysfunction syndrome: a disease of canine and feline brain aging. *The Veterinary clinics of North America Small animal practice.* 2012;42(4):749-768, vii.
132. Azkona G, Garcia-Belenguer S, Chacón G, Rosado B, León M, Palacio J. Prevalence and risk factors of behavioural changes associated with age-related cognitive impairment in geriatric dogs. *Journal of Small Animal Practice.* 2009;50(2):87-91.
133. Chan AD, Nippak P, Murphey H, et al. Visuospatial impairments in aged canines (Canis familiaris): the role of cognitive-behavioral flexibility. *Behavioral neuroscience.* 2002;116(3):443.
134. Landsberg GM, Nichol J, Araujo JA. Cognitive dysfunction syndrome: a disease of canine and feline brain aging. *Veterinary Clinics: Small Animal Practice.* 2012;42(4):749-768.

135. Osella MC, Re G, Odore R, et al. Canine cognitive dysfunction syndrome: Prevalence, clinical signs and treatment with a neuroprotective nutraceutical. *Applied Animal Behaviour Science.* 2007;105(4):297-310.
136. Cummings BJ, Head E, Ruehl W, Milgram NW, Cotman CW. The canine as an animal model of human aging and dementia. *Neurobiology of aging.* 1996;17(2):259-268.
137. Papaioannou N, Tooten PC, van Ederen AM, et al. Immunohistochemical investigation of the brain of aged dogs. I. Detection of neurofibrillary tangles and of 4-hydroxynonenal protein, an oxidative damage product, in senile plaques. *Amyloid.* 2001;8(1):11-21.
138. Rofina JE, van Ederen AM, Toussaint MJ, et al. Cognitive disturbances in old dogs suffering from the canine counterpart of Alzheimer's disease. *Brain research.* 2006;1069(1):216-226.
139. Salvin HE, McGreevy PD, Sachdev PS, Valenzuela MJ. The canine cognitive dysfunction rating scale (CCDR): a data-driven and ecologically relevant assessment tool. *Veterinary journal (London, England : 1997).* 2011;188(3):331-336.
140. Kiatipattanasakul W, Nakamura S, Hossain MM, et al. Apoptosis in the aged dog brain. *Acta Neuropathol.* 1996;92(3):242-248.
141. Ozawa M, Inoue M, Uchida K, Chambers JK, Takeuch Y, Nakayama H. Physical signs of canine cognitive dysfunction. *The Journal of veterinary medical science.* 2019;81(12):1829-1834.
142. Pugliese M, Mascort J, Mahy N, Ferrer I. Diffuse beta-amyloid plaques and hyperphosphorylated tau are unrelated processes in aged dogs with behavioral deficits. *Acta Neuropathol.* 2006;112(2):175-183.
143. Schmidt F, Boltze J, Jäger C, et al. Detection and Quantification of β-Amyloid, Pyroglutamyl Aβ, and Tau in Aged Canines. *Journal of neuropathology and experimental neurology.* 2015;74(9):912-923.
144. Abey A, Davies D, Goldsbury C, Buckland M, Valenzuela M, Duncan T. Distribution of tau hyperphosphorylation in canine dementia resembles early Alzheimer's disease and other tauopathies. *Brain pathology (Zurich, Switzerland).* 2020.
145. Head E. A canine model of human aging and Alzheimer's disease. *Biochimica et biophysica acta.* 2013;1832(9):1384-1389.
146. Head E, McCleary R, Hahn FF, Milgram NW, Cotman CW. Region-specific age at onset of beta-amyloid in dogs. *Neurobiology of aging.* 2000;21(1):89-96.
147. Borghys H, Van Broeck B, Dhuyvetter D, et al. Young to Middle-Aged Dogs with High Amyloid-β Levels in Cerebrospinal Fluid are Impaired on Learning in Standard Cognition tests. *J Alzheimers Dis.* 2017;56(2):763-774.
148. Braak H, Braak E. Neuropathological stageing of Alzheimer-related changes. *Acta Neuropathol.* 1991;82(4):239-259.
149. Ozawa M, Chambers JK, Uchida K, Nakayama H. The Relation between canine cognitive dysfunction and age-related brain lesions. *The Journal of veterinary medical science.* 2016;78(6):997-1006.
150. Colle MA, Hauw JJ, Crespeau F, et al. Vascular and parenchymal Abeta deposition in the aging dog: correlation with behavior. *Neurobiology of aging.* 2000;21(5):695-704.
151. Gonzalez-Martinez A, Rosado B, Pesini P, et al. Plasma beta-amyloid peptides in canine aging and cognitive dysfunction as a model of Alzheimer's disease. *Exp Gerontol.* 2011;46(7):590-596.
152. Janelidze S, Stomrud E, Palmqvist S, et al. Plasma β-amyloid in Alzheimer's disease and vascular disease. *Scientific reports.* 2016;6(1):26801.

153. Doecke JD, Pérez-Grijalba V, Fandos N, et al. Total Aβ(42)/Aβ(40) ratio in plasma predicts amyloid-PET status, independent of clinical AD diagnosis. *Neurology.* 2020;94(15):e1580-e1591.
154. Yu CH, Song GS, Yhee JY, et al. Histopathological and immunohistochemical comparison of the brain of human patients with Alzheimer's disease and the brain of aged dogs with cognitive dysfunction. *J Comp Pathol.* 2011;145(1):45-58.
155. Wegiel J, Wisniewski HM, Sołtysiak Z. Region- and cell-type-specific pattern of tau phosphorylation in dog brain. *Brain research.* 1998;802(1-2):259-266.
156. Kawas CH, Corrada MM, Brookmeyer R, et al. Visual memory predicts Alzheimer's disease more than a decade before diagnosis. *Neurology.* 2003;60(7):1089-1093.
157. Sperling RA, Aisen PS, Beckett LA, et al. Toward defining the preclinical stages of Alzheimer's disease: recommendations from the National Institute on Aging-Alzheimer's Association workgroups on diagnostic guidelines for Alzheimer's disease. *Alzheimer's & dementia : the journal of the Alzheimer's Association.* 2011;7(3):280-292.
158. Götz J, Bodea LG, Goedert M. Rodent models for Alzheimer disease. *Nature reviews Neuroscience.* 2018;19(10):583-598.
159. Kitazawa M, Medeiros R, Laferla FM. Transgenic mouse models of Alzheimer disease: developing a better model as a tool for therapeutic interventions. *Curr Pharm Des.* 2012;18(8):1131-1147.
160. Sarasa M, Pesini P. Natural non-trasgenic animal models for research in Alzheimer's disease. *Current Alzheimer research.* 2009;6(2):171-178.
161. Stylianaki I, Polizopoulou ZS, Theodoridis A, Koutouzidou G, Baka R, Papaioannou NG. Amyloid-beta plasma and cerebrospinal fluid biomarkers in aged dogs with cognitive dysfunction syndrome. *Journal of veterinary internal medicine.* 2020;34(4):1532-1540.
162. Lindblad-Toh K, Wade CM, Mikkelsen TS, et al. Genome sequence, comparative analysis and haplotype structure of the domestic dog. *Nature.* 2005;438(7069):803-819.
163. Liu GE, Matukumalli LK, Sonstegard TS, Shade LL, Van Tassell CP. Genomic divergences among cattle, dog and human estimated from large-scale alignments of genomic sequences. *BMC Genomics.* 2006;7:140-140.
164. Johnstone EM, Chaney MO, Norris FH, Pascual R, Little SP. Conservation of the sequence of the Alzheimer's disease amyloid peptide in dog, polar bear and five other mammals by cross-species polymerase chain reaction analysis. *Brain research Molecular brain research.* 1991;10(4):299-305.
165. Blizard DA, Klein LC, Cohen R, McClearn GE. A novel mouse-friendly cognitive task suitable for use in aging studies. *Behav Genet.* 2003;33(2):181-189.
166. American Kennel Club. Dog Years to Human Years. 2018, January 02; https://www.akcpetinsurance.com/blog/year-of-the-dog.
167. Mehta D, Jackson R, Paul G, Shi J, Sabbagh M. Why do trials for Alzheimer's disease drugs keep failing? A discontinued drug perspective for 2010-2015. *Expert Opin Investig Drugs.* 2017;26(6):735-739.
168. Oxford AE, Stewart ES, Rohn TT. Clinical Trials in Alzheimer's Disease: A Hurdle in the Path of Remedy. *Int J Alzheimers Dis.* 2020;2020:5380346.
169. ALZForum. 5xFAD mouse model. 15 Mar 2019.
170. ALZForum. APP/PS1 mouse model. 2021.
171. Tayebi M, Enever P, Sattar Z, Collinge J, Hawke S. Disease-associated prion protein elicits immunoglobulin M responses in vivo. *Mol Med.* 2004;10(7-12):104-111.

172. Mahmood T, Yang PC. Western blot: technique, theory, and trouble shooting. *North American journal of medical sciences.* 2012;4(9):429-434.
173. David MA, Jones DR, Tayebi M. Potential candidate camelid antibodies for the treatment of protein-misfolding diseases. *J Neuroimmunol.* 2014;272(1-2):76-85.
174. Beyreuther K, Masters CL. Amyloid precursor protein (APP) and beta A4 amyloid in the etiology of Alzheimer's disease: precursor-product relationships in the derangement of neuronal function. *Brain pathology (Zurich, Switzerland).* 1991;1(4):241-251.
175. Selkoe DJ, Hardy J. The amyloid hypothesis of Alzheimer's disease at 25 years. *EMBO Mol Med.* 2016;8(6):595-608.
176. Clark CM, Karlawish JH. Alzheimer disease: current concepts and emerging diagnostic and therapeutic strategies. *Ann Intern Med.* 2003;138(5):400-410.
177. Cai XD, Golde TE, Younkin SG. Release of excess amyloid beta protein from a mutant amyloid beta protein precursor. *Science (New York, NY).* 1993;259(5094):514-516.
178. Kang J, Lemaire HG, Unterbeck A, et al. The precursor of Alzheimer's disease amyloid A4 protein resembles a cell-surface receptor. *Nature.* 1987;325(6106):733-736.
179. Suzuki N, Cheung TT, Cai XD, et al. An increased percentage of long amyloid beta protein secreted by familial amyloid beta protein precursor (beta APP717) mutants. *Science (New York, NY).* 1994;264(5163):1336-1340.
180. Chow VW, Mattson MP, Wong PC, Gleichmann M. An overview of APP processing enzymes and products. *Neuromolecular medicine.* 2010;12(1):1-12.
181. Alafuzoff I, Arzberger T, Al-Sarraj S, et al. Staging of neurofibrillary pathology in Alzheimer's disease: a study of the BrainNet Europe Consortium. *Brain pathology (Zurich, Switzerland).* 2008;18(4):484-496.
182. Murphy MP, LeVine H, 3rd. Alzheimer's disease and the amyloid-beta peptide. *J Alzheimers Dis.* 2010;19(1):311-323.
183. Broersen K, Rousseau F, Schymkowitz J. The culprit behind amyloid beta peptide related neurotoxicity in Alzheimer's disease: oligomer size or conformation? *Alzheimer's research & therapy.* 2010;2(4):12.
184. Goure WF, Krafft GA, Jerecic J, Hefti F. Targeting the proper amyloid-beta neuronal toxins: a path forward for Alzheimer's disease immunotherapeutics. *Alzheimer's research & therapy.* 2014;6(4):42.
185. Glabe CG. Structural classification of toxic amyloid oligomers. *The Journal of biological chemistry.* 2008;283(44):29639-29643.
186. Mroczko B, Groblewska M, Litman-Zawadzka A, Kornhuber J, Lewczuk P. Amyloid β oligomers (AβOs) in Alzheimer's disease. *Journal of neural transmission (Vienna, Austria : 1996).* 2018;125(2):177-191.
187. Benilova I, Karran E, De Strooper B. The toxic Aβ oligomer and Alzheimer's disease: an emperor in need of clothes. *Nature neuroscience.* 2012;15(3):349-357.
188. Zhao LN, Long H, Mu Y, Chew LY. The toxicity of amyloid β oligomers. *International journal of molecular sciences.* 2012;13(6):7303-7327.
189. Frackowiak J, Zoltowska A, Wisniewski HM. Non-fibrillar beta-amyloid protein is associated with smooth muscle cells of vessel walls in Alzheimer disease. *Journal of neuropathology and experimental neurology.* 1994;53(6):637-645.
190. Katz B, Rimmer S. Ophthalmologic manifestations of Alzheimer's disease. *Survey of ophthalmology.* 1989;34(1):31-43.

191. Sadun AA, Borchert M, DeVita E, Hinton DR, Bassi CJ. Assessment of visual impairment in patients with Alzheimer's disease. *American journal of ophthalmology.* 1987;104(2):113-120.
192. Paquet C, Boissonnot M, Roger F, Dighiero P, Gil R, Hugon J. Abnormal retinal thickness in patients with mild cognitive impairment and Alzheimer's disease. *Neurosci Lett.* 2007;420(2):97-99.
193. Fotiou DF, Brozou CG, Haidich AB, et al. Pupil reaction to light in Alzheimer's disease: evaluation of pupil size changes and mobility. *Aging clinical and experimental research.* 2007;19(5):364-371.
194. Frost S, Kanagasingam Y, Sohrabi H, et al. Pupil response biomarkers for early detection and monitoring of Alzheimer's disease. *Current Alzheimer research.* 2013;10(9):931-939.
195. Nguyen CTO, Hui F, Charng J, et al. Retinal biomarkers provide "insight" into cortical pharmacology and disease. *Pharmacol Ther.* 2017;175:151-177.
196. Cronin-Golomb A, Corkin S, Rizzo JF, Cohen J, Growdon JH, Banks KS. Visual dysfunction in Alzheimer's disease: relation to normal aging. *Annals of neurology.* 1991;29(1):41-52.
197. Cronin-Golomb A, Sugiura R, Corkin S, Growdon JH. Incomplete achromatopsia in Alzheimer's disease. *Neurobiology of aging.* 1993;14(5):471-477.
198. Armstrong RA, Winsper SJ, Blair JA. Aluminium and Alzheimer's disease: review of possible pathogenic mechanisms. *Dementia.* 1996;7(1):1-9.
199. Trick GL, Trick LR, Morris P, Wolf M. Visual field loss in senile dementia of the Alzheimer's type. *Neurology.* 1995;45(1):68-74.
200. Valenti DA. Alzheimer's disease: screening biomarkers using frequency doubling technology visual field. *ISRN Neurol.* 2013;2013:989583.
201. Rizzo M, Anderson SW, Dawson J, Nawrot M. Vision and cognition in Alzheimer's disease. *Neuropsychologia.* 2000;38(8):1157-1169.
202. Blanks JC, Torigoe Y, Hinton DR, Blanks RH. Retinal pathology in Alzheimer's disease. I. Ganglion cell loss in foveal/parafoveal retina. *Neurobiology of aging.* 1996;17(3):377-384.
203. Blanks JC, Hinton DR, Sadun AA, Miller CA. Retinal ganglion cell degeneration in Alzheimer's disease. *Brain research.* 1989;501(2):364-372.
204. Dutescu RM, Li QX, Crowston J, Masters CL, Baird PN, Culvenor JG. Amyloid precursor protein processing and retinal pathology in mouse models of Alzheimer's disease. *Graefe's archive for clinical and experimental ophthalmology = Albrecht von Graefes Archiv fur klinische und experimentelle Ophthalmologie.* 2009;247(9):1213-1221.
205. Hinton DR, Sadun AA, Blanks JC, Miller CA. Optic-nerve degeneration in Alzheimer's disease. *The New England journal of medicine.* 1986;315(8):485-487.
206. Koronyo Y, Biggs D, Barron E, et al. Retinal amyloid pathology and proof-of-concept imaging trial in Alzheimer's disease. *JCI insight.* 2017;2(16).
207. La Morgia C, Ross-Cisneros FN, Koronyo Y, et al. Melanopsin retinal ganglion cell loss in Alzheimer disease. *Annals of neurology.* 2016;79(1):90-109.
208. Lu Y, Li Z, Zhang X, et al. Retinal nerve fiber layer structure abnormalities in early Alzheimer's disease: evidence in optical coherence tomography. *Neurosci Lett.* 2010;480(1):69-72.
209. Ratnayaka JA, Serpell LC, Lotery AJ. Dementia of the eye: the role of amyloid beta in retinal degeneration. *Eye (London, England).* 2015;29(8):1013-1026.
210. Oakley H, Cole SL, Logan S, et al. Intraneuronal beta-amyloid aggregates, neurodegeneration, and neuron loss in transgenic mice with five familial Alzheimer's

disease mutations: potential factors in amyloid plaque formation. *The Journal of neuroscience : the official journal of the Society for Neuroscience.* 2006;26(40):10129-10140.
211. Anstee DJ, Gardner B, Spring FA, et al. New monoclonal antibodies in CD44 and CD58: their use to quantify CD44 and CD58 on normal human erythrocytes and to compare the distribution of CD44 and CD58 in human tissues. *Immunology.* 1991;74(2):197-205.
212. Avent ND, Ridgwell K, Mawby WJ, Tanner MJ, Anstee DJ, Kumpel B. Protein-sequence studies on Rh-related polypeptides suggest the presence of at least two groups of proteins which associate in the human red-cell membrane. *The Biochemical journal.* 1988;256(3):1043-1046.
213. Hardy J, Allsop D. Amyloid deposition as the central event in the aetiology of Alzheimer's disease. *Trends Pharmacol Sci.* 1991;12(10):383-388.
214. Teboul O, Feki A, Dubois A, et al. A standardized method to automatically segment amyloid plaques in Congo Red stained sections from Alzheimer transgenic mice. *Conference proceedings : Annual International Conference of the IEEE Engineering in Medicine and Biology Society IEEE Engineering in Medicine and Biology Society Annual Conference.* 2007;2007:5593-5596.
215. Hardy J, Selkoe DJ. The amyloid hypothesis of Alzheimer's disease: progress and problems on the road to therapeutics. *Science (New York, NY).* 2002;297(5580):353-356.
216. Laske C, Sohrabi HR, Frost SM, et al. Innovative diagnostic tools for early detection of Alzheimer's disease. *Alzheimer's & dementia : the journal of the Alzheimer's Association.* 2015;11(5):561-578.
217. Schindler SE, Bollinger JG, Ovod V, et al. High-precision plasma β-amyloid 42/40 predicts current and future brain amyloidosis. *Neurology.* 2019;93(17):e1647-e1659.
218. Wang MJ, Yi S, Han JY, et al. Oligomeric forms of amyloid-β protein in plasma as a potential blood-based biomarker for Alzheimer's disease. *Alzheimer's research & therapy.* 2017;9(1):98.
219. Criscuolo C, Cerri E, Fabiani C, Capsoni S, Cattaneo A, Domenici L. The retina as a window to early dysfunctions of Alzheimer's disease following studies with a 5xFAD mouse model. *Neurobiology of aging.* 2018;67:181-188.
220. Adamec E, Mohan PS, Cataldo AM, Vonsattel JP, Nixon RA. Up-regulation of the lysosomal system in experimental models of neuronal injury: implications for Alzheimer's disease. *Neuroscience.* 2000;100(3):663-675.
221. Cataldo AM, Petanceska S, Terio NB, et al. Abeta localization in abnormal endosomes: association with earliest Abeta elevations in AD and Down syndrome. *Neurobiology of aging.* 2004;25(10):1263-1272.
222. Pasternak SH, Callahan JW, Mahuran DJ. The role of the endosomal/lysosomal system in amyloid-beta production and the pathophysiology of Alzheimer's disease: reexamining the spatial paradox from a lysosomal perspective. *J Alzheimers Dis.* 2004;6(1):53-65.
223. Wolfe DM, Lee JH, Kumar A, Lee S, Orenstein SJ, Nixon RA. Autophagy failure in Alzheimer's disease and the role of defective lysosomal acidification. *The European journal of neuroscience.* 2013;37(12):1949-1961.
224. El-Agnaf OM, Salem SA, Paleologou KE, et al. Detection of oligomeric forms of alpha-synuclein protein in human plasma as a potential biomarker for Parkinson's disease. *FASEB journal : official publication of the Federation of American Societies for Experimental Biology.* 2006;20(3):419-425.

225. El-Agnaf OM, Walsh DM, Allsop D. Soluble oligomers for the diagnosis of neurodegenerative diseases. *The Lancet Neurology.* 2003;2(8):461-462.
226. Doecke JD, Laws SM, Faux NG, et al. Blood-based protein biomarkers for diagnosis of Alzheimer disease. *Arch Neurol.* 2012;69(10):1318-1325.
227. Snyder HM, Carrillo MC, Grodstein F, et al. Developing novel blood-based biomarkers for Alzheimer's disease. *Alzheimers Dement.* 2014;10(1):109-114.
228. Gong Y, Chang L, Viola KL, et al. Alzheimer's disease-affected brain: presence of oligomeric A beta ligands (ADDLs) suggests a molecular basis for reversible memory loss. *Proceedings of the National Academy of Sciences of the United States of America.* 2003;100(18):10417-10422.
229. Larson ME, Lesné SE. Soluble Aβ oligomer production and toxicity. *J Neurochem.* 2012;120 Suppl 1(Suppl 1):125-139.
230. Sakono M, Zako T. Amyloid oligomers: formation and toxicity of Abeta oligomers. *The FEBS journal.* 2010;277(6):1348-1358.
231. Santos AN, Simm A, Holthoff V, Boehm G. A method for the detection of amyloid-beta1-40, amyloid-beta1-42 and amyloid-beta oligomers in blood using magnetic beads in combination with Flow cytometry and its application in the diagnostics of Alzheimer's disease. *J Alzheimers Dis.* 2008;14(2):127-131.
232. Xia W, Yang T, Shankar G, et al. A specific enzyme-linked immunosorbent assay for measuring beta-amyloid protein oligomers in human plasma and brain tissue of patients with Alzheimer disease. *Arch Neurol.* 2009;66(2):190-199.
233. Zhou L, Chan KH, Chu LW, et al. Plasma amyloid-β oligomers level is a biomarker for Alzheimer's disease diagnosis. *Biochemical and biophysical research communications.* 2012;423(4):697-702.
234. Nakamura A, Kaneko N, Villemagne VL, et al. High performance plasma amyloid-β biomarkers for Alzheimer's disease. *Nature.* 2018;554(7691):249-254.
235. Zachary JF, McGavin MD. *Pathologic Basis of Veterinary Disease Expert Consult-E-BOOK.* Elsevier Health Sciences; 2016.
236. Armstrong RA. Alzheimer's Disease and the Eye. *Journal of Optometry.* 2009;2(3):103-111.
237. Hadoux X, Hui F, Lim JKH, et al. Non-invasive in vivo hyperspectral imaging of the retina for potential biomarker use in Alzheimer's disease. *Nat Commun.* 2019;10(1):4227.
238. Kawarabayashi T, Younkin LH, Saido TC, Shoji M, Ashe KH, Younkin SG. Age-dependent changes in brain, CSF, and plasma amyloid (beta) protein in the Tg2576 transgenic mouse model of Alzheimer's disease. *The Journal of neuroscience : the official journal of the Society for Neuroscience.* 2001;21(2):372-381.
239. DaRocha-Souto B, Scotton TC, Coma M, et al. Brain oligomeric β-amyloid but not total amyloid plaque burden correlates with neuronal loss and astrocyte inflammatory response in amyloid precursor protein/tau transgenic mice. *Journal of neuropathology and experimental neurology.* 2011;70(5):360-376.
240. Liu B, Rasool S, Yang Z, et al. Amyloid-peptide vaccinations reduce {beta}-amyloid plaques but exacerbate vascular deposition and inflammation in the retina of Alzheimer's transgenic mice. *Am J Pathol.* 2009;175(5):2099-2110.
241. Morin PJ, Abraham CR, Amaratunga A, et al. Amyloid precursor protein is synthesized by retinal ganglion cells, rapidly transported to the optic nerve plasma membrane and nerve terminals, and metabolized. *J Neurochem.* 1993;61(2):464-473.
242. Gouras GK, Tsai J, Naslund J, et al. Intraneuronal Abeta42 accumulation in human brain. *Am J Pathol.* 2000;156(1):15-20.

243. Umeda T, Tomiyama T, Sakama N, et al. Intraneuronal amyloid β oligomers cause cell death via endoplasmic reticulum stress, endosomal/lysosomal leakage, and mitochondrial dysfunction in vivo. *J Neurosci Res.* 2011;89(7):1031-1042.
244. Bayer TA, Wirths O, Majtényi K, et al. Key factors in Alzheimer's disease: beta-amyloid precursor protein processing, metabolism and intraneuronal transport. *Brain pathology (Zurich, Switzerland).* 2001;11(1):1-11.
245. Iwatsubo T, Odaka A, Suzuki N, Mizusawa H, Nukina N, Ihara Y. Visualization of A beta 42(43) and A beta 40 in senile plaques with end-specific A beta monoclonals: evidence that an initially deposited species is A beta 42(43). *Neuron.* 1994;13(1):45-53.
246. Wirths O, Multhaup G, Czech C, et al. Intraneuronal Abeta accumulation precedes plaque formation in beta-amyloid precursor protein and presenilin-1 double-transgenic mice. *Neurosci Lett.* 2001;306(1-2):116-120.
247. Yu WH, Cuervo AM, Kumar A, et al. Macroautophagy--a novel Beta-amyloid peptide-generating pathway activated in Alzheimer's disease. *The Journal of cell biology.* 2005;171(1):87-98.
248. Langui D, Girardot N, El Hachimi KH, et al. Subcellular topography of neuronal Abeta peptide in APPxPS1 transgenic mice. *Am J Pathol.* 2004;165(5):1465-1477.
249. Zheng L, Kågedal K, Dehvari N, et al. Oxidative stress induces macroautophagy of amyloid beta-protein and ensuing apoptosis. *Free radical biology & medicine.* 2009;46(3):422-429.
250. Takahashi RH, Milner TA, Li F, et al. Intraneuronal Alzheimer abeta42 accumulates in multivesicular bodies and is associated with synaptic pathology. *Am J Pathol.* 2002;161(5):1869-1879.
251. Viola KL, Klein WL. Amyloid beta oligomers in Alzheimer's disease pathogenesis, treatment, and diagnosis. *Acta Neuropathol.* 2015;129(2):183-206.
252. Price JL, McKeel Jr DW, Buckles VD, et al. Neuropathology of nondemented aging: presumptive evidence for preclinical Alzheimer disease. *Neurobiology of aging.* 2009;30(7):1026-1036.
253. Braak H, Braak E. Frequency of stages of Alzheimer-related lesions in different age categories. *Neurobiology of aging.* 1997;18(4):351-357.
254. Rizzo M, Anderson SW, Dawson J, Nawrot M. Vision and cognition in Alzheimer's disease. *Neuropsychologia.* 2000;38(8):1157-1169.
255. Cronin-Golomb A, Corkin S, Rizzo JF, Cohen J, Growdon JH, Banks KS. Visual dysfunction in Alzheimer's disease: relation to normal aging. *Annals of Neurology: Official Journal of the American Neurological Association and the Child Neurology Society.* 1991;29(1):41-52.
256. Iseri PK, Altinas O, Tokay T, Yuksel N. Relationship between cognitive impairment and retinal morphological and visual functional abnormalities in Alzheimer disease. *Journal of neuro-ophthalmology : the official journal of the North American Neuro-Ophthalmology Society.* 2006;26(1):18-24.
257. Coppola G, Parisi V, Manni G, Pierelli F, Sadun AA. Optical coherence tomography in alzheimer's disease. In: *OCT and Imaging in Central Nervous System Diseases.* Springer; 2020:263-288.
258. Qiu Y, Jin T, Mason E, Campbell MCW. Predicting Thioflavin Fluorescence of Retinal Amyloid Deposits Associated With Alzheimer's Disease from Their Polarimetric Properties. *Translational vision science & technology.* 2020;9(2):47.
259. Mirzaei N, Shi H, Oviatt M, et al. Alzheimer's Retinopathy: Seeing Disease in the Eyes. *Frontiers in neuroscience.* 2020;14:921.

260. Jovčevska I, Muyldermans S. The Therapeutic Potential of Nanobodies. *BioDrugs.* 2019:1-16.
261. Li T, Vandesquille M, Koukouli F, et al. Camelid single-domain antibodies: A versatile tool for in vivo imaging of extracellular and intracellular brain targets. *J Control Release.* 2016;243:1-10.
262. Lafaye P, Achour I, England P, Duyckaerts C, Rougeon F. Single-domain antibodies recognize selectively small oligomeric forms of amyloid beta, prevent Abeta-induced neurotoxicity and inhibit fibril formation. *Molecular immunology.* 2009;46(4):695-704.
263. Vandesquille M, Li T, Po C, et al. Chemically-defined camelid antibody bioconjugate for the magnetic resonance imaging of Alzheimer's disease. *mAbs.* 2017;9(6):1016-1027.
264. Volianskis A, Køstner R, Mølgaard M, Hass S, Jensen MS. Episodic memory deficits are not related to altered glutamatergic synaptic transmission and plasticity in the CA1 hippocampus of the APPswe/PS1ΔE9-deleted transgenic mice model of β-amyloidosis. *Neurobiology of aging.* 2010;31(7):1173-1187.
265. Serneels L, Van Biervliet J, Craessaerts K, et al. gamma-Secretase heterogeneity in the Aph1 subunit: relevance for Alzheimer's disease. *Science.* 2009;324(5927):639-642.
266. Reiserer RS, Harrison FE, Syverud DC, McDonald MP. Impaired spatial learning in the APPSwe + PSEN1DeltaE9 bigenic mouse model of Alzheimer's disease. *Genes, brain, and behavior.* 2007;6(1):54-65.
267. Holcomb L, Gordon MN, McGowan E, et al. Accelerated Alzheimer-type phenotype in transgenic mice carrying both mutant amyloid precursor protein and presenilin 1 transgenes. *Nat Med.* 1998;4(1):97-100.
268. Radde R, Bolmont T, Kaeser SA, et al. Abeta42-driven cerebral amyloidosis in transgenic mice reveals early and robust pathology. *EMBO Rep.* 2006;7(9):940-946.
269. Yi J, Chen B, Yao X, Lei Y, Ou F, Huang F. Upregulation of the lncRNA MEG3 improves cognitive impairment, alleviates neuronal damage, and inhibits activation of astrocytes in hippocampus tissues in Alzheimer's disease through inactivating the PI3K/Akt signaling pathway. *J Cell Biochem.* 2019;120(10):18053-18065.
270. Mowat FM, Avelino J, Bowyer A, et al. Detection of circulating anti-retinal antibodies in dogs with sudden acquired retinal degeneration syndrome using indirect immunofluorescence: A case-control study. *Experimental eye research.* 2020;193:107989.
271. Palfi A, Yesmambetov A, Humphries P, Hokamp K, Farrar GJ. Non-photoreceptor Expression of Tulp1 May Contribute to Extensive Retinal Degeneration in Tulp1-/- Mice. *Frontiers in neuroscience.* 2020;14:656.
272. Habiba U, Merlin S, Lim JKH, et al. Age-Specific Retinal and Cerebral Immunodetection of Amyloid-β Plaques and Oligomers in a Rodent Model of Alzheimer’s Disease. *Journal of Alzheimer's Disease.* 2020;Preprint:1-6.
273. Youn YC, Kang S, Suh J, et al. Blood amyloid-β oligomerization associated with neurodegeneration of Alzheimer's disease. *Alzheimer's research & therapy.* 2019;11(1):40.
274. Ding Y, Zhao J, Zhang X, et al. Amyloid Beta Oligomers Target to Extracellular and Intracellular Neuronal Synaptic Proteins in Alzheimer's Disease. *Frontiers in neurology.* 2019;10:1140-1140.
275. Cagnin A, Brooks DJ, Kennedy AM, et al. In-vivo measurement of activated microglia in dementia. *Lancet.* 2001;358(9280):461-467.

276. Parachikova A, Agadjanyan MG, Cribbs DH, et al. Inflammatory changes parallel the early stages of Alzheimer disease. *Neurobiology of aging.* 2007;28(12):1821-1833.
277. Chun H, Marriott I, Lee CJ, Cho H. Elucidating the Interactive Roles of Glia in Alzheimer's Disease Using Established and Newly Developed Experimental Models. *Front Neurol.* 2018;9:797.
278. Wang W, Hou TT, Jia LF, Wu QQ, Quan MN, Jia JP. Toxic amyloid-β oligomers induced self-replication in astrocytes triggering neuronal injury. *EBioMedicine.* 2019;42:174-187.
279. Lesne SE. Toxic oligomer species of amyloid-β in Alzheimer's disease, a timing issue. *Swiss Med Wkly.* 2014;144:w14021.
280. Gao CM, Yam AY, Wang X, et al. Aβ40 oligomers identified as a potential biomarker for the diagnosis of Alzheimer's disease. *PLoS One.* 2010;5(12):e15725.
281. Turner RS, Stubbs T, Davies DA, Albensi BC. Potential New Approaches for Diagnosis of Alzheimer's Disease and Related Dementias. *Frontiers in neurology.* 2020;11:496-496.
282. Kuo YM, Emmerling MR, Vigo-Pelfrey C, et al. Water-soluble Abeta (N-40, N-42) oligomers in normal and Alzheimer disease brains. *The Journal of biological chemistry.* 1996;271(8):4077-4081.
283. Lambert MP, Barlow AK, Chromy BA, et al. Diffusible, nonfibrillar ligands derived from Abeta1-42 are potent central nervous system neurotoxins. *Proceedings of the National Academy of Sciences of the United States of America.* 1998;95(11):6448-6453.
284. Cizas P, Budvytyte R, Morkuniene R, et al. Size-dependent neurotoxicity of beta-amyloid oligomers. *Arch Biochem Biophys.* 2010;496(2):84-92.
285. Kayed R, Head E, Sarsoza F, et al. Fibril specific, conformation dependent antibodies recognize a generic epitope common to amyloid fibrils and fibrillar oligomers that is absent in prefibrillar oligomers. *Molecular neurodegeneration.* 2007;2:18.
286. Adlard PA, Li QX, McLean C, et al. β-amyloid in biological samples: not all Aβ detection methods are created equal. *Front Aging Neurosci.* 2014;6:203.
287. Hart NJ, Koronyo Y, Black KL, Koronyo-Hamaoui M. Ocular indicators of Alzheimer's: exploring disease in the retina. *Acta Neuropathol.* 2016;132(6):767-787.
288. Le Bastard N, Aerts L, Leurs J, Blomme W, De Deyn PP, Engelborghs S. No correlation between time-linked plasma and CSF Abeta levels. *Neurochem Int.* 2009;55(8):820-825.
289. Freddo TF. A contemporary concept of the blood-aqueous barrier. *Prog Retin Eye Res.* 2013;32:181-195.
290. Organisation WH. Ageing. 2020; https://www.who.int/health-topics/ageing#tab=tab_1.
291. Adams B, Chan A, Callahan H, Milgram NW. The canine as a model of human cognitive aging: recent developments. *Prog Neuropsychopharmacol Biol Psychiatry.* 2000;24(5):675-692.
292. Wallis LJ, Szabó D, Erdélyi-Belle B, Kubinyi E. Demographic Change Across the Lifespan of Pet Dogs and Their Impact on Health Status. *Front Vet Sci.* 2018;5:200.
293. Greer KA, Canterberry SC, Murphy KE. Statistical analysis regarding the effects of height and weight on life span of the domestic dog. *Research in veterinary science.* 2007;82(2):208-214.
294. Zhao Y, Flandin P, Long JE, Cuesta MD, Westphal H, Rubenstein JL. Distinct molecular pathways for development of telencephalic interneuron subtypes revealed through analysis of Lhx6 mutants. *J Comp Neurol.* 2008;510(1):79-99.

295. Braak H, Alafuzoff I, Arzberger T, Kretzschmar H, Del Tredici K. Staging of Alzheimer disease-associated neurofibrillary pathology using paraffin sections and immunocytochemistry. *Acta Neuropathol.* 2006;112(4):389-404.
296. Head E, Pop V, Sarsoza F, et al. Amyloid-beta peptide and oligomers in the brain and cerebrospinal fluid of aged canines. *J Alzheimers Dis.* 2010;20(2):637-646.
297. Rusbridge C, Salguero FJ, David MA, et al. An Aged Canid with Behavioral Deficits Exhibits Blood and Cerebrospinal Fluid Amyloid Beta Oligomers. *Front Aging Neurosci.* 2018;10:7.
298. Smolek T, Madari A, Farbakova J, et al. Tau hyperphosphorylation in synaptosomes and neuroinflammation are associated with canine cognitive impairment. *J Comp Neurol.* 2016;524(4):874-895.
299. Bennett RE, DeVos SL, Dujardin S, et al. Enhanced Tau Aggregation in the Presence of Amyloid β. *Am J Pathol.* 2017;187(7):1601-1612.
300. Bilousova T, Miller CA, Poon WW, et al. Synaptic Amyloid-β Oligomers Precede p-Tau and Differentiate High Pathology Control Cases. *Am J Pathol.* 2016;186(1):185-198.
301. Chambers JK, Tokuda T, Uchida K, et al. The domestic cat as a natural animal model of Alzheimer's disease. *Acta Neuropathol Commun.* 2015;3:78.
302. Gołaszewska A, Bik W, Motyl T, Orzechowski A. Bridging the Gap between Alzheimer's Disease and Alzheimer's-like Diseases in Animals. *International journal of molecular sciences.* 2019;20(7).
303. Meuten DJ, Moore FM, George JW. Mitotic Count and the Field of View Area: Time to Standardize. *Vet Pathol.* 2016;53(1):7-9.
304. Cummings BJ, Head E, Afagh AJ, Milgram NW, Cotman CW. Beta-amyloid accumulation correlates with cognitive dysfunction in the aged canine. *Neurobiol Learn Mem.* 1996;66(1):11-23.
305. Malek-Ahmadi M, Perez SE, Chen K, Mufson EJ. Neuritic and Diffuse Plaque Associations with Memory in Non-Cognitively Impaired Elderly. *J Alzheimers Dis.* 2016;53(4):1641-1652.
306. Studzinski CM, Christie LA, Araujo JA, et al. Visuospatial function in the beagle dog: an early marker of cognitive decline in a model of human aging and dementia. *Neurobiol Learn Mem.* 2006;86(2):197-204.
307. Su MY, Tapp PD, Vu L, et al. A longitudinal study of brain morphometrics using serial magnetic resonance imaging analysis in a canine model of aging. *Prog Neuropsychopharmacol Biol Psychiatry.* 2005;29(3):389-397.
308. Thompkins AM, Deshpande G, Waggoner P, Katz JS. Functional Magnetic Resonance Imaging of the Domestic Dog: Research, Methodology, and Conceptual Issues. *Comparative cognition & behavior reviews.* 2016;11:63-82.
309. Clark CM, Karlawish JH. Alzheimer disease: current concepts and emerging diagnostic and therapeutic strategies. *Annals of internal medicine.* 2003;138(5):400-410.
310. Mott RT, Hulette CM. Neuropathology of Alzheimer's disease. *Neuroimaging Clinics.* 2005;15(4):755-765.
311. Jack CR, Jr., Wiste HJ, Weigand SD, et al. Age, Sex, and APOE ε4 Effects on Memory, Brain Structure, and β-Amyloid Across the Adult Life Span. *JAMA Neurol.* 2015;72(5):511-519.
312. Rentz DM, Locascio JJ, Becker JA, et al. Cognition, reserve, and amyloid deposition in normal aging. *Annals of neurology.* 2010;67(3):353-364.
313. Rodrigue KM, Kennedy KM, Park DC. Beta-amyloid deposition and the aging brain. *Neuropsychol Rev.* 2009;19(4):436-450.

314. Oh H, Mormino EC, Madison C, Hayenga A, Smiljic A, Jagust WJ. β-Amyloid affects frontal and posterior brain networks in normal aging. *NeuroImage.* 2011;54(3):1887-1895.
315. Bourgeat P, Chételat G, Villemagne VL, et al. Beta-amyloid burden in the temporal neocortex is related to hippocampal atrophy in elderly subjects without dementia. *Neurology.* 2010;74(2):121-127.
316. Rowe CC, Ellis KA, Rimajova M, et al. Amyloid imaging results from the Australian Imaging, Biomarkers and Lifestyle (AIBL) study of aging. *Neurobiology of aging.* 2010;31(8):1275-1283.
317. Petersen RC, Aisen P, Boeve BF, et al. Mild cognitive impairment due to Alzheimer disease in the community. *Annals of neurology.* 2013;74(2):199-208.
318. Erten-Lyons D, Woltjer RL, Dodge H, et al. Factors associated with resistance to dementia despite high Alzheimer disease pathology. *Neurology.* 2009;72(4):354-360.
319. Bischof GN, Rodrigue KM, Kennedy KM, Devous MD, Sr., Park DC. Amyloid deposition in younger adults is linked to episodic memory performance. *Neurology.* 2016;87(24):2562-2566.
320. Hanseeuw BJ, Betensky RA, Jacobs HIL, et al. Association of Amyloid and Tau With Cognition in Preclinical Alzheimer Disease: A Longitudinal Study. *JAMA Neurol.* 2019;76(8):915-924.
321. Rowe CC, Bourgeat P, Ellis KA, et al. Predicting Alzheimer disease with β-amyloid imaging: results from the Australian imaging, biomarkers, and lifestyle study of ageing. *Annals of neurology.* 2013;74(6):905-913.
322. Pugliese M, Gangitano C, Ceccariglia S, et al. Canine cognitive dysfunction and the cerebellum: acetylcholinesterase reduction, neuronal and glial changes. *Brain research.* 2007;1139:85-94.
323. Adams B, Chan A, Callahan H, Milgram NW. The canine as a model of human cognitive aging: recent developments. *Progress in neuro-psychopharmacology & biological psychiatry.* 2000.
324. Head E. A canine model of human aging and Alzheimer's disease. *Biochimica et Biophysica Acta (BBA)-Molecular Basis of Disease.* 2013;1832(9):1384-1389.
325. Rofina J, Van Ederen A, Toussaint M, et al. Cognitive disturbances in old dogs suffering from the canine counterpart of Alzheimer's disease. *Brain research.* 2006;1069(1):216-226.
326. Hardy J, Selkoe DJ. The amyloid hypothesis of Alzheimer's disease: progress and problems on the road to therapeutics. *Science (New York, NY).* 2002;297(5580):353-356.
327. Head E, Pop V, Sarsoza F, et al. Amyloid-β peptide and oligomers in the brain and cerebrospinal fluid of aged canines. *Journal of Alzheimer's Disease.* 2010;20(2):637-646.
328. Armstrong RA. Alzheimer's Disease and the Eye. *Journal of Optometry.* 2009;2(3):103-111.
329. Santos CY, Johnson LN, Sinoff SE, Festa EK, Heindel WC, Snyder PJ. Change in retinal structural anatomy during the preclinical stage of Alzheimer's disease. *Alzheimers Dement (Amst).* 2018;10:196-209.
330. Lee ATC, Richards M, Chan WC, Chiu HFK, Lee RSY, Lam LCW. Higher Dementia Incidence in Older Adults with Poor Visual Acuity. *J Gerontol A Biol Sci Med Sci.* 2020;75(11):2162-2168.
331. Tsai Y, Lu B, Ljubimov AV, et al. Ocular changes in TgF344-AD rat model of Alzheimer's disease. *Investigative ophthalmology & visual science.* 2014;55(1):523-534.

332. van Eersel J, Stevens CH, Przybyla M, et al. Early-onset axonal pathology in a novel P301S-Tau transgenic mouse model of frontotemporal lobar degeneration. *Neuropathol Appl Neurobiol.* 2015;41(7):906-925.
333. Nakayama H, Uchida K, Doi K. A comparative study of age-related brain pathology--are neurodegenerative diseases present in nonhuman animals ? *Med Hypotheses.* 2004;63(2):198-202.
334. Cummings BJ, Pike CJ, Shankle R, Cotman CW. Beta-amyloid deposition and other measures of neuropathology predict cognitive status in Alzheimer's disease. *Neurobiology of aging.* 1996;17(6):921-933.
335. Breydo L, Uversky VN. Structural, morphological, and functional diversity of amyloid oligomers. *FEBS letters.* 2015;589(19 Pt A):2640-2648.
336. Rofina J, van Andel I, van Ederen AM, Papaioannou N, Yamaguchi H, Gruys E. Canine counterpart of senile dementia of the Alzheimer type: amyloid plaques near capillaries but lack of spatial relationship with activated microglia and macrophages. *Amyloid.* 2003;10(2):86-96.
337. da Silva EG, Dubielzig R, Zarfoss MK, Anibal A. Distinctive histopathologic features of canine optic nerve hypoplasia and aplasia: a retrospective review of 13 cases. *Veterinary ophthalmology.* 2008;11(1):23-29.
338. Rüttimann G, Daicker B. [Complex colobomas in the anterior eye segment in a beagle hound]. *Zentralblatt fur Veterinarmedizin Reihe A.* 1982;29(7):528-537.
339. Williams DL. A comparative approach to anterior segment dysgenesis. *Eye (London, England).* 1993;7 (Pt 5):607-616.
340. Morris JC. Early-stage and preclinical Alzheimer disease. *Alzheimer Dis Assoc Disord.* 2005;19(3):163-165.
341. Sperling RA, Rentz DM, Johnson KA, et al. The A4 study: stopping AD before symptoms begin? *Sci Transl Med.* 2014;6(228):228fs213.
342. Jack CR, Jr., Bennett DA, Blennow K, et al. NIA-AA Research Framework: Toward a biological definition of Alzheimer's disease. *Alzheimer's & dementia : the journal of the Alzheimer's Association.* 2018;14(4):535-562.
343. Zahs KR, Ashe KH. β-Amyloid oligomers in aging and Alzheimer's disease. *Front Aging Neurosci.* 2013;5:28.
344. Casaletto KB, Ward ME, Baker NS, et al. Retinal thinning is uniquely associated with medial temporal lobe atrophy in neurologically normal older adults. *Neurobiology of aging.* 2017;51:141-147.
345. Alonso-Caneiro D, Read SA, Collins MJ. Automatic segmentation of choroidal thickness in optical coherence tomography. *Biomed Opt Express.* 2013;4(12):2795-2812.
346. Ko F, Muthy ZA, Gallacher J, et al. Association of Retinal Nerve Fiber Layer Thinning With Current and Future Cognitive Decline: A Study Using Optical Coherence Tomography. *JAMA Neurol.* 2018;75(10):1198-1205.
347. Schütt T, Helboe L, Pedersen L, Waldemar G, Berendt M, Pedersen JT. Dogs with Cognitive Dysfunction as a Spontaneous Model for Early Alzheimer's Disease: A Translational Study of Neuropathological and Inflammatory Markers. *J Alzheimers Dis.* 2016;52(2):433-449.
348. Chin AL, Negash S, Hamilton R. Diversity and disparity in dementia: the impact of ethnoracial differences in Alzheimer disease. *Alzheimer Dis Assoc Disord.* 2011;25(3):187-195.
349. Gurland BJ, Wilder DE, Lantigua R, et al. Rates of dementia in three ethnoracial groups. *Int J Geriatr Psychiatry.* 1999;14(6):481-493.

350. Babulal GM, Quiroz YT, Albensi BC, et al. Perspectives on ethnic and racial disparities in Alzheimer's disease and related dementias: Update and areas of immediate need. *Alzheimer's & dementia : the journal of the Alzheimer's Association.* 2019;15(2):292-312.
351. Fillenbaum GG, Heyman A, Huber MS, et al. The prevalence and 3-year incidence of dementia in older Black and White community residents. *Journal of clinical epidemiology.* 1998;51(7):587-595.
352. Kaeberlein M, Creevy KE, Promislow DE. The dog aging project: translational geroscience in companion animals. *Mammalian genome : official journal of the International Mammalian Genome Society.* 2016;27(7-8):279-288.
353. Mucke L, Selkoe DJ. Neurotoxicity of amyloid β-protein: synaptic and network dysfunction. *Cold Spring Harb Perspect Med.* 2012;2(7):a006338.
354. Kim HJ, Chae SC, Lee DK, et al. Selective neuronal degeneration induced by soluble oligomeric amyloid beta protein. *FASEB journal : official publication of the Federation of American Societies for Experimental Biology.* 2003;17(1):118-120.
355. McLean CA, Cherny RA, Fraser FW, et al. Soluble pool of Abeta amyloid as a determinant of severity of neurodegeneration in Alzheimer's disease. *Annals of neurology.* 1999;46(6):860-866.
356. Lynn SA, Johnston DA, Scott JA, et al. Oligomeric Aβ(1-42) Induces an AMD-Like Phenotype and Accumulates in Lysosomes to Impair RPE Function. *Cells.* 2021;10(2).
357. Luibl V, Isas JM, Kayed R, Glabe CG, Langen R, Chen J. Drusen deposits associated with aging and age-related macular degeneration contain nonfibrillar amyloid oligomers. *J Clin Invest.* 2006;116(2):378-385.
358. Denenberg S, Liebel F-X, Rose J. Behavioural and Medical Differentials of Cognitive Decline and Dementia in Dogs and Cats. *Canine and Feline Dementia.* 2017:13-58.
359. Acland GM, Aguirre GD. Retinal degenerations in the dog: IV. Early retinal degeneration (erd) in Norwegian elkhounds. *Experimental eye research.* 1987;44(4):491-521.
360. Weber SA, Patel RK, Lutsep HL. Cerebral amyloid angiopathy: diagnosis and potential therapies. *Expert Rev Neurother.* 2018;18(6):503-513.
361. Sharafi SM, Sylvestre JP, Chevrefils C, et al. Vascular retinal biomarkers improves the detection of the likely cerebral amyloid status from hyperspectral retinal images. *Alzheimers Dement (N Y).* 2019;5:610-617.
362. Fast R, Schütt T, Toft N, Møller A, Berendt M. An observational study with long-term follow-up of canine cognitive dysfunction: clinical characteristics, survival, and risk factors. *Journal of veterinary internal medicine.* 2013;27(4):822-829.
363. Katina S, Farbakova J, Madari A, Novak M, Zilka N. Risk factors for canine cognitive dysfunction syndrome in Slovakia. *Acta veterinaria Scandinavica.* 2016;58:17.
364. Azkona G, García-Belenguer S, Chacón G, Rosado B, León M, Palacio J. Prevalence and risk factors of behavioural changes associated with age-related cognitive impairment in geriatric dogs. *The Journal of small animal practice.* 2009;50(2):87-91.
365. Hart BL. Effect of gonadectomy on subsequent development of age-related cognitive impairment in dogs. *Journal of the American Veterinary Medical Association.* 2001;219(1):51-56.
366. Arnsten AFT, Datta D, Tredici KD, Braak H. Hypothesis: Tau pathology is an initiating factor in sporadic Alzheimer's disease. *Alzheimer's & dementia : the journal of the Alzheimer's Association.* 2021;17(1):115-124.

367. Fein JA, Sokolow S, Miller CA, et al. Co-localization of amyloid beta and tau pathology in Alzheimer's disease synaptosomes. *Am J Pathol.* 2008;172(6):1683-1692.
368. Takahashi RH, Capetillo-Zarate E, Lin MT, Milner TA, Gouras GK. Co-occurrence of Alzheimer's disease ß-amyloid and τ pathologies at synapses. *Neurobiology of aging.* 2010;31(7):1145-1152.
369. Lockhart SN, Schöll M, Baker SL, et al. Amyloid and tau PET demonstrate region-specific associations in normal older people. *NeuroImage.* 2017;150:191-199.
370. Golde TE, Schneider LS, Koo EH. Anti-aβ therapeutics in Alzheimer's disease: the need for a paradigm shift. *Neuron.* 2011;69(2):203-213.
371. Parker HG, Kim LV, Sutter NB, et al. Genetic structure of the purebred domestic dog. *Science (New York, NY).* 2004;304(5674):1160-1164.
372. Davis PR, Head E. Prevention approaches in a preclinical canine model of Alzheimer's disease: benefits and challenges. *Front Pharmacol.* 2014;5:47.
373. Alzheimer Forum (ALZFORUM). Dogs May Provide First Natural Animal Model for ALS. 2008.
374. Zhang Y, Wang Y, Shi C, Shen M, Lu F. Advances in retina imaging as potential biomarkers for early diagnosis of Alzheimer's disease. *Translational neurodegeneration.* 2021;10(1):6.
375. Andrew MK, Tierney MC. The puzzle of sex, gender and Alzheimer’s disease: Why are women more often affected than men? *Womens Health (Lond).* 2018;14:1745506518817995.
376. Perl DP. Neuropathology of Alzheimer's disease. *Mount Sinai Journal of Medicine: A Journal of Translational and Personalized Medicine.* 2010;77(1):32-42.
377. Dodart JC, Bales KR, Gannon KS, et al. Immunization reverses memory deficits without reducing brain Abeta burden in Alzheimer's disease model. *Nature neuroscience.* 2002;5(5):452-457.
378. Sloane JA, Pietropaolo MF, Rosene DL, et al. Lack of correlation between plaque burden and cognition in the aged monkey. *Acta Neuropathol.* 1997;94(5):471-478.
379. Kayed R, Lasagna-Reeves CA. Molecular mechanisms of amyloid oligomers toxicity. *J Alzheimers Dis.* 2013;33 Suppl 1:S67-78.
380. Ono K, Condron MM, Teplow DB. Structure-neurotoxicity relationships of amyloid beta-protein oligomers. *Proceedings of the National Academy of Sciences of the United States of America.* 2009;106(35):14745-14750.
381. Buttini M, Yu GQ, Shockley K, et al. Modulation of Alzheimer-like synaptic and cholinergic deficits in transgenic mice by human apolipoprotein E depends on isoform, aging, and overexpression of amyloid beta peptides but not on plaque formation. *The Journal of neuroscience : the official journal of the Society for Neuroscience.* 2002;22(24):10539-10548.
382. Mucke L, Masliah E, Yu GQ, et al. High-level neuronal expression of abeta 1-42 in wild-type human amyloid protein precursor transgenic mice: synaptotoxicity without plaque formation. *The Journal of neuroscience : the official journal of the Society for Neuroscience.* 2000;20(11):4050-4058.
383. Kwon JY, Yang JH, Han JS, Kim DG. Analysis of the Retinal Nerve Fiber Layer Thickness in Alzheimer Disease and Mild Cognitive Impairment. *Korean journal of ophthalmology : KJO.* 2017;31(6):548-556.
384. Meng X, Li T, Wang X, et al. Association between increased levels of amyloid-β oligomers in plasma and episodic memory loss in Alzheimer's disease. *Alzheimer's research & therapy.* 2019;11(1):89.

385. Olesen L, Bouzinova EV, Severino M, et al. Behavioural Phenotyping of APPswe/PS1δE9 Mice: Age-Rrelated Changes and Effect of Long-Term Paroxetine Treatment. *PloS one.* 2016;11(11):e0165144.
386. Savonenko A, Xu GM, Melnikova T, et al. Episodic-like memory deficits in the APPswe/PS1dE9 mouse model of Alzheimer's disease: relationships to beta-amyloid deposition and neurotransmitter abnormalities. *Neurobiology of disease.* 2005;18(3):602-617.
387. Hsiao K, Chapman P, Nilsen S, et al. Correlative memory deficits, Abeta elevation, and amyloid plaques in transgenic mice. *Science (New York, NY).* 1996;274(5284):99-102.
388. Webster SJ, Bachstetter AD, Van Eldik LJ. Comprehensive behavioral characterization of an APP/PS-1 double knock-in mouse model of Alzheimer's disease. *Alzheimer's research & therapy.* 2013;5(3):28-28.
389. Zhang W, Hao J, Liu R, et al. Soluble Aβ levels correlate with cognitive deficits in the 12-month-old APPswe/PS1dE9 mouse model of Alzheimer's disease. *Behav Brain Res.* 2011;222(2):342-350.
390. Runkle EA, Antonetti DA. The blood-retinal barrier: structure and functional significance. *Methods Mol Biol.* 2011;686:133-148.
391. Cunha-Vaz J, Bernardes R, Lobo C. Blood-retinal barrier. *Eur J Ophthalmol.* 2011;21 Suppl 6:S3-9.
392. Vinores SA. Breakdown of the Blood–Retinal Barrier. *Encyclopedia of the Eye.* 2010:216-222.
393. Campbell M, Humphries P. The blood-retina barrier: tight junctions and barrier modulation. *Adv Exp Med Biol.* 2012;763:70-84.
394. Xu HZ, Le YZ. Significance of outer blood-retina barrier breakdown in diabetes and ischemia. *Investigative ophthalmology & visual science.* 2011;52(5):2160-2164.
395. Hudson N, Cahill M, Campbell M. Inner blood-retina barrier involvement in dry age-related macular degeneration (AMD) pathology. *Neural Regen Res.* 2020;15(9):1656-1657.
396. Shi H, Koronyo Y, Fuchs DT, et al. Retinal capillary degeneration and blood-retinal barrier disruption in murine models of Alzheimer's disease. *Acta Neuropathol Commun.* 2020;8(1):202.
397. Murphy MP, LeVine H, 3rd. Alzheimer's disease and the amyloid-beta peptide. *J Alzheimers Dis.* 2010;19(1):311-323.
398. Vitek MP, Araujo JA, Fossel M, et al. Translational animal models for Alzheimer's disease: An Alzheimer's Association Business Consortium Think Tank. *Alzheimers Dement (N Y).* 2020;6(1):e12114.
399. Jankowsky JL, Zheng H. Practical considerations for choosing a mouse model of Alzheimer's disease. *Molecular neurodegeneration.* 2017;12(1):89.
400. Prpar Mihevc S, Majdič G. Canine Cognitive Dysfunction and Alzheimer's Disease - Two Facets of the Same Disease? *Frontiers in neuroscience.* 2019;13:604.
401. Cummings BJ, Su JH, Cotman CW, White R, Russell MJ. Beta-amyloid accumulation in aged canine brain: a model of early plaque formation in Alzheimer's disease. *Neurobiology of aging.* 1993;14(6):547-560.
402. Lacor PN, Buniel MC, Chang L, et al. Synaptic targeting by Alzheimer's-related amyloid beta oligomers. *The Journal of neuroscience : the official journal of the Society for Neuroscience.* 2004;24(45):10191-10200.
403. Zempel H, Thies E, Mandelkow E, Mandelkow EM. Abeta oligomers cause localized Ca(2+) elevation, missorting of endogenous Tau into dendrites, Tau phosphorylation,

and destruction of microtubules and spines. *The Journal of neuroscience : the official journal of the Society for Neuroscience.* 2010;30(36):11938-11950.
404. Chabrier MA, Blurton-Jones M, Agazaryan AA, Nerhus JL, Martinez-Coria H, LaFerla FM. Soluble aβ promotes wild-type tau pathology in vivo. *The Journal of neuroscience : the official journal of the Society for Neuroscience.* 2012;32(48):17345-17350.
405. Mairet-Coello G, Courchet J, Pieraut S, Courchet V, Maximov A, Polleux F. The CAMKK2-AMPK kinase pathway mediates the synaptotoxic effects of Aβ oligomers through Tau phosphorylation. *Neuron.* 2013;78(1):94-108.
406. Mormino EC, Papp KV. Amyloid Accumulation and Cognitive Decline in Clinically Normal Older Individuals: Implications for Aging and Early Alzheimer's Disease. *J Alzheimers Dis.* 2018;64(s1):S633-s646.
407. Weigand AJ, Bangen KJ, Thomas KR, et al. Is tau in the absence of amyloid on the Alzheimer's continuum?: A study of discordant PET positivity. *Brain Commun.* 2020;2(1):fcz046.
408. Schuman SG, Koreishi AF, Farsiu S, Jung SH, Izatt JA, Toth CA. Photoreceptor layer thinning over drusen in eyes with age-related macular degeneration imaged in vivo with spectral-domain optical coherence tomography. *Ophthalmology.* 2009;116(3):488-496.e482.
409. Virgili G, Menchini F, Dimastrogiovanni AF, et al. Optical coherence tomography versus stereoscopic fundus photography or biomicroscopy for diagnosing diabetic macular edema: a systematic review. *Investigative ophthalmology & visual science.* 2007;48(11):4963-4973.
410. Müller PL, Wolf S, Dolz-Marco R, Tafreshi A, Schmitz-Valckenberg S, Holz FG. Ophthalmic Diagnostic Imaging: Retina. In: Bille JF, ed. *High Resolution Imaging in Microscopy and Ophthalmology: New Frontiers in Biomedical Optics.* Cham (CH): Springer

Copyright 2019, The Author(s). 2019:87-106.
411. Muakkassa NW, Chin AT, de Carlo T, et al. CHARACTERIZING THE EFFECT OF ANTI-VASCULAR ENDOTHELIAL GROWTH FACTOR THERAPY ON TREATMENT-NAIVE CHOROIDAL NEOVASCULARIZATION USING OPTICAL COHERENCE TOMOGRAPHY ANGIOGRAPHY. *Retina (Philadelphia, Pa).* 2015;35(11):2252-2259.

Appendices

Published paper (Paper 1)

Citation details: Habiba U, Merlin S, Lim JKH, Wong VHY, Nguyen CTO, Morley JW, Bui BV, Tayebi M. Age-Specific Retinal and Cerebral Immunodetection of Amyloid-β Plaques and Oligomers in a Rodent Model of Alzheimer's Disease. J Alzheimers Dis. 2020;76(3):1135-1150. doi: 10.3233/JAD-191346. PMID: 32597800.

Link to publisher versions:

https://content.iospress.com/articles/journal-of-alzheimers-disease/jad191346

Published Paper (Paper 2)

Citation details: Habiba U, Ozawa M, Chambers JK, Uchida K, Descallar J, Nakayama H, Summers BA, Morley JW, Tayebi M. Neuronal Deposition of Amyloid-β Oligomers and Hyperphosphorylated Tau Is Closely Connected with Cognitive Dysfunction in Aged Dogs. J Alzheimers Dis Rep. 2021 Oct 6;5(1):749-760. doi: 10.3233/ADR-210035. PMID: 34870101; PMCID: PMC8609497.

Link to publisher versions:

https://content.iospress.com/articles/journal-of-alzheimers-disease-reports/adr210035?resultNumber=0&totalResults=459&start=0&q=Neuronal+Deposition+of+Amyloid-%CE%B2+Oligomers+and+Hyperphosphorylated+Tau+Is+Closely+Connected+with+Cognitive+Dysfunction+in+Aged+Dogs&resultsPageSize=10&rows=10

Published paper (Paper 3)

Received: 6 January 2021 | Revised: 13 April 2021 | Accepted: 13 April 2021 | Published online: 4 May 2021

DOI: 10.1002/dad2.12193

Alzheimer's & Dementia: Diagnosis, Assessment & Disease Monitoring

RESEARCH ARTICLE

Detection of retinal and blood Aβ oligomers with nanobodies

Umma Habiba[1] | Joseph Descallar[2,3] | Fabian Kreilaus[1] | Utpal K. Adhikari[1] | Sachin Kumar[1] | John W Morley[1] | Bang V Bui[4] | Maya K. Hamaoui[5] | Mourad Tayebi[1]

[1] School of Medicine, Western Sydney University, Campbelltown, New South Wales, Australia

[2] South Western Sydney Clinical School, Faculty of Medicine, UNSW, Liverpool Hospital, Liverpool, New South Wales, Australia

[3] Ingham Institute of Applied Medical Research, Liverpool, New South Wales, Australia

[4] Department of Optometry and Vision Sciences, University of Melbourne, Melbourne, Victoria, Australia

[5] Department of Neurosurgery, Maxine Dunitz Neurosurgical Research Institute and Department of Biomedical Sciences, Cedars-Sinai Medical Center, Los Angeles, California, USA

Correspondence
Mourad Tayebi, Biomedical Sciences, School of Medicine, Western Sydney University, Campbelltown, Sydney, NSW 2560, Australia.
E-mail: m.tayebi@westernsydney.edu.au

Funding information
Ainsworth Medical Research Innovation Fund

Abstract

Introduction: Abnormal retinal changes are increasingly recognized as an early pathological change in Alzheimer's disease (AD). Although amyloid beta oligomers (Aβo) have been shown to accumulate in the blood and retina of AD patients and animals, it is not known whether the early Aβo deposition precedes their accumulation in brain.

Methods and results: Using nanobodies targeting $A\beta_{1-40}$ and $A\beta_{1-42}$ oligomers we were able to detect Aβ oligomers in the retina and blood but not in the brain of 3-month-old APP/PS1 mice. Furthermore, Aβ plaques were detected in the brain but not the retina of 3-month-old APP/PS1 mice.

Conclusion: These results suggest that retinal accumulation of Aβo originates from peripheral blood and precedes cognitive decline and Aβo deposition in the brain. This provides a very strong basis to develop and implement an "eye test" for early detection of AD using nanobodies targeting retinal Aβ.

KEYWORDS

amyloid beta oligomers, Alzheimer's disease, APP/PS1 mice, blood immunodetection, early Alzheimer's disease diagnosis, nanobodies, retinal immunodetection

1 | INTRODUCTION

The importance of amyloid beta oligomer (Aβo) detection has gained momentum and experimental studies using human Alzheimer's disease (AD) samples have shown that this form can be detected as much as two decades before clinical onset of AD.[1-4] Aβo can potentially become a strong biomarker for early AD detection and could provide accurate biochemical information about various preclinical stages of AD. Several investigators have shown experimentally that blood-borne Aβo is a viable biomarker for human AD. A study by Nakamura et al.[5] has identified high-performance plasma Aβ biomarkers using a combination of immunoprecipitation and mass spectrometry and suggested that plasma Aβ ratio can predict brain Aβ burden. Plasma Aβ precursor protein $(APP)_{669-711}/A\beta_{1-42}$ and $A\beta_{1-40}/A\beta_{1-42}$ were correlated with brain Aβ levels determined by Aβ positron emission tomography (PET) imaging.

Ocular disturbances are an early complaint in AD patients[6-8] with reported changes in color vision, contrast sensitivity, visual memory and perception,[9-11] nerve damage, and loss of nerve fibers.[12] Ganglion cell loss[13] and thinning of the retinal nerve fiber layer (RNFL)[14,15] have also been reported. A recent study by Coppola et al.[16] reported that RNFL thinning was associated with neurodegenerative progressions in mild cognitive impaired (MCI) and AD patients compared to cognitively healthy individuals. Similar color vision and contrast sensitivity deficits were shown in a murine model of AD. In addition to neuronal changes in the retina, alteration of retinal blood flow and morphology has also been noted.[17] Importantly, Aβ deposits in the retina of AD patients were identified by histology[18] and in vivo imaging of MCI and AD patients.[19] Subsequent studies have corroborated these findings and showed accumulation of Aβ and hyperphosphorylated tau (p-tau) in the retina of AD patients[20–22] and animal models.[23]

Nanobodies are camelid-derived antibody fragments with unique biological features, including lack of light chains, smaller size (more diffusible in tissues), hydrophilic (soluble in aqueous solution), highly stable, and more resistant against chemical denaturation.[24] Previous studies reported that nanobodies targeting Aβ and neurofibrillary tangles in mice brain parenchyma are able to cross the blood-brain barrier (BBB).[25] Another study demonstrated that nanobodies specific for Aβ oligomers prevent neurotoxicity and fibril formation.[26] Moreover, Vandesquille et al. showed that nanobodies were able to detect cerebral Aβ plaque deposits via magnetic resonance imaging (MRI) after intravenous injection.[27]

In the current study, we used nanobody anti-A$\beta_{1\text{-}40}$ (PrioAD12) and anti-A$\beta_{1\text{-}42}$ (PrioAD13) oligomer antibodies[28] to measure the levels of Aβo in the brain and retina of the APP/PS1 mice[25] at 3 to 4 months of age with immunohistochemistry (IHC), before behavioral changes and appearance of cognitive deficits. We showed that retinal A$\beta_{1\text{-}40}$ and A$\beta_{1\text{-}42}$ oligomer levels were significantly higher in APP/PS1 mice compared to age-matched WT controls. Furthermore, immunofluorescence (FL) analysis confirmed our IHC results and surprisingly resulted in the detection of large amounts of Aβo in the 18-month-old APP/PS1 age group. We also confirmed the localization of both A$\beta_{1\text{-}40}$ and A$\beta_{1\text{-}42}$ oligomers to neuronal late-endosomal compartments in the retina and brain[29] that was associated with activated astrocytes and microglia in APP/PS1 mice. Of importance, A$\beta_{1\text{-}40}$ and A$\beta_{1\text{-}42}$ levels in whole blood quantified by western blotting with the nanobodies were elevated in 3- and 18-month-old APP/PS1 mice compared to wild-type (WT) controls. The observation that Aβo was detectable in the retina and blood but not in the brain of young APP/PS1 mice suggests that deposition of retinal Aβo might originate from the blood. Taken together, our results provide an important milestone in achieving an "eye" and/or blood-based screening test for AD.

RESEARCH IN CONTEXT

1. **Systematic review:** Although several experimental studies have demonstrated the presence of blood-borne amyloid beta oligomers (Aβo) decades before clinical Alzheimer's disease (AD) and neuropathology have ensued, few studies have focused on the early detection of Aβ oligomers in the retina and other eye structures.
2. **Interpretation:** The results of this study involving the double-transgenic APP/PS1 AD mouse model showed that Aβo could be detected simultaneously in blood and retina before its deposition in the brain and appearance of cognitive decline.
3. **Future directions:** Future research in this field should aim to establish a routine clinical optical retinal and/or blood-based test for the detection of human AD before cognitive decline and neuropathology have ensued. The ability to detect AD before clinical disease will potentially facilitate implementation of effective therapies.

2 | METHODS

2.1 | Animals and ethics statement

All procedures followed the requirements of the National Health and Medical Research Council of Australia statement for the use of animals in research and were approved by the Western Sydney University Animal Ethics Committee (ACEC # A12905). Mice were housed with free access to water and standard rodent chow (Gordon's Specialty Stock Feeds). APP/PS1 mice have the APP Swedish mutation K595N and M596L[30] and PSEN1 with L166P mutation controlled by the Thy1 promoter (ww.alzforum.org). Cognitive impairment is usually observed after 7 months.[31,32] The APP/PS1 mouse model has high brain levels of A$\beta_{1\text{-}42}$ over A$\beta_{1\text{-}40}$, which increases with age.[33,34] Age-matched WT littermates were used as a control.

2.2 | Immunohistochemistry

APP/PS1 mice (n = 28) and WT littermates (n = 20) were first euthanized (Advanced Anesthesia Specialists, DarvallVet) before perfusion with saline followed with 10% neutral buffered formalin. Formalin fixed paraffin embedded blocks (FFPE) were prepared using 10% neutral buffered formalin as a fixative followed by graded ethanol and xylene. 6μm thick brain and eye tissue sections were cut using a microtome (Thermo Fisher Scientific). Sections were then deparaffinized with xylene and rehydrated through graded alcohols and finally washed with deionized water.

Sections were pretreated using the 2100 antigen retriever (Aptum Biologics Ltd) to expose the target epitopes. Sections were then treated with 90% formic acid for 5 minutes at room temperature followed by cell membrane permeabilization, which was achieved by using 1% triton X for 1 minute prior to addition of 0.3% H_2O_2 for 15 minutes to inactivate endogenous peroxidases. Sections were then blocked with Protein Block Serum-Free (Agilent) for 15 minutes. Sections were then stained for 1 hour with the following primary antibodies in phosphate-buffered saline (PBS): anti-A$\beta_{1\text{-}40}$ (PrioAD12), anti-Aβ_{1-42} (PrioAD13) antibodies (1:500),[28] or mouse anti-Aβ purified 4G8 antibody (1:500; BioLegend). After washing with PBS, sections were incubated for 1 hour at room temperature with secondary antibodies in PBS:horseradish peroxidase (HRP)-conjugated anti-llama immunoglobulin G (IgG; Bethyl Laboratories) or anti-mouse IgG (Sigma-Aldrich). Sections were then washed in PBS (x3) before addition of DAB substrate chromogen system and incubated for 5 to 10 minutes. Slides were then counterstained with hematoxylin for 1 minutes. The Olympus VS 120 Slide Scanner was used to visualize images and the Olympus OlyVIA and Olympus cellSens imaging software were used for analysis.

2.3 | Immunofluorescence co-localization studies

Double immuno-labeling was achieved by two different fluorescent labels, each having a separate emission wavelength. Sections were incubated overnight with anti-Aβ_{1-40} (PrioAD12), anti-Aβ_{1-42} (PrioAD13) or *4G8* antibody at 4°C. Sections were also incubated with camelid antibodies and mouse anti-lysosomal-associated membrane protein 2 (*LAMP2*, Stressgen Bioreagents Corp) antibody to assess whether Aβo localizes to lysosomes/late endosomes. Sections derived from the 3- to 4-month-old group were incubated with camelid antibodies and *GFAP* or Iba1 (Thermo Fisher Scientific). Finally, sections were incubated with camelid-derived antibodies and anti-NeuN mAb, clone *A60* (MilliporeSigma) to confirm the intra-neuronal localization of the Aβos. All the sections were incubated overnight at 4°C. After washing with PBS, sections were then incubated with goat anti-llama IgG conjugated to fluorescein isothiocyanate (FITC; Bethyl Laboratories, Inc) and donkey-anti-mouse IgG conjugated to Texas Red (Sigma-Aldrich) for 2 hours at 4°C. Sections were then mounted using fluorescence mounting media (Agilent) then visualized using an Olympus VS 120 slide scanner with a standard FITC/Texas Red double band-pass filter set.

2.4 | Image quantification

For the quantification of the age-dependent accumulation of Aβ plaque (Aβp) and Aβo, we used three sections derived from the 3- to 4-month-old APP/PS1 ($n = 8$) and WT ($n = 8$) mice as well as the 17- to 18-month-old APP/PS1 ($n = 8$) and WT ($n = 8$) mice. Three different hippocampus, cerebral cortex, and retinal sections were analyzed. Immunohistochemical signal intensity was visualized by capturing bright field images using the Olympus VS 120 slide scanner. Images were analyzed using OlyVIA software.[35,36] Age-dependent accumulation of Aβp and Aβo in APP/PS1 mice was quantified using cellSens image processing software. The mean intensity of particles was calculated in several brain and retinal regions from each age group and the result was presented as percentage intensity and expressed as mean $\pm$ standard error of the mean.

2.5 | Immunoprecipitation and western blot analysis of Aβo in whole blood

To measure blood levels of Aβo in APP/PS1 mice, we performed immunoprecipitation to enrich/isolate Aβ from 3 to 4- and 17 to 18-month-old mice as described.[37] Samples were loaded on precast gels (Bio-Rad) and electrophoresed and 1 μg/mL of nanobody Aβ_{1-40} (PrioAD12), Aβ_{1-42} (PrioAD13) anti-oligomer antibodies[28] or A11 rabbit-anti-Aβo antibody (MilliporeSigma) was added followed by anti-llama (Bethyl Laboratories) or anti-rabbit IgG (Sigma-Aldrich) HRP conjugated antibody. The resulting digital images were analyzed with ImageJ processing program for the densitometry analysis and values between the transgenic APP/PS1 and WT controls were compared.

2.6 | Statistical analyses

Statistical analyses were performed using SAS Enterprise Guide version 8.2. A natural logarithm transformation was applied to the measurements. Shapiro-Wilk test was used to determine normality. Group differences were analyzed by Wilcoxon-Mann-Whitney test due to non-normality. The blood-borne Aβo performance at 3 to 4 months when predicting Aβp at 17 to 18 months in both brain and eye was not performed because these data were not measured on the same animal over time. There were 36 comparisons overall so a Bonferroni correction of $0.05/36 = 0.0014$ was applied, meaning *P*-values less than this were considered statistically significant.

3 | RESULTS

3.1 | Immunodetection of Aβ plaques and oligomers in the brain and retina of APP/PS1 mice using single-domain antibodies

In this study, we wanted to test the hypothesis that retinal Aβo accumulation precedes neurobehavioral deficits but also predates brain deposition of both Aβo and Aβp in young APP/PS1 mice using single-domain camelid-derived anti-Aβo antibody fragments and the 4G8 anti-Aβp antibody (Table 1 and Figures 1–4). Of note, the single-domain antibody fragments, called PrioAD12 and PrioAD13, were previously shown to bind to Aβ_{1-40} and Aβ_{1-42}, respectively.[28] Here, we showed widespread intra-neuronal Aβ_{1-40} and Aβ_{1-42} oligomers in the retinal inner nuclear layer (INL), outer nuclear layer (ONL), and ganglion cell layer (GCL) of the 3-month-old APP/PS1 mice (Figure 1C & F); in contrast, no Aβo depositions were seen in the brains at the same age (Figure 1A, B, D, E), indicating that retinal Aβo accumulation precedes its appearance in the brain. Furthermore, no 4G8-specific Aβp was found in the brain and retina of the 3-month-old APP/PS1 mice (Figure 1G, H, I). Interestingly, both Aβ_{1-40} and Aβ_{1-42} were detected at 8 months of age in the cerebral cortex and hippocampus of APP/PS1 mice

TABLE 1 Age-dependent accumulation of Aβ oligomers and plaques in the blood, retina and brain of APP/PS1 mice

Age groups (months)	PRIOAD12 (Aβ1-40) or PRIOAD13 (Aβ1-42)				4G8 (Aβ plaques)		
	Blood	Retinal layers	Brain		Retinal layers	Brain	
			Cerebral cortex	Hippocampus		Cerebral cortex	Hippocampus
3–4 (n = 16)	Present	Present	Absent	Absent	Absent	Absent	Absent
8–11 (n = 16)	Nd*	Present	Present	Present	Present	Present	Present
17–18 (n = 16)	Present	Absent	Absent	Absent	Present	Present	Present

Abbreviations: Aβ, amyloid beta; Nd, Not determined.

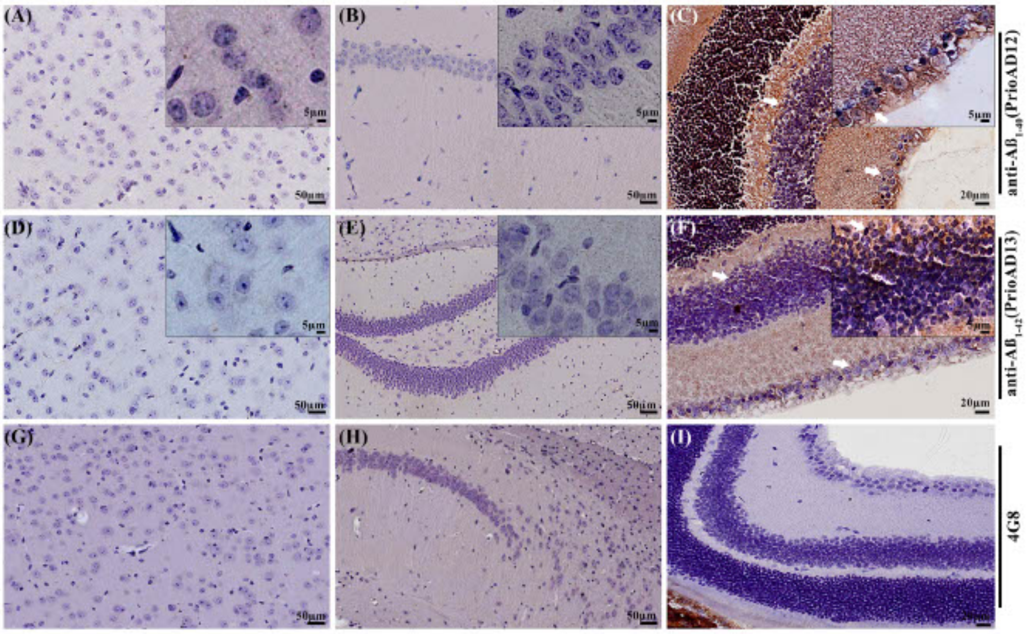

FIGURE 1 Immunohistochemical staining of amyloid beta (Aβ) in the brain and retina of 3-month-old APP/PS1 mice. Immunohistochemical staining with anti-A$\beta_{1\text{-}40}$ and anti-A$\beta_{1\text{-}42}$ oligomer nanobodies and 4G8 anti-Aβ plaque antibody of 3-month-old APP/PS1 mice. Immunohistochemical staining with anti-A$\beta_{1\text{-}40}$ (PrioAD12) and anti-A$\beta_{1\text{-}42}$ (PrioAD13) nanobodies of a 3-month-old APP/PS1 mice did not demonstrate A$\beta_{1\text{-}40}$ depositions in the (A) cerebral cortex and (B) hippocampus as well as A$\beta_{1\text{-}42}$ depositions in the (D) cerebral cortex and (E) hippocampus. A$\beta_{1\text{-}40}$ and A$\beta_{1\text{-}42}$ depositions were observed in the (C, F) ganglion cell layer (GCL), inner nuclear layer (INL), and outer nuclear layer (ONL) of the retina. The photomicrograph was derived from peripheral region of the retina—away from the optic disc. Immunohistochemical staining with 4G8 antibody of 3-month-old APP/PS1 mice did not display characteristic extracellular Aβ plaques in the (G) hippocampus, (H) cerebral cortex, and (I) retina. Representative of all affected mice in this age group

(Figure 2A, B, D, E) as well as in the retina similar to 3-month-old APP/PS1 mice (Figure 2C, F). 4G8-specific Aβp was also observed in the cerebral cortex, hippocampus, and INL of the retina at 8 months (Figure 2G, H, I). Both Aβo and Aβp were detectable in the cerebral cortex, hippocampus, and retinal layers of 11-month-old APP/PS1 mice (Figure 3A-I). Finally, no Aβo were detected in 18-month-old APP/PS1 mice (Figure 4A, B, C, D, E, F), whereas extensive, widespread, and conspicuous Aβp was observed in the cerebral cortex, hippocampus (Figure 4 G, H), and retinal INL (Figure 4 I). No Aβo or Aβp deposits were seen in age-matched WT littermates (data not shown). Overall our data confirm that Aβo deposits first appear in the retina months before they are detectable in the brain and support the

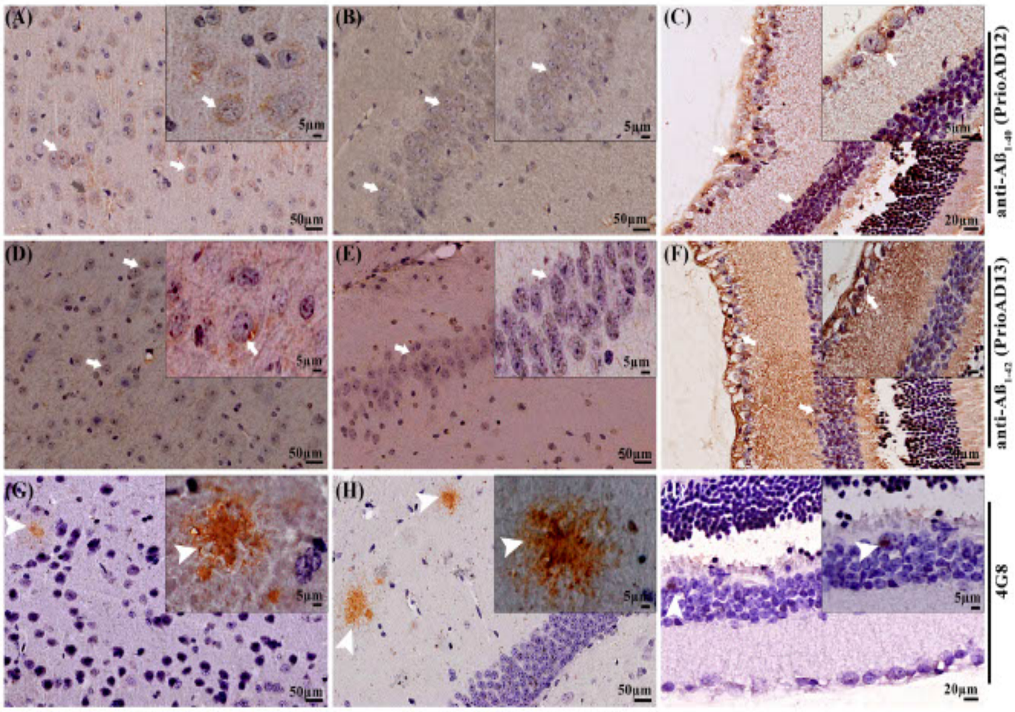

FIGURE 2 Immunohistochemical staining of amyloid beta (Aβ) in the brain and retina of 8-month-old APP/PS1 mice. Immunohistochemical staining with anti-Aβ_{1-40} and anti-Aβ_{1-42} oligomer nanobodies and 4G8 anti-Aβ plaque antibody of 8-month-old APP/PS1 mice. Immunohistochemical staining with anti-Aβ_{1-40} (PrioAD12) and anti-Aβ_{1-42} (PrioAD13) nanobodies of 8-month-old APP/PS1 mice showed presence of Aβ_{1-40} depositions in the (A) cerebral cortex and (B) hippocampus as well as Aβ_{1-42} depositions in the (D) cerebral cortex and (E) hippocampus. Aβ_{1-40} and Aβ_{1-42} depositions were observed in the (C, F) ganglion cell layer (GCL), inner nuclear layer (INL), and outer nuclear layer (ONL) of the retina. The photomicrograph was derived from peripheral region of the retina—away from the optic disc. Immunohistochemical staining with 4G8 antibody of 8-month-old APP/PS1 mice displayed extensive extracellular Aβ plaque staining in the (G) hippocampus, (H) cerebral cortex, and (I) retina. Representative of all affected mice in this age group

proposition that the retinal oligomers probably originate from the blood.[38] These results also validate our previous findings that showed Aβp burden increased over the course of the disease in both brain and retina, whereas Aβo levels appeared to decrease in an age-dependent manner.[39]

3.2 | Quantitative analysis of Aβ plaques and oligomers in the brain, retina, and whole blood of APP/PS1 mice using single-domain antibodies

Age-dependent retinal and brain accumulation of Aβp and Aβo in the 3- to 4-month-old APP/PS1 mice (n = 8) and WT littermates (n = 8) was quantified and compared to Aβp and Aβo levels in the 17- to 18-month-old APP/PS1 mice (n = 8) and WT littermates (n = 8; Tables 2 and 3; Figure 5). Three different areas of retina, hippocampus, and cerebral cortex of each section (32 x 3 sections) were analyzed. Figure 5 shows the normalized intensity of retinal and brain Aβ as measured by the cellSens image processing software and the values for Aβ_{1-40} (PRIOAD12 antibody), Aβ_{1-42} (PRIOAD13 antibody), and total Aβ (4G8 antibody). We found that the normalized intensity of retinal Aβ_{1-40} and Aβ_{1-42} oligomers were significantly higher in 3- to 4-month-old compared to the 17- to 18-month-old APP/PS1 mice ($P = .0002$; Tables 2 and 3), whereas normalized intensity of brain Aβp was significantly higher in the retina and brain of 17- to 18-month-old compared to the 3- to 4-month-old APP/PS1 mice ($P = .0002$; Tables 2 and 3; Figure 5).

Several studies have demonstrated the presence of Aβo in plasma of patients with MCI and AD;[5,40,41] plasma levels may also predict the brain Aβ burden. In this study, we hypothesized that Aβo accumulation in blood might also precede retinal accumulation or at least occur simultaneously with retinal accumulation. Here, we used fresh whole blood in blood lysis buffer to enrich Aβo. Initially and after lysing whole blood derived from APP/PS1 mice, anti-oligomer-A11-coated immunomagnetic microbeads were used to isolate Aβ from APP/PS1 mice and WT littermates (APP/PS1, n = 16, and WT, n = 16). After western blotting, anti-Aβ_{1-40} (PrioAD12) or anti-Aβ_{1-42} (PrioAD13) oligomer single-domain antibodies were used to immunodetect Aβo isoforms in 3- and 18-month-old APP/PS1 and WT mice. Anti-Aβ_{1-40} PrioAD12 displayed

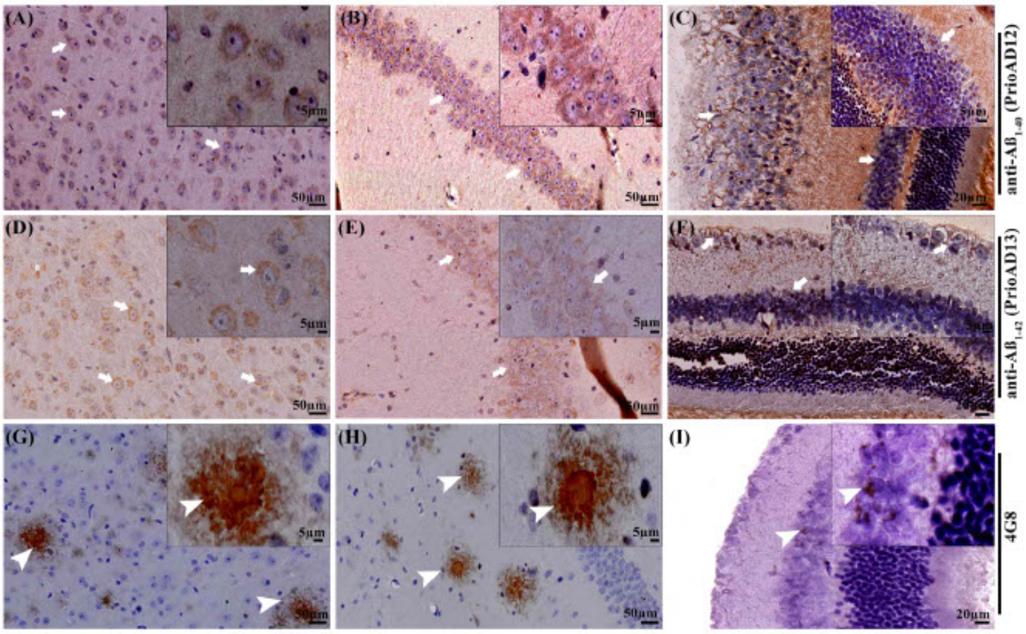

FIGURE 3 Immunohistochemical staining of amyloid beta (Aβ) in the brain and retina of 11-month-old APP/PS1 mice. Immunohistochemical staining with anti-$A\beta_{1-40}$ and anti-$A\beta_{1-42}$ oligomer nanobodies and 4G8 anti-Aβ plaque antibody of 11-month-old APP/PS1 mice. Immunohistochemical staining with anti-$A\beta_{1-40}$ (PrioAD12) and anti-$A\beta_{1-42}$ (PrioAD13) nanobodies of 11-month-old APP/PS1 mice showed presence of $A\beta_{1-40}$ oligomer depositions in the (A) cerebral cortex and (B) hippocampus as well as $A\beta_{1-42}$ oligomer depositions in the (D) cerebral cortex and (E) hippocampus. $A\beta_{1-40}$ and $A\beta_{1-42}$ depositions were observed in the (C, F) ganglion cell layer (GCL), inner nuclear layer (INL), and outer nuclear layer (ONL) of the retina. The photomicrograph was derived from peripheral region of the retina—away from the optic disc. Immunohistochemical staining with 4G8 antibody of 11-month-old APP/PS1 mice displayed extensive extracellular Aβ plaque staining in the (G) hippocampus, (H) cerebral cortex, and (I) retina. Representative of all affected mice in this age group

a two-band pattern ranging between 10 and 15 kDa in the 3-month-old APP/PS1 mice, whereas only one band at 10 to 15 kDa was seen in the 18-month-old APP/PS1 age group (Figure S1A, B in supporting information). In contrast, anti-$A\beta_{1-42}$ PrioAD13 showed only one band at 10 to 15 KDa in both the 3- and 18-month-old APP/PS1 age groups (Figure S1A, B). Furthermore, we also used A11 rabbit anti-Aβo antibody to immuno-compare $A\beta_{1-40}$ and $A\beta_{1-42}$ levels detected with PrioAD12 and PrioAD13. In both age groups A11 displayed a different band pattern compared to the single-domain antibodies and ranged between 70 and 80 kDa (Figure S1A, B). We then performed densitometric analysis of scanned western blot membranes.[42] Table 2 shows the normalized intensity of whole-blood Aβ as measured by *ImageJ* software and the values for $A\beta_{1-40}$ (PRIOAD12 antibody) and $A\beta_{1-42}$ (PRIOAD13 antibody). Levels of both $A\beta_{1-40}$ and $A\beta_{1-42}$ oligomers were not significantly higher compared to the WT levels in the 3-month age group ($P = .0286$) when a Bonferroni correction was applied. However, when the statistical analysis was performed using paired *t*-tests (*P*-values below .05 were deemed significant in this case) to compare levels of both $A\beta_{1-40}$ and $A\beta_{1-42}$ oligomers in APP/PS1 versus WT, these were significant ($P < .05$; Figure 6). Levels of $A\beta_{1-40}$ increased significantly from 3 to 18 months while $A\beta_{1-42}$ decreased by at least three-fold in the 18-month-old APP/PS1 mice (Figure 6). These results also highlight the high binding affinity of the camelid-derived single domain antibodies for detection of $A\beta_{1-40}$ and $A\beta_{1-42}$ oligomers in whole blood.

3.3 | Co-localization of Aβ oligomers and plaques in the retina and brain of APP/PS1 mice

To determine whether $A\beta_{1-40}$ or $A\beta_{1-42}$ oligomers co-localized with Aβp in different anatomical regions and structures of the retina and brain, we co-stained brain and retinal sections with 4G8 antibody with either anti-$A\beta_{1-40}$ (PrioAD12) or anti-$A\beta_{1-42}$ (PrioAD13) oligomer single-domain antibodies (Figure 7). We did not observe any co-localization in the brain and retina of the 3-month-old APP/PS1 mice (Figure 7A-F) but confirmed the presence of $A\beta_{1-40}$ or $A\beta_{1-42}$ oligomer in the retinal layers (Figure 7C, F). However, both retinal Aβp and $A\beta_{1-40}$ or Aβp and $A\beta_{1-42}$ were shown to co-localize in the GCL, IPL, and INL of

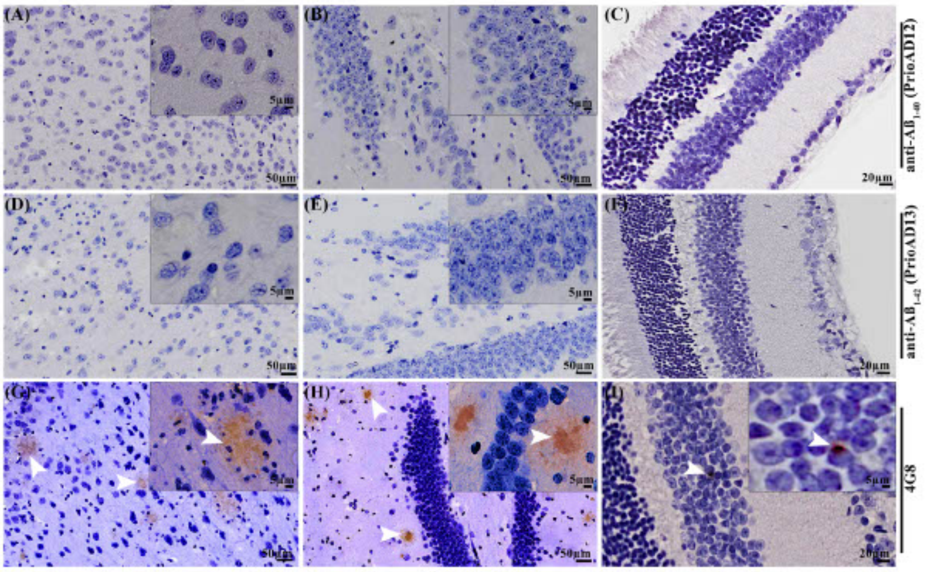

FIGURE 4 Immunohistochemical staining of amyloid beta (Aβ) in the brain and retina of 18-month-old APP/PS1 mice. Immunohistochemical staining with anti-A$\beta_{1\text{-}40}$ and anti-A$\beta_{1\text{-}42}$ oligomer nanobodies and 4G8 anti-Aβ plaque antibody of 18-month-old APP/PS1 mice. Immunohistochemical staining with anti-A$\beta_{1\text{-}40}$ (PrioAD12) and anti-A$\beta_{1\text{-}42}$ (PrioAD13) nanobodies of 18-month-old APP/PS1 mice did not show presence of A$\beta_{1\text{-}40}$ depositions in the (A) cerebral cortex and (B) hippocampus as well as A$\beta_{1\text{-}42}$ in the (D) cerebral cortex and (E) hippocampus. A$\beta_{1\text{-}40}$ and A$\beta_{1\text{-}42}$ depositions were not observed (C, F) in the ganglion cell layer (GCL), inner nuclear layer (INL), and outer nuclear layer (ONL) of the retina. The photomicrograph was derived from peripheral region of the retina—away from the optic disc. Immunohistochemical staining with 4G8 antibody of 18-month-old APP/PS1 mice displayed extensive extracellular Aβ plaque staining in the (G) hippocampus and (H) cerebral cortex and (I) plaques were observed in the retina (white arrows). Representative of all affected mice in this age group

the 8-month-old APP/PS1 age group (Figure 7I, L). Furthermore, co-accumulation of Aβp and A$\beta_{1\text{-}40}$ or Aβp and A$\beta_{1\text{-}42}$ was also seen in the cerebral cortex and hippocampus (Figure 7G, H, J, K), noticeably higher levels of Aβo in this age group compared to plaques. Aβp in 11-month-old APP/PS1 mice was markedly increased while A$\beta_{1\text{-}40}$ and A$\beta_{1\text{-}42}$ oligomers decreased in the brain (Figure 7M, N, P, Q). High levels of A$\beta_{1\text{-}40}$ and A$\beta_{1\text{-}42}$ oligomers were consistently found in the retina (Figure 7O, R). Finally, 18-month-old APP/PS1 mice showed that both A$\beta_{1\text{-}40}$ and A$\beta_{1\text{-}42}$ co-localized with Aβp in the cerebral cortex and hippocampus and in the retinal GCL, INL, and ONL (Figure 7S-X). Surprisingly, high levels of A$\beta_{1\text{-}40}$ and A$\beta_{1\text{-}42}$ oligomers were observed in the retina and brain of 18-month-old APP/PS1 mice (Figure 7S-X), perhaps confirming the hypothesis that plaques act as a reservoir for the toxic Aβo.[43] WT age-matched littermates did not show any co-localization of Aβp with A$\beta_{1\text{-}40}$ or A$\beta_{1\text{-}42}$ (data not shown).

4 | DISCUSSION

Behavioral assessment of the APP/PS1 AD mouse model demonstrated that memory decline and cognitive deficits start after 7 months of age.[32] Although our study did not include behavioral assessments, mice appeared healthy until 10 months of age. Of importance, we show that increased Aβo in blood and retinal accumulation of Aβo was observed at 3 months in APP/PS1 mice in the absence of Aβp accumulation in the retina and before appearance of both Aβo and Aβp in brain. The accumulation of blood and retinal Aβo occur at a very early age, likely months before the expected memory and cognitive deficits in APP/PS1 mice. These data indicate that these assemblies are likely to be responsible for the toxic effects associated with AD,[44,45] can be detected before AD onset,[46] and might originate from the blood.[38] Several diagnostic strategies have been developed for early AD detection, including systems for the detection of Aβo in plasma[40] and in the cerebrospinal fluid (CSF).[47] The experimental value of detecting blood-borne Aβ biomarkers has gained considerable momentum;[48,49] however, a decade of research efforts in this area has not yet led to a clinical diagnostic due to the complexity and lack of reproducibility of these approaches.[50] Nonetheless, pursuing a blood-detection approach might have great diagnostic value.[51] A recent study combining immunoprecipitation and mass spectrometry led to the identification of high-performance blood-borne Aβs derived from human MCI and AD.[5] Similarly, using our unique camelid single-domain anti-A$\beta_{1\text{-}40}$ or anti-A$\beta_{1\text{-}42}$ oligomer antibody, we were able to detect both A$\beta_{1\text{-}40}$ and A$\beta_{1\text{-}42}$ oligomer in whole blood derived from 3- to 18-month-old

TABLE 2 Statistical analysis of the age-dependent retinal, brain, and blood accumulation of Aβp and Aβo in the 3- to 4-month- and 17- to 18-month-old APP/PS1 mice and compared to wild-type littermates. Bonferroni correction of 0.05/36 =0.0014 was applied, meaning *P*-values less than this value were considered statistically significant

Antibody	Age	Predictor	APP/PS1					Wild type					Difference	
			N	Median	Lower quartile	Upper quartile	IQR	N	Median	Lower quartile	Upper quartile	IQR	z	P
PRIOAD12	3–4 months	logeye	8	8.67	8.53	8.84	0.32	8	3.28	2.51	4.04	1.53	-3.3082	.0002
PRIOAD12		logbrain	8	4.00	3.82	4.04	0.22	8	2.55	2.43	2.63	0.20	-3.3082	.0002
PRIOAD12		logblood	8	3.94	3.78	4.28	0.51	8	2.30	2.30	2.56	0.25	-2.2185	.0286
PRIOAD13		logeye	8	8.34	7.99	8.57	0.58	8	3.01	2.43	3.97	1.53	-3.3106	.0002
PRIOAD13		logbrain	8	3.83	3.40	4.11	0.71	8	2.50	2.33	2.88	0.55	-3.3106	.0002
PRIOAD13		logblood	8	4.08	3.96	4.12	0.16	8	2.30	2.30	2.30	0.00	-2.3067	.0286
4G8		logeye	8	2.30	2.30	2.30	0.00	8	2.30	2.30	2.30	0.00	0	1
4G8		logbrain	8	2.30	2.30	2.30	0.00	8	2.30	2.30	2.30	0.00	0	1
PRIOAD12	17–18 months	logeye	8	2.93	2.33	3.77	1.43	8	2.30	2.30	2.30	0.00	2.8359	.007
PRIOAD12		logbrain	8	2.57	2.38	2.80	0.42	8	2.30	2.30	2.30	0.00	3.1854	.0014
PRIOAD12		logblood	8	4.43	4.28	4.47	0.19	8	2.30	2.30	2.30	0.00	2.3067	.0286
PRIOAD13		logeye	8	2.74	2.35	2.93	0.58	8	2.30	2.30	2.30	0.00	2.8359	.007
PRIOAD13		logbrain	8	2.76	2.57	2.98	0.41	8	2.30	2.30	2.30	0.00	3.1825	.0014
PRIOAD13		logblood	8	2.83	2.72	3.22	0.50	8	2.30	2.30	2.30	0.00	2.3067	.0286
4G8		logeye	8	4.35	4.06	4.66	0.60	8	2.30	2.30	2.30	0.00	3.5336	.0002
4G8		logbrain	8	7.73	7.68	7.77	0.09	8	2.30	2.30	2.30	0.00	3.5366	.0002

TABLE 3 Age-dependent retinal and brain accumulation of Aβp and Aβo in the 3- to 4-month-old APP/PS1 mice were quantified and compared to Aβp and Aβo levels in the 17- to 18-month-old APP/PS1 mice. Bonferroni correction of 0.05/36 = 0.0014 was applied, meaning *P*-values less than this value were considered statistically significant

Antibody	Group	Log	N	Age (month)	Difference	
					z	P
PRIOAD12	APP/PS1	EYE	8	3–4 vs. 17–18	-3.3106	.0002
PRIOAD13		EYE			-3.3106	
4G8		EYE			3.5336	
4G8		BRAIN			3.5366	

Abbreviations: Aβ, amyloid beta; Aβo, amyloid beta oligomers; Aβp, amyloid beta plaques.

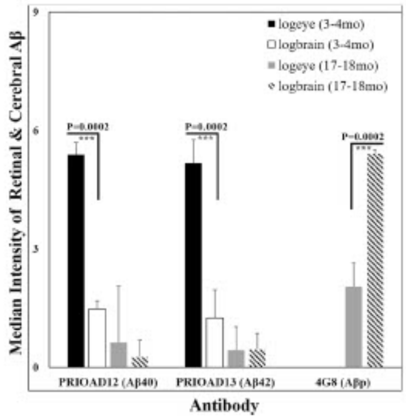

FIGURE 5 Age-dependent accumulation of amyloid beta (Aβ) oligomers and Aβ plaques. Quantification of the age dependent accumulation of cerebral and retinal Aβ oligomers and Aβ plaques with nanobodies: Immunodetection and quantification of retinal and cerebral $A\beta_{1-40}$ and $A\beta_{1-42}$ with PrioAD12 and PrioAD13 nanobodies in the cerebral cortex and hippocampus and retina of 3- to 4-month-old (n = 8) and 17- to 18-month-old (n = 8) APP/PS1 mice using cellSens software image analysis after immunohistochemical staining. Total Aβ plaque burden (Aβp) was quantified in the cerebral cortex and hippocampus and retina of 3- to 4-month-old (n = 8) and 17- to 18-month-old (n = 8) APP/PS1 mice. Wilcoxon-Mann-Whitney test was performed and normalized intensity of both $A\beta_{1-40}$ and $A\beta_{1-42}$ oligomers were significantly higher in the retina of 3- to 4-month-old compared to the 17- to 18-month-old age group APP/PS1 mice (P = .0002) whereas Aβp load was significantly higher in brain and retina of the 17- to 18-month-old age group compared to the 3- to 4-month-old age group (P = .0002). Error bars represent interquartile range

APP/PS1 mice via immunoprecipitation followed by western blotting. $A\beta_{1-40}$ and $A\beta_{1-42}$ oligomer levels were significantly higher compared to WT mice in the 3-month-old age group, while their levels were elevated for $A\beta_{1-40}$ oligomers and reduced for $A\beta_{1-42}$ oligomers in the 18-month-old age group compared to the 3-month-old age group. The

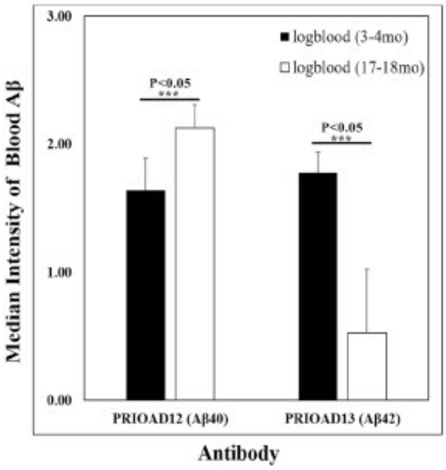

FIGURE 6 Quantification of amyloid beta (Aβ) oligomers in blood. Quantification of the age-dependent accumulation of blood-borne Aβ oligomers with nanobodies. Immunodetection and quantification of blood-borne $A\beta_{1-40}$ and $A\beta_{1-42}$ with PrioAD12 and PrioAD13 nanobodies in whole blood of 3- to 4-month-old (n = 8) and 17- to 18-month-old (n = 8) APP/PS1 mice using ImageJ software analysis after western blotting. The normalized intensity was calculated in three independent experiments for each age group and the final result was presented as median intensity. Paired *t*-tests were performed and *P*-values below .05 were considered significant. Levels of both $A\beta_{1-40}$ and $A\beta_{1-42}$ oligomers were significantly higher in the 3- to 4-month age group. $A\beta_{1-40}$ oligomer level increased significantly from 3 to 4 to 17 to 18 months whereas $A\beta_{1-42}$ oligomer level decreased by at least three-fold in the 17- to 18-month-old APP/PS1 mice. Error bars represent interquartile range

reduction of $A\beta_{1-42}$ in the older age group mirrors the biological behavior of this assembly in human AD in which plasma $A\beta_{1-42}$ or total $A\beta_{1-42}/A\beta_{1-40}$ ratio is used as a strong predictor of amyloid-PET status.[51,52] Although the levels of blood-borne Aβ levels were significantly higher in APP/PS1 compared to the levels in the WT littermates, the western blot technique has its limitations and might generally lead to false positives.[53]

We have previously shown a strong inverse correlation between retinal Aβo and brain Aβp deposition.[39] This previous study provided the rationale for assessing and comparing age-dependent accumulation of Aβo in the retina, whole blood, and brain. In this current study, the 3- to 4-month-old APP/PS1 age group displayed extensive accumulation of Aβo deposits in the ONL, INL, and GCL of the retina, whereas the brain remained free of Aβo deposition. In addition, Aβ plaques were completely absent in both brain and retina in this age group. Retinal Aβo deposition was lower with age, and was no longer detected in the 17- to 18-month-old age group using IHC. In contrast, cerebral Aβo was first detected at 8 months of age in our APP/PS1 mice and remained unchanged in 11-month-old mice, but was undetectable in 18-month-old APP/PS1 mice. Consistent with our previous study,[39] retinal Aβp

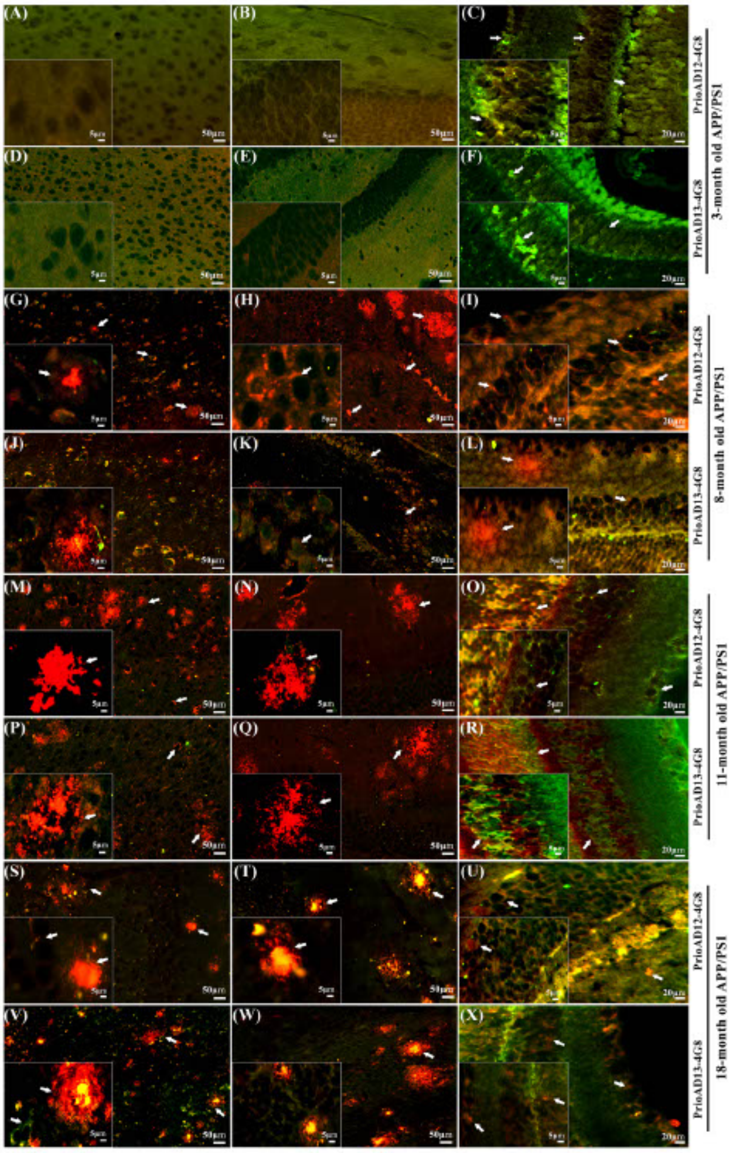

FIGURE 7 Co-localization of amyloid beta (Aβ) oligomers and plaques. Immunofluorescence co-localization of cerebral and retinal Aβ oligomers and Aβ plaques in different APP/PS1 age groups. Cerebral and retinal co-staining with anti-A$\beta_{1\text{-}40}$ (PrioAD12) and anti-A$\beta_{1\text{-}42}$ (PrioAD13) nanobodies (GREEN) and 4G8 antibody (RED) of 3- (A-F), 8- (G-L), 11- (M-R), and 18-month-old (S-X) APP/PS1 mice. No distinctive oligomers co-localized with plaques in the brain cortical region (A, D) and in the hippocampus (B, E). Large number of oligomers found in the (C, F) retinal ganglion cell layer (GCL), inner nuclear layer (INL), and outer nuclear layer (ONL) but no co-localization observed in the 3-month-old mice (white arrows). Then A$\beta_{1\text{-}40}$ (G, H) and A$\beta_{1\text{-}42}$ (J, K) oligomers co-localized with plaques in the brain cortical region and hippocampus, respectively, and in the retinal GCL and INL (I, L) of the 8-month-old mice (white arrows), respectively. With age progression, A$\beta_{1\text{-}40}$ (M, N) and A$\beta_{1\text{-}42}$ (P, Q) oligomers co-localized with plaques in the brain cortical region and hippocampus, respectively, and in the retinal INL (O, R) of the 11-month-old mice (white arrows). Finally, in 18-month-old APP/PS1 mice, Aβ oligomers co-localized with plaques in the brain cortical region (S, V) and in the hippocampus (T, W) and also in the retinal GCL, INL, and ONL (U, X) of the 18-month-old mice, respectively (white arrows). Representative of all affected mice in all age groups

was first detected in 8- to 11-month-old APP/PS1 and increased in the 18-month age group. The lack of detection of Aβo in older animals supports the hypothesis of Aβo conversion to plaques as the disease progresses. This is highly speculative as this "conversion" from oligomers to plaques has not been demonstrated at a molecular level; however, in our study, the mere fact that Aβo are present in the retina and not in the brain provides momentum to pursue this diagnostic strategy in vivo. Taken together, and acknowledging the limitations of the study in relation to the lack of data related to animal behavior in our current study, these results suggest that retinal Aβo accumulation precedes its cerebral deposition and that its simultaneous presence in the blood at high levels strongly suggests that retinal Aβo originate from the blood,[18,54] albeit a lymphatic and/or a CSF origin cannot be ruled out.[55] Of note, fluorescence assessment also showed presence of cerebral Aβo depositions forming the dense core of the Aβp plaques in the 18-month age group. This data strengthens the hypothesis of Haass et al.[43] suggesting that Aβ plaques might act as a reservoir for Aβ oligomers.

In this study, we established that Aβo could be detected simultaneously in the blood and retina of APP/PS1 mice before their appearance in the brain. Aβo neuroinvasion appears to originate from blood before reaching the retina probably via "leaky" blood–ocular barriers.[56] A study by Morin et al.[57] reported that APP is synthesized in retinal ganglion cells and transported to the optic nerve in small transport vesicles. It can be speculated that blood-borne Aβo deposition in the retina might initiate a seeding reaction leading to aggregation and spread to the brain.[38] The ability to detect Aβo concurrently in the blood and retina using nanobodies that specifically bind $A\beta_{1-40}$ and $A\beta_{1-42}$ oligomers before cognitive decline and neuropathology are evident offers a real possibility to establish a screening platform (retinal imaging of Aβo) and a reference diagnostic testing platform (blood testing of Aβo).

ACKNOWLEDGMENTS

We wish to thank Professor Tim Karl at Western Sydney University for providing the APP/PS1 mice. We also thank Dr Hong Yu at the Westmead Institute for Medical Research, Sydney, Australia for help with image acquisition using the Olympus VS 120. This work was supported by an Ainsworth Medical Research Innovation Fund Grant awarded to MT. UH was awarded an Australian Government Research Training Program Stipend Scholarship for PhD support.

CONFLICTS OF INTEREST

The authors declare that the research was conducted in the absence of any commercial or financial and non-financial competing interests that could be construed as a potential conflict of interest.

ORCID

Mourad Tayebi https://orcid.org/0000-0001-8664-6918

REFERENCES

1. Viola KL, Klein WL. Amyloid beta oligomers in Alzheimer's disease pathogenesis, treatment, and diagnosis. *Acta Neuropathol*. 2015;129(2):183-206.
2. Price JL, McKeel DW, Jr, Buckles VD, et al. Neuropathology of nondemented aging: presumptive evidence for preclinical Alzheimer disease. *Neurobiol Aging*. 2009;30(7):1026-1036.
3. Braak H, Braak E. Frequency of stages of Alzheimer-related lesions in different age categories. *Neurobiol Aging*. 1997;18(4):351-357.
4. Funke SA. Detection of soluble amyloid-oligomers and insoluble high-molecular-weight particles in CSF: development of methods with potential for diagnosis and therapy monitoring of Alzheimer's disease. *Int J Alzheimer's Dis*. 2011;2011:151645.
5. Nakamura A, Kaneko N, Villemagne VL, et al. High performance plasma amyloid-β biomarkers for Alzheimer's disease. *Nature*. 2018;554(7691):249-254.
6. Fotiou DF, Brozou CG, Haidich AB, et al. Pupil reaction to light in Alzheimer's disease: evaluation of pupil size changes and mobility. *Aging Clin Exp Res*. 2007;19(5):364-371.
7. Katz B, Rimmer S. Ophthalmologic manifestations of Alzheimer's disease. *Survey Ophthalmol*. 1989;34(1):31-43.
8. Sadun AA, Borchert M, DeVita E, Hinton DR, Bassi CJ. Assessment of visual impairment in patients with Alzheimer's disease. *Am J Ophthalmol*. 1987;104(2):113-120.
9. Rizzo M, Anderson SW, Dawson J, Nawrot M. Vision and cognition in Alzheimer's disease. *Neuropsychologia*. 2000;38(8):1157-1169.
10. Cronin-Golomb A, Corkin S, Rizzo JF, Cohen J, Growdon JH, Banks KS. Visual dysfunction in Alzheimer's disease: relation to normal aging. *Ann Neurol*. 1991;29(1):41-52.
11. Trick GL, Trick LR, Morris P, Wolf M. Visual field loss in senile dementia of the Alzheimer's type. *Neurology*. 1995;45(1):68-74.
12. Danesh-Meyer HV, Birch H, Ku JY, Carroll S, Gamble G. Reduction of optic nerve fibers in patients with Alzheimer disease identified by laser imaging. *Neurology*. 2006;67(10):1852-1854.
13. Blanks JC, Hinton DR, Sadun AA, Miller CA. Retinal ganglion cell degeneration in Alzheimer's disease. *Brain Res*. 1989;501(2):364-372.
14. Colligris P, Perez de Lara MJ, Colligris B, Pintor J. Ocular manifestations of Alzheimer's and other neurodegenerative diseases: the prospect of the eye as a tool for the early diagnosis of Alzheimer's disease. *J Ophthalmol*. 2018;2018:8538573.
15. Iseri PK, Altinas O, Tokay T, Yuksel N. Relationship between cognitive impairment and retinal morphological and visual functional abnormalities in Alzheimer disease. *J Neuro Ophthalmol*. 2006;26(1):18-24.
16. Coppola G, Parisi V, Manni G, Pierelli F, Sadun AA. Optical coherence tomography in Alzheimer's disease. *OCT and Imaging in Central Nervous System Diseases*: Springer; 2020:263-288.
17. Berisha F, Feke GT, Trempe CL, McMeel JW, Schepens CL. Retinal abnormalities in early Alzheimer's disease. *Investig Ophthalmol Vis Sci*. 2007;48(5):2285-2289.
18. Koronyo-Hamaoui M, Koronyo Y, Ljubimov AV, et al. Identification of amyloid plaques in retinas from Alzheimer's patients and noninvasive in vivo optical imaging of retinal plaques in a mouse model. *NeuroImage*. 2011;54(Suppl 1):S204-217.
19. Koronyo Y, Biggs D, Barron E, et al. Retinal amyloid pathology and proof-of-concept imaging trial in Alzheimer's disease. *JCI Insight*. 2017;2(16):e93621.
20. La Morgia C, Ross-Cisneros FN, Koronyo Y, et al. Melanopsin retinal ganglion cell loss in Alzheimer disease. *Ann Neurol*. 2016;79(1):90-109.
21. Lee S, Jiang K, McIlmoyle B, et al. Amyloid beta immunoreactivity in the retinal ganglion cell layer of the Alzheimer's eye. *Front Neurosci*. 2020;14:758.
22. Qiu Y, Jin T, Mason E, Campbell MCW. Predicting thioflavin fluorescence of retinal amyloid deposits associated with Alzheimer's disease from their polarimetric properties. *Transl Vis Sci Technol*. 2020;9(2):47.
23. Mirzaei N, Shi H, Oviatt M, et al. Alzheimer's retinopathy: seeing disease in the eyes. *Front Neurosci*. 2020;14:921.
24. Jovčevska I, Muyldermans S. The therapeutic potential of nanobodies. *BioDrugs*. 2019:1-16.

25. Li T, Vandesquille M, Koukouli F, et al. Camelid single-domain antibodies: a versatile tool for in vivo imaging of extracellular and intracellular brain targets. *J Control Release*. 2016;243:1-10.
26. Lafaye P, Achour I, England P, Duyckaerts C, Rougeon F. Single-domain antibodies recognize selectively small oligomeric forms of amyloid beta, prevent Abeta-induced neurotoxicity and inhibit fibril formation. *Mol Immunol*. 2009;46(4):695-704.
27. Vandesquille M, Li T, Po C, et al. Chemically-defined camelid antibody bioconjugate for the magnetic resonance imaging of Alzheimer's disease. *mAbs*. 2017;9(6):1016-1027.
28. David MA, Jones DR, Tayebi M. Potential candidate camelid antibodies for the treatment of protein-misfolding diseases. *J Neuroimmunol*. 2014;272(1-2):76-85.
29. Yang AJ, Chandswangbhuvana D, Margol L, Glabe CG. Loss of endosomal/lysosomal membrane impermeability is an early event in amyloid Abeta1-42 pathogenesis. *J Neurosci Res*. 1998;52(6):691-698.
30. Volianskis A, Køstner R, Mølgaard M, Hass S, Jensen MS. Episodic memory deficits are not related to altered glutamatergic synaptic transmission and plasticity in the CA1 hippocampus of the APPswe/PS1ΔE9-deleted transgenic mice model of β-amyloidosis. *Neurobiol Aging*. 2010;31(7):1173-1187.
31. Serneels L, Van Biervliet J, Craessaerts K, et al. gamma-Secretase heterogeneity in the Aph1 subunit: relevance for Alzheimer's disease. *Science*. 2009;324(5927):639-642.
32. Reiserer RS, Harrison FE, Syverud DC, McDonald MP. Impaired spatial learning in the APPSwe + PSEN1DeltaE9 bigenic mouse model of Alzheimer's disease. *Genes Brain Behav*. 2007;6(1):54-65.
33. Holcomb L, Gordon MN, McGowan E, et al. Accelerated Alzheimer-type phenotype in transgenic mice carrying both mutant amyloid precursor protein and presenilin 1 transgenes. *Nat Med*. 1998;4(1):97-100.
34. Radde R, Bolmont T, Kaeser SA, et al. Abeta42-driven cerebral amyloidosis in transgenic mice reveals early and robust pathology. *EMBO Rep*. 2006;7(9):940-946.
35. Mowat FM, Avelino J, Bowyer A, et al. Detection of circulating anti-retinal antibodies in dogs with sudden acquired retinal degeneration syndrome using indirect immunofluorescence: a Case-Control Study. *Exp Eye Res*. 2020;193:107989.
36. Palfi A, Yesmambetov A, Humphries P, Hokamp K, Farrar GJ. Non-photoreceptor expression of Tulp1 may contribute to extensive retinal degeneration in Tulp1-/- Mice. *Front Neurosci*. 2020;14:656.
37. Tayebi M, Enever P, Sattar Z, Collinge J, Hawke S. Disease-associated prion protein elicits immunoglobulin M responses in vivo. *Mol Med*. 2004;10(7-12):104-111.
38. Shi H, Koronyo Y, Rentsendorj A, et al. Identification of early pericyte loss and vascular amyloidosis in Alzheimer's disease retina. *Acta Neuropathol*. 2020;139(5):813-836.
39. Habiba U, Merlin S, Lim JKH, et al. Age-specific retinal and cerebral immunodetection of amyloid-β plaques and oligomers in a rodent model of Alzheimer's disease. *J Alzheimer's Dis*. 2020;Preprint:1-6.
40. Youn YC, Kang S, Suh J, et al. Blood amyloid-β oligomerization associated with neurodegeneration of Alzheimer's disease. *Alzheimers Res Ther*. 2019;11(1):40.
41. Youn YC, Lee BS, Kim GJ, et al. Blood amyloid-β oligomerization as a biomarker of Alzheimer's disease: a Blinded Validation Study. *J Alzheimers Dis*. 2020;75(2):493-499.
42. Ding Y, Zhao J, Zhang X, et al. Amyloid beta oligomers target to extracellular and intracellular neuronal synaptic proteins in Alzheimer's disease. *Front Neurol*. 2019;10:1140-1140.
43. Haass C, Selkoe DJ. Soluble protein oligomers in neurodegeneration: lessons from the Alzheimer's amyloid beta-peptide. *Nat Rev Mol Cell Biol*. 2007;8(2):101-112.
44. Lesne SE. Toxic oligomer species of amyloid-β in Alzheimer's disease, a timing issue. *Swiss Med Wkly*. 2014;144:w14021.
45. Sengupta U, Nilson AN, Kayed R. The role of amyloid-β oligomers in toxicity, propagation, and immunotherapy. *EBioMedicine*. 2016;6:42-49.
46. Lesné SE, Sherman MA, Grant M, et al. Brain amyloid-β oligomers in ageing and Alzheimer's disease. *Brain*. 2013;136(Pt 5):1383-1398.
47. Gao CM, Yam AY, Wang X, et al. Aβ40 oligomers identified as a potential biomarker for the diagnosis of Alzheimer's disease. *PLoS One*. 2010;5(12):e15725.
48. Doecke JD, Laws SM, Faux NG, et al. Blood-based protein biomarkers for diagnosis of Alzheimer disease. *Arch Neurol*. 2012;69(10):1318-1325.
49. Snyder HM, Carrillo MC, Grodstein F, et al. Developing novel blood-based biomarkers for Alzheimer's disease. *Alzheimers Dement*. 2014;10(1):109-114.
50. Turner RS, Stubbs T, Davies DA, Albensi BC. Potential new approaches for diagnosis of Alzheimer's disease and related dementias. *Front Neurol*. 2020;11:496-496.
51. Schindler SE, Bollinger JG, Ovod V, et al. High-precision plasma β-amyloid 42/40 predicts current and future brain amyloidosis. *Neurology*. 2019;93(17):e1647-e1659.
52. Doecke JD, Pérez-Grijalba V, Fandos N, et al. Total Aβ(42)/Aβ(40) ratio in plasma predicts amyloid-PET status, independent of clinical AD diagnosis. *Neurology*. 2020;94(15):e1580-e1591.
53. Adlard PA, Li QX, McLean C, et al. β-amyloid in biological samples: not all Aβ detection methods are created equal. *Front Aging Neurosci*. 2014;6:203.
54. Hart NJ, Koronyo Y, Black KL, Koronyo-Hamaoui M. Ocular indicators of Alzheimer's: exploring disease in the retina. *Acta Neuropathol*. 2016;132(6):767-787.
55. Le Bastard N, Aerts L, Leurs J, Blomme W, De Deyn PP, Engelborghs S. No correlation between time-linked plasma and CSF Abeta levels. *Neurochem Int*. 2009;55(8):820-825.
56. Freddo TF. A contemporary concept of the blood-aqueous barrier. *Prog Retin Eye Res*. 2013;32:181-195.
57. Morin PJ, Abraham CR, Amaratunga A, et al. Amyloid precursor protein is synthesized by retinal ganglion cells, rapidly transported to the optic nerve plasma membrane and nerve terminals, and metabolized. *J Neurochem*. 1993;61(2):464-473.

SUPPORTING INFORMATION

Additional supporting information may be found online in the Supporting Information section at the end of the article.

How to cite this article: Habiba U, Descallar J, Kreilaus F, et al. Detection of retinal and blood Aβ oligomers with nanobodies. *Alzheimer's Dement*. 2021;13:e12193. https://doi.org/10.1002/dad2.12193